UNIVERSIDADE FEDERAL DO CEARÁ
Centro de tecnologia
Departamento de engenharia química
Programa de pós-graduação em engenharia química

UNIVERSITÉ DE PAU ET DES PAYS DE L'ADOUR
Laboratoire des Fluides Complexes et leurs Réservoirs (LFCR)
École doctorale des sciences exactes et leurs applications

ALANDERSON ARTHU ARAÚJO ALVES

THERMOPHYSICAL PROPERTIES OF BIOFUEL SYSTEMS UNDER HIGH-PRESSURE CONDITIONS

FORTALEZA (BRAZIL) / PAU (FRANCE)
2025

ALANDERSON ARTHU ARAÚJO ALVES

THERMOPHYSICAL PROPERTIES OF BIOFUEL SYSTEMS UNDER HIGH-PRESSURE CONDITIONS

Tese apresentada ao Programa de Pós-graduação em Engenharia Química da Universidade Federal do Ceará, em cotutela com a Université de Pau et des Pays de l'Adour como requisito parcial à obtenção do título de Doutor em Engenharia Química, na área de concentração de Processos Químicos e Bioquímicos pela UFC, e Doutor em Engenharia de Petróleo pela UPPA.

Orientador:
Prof. Dr. Filipe Xavier Feitosa
Prof. Dr. Jean-Luc Daridon

FORTALEZA (BRAZIL) / PAU (FRANCE)
2025

ALANDERSON ARTHU ARAÚJO ALVES

THERMOPHYSICAL PROPERTIES OF BIOFUEL SYSTEMS UNDER HIGH-PRESSURE CONDITIONS

Thesis presented to the Post-Graduation Program in Chemical Engineering at the Federal University of Ceará (UFC), in cotutelle with Université de Pau et des Pays de l'Adour (UPPA) as a partial requirement to obtain the degree of Doctor in Chemical Engineering by UFC, and Doctor in Petroleum Engineering by UPPA

Advisors:
Prof. Dr. Filipe Xavier Feitosa
Prof. Dr. Jean-Luc Daridon

Date : 01/10/2025

EXAMINATION BOARD

Prof. Dr. Hervé Carrier (Committee Chair)
Université de Pau et des Pays de l'Adour (UPPA)

Profª. Drª. Roberta Ceriani (Rapporteur)
Universidade Estadual de Campinas (UNICAMP)

Prof. Dr. Márcio Luis Lyra Paredes (Rapporteur)
Universidade do Estado do Rio de Janeiro (UERJ)

Prof. Dr. Jean-Luc Daridon (Advisors and Jury)
Université de Pau et des Pays de l'Adour (UPPA)

Prof. Dr. Filipe Xavier Feitosa (Advisors)
Universidade Federal do Ceará (UFC)

A Deus,

Aos meus pais, **Arinaldo Alves** e **Maria Liliane Santos de Araújo Alves**, e a todos os meus **familiares.**

AGRADECIMENTOS

Primeiramente, agradeço a Deus, por ter sido a base e o alicerce durante toda essa desafiadora caminhada, concedendo-me sabedoria, motivação e força para alcançar meus objetivos.

Aos meus pais, Arinaldo Alves e Maria Liliane Santos de Araújo Alves, expresso minha mais profunda gratidão por todo o amor, carinho, atenção e, sobretudo, pela educação e os estudos que me proporcionaram. Sem esse suporte, não teria chegado até aqui.

Agradeço também aos meus avós paternos e à minha avó materna, por todo o apoio e palavras de encorajamento ao longo da jornada. Aos meus irmãos, Arinaldo Alves Filho e Amanda Luanna de Araújo Alves, pela ajuda constante e apoio nos momentos em que mais precisei.

À minha futura esposa, Thaís do Carmo Oliveira Silva, agradeço imensamente pelo amor, paciência, incentivo e presença constante. Seu apoio foi fundamental para que eu superasse os momentos mais difíceis dessa trajetória. Sem você, essa conquista não teria sido possível. Muito obrigado por tudo.

Aos amigos e companheiros de jornada na pesquisa e no dia a dia, Hugo Andersson, Lucas Henrique Gomes de Medeiros e Moacir Leal da Costa sou grato por cada momento compartilhado durante o doutorado. Agradeço ainda aos colegas e membros do Grupo de Pesquisa em Termofluidodinâmica Aplicada (GPTA): Ana Carolina, Peterson Yamagushi, Willam Trujillo, David Matheus, Davi Cezar, Elton Erick, Júlia Alves, Mauro Anderson, Samuel Santos, Letícia Trindade e Vinícius de Oliveira. Foi uma honra dividir essa experiência com vocês.

Ao professor Frederico Ribeiro do Carmo, meus sinceros agradecimentos pelo apoio desde a graduação e pela confiança depositada em meu trabalho ao longo dessa trajetória. Ao meu amigo Maxwell Silva, muito obrigado por estar sempre disposto a ajudar, com generosidade e prontidão.

Aos professores e coordenadores do GPTA, Prof. Dr. Hosiberto Batista de Sant'Ana e Prof. Dr. Filipe Xavier Feitosa, minha profunda gratidão pela excelente orientação, paciência, confiança e parceria ao longo de toda a pesquisa.

Também agradeço aos membros do *Laboratoire des Fluides Complexes et leurs Réservoirs* (LFCR), onde tive a oportunidade de ampliar meus conhecimentos sob a orientação do Prof. Dr. Jean-Luc Daridon e com o valioso apoio de Jean-Patrick Bazile e Djamel Nasri. A

convivência e os aprendizados durante minha estadia na França enriqueceram significativamente esta jornada acadêmica.

Agradeço, ainda, à Fundação Cearense de Apoio ao Desenvolvimento Científico e Tecnológico (FUNCAP), pelo apoio financeiro por meio da bolsa de estudos concedida.

Por fim, a todos que, de alguma forma, contribuíram para a realização deste trabalho, deixo aqui meu sincero agradecimento. Esta conquista também é de vocês.

ABSTRACT

The growing demand for sustainable alternatives to fossil fuels presents technical and scientific challenges related to the use of biofuels, particularly in understanding their thermophysical behavior under real operating conditions, such as high pressure. This thesis provides a comprehensive investigation of the thermophysical properties of biodiesel-based systems, encompassing both pure fuels and blends with 1-butanol and diesel. The objective is to address gaps in the literature, evaluate the feasibility of alternative formulations, and propose advances in predictive modeling. Properties such as density, speed of sound, isobaric heat capacity, and distillation profile were analyzed, along with derived properties such as compressibility, thermal expansivity, and excess properties. Experimental measurements were conducted over a wide pressure range, from atmospheric conditions to levels representative of the real operating environment of internal combustion engines, which can reach pressures up to 200 MPa. The addition of 1-butanol was explored as a strategy to mitigate the limitations of biodiesel, including its low volatility and poor performance at reduced temperatures, highlighting the potential of this alcohol as a promising renewable additive. In addition to generating novel experimental data, the study incorporates various modeling approaches, including the PC-SAFT equation of state, corresponding states models, and empirical correlations based on fatty ester composition, with the aim of improving the accuracy of property predictions. The results indicate that, although the evaluated models perform satisfactorily in specific contexts, targeted adaptations and parameterizations are essential for the accurate representation of multicomponent mixtures under high pressure. This work makes a significant contribution to the advanced characterization of biofuels, supporting the development of more efficient and sustainable fuels and enhancing modeling tools in process engineering.

Keywords: biofuels; high pressure; thermophysical properties; thermodynamic modeling; renewable additive.

RESUMO

A crescente demanda por alternativas sustentáveis aos combustíveis fósseis impõe desafios técnicos e científicos relacionados ao uso de biocombustíveis, especialmente no que se refere à compreensão de seu comportamento termofísico sob condições operacionais reais, como as de alta pressão. Esta tese investiga, de forma abrangente, as propriedades termofísicas de sistemas à base de biodiesel, abrangendo tanto combustíveis puros quanto misturas com 1-butanol e diesel, com o objetivo de suprir lacunas existentes na literatura, avaliar a viabilidade de formulações alternativas e propor avanços em modelagens preditivas. Foram analisadas propriedades como densidade, velocidade do som, capacidade calorífica isobárica e perfil de destilação, além de propriedades derivadas como compressibilidade, expansividade térmica e propriedades em excesso, por meio de experimentação em ampla faixa de pressões, desde a condição atmosférica até níveis que simulam o ambiente real de operação de motores de combustão interna, que podem atingir pressões da ordem de 200 MPa. A adição de 1-butanol foi estudada como estratégia para mitigar limitações do biodiesel, como sua baixa volatilidade e desempenho insatisfatório em temperaturas reduzidas, evidenciando o potencial desse álcool como aditivo renovável promissor. Além da geração de dados experimentais inéditos, a pesquisa incorpora diferentes abordagens de modelagem, incluindo a equação de estado PC-SAFT, modelos de estados correspondentes e correlações empíricas baseadas na composição em ésteres graxos, com o objetivo de prever com maior precisão o comportamento dos sistemas estudados. Os resultados demonstram que, embora os modelos avaliados apresentem desempenho satisfatório em determinados contextos, adaptações e parametrizações específicas são essenciais para a representação adequada de misturas multicomponentes sob alta pressão. Dessa forma, o presente trabalho contribui de maneira significativa para a caracterização avançada de biocombustíveis, oferecendo subsídios relevantes ao desenvolvimento de combustíveis mais eficientes e sustentáveis, bem como ao aprimoramento de ferramentas de modelagem na engenharia de processos.

Palavras-chave: biocombustíveis; alta Pressão; propriedades termofísicas; modelagem termodinâmica; aditivo renovável.

RÉSUMÉ

La demande croissante pour des alternatives durables aux combustibles fossiles soulève des défis techniques et scientifiques, notamment en ce qui concerne la compréhension du comportement thermophysique des biocarburants dans des conditions réelles de fonctionnement, telles que les hautes pressions. Cette thèse propose une étude approfondie des propriétés thermophysiques de systèmes à base de biodiesel, incluant les combustibles purs ainsi que des mélanges avec du 1-butanol et du diesel. L'objectif est de combler certaines lacunes présentes dans la littérature, d'évaluer la viabilité de formulations alternatives et de proposer des avancées en matière de modélisation prédictive. Les propriétés telles que la densité, la vitesse du son, la capacité calorifique isobare et le profil de distillation ont été analysées, de même que des propriétés dérivées telles que la compressibilité, l'expansivité thermique et les propriétés en excès. Les mesures expérimentales ont été réalisées dans une large gamme de pressions, allant des conditions atmosphériques jusqu'à des niveaux représentatifs de l'environnement réel de fonctionnement des moteurs à combustion interne, pouvant atteindre 200 MPa. L'ajout de 1-butanol a été exploré comme stratégie pour atténuer les limitations du biodiesel, notamment sa faible volatilité et ses mauvaises performances à basse température, mettant en évidence le potentiel de cet alcool comme additif renouvelable prometteur. En plus de générer des données expérimentales inédites, ce travail intègre plusieurs approches de modélisation, incluant l'équation d'état PC-SAFT, les modèles des états correspondants et des corrélations empiriques fondées sur la composition en esters gras, dans le but d'améliorer la précision des prédictions. Les résultats montrent que, bien que les modèles évalués offrent des performances satisfaisantes dans certains contextes, des adaptations ciblées et des paramétrages spécifiques sont nécessaires pour représenter avec précision les mélanges multicomposants sous haute pression. Ce travail constitue une contribution importante à la caractérisation avancée des biocarburants, soutenant le développement de combustibles plus efficaces et durables et renforçant les outils de modélisation en génie des procédés.

Mots-clés : biocarburants ; haute pression ; propriétés thermophysiques ; modélisation thermodynamique ; additif renouvelable.

FIGURES LIST

TABLES LIST

SUMMARY

1 INTRODUCTION

1.1 Relevance and Scientific Motivation of the Study

The intensified use of fossil fuels in recent decades has significantly contributed to the worsening of global environmental issues, such as the increase in greenhouse gas emissions, air pollution, and the progression of climate change. In response to this situation, the partial or complete replacement of fossil fuels with biofuels, particularly biodiesel, has emerged as a key strategy adopted by several countries to promote a more sustainable energy matrix Van Gerpen (2005 e Knothe et al. (2010). Produced from renewable sources such as vegetable oils and fatty residues, biodiesel possesses favorable characteristics, including biodegradability and lower pollutant emissions compared to conventional petroleum-derived diesel, making it a more environmentally responsible alternative. Furthermore, biodiesel blends with fossil diesel, such as B10, B20, and B30, have been widely promoted through public policies, mandatory blending programs, and decarbonization targets, such as Brazil's RenovaBio Tiburcio et al. (2023), as well as by guidelines established by the European Union and the International Energy Agency Daugbjerg; Swinbank (2015 e Switzer; McMahon (2011). These political measures aim not only to reduce dependence on fossil fuels but also to encourage the development of technologies compatible with biofuels while leveraging the existing transport, storage, and distribution infrastructures. In this context, the advancement of biofuels relies heavily on a deep understanding of their thermophysical properties, especially under extreme operating conditions, such as those encountered in modern internal combustion engines. These engines are equipped with injection systems, including common rail injectors, capable of operating at pressures exceeding 200 MPa Araújo Alves et al. (2025 e Boudy; Seers (2009 e Kamil et al. (2010).

The use of biodiesel in its pure form (B100) still presents significant technical challenges, primarily due to uncertainties regarding its behavior under high pressure and the presence of unfavorable properties in certain conditions, such as high viscosity, high density, and low volatility. These characteristics can compromise fuel atomization, combustion efficiency, and overall engine performance. Given this situation, medium-chain alcohols, such as 1-butanol, have been widely investigated as additives or co-solvents that can modify and improve the physicochemical properties of biodiesel. Butanol, in particular, is notable for its complete miscibility with biodiesel, higher energy content compared to lighter alcohols like ethanol, and favorable ignition and volatility characteristics. Recent studies Imtenan et al. (2015

e Killol et al. (2019a e Kuszewski et al. (2023 e Liu et al. (2011a e Rakopoulos et al. (2010 e Thakkar et al. (2021a e Wang et al. (2015a, 2015b e Zheng et al. (2016a) have explored the potential of butanol in developing more efficient fuel mixtures that meet the operational demands of modern engines, highlighting its promising role in the transition toward liquid fuels with a lower environmental impact.

As mentioned previously, facilitating the use of alternative fuels in internal combustion engines requires a detailed understanding of their thermophysical properties. Properties such as density, viscosity, speed of sound, refractive index, distillation temperature, and flash point, among others, directly influence fuel performance during critical stages such as injection, atomization, mixture formation, and combustion Anitescu; Bruno (2012a e Bukkarapu; Krishnasamy (2022). In this context, obtaining reliable experimental data is essential not only for evaluating the behavior of these fuels and their mixtures but also for supporting the development and validation of predictive models De Hemptinne et al. (2022). Modeling tools, including molecularly based equations of state, group contribution models, empirical correlations, and state matching methods, play a crucial role in simulating operational scenarios, optimizing processes, and advancing scientific knowledge. Therefore, the integration of experimentation and modeling is a key element in the development of more efficient, safer, and environmentally sustainable fuels De Hemptinne et al. (2022 e Kontogeorgis et al. (2021).

Models capable of reproducing experimental data with deviations close to measurement uncertainties Daridon (2020, 2022a, 2022b) are particularly valuable, as they provide greater reliability for the simulations and projections conducted using them. When a model demonstrates performance consistent with experimental error limits, it becomes a robust tool for extrapolating properties under conditions not yet evaluated in the laboratory, in addition to being widely applicable in simulation environments and process optimization with greater safety and precision. This capability is especially important in the context of alternative fuels, whose properties can vary significantly depending on the raw material, production routes, and operating conditions. In the specific case of biodiesel, for example, these variations can be attributed to the diversity of oil sources used, the type of alcohol employed in transesterification (such as methanol, resulting in methyl esters (FAME), or ethanol, producing ethyl esters (FAEE)), as well as variations in pressure and temperature during application. Therefore, the development and validation of highly accurate models not only strengthen the scientific foundation for the application of these fuels but also provide essential technical support for their integration into commercial technologies and the establishment of more effective

environmental regulations (DO CARMO et al., 2015a, 2020b; EVANGELISTA; DO CARMO; DE SANT'ANA, 2017b, 2018).

Taking into account the need for biodiesels and biodiesel blends thermophysical data, this thesis proposes a comprehensive approach for characterizing biofuel systems under high pressure by obtaining experimental data on density, speed of sound, heat capacity, and distillation profiles in both pure and mixed systems (biodiesel + 1-butanol; biodiesel + diesel). In addition to the experimental characterization, the work includes specific modeling for each property studied, with an emphasis on the PC-SAFT equation of state, known for its effectiveness in representing associative and polar systems, and whose set of parameters allows the derivation of several thermodynamic properties Gross; Sadowski (2001a). Corresponding state models, correlations based on chemical composition Daridon (2020, 2022b) and Tait-type models Dymond; Malhotra (1988), are also used, enabling accurate adjustments and extrapolation or interpolation of properties under conditions not experimentally evaluated. These tools are critically evaluated for their ability to predict the behavior of complex, multicomponent systems under high pressure, aiming to identify their limitations and propose specific parameterizations when necessary. Furthermore, the modeling aims to achieve a level of precision that matches experimental uncertainties, improving the reliability of the results and supporting the application of the models in simulations and process optimization.

1.2 Biodiesel: Production, Potential, and Relevance for Research

Biodiesel is defined as a renewable fuel obtained through a chemical process known as transesterification. This process involves the reaction of triglycerides, found in vegetable oils or animal fats, with a primary alcohol (usually methanol or ethanol) in the presence of a catalyst, resulting in the formation of fatty acid esters (biodiesel) and glycerol as a by-product. Transesterification typically consists of an organic reaction in which one ester is converted into another by replacing the alkoxide group. During this reaction, triglycerides are transformed into fatty acid monoesters, which constitute biodiesel. The type of alcohol used, as well as the composition of the feedstock (biomass), directly influences the physicochemical properties of the resulting biodiesel, leading to ester chains with varying lengths and degrees of unsaturation Knothe et al. (2010).

Basic catalysts such as sodium hydroxide (NaOH) and potassium hydroxide (KOH) are commonly used due to their high efficiency and low cost. However, there are also alternative production routes, such as acid esterification (particularly useful for feedstocks with a high

content of free fatty acids), supercritical processes, enzymatic processes, and others Sahu et al. (2018). Figure 1 illustrates the mechanism of the transesterification reaction using two different alcohols. The molecular structure of the resulting biodiesel is determined by the nature of the alcohol used and by the R_1, R_2, and R_3 chains, which represent the alkyl radicals derived from the biomass. These variables directly influence the final properties of the fuel, such as viscosity, density, flash point, cold flow behavior, and engine performance Baiju et al. (2009).

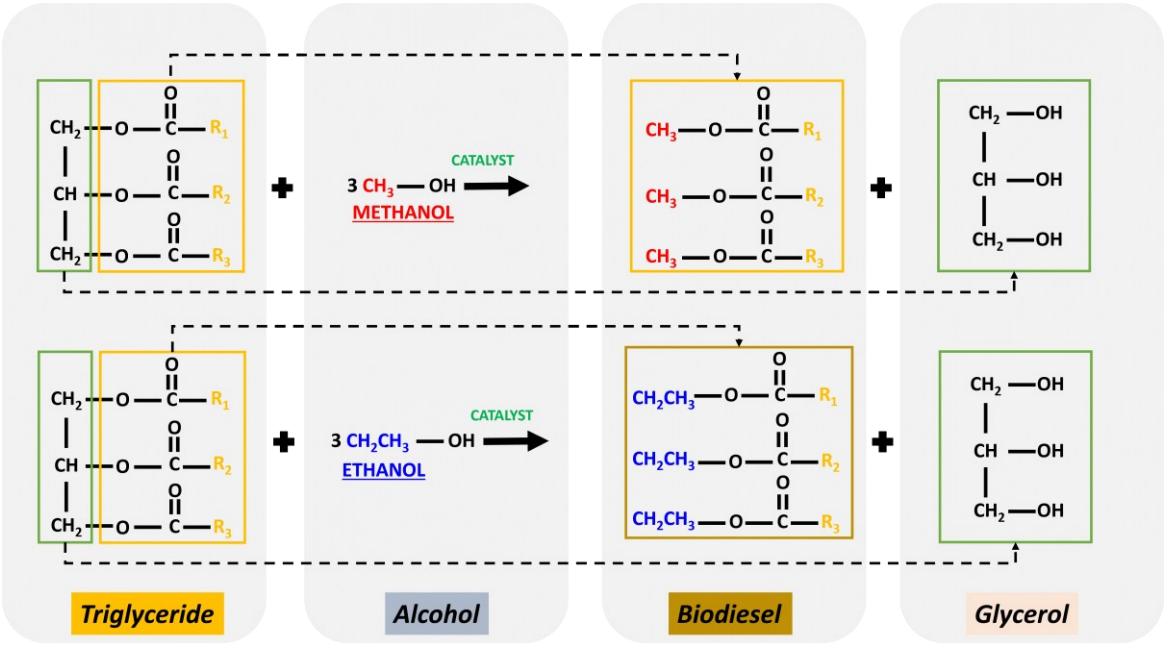

Figure 1 – Illustration of biodiesel transesterification reaction routes using methanol and ethanol. (Created by the author, 2025)

Biodiesel stands out as a promising alternative to fossil fuels not only because it is renewable and biodegradable, but also due to its potential to reduce greenhouse gas emissions and contribute to sustainable development Salina et al. (2019). Despite significant progress in production technologies, the selection of feedstocks remains a critical issue. Currently, the biodiesel industry is largely dependent on edible vegetable oils, particularly soybean and palm oils, which together account for more than 90% of global production. This reliance raises concerns about competition with the food supply chain and increased pressure on land use. Despite this situation, the International Energy Agency (IEA) projects that the use of vegetable oils for biofuel production will grow by 46% between 2022 and 2027, maintaining its position as the primary raw material source for biodiesels. Considering these projections, there is an urgent need to diversify feedstocks by exploring non-edible oils, industrial residues, and algal biomass to ensure the long-term environmental and socioeconomic sustainability of the biodiesel production chain Alves, Alanderson A.A. et al. (2025). However, in this thesis, many

investigations focus on edible oils, solely and exclusively due to their wide availability and experimental accessibility. Furthermore, these oils still represent the main raw material used in both research and the commercial production of biodiesel, reinforcing their relevance in the current context and justifying their choice as the object of study in this work. Research on biodiesel holds high scientific, technological, and socio-environmental relevance in today's energy context Sangeeta et al. (2014). Given the growing concerns over the environmental impacts of fossil fuel use, systematic investigations into the physicochemical properties of biodiesel and its mixtures are crucial. This research, along with studies on the performance of various synthesis routes and raw materials, is essential to ensure the efficiency, operational safety, and economic viability of biodiesel on a large scale.

In addition to research works on biodiesel from edible oils, there is a growing trend in research focusing on non-petroleum and non-food sources, such as microalgae, and blending biodiesel with alcohols as well as the development of alternative synthesis routes, such as enzymatic and supercritical processes. These approaches aim to further mitigate the environmental impacts associated with conventional biodiesel production Demirbas; Fatih Demirbas (2011 e Galadima; Muraza (2014 e Scott et al. (2010). This thesis contributes to this panorama by examining the thermophysical properties of biodiesel blends with butanol, a longer-chain alcohol that has the potential to modify the properties of the biofuel. Such blends can enhance the performance of alternative fuels, enabling both an increase in the renewable fraction in blends with fossil diesel and direct use as fuel, aligning with transition strategies toward a more sustainable energy matrix.

1.3 The Potential of Butanol as a Biofuel

Butanol is a four-carbon chain alcohol that stands out as a promising alternative to fossil fuels, both due to its potential as a biofuel and its effectiveness as an additive in diesel and biodiesel blends. Its physical and chemical properties, such as high calorific value, lower volatility compared to ethanol, and greater miscibility with petroleum-based fuels, confer significant versatility for applications in the energy sector. These characteristics make 1-butanol an attractive option for enhancing the performance and stability of alternative fuels, as well as contributing to the reduction of pollutant emissions Fernández-Rodríguez et al. (2021).

Butanol can be produced from several raw materials, primarily biomass rich in sugars, starches or cellulose. Conventional butanol production occurs through anaerobic fermentation using *Clostridium* bacteria, which convert simple sugars into butanol. However,

the conversion of lignocellulosic biomass, such as agricultural and forestry waste, into butanol has gained increasing attention, offering a more sustainable pathway by utilizing non-edible materials and avoiding competition with food production. Nevertheless, biomass pre-treatment and the use of specialized microbial strains are still required to enhance process efficiency. Emerging approaches, including genetic engineering and the development of more efficient bioreactors, are being investigated to make butanol production more economically viable and environmentally sustainable. When combined with carbon capture technologies, this production pathway can offer even greater environmental benefits by contributing to the reduction of greenhouse gas emissions Kolesinska et al. (2019 e Rajagopalan; Krishnan (2022).

In addition, butanol exhibits better compatibility with existing engines compared to ethanol, due to its lower corrosiveness and higher solubilizing power, making it more suitable for blending with diesel or biodiesel. Its low volatility also reduces evaporation during combustion, which can contribute to lower pollutant emissions Thakkar et al. (2021a e Wang et al. (2015b). As shown in Table 1, the physicochemical properties of gasoline, diesel, methanol, ethanol, and n-butanol indicate that the latter possesses advantageous characteristics over the other fuels.

Table 1 – Specification of alcohols and conventional fossil fuels Jin et al. (2011).

Information/properties	Gasoline	Diesel	Methanol	Ethanol	n-Butanol
Molecular formula	C4–C12	C12–C25	CH3OH	C2H5OH	C4H9OH
Cetane number	0–10	40–55	3	8	25
Octane number	80–99	20–30	111	108	96
Oxygen content (% weight)	–	–	50	34.8	21.6
Density (g/mL) at 20 °C	0.72–0.78	0.82–0.86	0.796	0.790	0.808
Autoignition temperature (°C)	∼300	∼210	470	434	385
Flash point (°C) at closed cup	−45 to −38	65–88	12	8	35
Lower heating value (MJ/kg)	42.7	42.5	19.9	26.8	33.1
Boiling point (°C)	25–215	180–370	64.5	78.4	117.7
Stoichiometric ratio	14.7	14.3	6.49	9.02	11.21
Latent heating (kJ/kg) at 25 °C	380–500	270	1109	904	582
Flammability limits (%vol.)	0.6–8	1.5–7.6	6.0–36.5	4.3–19	1.4–11.2

Information/properties	Gasoline	Diesel	Methanol	Ethanol	n-Butanol
Saturation pressure (kPa) at 38 °C	31.01	1.86	31.69	13.8	2.27
Viscosity (mm2/s) at 40 °C	0.4–0.8 (20 °C)	1.9–4.1	0.59	1.08	2.63

It can be seen in Table 1.1 that n-butanol presents a higher heating value and a lower boiling temperature compared to ethanol and methanol. This higher calorific value enhances energy efficiency, while its lower volatility reduces issues related to cavitation and vapor lock. Additionally, its lower autoignition temperature and reduced heat of vaporization facilitate cold starts, ensuring greater operational reliability Jin et al. (2011).

Its relatively high viscosity improves engine lubrication, thereby reducing wear, and its good miscibility with diesel and gasoline eliminates the need for cosolvents. From a safety perspective, its high flash point and low vapor pressure make it less flammable than gasoline and lighter alcohols. Furthermore, its resistance to water contamination and lower corrosivity facilitate transportation through conventional pipelines. Its potential for hydrogen production in fuel cells further reinforces its long-term relevance in the energy sector Jin et al. (2011).

Despite these advantages, the direct use of n-butanol in engines presents certain challenges. Its lower calorific value compared to gasoline and diesel necessitates a higher fuel flow to maintain equivalent performance. Additionally, alcohol-based fuels may be incompatible with components of the fuel injection system and may impair the functionality of capacitive fuel level detection. Although its high viscosity is beneficial for lubrication in diesel engines, it may cause issues related to fuel atomization and increased corrosivity when blended with gasoline in spark ignition (SI) engines Jin et al. (2011).

Given the challenges associated with the direct use of n-butanol as a fuel, research into its blending with other biofuels and with diesel itself has emerged as a strategic alternative. The formulation of such blends can help overcome limitations related to its lower calorific value, incompatibility with combustion system components, and potential corrosivity. Moreover, blending with diesel promotes a balance of physical and chemical properties, preserving both energy efficiency and engine operability without requiring major modifications Rakopoulos et al. (2010). Comparative analyses with other alcohols further reinforce the potential of n-butanol, as its properties, particularly viscosity, miscibility, and thermal stability, are more closely aligned with those of diesel. This similarity makes n-butanol a promising candidate for alternative fuel formulations and highlights the relevance of the present study in

the pursuit of viable and sustainable solutions to expand its use as a partial substitute for fossil fuels Liu et al. (2011b, 2011a e Rakopoulos et al. (2010).

1.4 Internal Combustion Engines: Principles, Operation, and Technological Development

Internal combustion engines play a pivotal role in the transportation sector and in the generation of mechanical energy, by converting the chemical energy of fuels into mechanical work through combustion within a confined chamber. Since their inception, spark ignition and compression ignition engines have been extensively employed and continuously refined, aiming to enhance energy efficiency and reduce pollutant emissions Alagumalai (2014).

The spark ignition engine, commonly referred to as the Otto engine, was developed by Nikolaus August Otto in 1876 and operates based on the four-stroke thermodynamic cycle. In this engine, the air-fuel mixture is prepared prior to ignition, which is triggered by an electric spark produced by a spark plug. Conversely, the compression ignition engine, introduced by Rudolf Diesel in 1892, does not require spark plugs. Instead, it utilizes a high compression ratio to elevate the temperature of the air inside the cylinder, thereby initiating the autoignition of the injected fuel. Owing to this principle of operation, diesel engines typically offer superior thermal efficiency and higher torque, making them particularly suitable for heavy-duty vehicles and industrial applications Mollenhauer; Schreiner (2010).

In compression ignition engines, the high compression ratio enables more efficient utilization of the fuel's energy, resulting in greater thermal efficiency compared to spark ignition engines. During operation, the incoming air is compressed to a point where the temperature becomes sufficiently high to spontaneously ignite the atomized fuel. This process promotes slower and more controlled combustion, which enhances energy conversion and reduces specific fuel consumption.

However, factors such as fuel spray quality, turbulence within the combustion chamber, and injection timing have a direct impact on the overall efficiency of the process. In this context, common rail injection systems represent a major technological advancement, as they provide precise control over the quantity, pressure, and timing of fuel injection. Operating at pressures exceeding 200 MPa, these systems significantly improve fuel atomization and promote more homogeneous combustion Sadeghinezhad et al. (2014 e Taylor (2008), leading to enhanced thermal efficiency, reduced fuel consumption, and lower pollutant emissions.

Studying the behavior of fuels under high-pressure conditions is therefore essential for optimizing the application of emerging engine technologies, particularly in light of the increasing demand for alternative fuels. In this context, biofuels such as biodiesel have emerged as promising alternatives to fossil fuels, driven by growing environmental concerns and the need to diversify the global energy matrix. However, despite their environmental benefits and the potential for production from renewable sources, the use of biofuels in internal combustion engines still poses technical challenges. The performance of an engine running on biodiesel can be significantly affected by the physicochemical properties of the fuel, such as density, viscosity, compressibility and thermal behavior, as well as by operational parameters including compression ratio, ignition timing and combustion chamber geometry. These factors directly influence fuel atomization, air-fuel mixture formation and the combustion process as a whole Alagumalai (2014 e Damanik et al. (2018 e Rajendran (2021).

In this context, the present study aims to contribute to the understanding of the behavior of binary blends of biodiesel with 1-butanol, diesel, and nitrogen under high-pressure and high-temperature conditions. To this end, fundamental experimental data on thermophysical properties, such as density and speed of sound, are provided. These data are essential for the development, calibration, and validation of advanced thermodynamic models capable of more accurately predicting the performance of these fuels under real operating conditions.

1.5 Aligning Scientific Research with the Sustainable Development Goals (SDGs)

The growing concern about climate change, the scarcity of natural resources, and the environmental impacts associated with the current development model have driven the global pursuit of more sustainable solutions. In response to these challenges, the United Nations (UN) established the Sustainable Development Goals (SDGs) in 2015 as part of the 2030 Agenda. This set of 17 interconnected goals aims to eradicate poverty, protect the planet, and ensure that all people can enjoy peace and prosperity by the year 2030 (Figure 2).

Figure 2 – The 17 Sustainable Development Goals (SDGs). Source: United Nations (2015)

Among the central pillars of the 2030 Agenda are energy transition, technological innovation, and climate change mitigation. In this context, research into the development of alternative and renewable fuels has gained prominence, as the transportation sector has historically been one of the largest emitters of greenhouse gases. The partial or complete replacement of fossil fuels with renewable sources, such as biodiesel and 1-butanol, represents an important step toward building a cleaner and more resilient energy matrix.

The work presented in this thesis is part of this broader energy transformation effort. By experimentally characterizing the thermophysical properties of systems containing biodiesel, fossil diesel, and renewable additives, this research aims to provide essential technical data to support the efficient and safe use of these fuels in internal combustion engines. In addition to addressing knowledge gaps under extreme operating conditions typical of the modern automotive industry, the study contributes directly to the formulation of strategies that support the decarbonization of the transportation sector.

By promoting the use of renewable resources, encouraging innovation in fuel technologies, and enabling the development of more energy and environmentally efficient solutions, this research aligns directly with several SDGs, particularly SDG 7 (Affordable and Clean Energy), SDG 9 (Industry, Innovation and Infrastructure), SDG 12 (Responsible Consumption and Production), and SDG 13 (Climate Action). In this way, the thesis reaffirms the role of science and engineering as fundamental tools for achieving global sustainability

goals while proposing concrete pathways for the transition toward a more balanced and environmentally responsible energy future.

1.6 Objective of this work

This thesis is driven by the growing environmental concerns and the urgent need to mitigate the negative impacts associated with the extensive use of fossil fuels, such as diesel, which are major contributors to high greenhouse gas emissions and air pollution. In this context, the partial replacement of fossil diesel with biofuels, such as biodiesel, emerges as a promising strategy for promoting a more sustainable energy matrix. However, the use of biodiesel in internal combustion engines presents technical challenges, particularly in relation to its thermophysical properties. In this regard, an in-depth study of biodiesel, along with the incorporation of renewable additives, such as 1-butanol, has shown promise in addressing these limitations. Nevertheless, the lack of detailed experimental data on the thermophysical properties of these mixtures under high pressure and temperature conditions (conditions typical of modern engine operations) remains a barrier to the advancement of this technology. Therefore, the motivation for this thesis is to bridge this knowledge gap, with the central objective of:

1.6.1 Central objective

To investigate the thermophysical behavior of biofuel systems containing biodiesel, 1-butanol, and fossil diesel under high-pressure conditions by obtaining new experimental data on key properties such as density, speed of sound, heat capacity, and distillation profiles. Additionally, to evaluate correlation and prediction models that provide a solid foundation for applications aimed at the efficient and sustainable use of these fuels in internal combustion engines, with a particular emphasis on the detailed study of their physical and thermodynamic properties.

1.6.2 Specific objectives

- To experimentally evaluate the density and speed of sound properties of various biodiesels under high pressure, using thermodynamic models such as the PC-SAFT equation of state, along with chemical composition-based models for correlation and prediction purposes

- Measure the isobaric heat capacity of different biodiesels and analyze the applicability of a corresponding state model adapted for complex mixtures, incorporating mixing rules to specifically represent the systems under study.
- Investigate the density behavior of 1-butanol and biodiesel mixtures at high pressures to understand the effect of adding renewable alcohol on the volumetric properties of these biofuels.
- Experimentally analyze the speed of sound in mixtures of 1-butanol and biodiesel under high pressure to deepen the understanding of acoustic behavior and its implications for combustion processes.
- Characterize binary blends of diesel and biodiesel in terms of distillation profiles and thermophysical properties, contributing to the development of more efficient and sustainable formulations for internal combustion engines, while also assessing compliance with ASTM standards for the entire range of diesel + biodiesel blends.

1.7 Thesis structure

To ensure better clarity and organization, this thesis is structured into seven chapters, which progressively address the main theoretical, experimental, and applied aspects of the research. The initial chapters discuss the fundamentals and relevance of studying biofuels and their applications, with an emphasis on strategies to increase renewable content through the addition of additives such as butanol, aimed at regulating physicochemical properties. Subsequently, the connection between this research and the United Nations Sustainable Development Goals (SDGs) is explored, reinforcing the alignment of the study with global sustainability targets. The thesis also provides a detailed description of the experimental apparatus and the modeling tools used to support the analysis of the systems under investigation. Finally, the analysis chapters (Chapters 3 to 7) focus on the presentation and discussion of the experimental results. A summary of the content of each chapter is provided below:

Chapter 1 presents the theoretical foundations that support and scientifically justify this research. It provides a comprehensive introduction to the topic of biofuels, addressing their relevance in the current energy landscape, their main physicochemical properties, and the challenges associated with their use. The chapter discusses the role of biodiesel as a viable alternative to fossil fuels and explores the potential of butanol as a promising additive in the formulation of renewable fuels. It also reviews the operating principles and technological

evolution of internal combustion engines, with particular emphasis on their adaptation to alternative fuels. The chapter concludes by establishing the connection between the aims of this study and the United Nations Sustainable Development Goals, highlighting the research's commitment to cleaner and more sustainable energy solutions.

Chapter 2 describes the experimental procedures employed to obtain speed of sound and density data under high pressure conditions, which are essential for analyzing the thermodynamic behavior of fuel mixtures. It details the measurement techniques and equipment, emphasizing their role in investigating complex systems. The chapter also outlines the thermodynamic models adopted as analytical tools, which were applied to interpret the experimental results. Particular attention is given to the PC-SAFT equation of state, whose theoretical basis and suitability for modeling the systems studied are thoroughly examined, demonstrating its capability to predict volumetric and acoustic properties across a wide pressure range.

Chapter 3 develops a detailed experimental investigation into the density and speed of sound of three biodiesels under a wide range of pressures, reaching up to 200 MPa, and at various temperatures. These data contribute to addressing a relevant gap in literature, particularly under high-pressure conditions that are critical for modern fuel injection systems. In parallel with the experimental work, the chapter evaluates the performance of two predictive models. The first is the PC-SAFT equation of state, known for its ability to represent the thermophysical behavior of complex systems. The second is an empirical approach based on the chemical composition of biofuels, calibrated using experimental data for individual esters, specifically fatty acid methyl esters (FAMEs) and ethyl esters (FAEEs), and applied to estimate the properties of biodiesel as a multicomponent mixture. The comparison between experimental results and model predictions enables an assessment of their accuracy and practical applicability under extreme conditions, supporting their use in process simulations and computational fluid dynamics studies focused on renewable fuel development.

Chapter 4 describes the experimental determination of the isobaric heat capacity of ten biodiesels obtained from different feedstocks, measured over a broad temperature range using differential scanning calorimetry (DSC). The experimental results were combined with data from literature to build a comprehensive database covering 22 types of biodiesels. The variation of heat capacity with temperature and the influence of biodiesel origin are analyzed in detail. The chapter also explores the applicability of a predictive model based on the principle of corresponding states, initially developed for pure esters, which is extended to estimate the heat capacity of biodiesel as a complex mixture through the use of blending rules and different

methodological approaches. A critical assessment of the model's performance in comparison to the compiled data set allows for a discussion of its robustness and its limitations in representing the compositional diversity inherent to biodiesels.

Chapter 5 investigates the density behavior of blends composed of 1-butanol and biodiesel under high pressure conditions, aiming to understand the impact of alcohol addiction on the volumetric properties of the resulting fuel. Experimental density data were obtained over a temperature range from 293.15 to 373.15 K and at pressures up to 100 MPa. The study includes an analysis of excess properties, enabling the identification of deviations from ideal mixing behavior. The experimental results were correlated using both the Tammann-Tait equation and the PC-SAFT equation of state, allowing for a comparison of their accuracy and underlying conceptual frameworks. From the Tammann-Tait parameters, key thermodynamic properties such as isothermal compressibility and isobaric thermal expansivity were derived. These same properties were also estimated using the PC-SAFT model, providing a comparative analysis that highlights the methodological differences and predictive capabilities of each approach.

Chapter 6 continues the investigations from Chapters 3 and 5 by presenting an experimental analysis of the speed of sound in binary mixtures of 1-butanol with biodiesels derived from canola and sucupira oils. Measurements were performed at temperatures ranging from 293.15 K to 333.15 K and pressures up to 100 MPa. The chapter explores the behavior of the quantity $cM\gamma$ as a function of composition, highlighting deviations from ideality and its dependence on temperature and pressure. A combination rule based on this parameter is proposed to predict the speed of sound in these mixtures with accuracy comparable to experimental uncertainty. Furthermore, the chapter evaluates the predictive capacity of the PC-SAFT equation of state for these systems using molecular parameters determined for the pure components, without the need for binary interaction adjustments. The findings contribute to expanding the understanding of thermophysical properties of renewable fuels under relevant operational conditions.

Chapter 7 addresses the thermophysical behavior of blends of biodiesel and low-sulfur diesel (S10), focusing on the distillation curve, a key property for characterizing volatility and technical performance in automotive fuels. The chapter presents detailed experimental data for binary systems containing biodiesels derived from grape seed, corn, and linseed oils, in volumetric proportions of 0%, 20%, 40%, 60%, 80%, and 100%. In addition to the distillation curve, important properties such as density, viscosity, refractive index, cetane number, and flash point are evaluated according to rigorous ASTM standards. A significant contribution of this

chapter is the proposal of two new correlations for modeling the distillation curve of pure biodiesel and its blends with diesel.

2 EXPERIMENTAL TECHNIQUES AND THERMODYNAMIC MODELS

2.1 Speed of Sound Measurement: Methods, Applications and Implications in the Thermodynamic Characterization of Fluids

The speed of sound refers to the velocity at which a mechanical disturbance propagates through a medium and is directly associated with its thermodynamic properties, such as density and isentropic compressibility Rasmussen; Wilthan (2024). It is a fundamental parameter in the characterization of fluids and materials, with broad relevance across various fields of engineering and science. In chemical engineering, the speed of sound is widely employed to determine thermodynamic derivative properties, validate mathematical models, and predict the behavior of mixtures under varying pressure and temperature conditions.

Accurate measurement of the speed of sound in fuels is particularly critical for the biofuels and petroleum sectors, as it provides insights into the interactions among biodiesel, diesel, and gases under high-pressure conditions. This enables the development of more precise models to optimize fuel formulations and predict performance in engines and transport systems. In internal combustion engines, especially in common rail injection systems, the speed of sound plays a key role in the acoustic phenomena caused by operating the injector at high frequency and which influence injection dynamics, fuel atomization, and consequently combustion efficiency. As these systems operate at pressures exceeding 2000 bar, variations in fuel compressibility significantly impact the propagation of pressure waves in the high-pressure lines, thereby affecting injector response and injection accuracy Freitas, S. V.D. et al. (2013 e Kamil et al. (2010). A low speed of sound can delay fuel delivery, compromise combustion quality, and increase pollutant emissions, whereas excessively high values can generate pressure spikes that compromise system durability Tat; Van Gerpen (2003a). In the context of this thesis, evaluating the speed of sound in pressurized mixtures plays a key role in understanding molecular interactions and in the development of equations of state such as PC-SAFT, which allow for more accurate modeling of the behavior of biofuels and their blends under extreme conditions.

Experimental measurements of the speed of sound in liquids are fundamental for the thermodynamic characterization and for the modeling of the physicochemical properties of these systems. Therefore, a variety of experimental techniques are available for this purpose, generally classified into direct and indirect methods, depending on whether the measurement is based on the propagation time of acoustic waves or inferred from other thermophysical

properties. Indirect methods infer the speed of sound by correlating it with other physical phenomena, such as interference or resonance, without directly measuring the wave's propagation time. In contrast, direct methods determine this property by measuring the propagation of an acoustic wave through the medium, typically by assessing the transit time between an emitter and a receiver.

As mentioned, indirect methods infer the speed of sound from correlated physical phenomena without directly measuring the transit time of the acoustic wave. The main methods include variable-path ultrasonic interferometry, which utilizes stationary waves formed between an emitting crystal and a moving reflector to determine the wavelength and calculate the speed of sound. This method can operate in both liquid and gas systems. However, it requires precise alignment, especially under high-pressure conditions Rasmussen; Wilthan (2024). Optical methods based on light diffraction analyze the interaction between ultrasonic waves and light beams to determine the speed of sound from the wavelength or diffraction angle, but they face limitations in highly opaque fluids. Another method relies on resonance phenomena, which excites the fluid with an acoustic signal and calculates the speed of sound from the resonance frequency and the system's eigenvalue equation. While widely used for gases, its accuracy decreases at pressures above 20 MPa due to potential mechanical deformations in the resonator Dzida et al. (2017).

In direct sound velocity measurement methods known as pulse-echo technique, the velocity is determined from the propagation of an ultrasonic wave through a fluid medium Khelladi et al. (2010) over a given path length. The technique consists in determining both the transit time of the acoustic wave and the path length. Several pulse-echo techniques were proposed. These techniques differ based on several factors, including how the ultrasonic wave is generated, the nature of the path length, the transmission or reflection mode, and the method of measuring the time of flight, as outlined below.

Wave Generation: The ultrasonic wave can be generated in two primary ways: as a pulse or as a burst of several sinusoidal cycles.

- Pulse Generation: In this method, a short electrical pulse of Dirac-type is generated and sent to a piezoelectric element, which undergoes mechanical deformation. The rapid change in the electric field causes the transducer to vibrate, producing an ultrasonic wave train consisting of a few oscillation cycles. The shape of this acoustic wave train typically resembles a damped sinusoidal wave: it begins with a sharp initial compression wave followed by oscillations that decay in amplitude, as shown in Figure 3. Its frequency is

determined by the resonant frequency of the transducer. This technique is often favored for its simplicity and effectiveness in various applications.

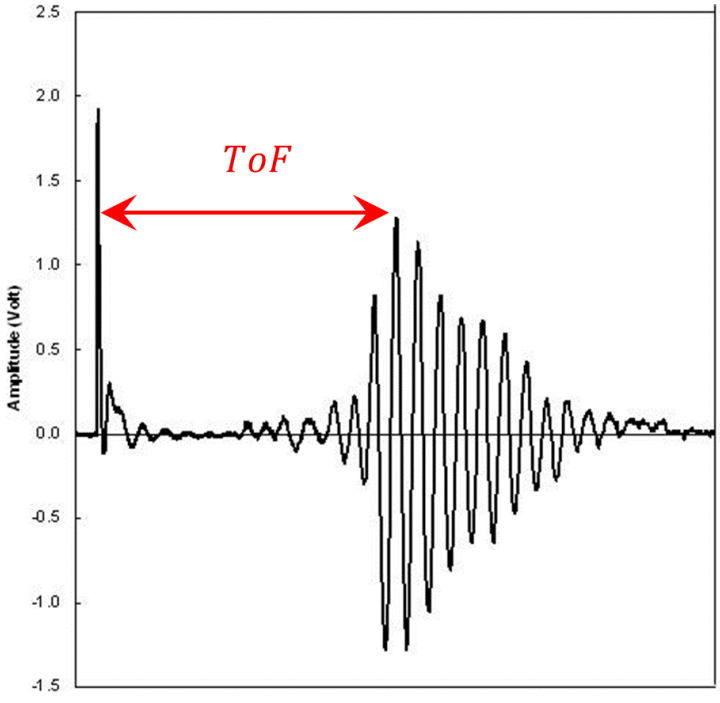

Figure 3 – Typical acoustic signal in the Time of Flight (ToF) technique, showing the damped waveform and the time interval between pulses used to calculate the speed of sound. (Created by the author, 2025)

- Tone Burst of Several Sinusoidal Cycles: In this approach, the transducer is energized by a single electrical burst of several sinusoidal cycles (around 10). This causes the transducer to emit an acoustic wave packet of the same frequency in the fluid. This method is particularly useful in applications requiring a fixed and stable frequency for signal analysis. It is also beneficial for measuring wave attenuation in addition to the speed of sound.
- *Path Length Consideration:* The path length can be classified as either variable or fixed, which influences the measurement method as primary (absolute) or secondary (relative).
- Variable Path Length: In this technique, the distance can change, and the time of flight is measured as a function of the distance, allowing for a direct measurement of path length and time of flight, leading to an absolute determination of the speed of sound.
- Fixed Path Length: In this configuration, the distance the wave travels remains constant throughout the measurement. This method is particularly suited for high-pressure conditions, as it simplifies the experimental setup by eliminating movable parts. However, it requires the path length to be determined by calibration prior to measurement with the sample studied. Therefore, it is considered as a secondary technique.

Transducer Modes: The way the transducers operate can be categorized into two methods: transmission and reflection.

- Transmission: In this method, two different transducers facing each other are used in the experimental setup. One acts as a transmitter, while the other serves as a receiver.
- Reflection: In this second method, a single transducer is used in the experiment, but one or more reflectors must be added to reflect the acoustic wave. In this configuration, the transducer generates the acoustic wave and, after a round trip through the studied medium, receives it and converts it into an electrical signal. This method is advantageous in high-pressure devices due to its simple configuration, as it requires only one transducer and consequently only one electrical connection.

Time of Flight Measurement: After the signal is received by the transducer and converted into an electrical signal, it is typically displayed on a digital oscilloscope. This device enables real-time visualization of the ultrasonic signal, recording with high precision the moments when the pulse is emitted and when it is received. Such accurate time-of-flight (ToF) measurement is essential for determining the speed of sound with minimal uncertainty. Using a digital oscilloscope, ToF can be measured with various techniques, each with its own advantages and limitations. Among these, we can mention, without being exhaustive the following techniques

- Direct Chronometry: This method involves measuring the ToF by determining the position of an arbitrary peak of the received echo on the oscilloscope's time base. It is widely used due to its precision, simplicity, and adaptability to various experimental conditions Habrioux (2015 e Ndiaye (2012). However, while straightforward, it may lack sufficient precision in some applications.
- Pulse-Echo Overlap: This technique involves superimposing two ultrasonic echo signals on the oscilloscope display Papadakis (1965). The superposition of the echoes is achieved using an external time base sweep, whose frequency enables precise measurement of the time interval between the two echoes.
- Digital Overlap Method: In this technique, two echoes are recorded and digitized. One echo is then shifted along the temporal axis to overlap the other Bazile et al. (2017). The time delay between echoes is estimated by determining the time shift that maximizes the overlap. This method improves accuracy compared to direct chronometry.

Regardless of the chosen method, it is preferable to measure the time delay between two successive echoes rather than the ToF of the first echo alone. This is because the single-echo measurement includes not only the wave's transit time through the fluid but also delays

introduced by the electronic components and the conversion of the electrical signal to an acoustic wave within the piezoelectric element. By measuring ΔToF, the time delay between two successive echoes (Figure 4), these additional times are effectively canceled out, isolating the true transit time of the acoustic wave in the fluid and enabling a more accurate determination of the speed of sound. The various echoes can be obtained either by configuring different propagation path lengths (using variable path lengths or double-path configurations - Figure 5) or by analyzing successive echoes resulting from multiple round-trips of the wave within the medium, as illustrated in Figure 6. In this context, the effective propagation length should correspond to the difference in the path lengths between the two successive echoes.

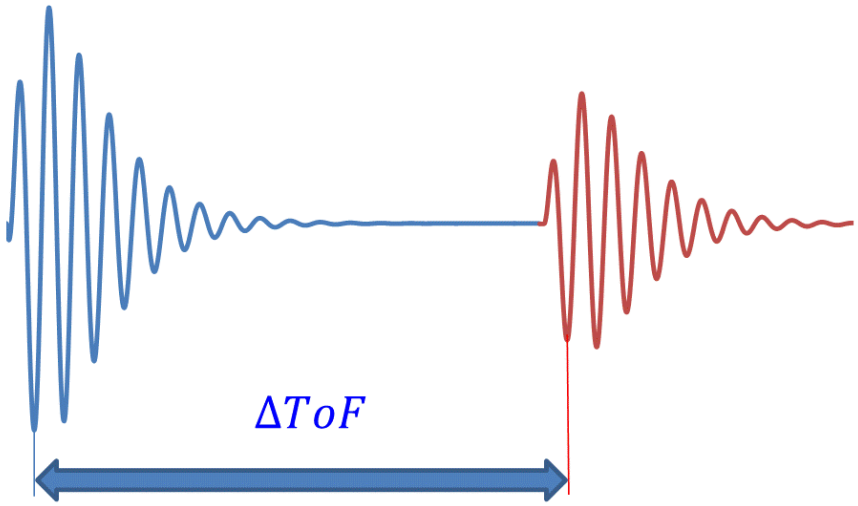

Figure 4 – Diagram illustrating the measurement of the time delay between two successive echoes (ΔToF). Measuring the interval between echoes eliminates electronic and transducer delays, isolating the actual transit time of the acoustic wave in the fluid. (Created by the author, 2025)

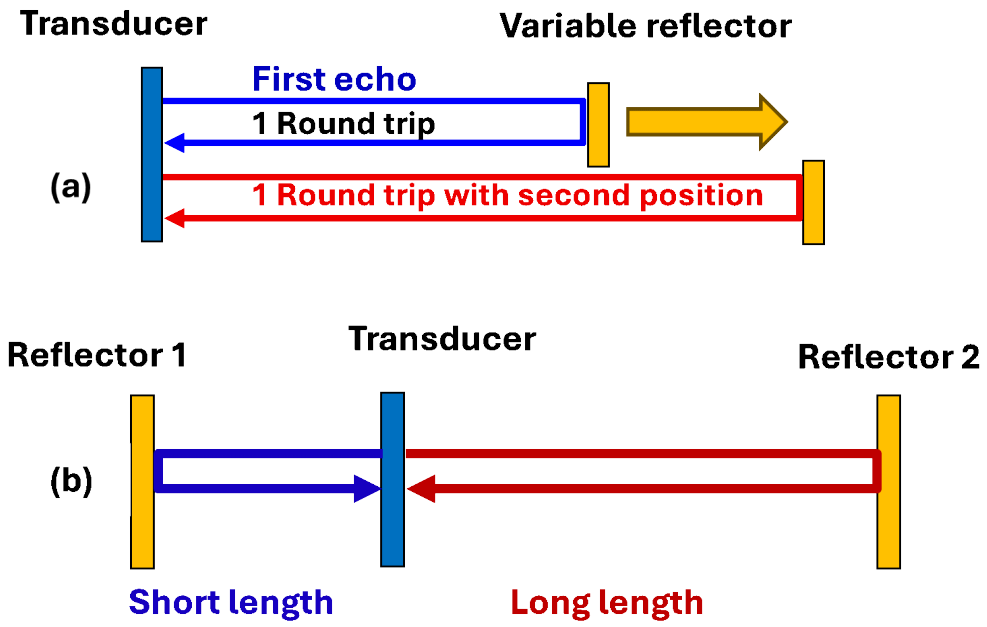

Figure 5 – Schematics of configurations with different path lengths for measuring the time of flight (ToF) of acoustic waves. (a) Single path method with relocation of the reflector position to obtain two different path lengths (short and long). (b) Double path method where waves travel short and long paths simultaneously, making it possible to measure the time delay between two consecutive echoes. (Created by the author, 2025)

Figure 6 – Diagram illustrating the first two acoustic echoes generated by multiple round trips of the wave between the transducers. The first echo corresponds to one complete trip (1 round trip) and the second echo to two complete trips (2 round trips), allowing precise measurement of the wave's transit time by the interval between consecutive echoes. (Created by the author, 2025)

In our study, we employed a pulsed-echo method combined with the digital overlap technique. At atmospheric pressure, measurements were conducted using a variable-path-length cell, while at high pressure, a fixed double-path-length configuration was used. The specific configurations of these devices will be detailed in the following paragraphs.

2.1.1 Experimental Apparatus for Measuring the Speed of Sound at Atmospheric Pressure

The experimental system used to determine the speed of sound in liquids employs the variable path pulse echo technique at 3 MHz. This method has been previously described in studies by Bazile et al. (2024), Daridon et al. (2013), and Plantier et al. (2000). Bazile et al. (2024 e Daridon et al. (2013a e Plantier et al. (2000).

The main configuration of the apparatus consists of a cylindrical stainless-steel cell, the base of which is sealed with a piezoelectric transducer. The cell is filled with the liquid sample under analysis. At the top end, an acoustic reflector in the form of a movable piston can be adjusted with high precision along the axis of the cylinder using a worm drive. The displacement of the piston is monitored by a mechanical comparator with an absolute uncertainty of 5 μm, allowing for precise determination of the variation in the length of the acoustic path. An illustrative diagram can be seen in Figure 7.

To ensure the thermal stability of the sample, the cell is positioned vertically inside a high-precision thermoregulatory bath with a stability of 0.01 K. Additionally, the cell is coated with a polymeric material to enhance its thermal insulation. The temperature of the sample is monitored using a PT 100 probe inserted directly into the liquid through an opening in the cell, ensuring measurements with an uncertainty of 0.1 K. The probe is connected to a reference thermometer, providing reliable readings throughout the experiments.

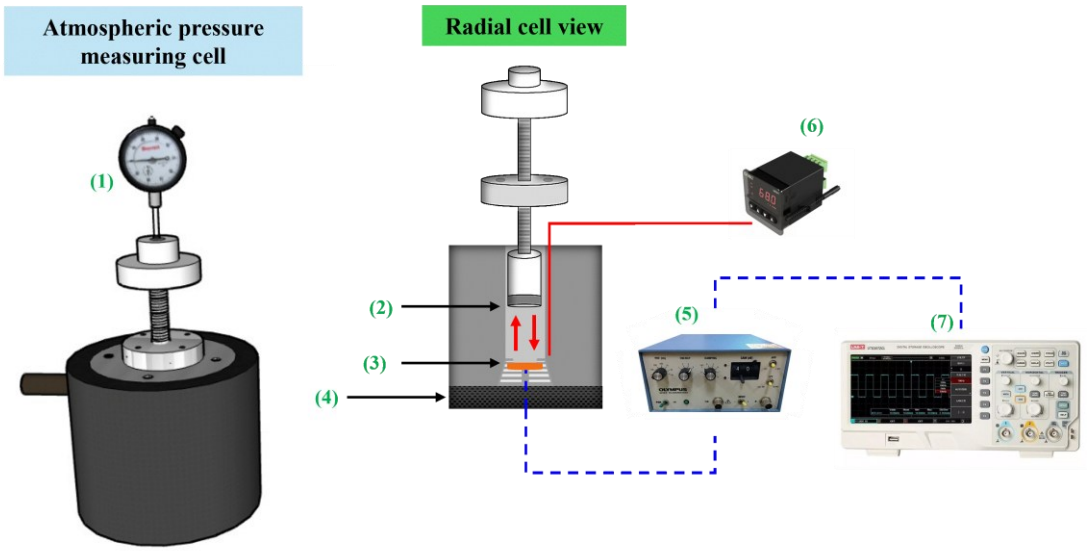

Figure 7 – System for measuring the speed of sound at atmospheric pressure. (1) Comparison, (2) Reflector, (3) Piezoelectric transducer, (4) Thermal insulation, (5) Impulse generator, (6) temperature marker, and (7) Oscilloscope. (Created by the author, 2025)

With this cell, the speed of sound is determined using digital overlap method for measuring the time-of-flight technique. A short ultrasonic pulse is generated by a pulsator/receiver and converted into an acoustic wave by the piezoelectric transducer. This wave travels through the sample until it is reflected by a stainless-steel reflector attached to a moving piston. It then returns to the transducer, which also functions as the receiver. The received signal is amplified and digitized by an oscilloscope and recorded for different positions of the reflector, allowing the analysis of the time elapsed between the first echo reflected at different positions of the piston.

The variation in the length of the acoustic path Δl is directly determined from the displacement of the piston, while the time difference between the echoes Δ_{tof} is obtained by digitally overlapping the different recorded signals. In this way, the speed of sound (c) is calculated absolutely, without the need for calibration, using the following equation:

$$c = \frac{\Delta l}{\Delta_{tof}} \tag{2.1}$$

This method demonstrates high precision, with an error margin of less than 0.1% as confirmed by tests conducted using water as the reference fluid (MARCZAK, 1997). A detailed analysis of the uncertainty calculations is provided in Appendix A1 of this thesis.

The experimental setup, combined with the precision in measuring the piston position and the ultrasonic signal's propagation time, enables reliable determination of the speed of sound in liquids across various temperature and composition conditions. Therefore, this apparatus serves as a robust and accurate tool for investigating the acoustic properties of liquid mixtures.

2.1.2 Experimental Apparatus for Measuring the Speed of Sound at High Pressure

The speed of sound in high-pressure liquids was measured using the pulse-echo technique in reflection mode. This method involves measuring the time of flight of two ultrasonic wave trains traveling through the sample placed on either side of a transducer. The experimental setup (Figure 8) features a double-path length acoustic sensor consisting of a 3 MHz piezoelectric disk mounted between two hollow cylindrical supports of varying lengths. Metal reflectors are positioned at the opposite ends of these supports to reflect the ultrasonic

waves, enabling their return to the piezoelectric element which functions as both an emitter and receiver.

The transducer emits ultrasonic waves in opposite directions, which are reflected by the acoustic mirrors and return, after a round trip in the fluid, to the transducer with a time delay Δt, corresponding to the difference $\Delta L\ (T, p)$ between the two path lengths. This time-of-flight difference is used to calculate the speed of sound (c) according to the following relation:

$$c = \frac{\Delta L(T,p)}{\Delta t} \tag{2.2}$$

The $\Delta L\ (T, p)$ difference is calibrated experimentally using water as the reference liquid, due to the availability of reliable data over a wide temperature and pressure range Wilson (1959). During calibration, the effects of thermal expansion and compression of the acoustic sensor are taken into account, assuming linear behavior of the geometry with temperature and pressure. The following equation represents the calibration process:

$$\Delta L\ (T, p) = \Delta L_0\ [1 + a(T - T0) + b(P - P0)] \tag{2.3}$$

where ΔL_0 is the value of the path difference under reference conditions (T_0 = 293,15 K, P_0 = 0,1013 MPa), and a and b are the thermal and barometric coefficients of linear expansion of the acoustic sensor, respectively. All these apparatus parameters were determined from calibration with water using data of Del Grosso; Mader (1972) for ΔL_0 and Wilson for *a* and *b*.

The time-of-flight measurements were obtained by digitally overlapping the two echoes using a digital oscilloscope (1 GS/s, 2500 points per acquisition). In this method, the first echo is temporally shifted until it overlaps with the second echo, minimizing the difference between the signals. During this process, the amplitude of the first echo is numerically adjusted to compensate for attenuation differences. The time delay Δt is then determined with high precision, allowing for the accurate calculation of the speed of sound.

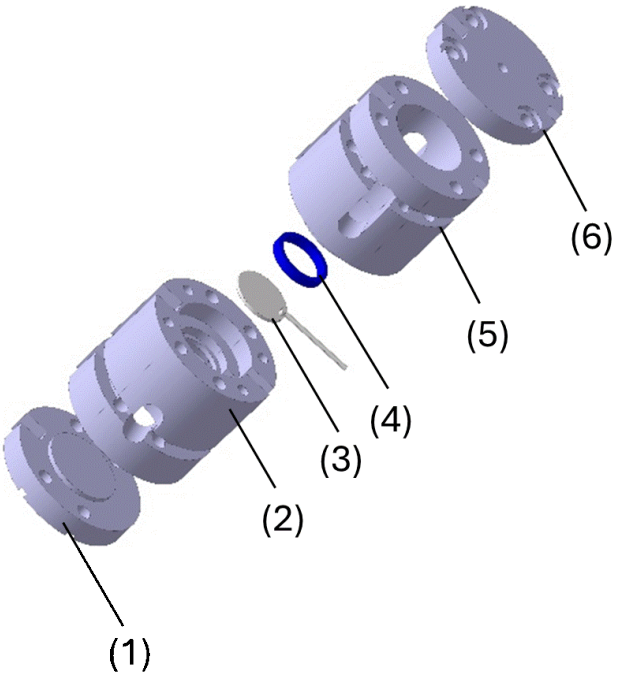

Figure 8 – Schematic diagram of the acoustic wave sensor: (1) stainless steel reflector; (2) short length cylinder; (3) electric insulator ring; (4) piezoelectric ceramic disc with its electrical connection; (5) long length cylinder; (6) stainless steel reflector. Source: Bazile et al. (2017).

The acoustic sensor is installed inside an autoclave cell (Figure 9) filled with the liquid of interest. Pressure is applied via a volumetric pump connected to the cell and is monitored by two pressure transducers. One of the sensors is calibrated for the full range of (0.1 to 200) MPa with an uncertainty of 0.1 MPa, while the other covers the range of (0.1 to 100) MPa with greater precision (0.01 MPa). The measuring cell is immersed in a highly stable thermostatic bath (±0.02 K), ensuring thermal uniformity during the experiments. Temperature is monitored by a 1.2 mm diameter Pt100 probe, housed in a metal finger inside the cell, with an uncertainty of less than 0.1 K. The procedures used to evaluate the measurement uncertainties are detailed in Appendix A1, and the uncertainty values associated with each system are reported in the corresponding chapters, alongside the experimental results.

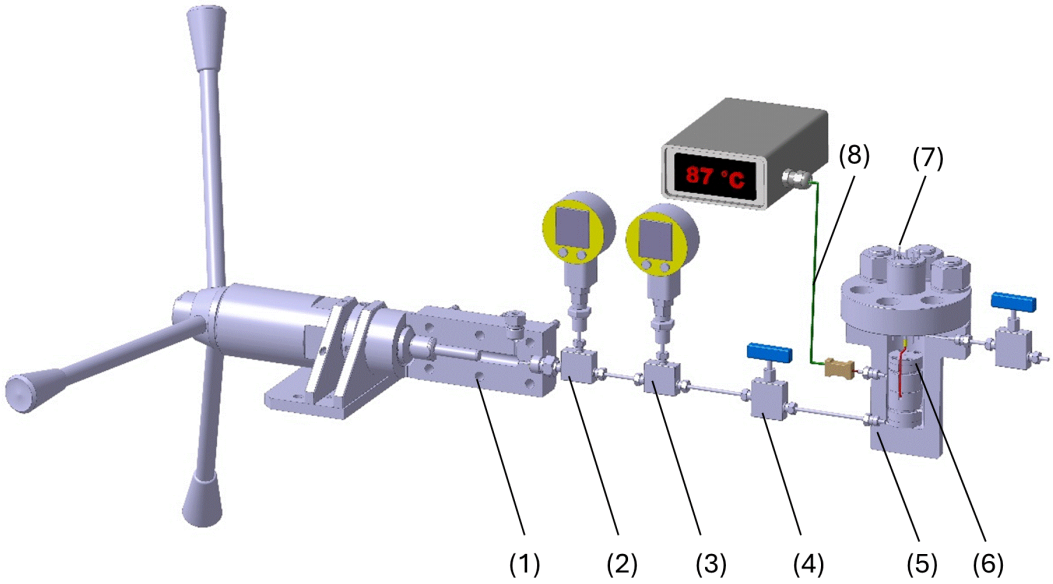

Figure 9 – Schematic diagram of speed of sound experimental setup: (1) high pressure volumetric pump; (2) pressure sensor (100 MPa); (3) pressure sensor (200 MPa); (4) cell inlet valve; (5) high pressure vessel; (6) acoustic wave sensor ; (7) thermostatic bath ; (8) temperature sensor inserted in a metal finger; (9) electrical feedthrough. Source: Bazile et al. (2017).

2.2 Density Measurement: Methods, Applications, and Implications for the Thermodynamic Characterization of Fluids

Density is one of the most fundamental physical properties in science and engineering, playing a central role in the characterization of materials and in understanding the behavior of systems under various operating conditions. From this property, it is possible to estimate several derived thermodynamic quantities, such as compressibility and thermal expansivity, which are essential for the modeling and simulation of physicochemical processes Webster (2023). In the context of liquid fuels, density becomes even more critical, as it directly affects operational parameters such as fuel injection and atomization efficiency, the performance of internal combustion engines, and the design of storage and transportation systems Alagumalai (2014).

In energy applications, accurate knowledge of density is indispensable for mass and volume calculations, mixture formulation, energy balances, and quality control, particularly when dealing with complex mixtures. In process engineering, the precise determination of density under high-pressure and high-temperature (HPHT) conditions is especially relevant for

the design, operation, and safety of equipment such as compressors, engines, reactors, and transport systems Torres-Jimenez et al. (2011 e Veny et al. (2009).

Techniques for determining density, like those used for measuring the speed of sound (Section 1.5), can be classified into direct and indirect methods. Direct methods involve measuring the volume occupied by a known mass of fluid and include techniques such as pycnometry, which employs flasks of known volume and precise mass measurements; hydrostatic weighing, which is based on the buoyant force acting on an immersed object; and the float densimeter, which applies Archimedes' principle to determine density from the degree of immersion of a floating body. Indirect methods estimate density based on other physical properties and require calibration using standard reference substances. These include the mechanical oscillation densimeter (or vibrating-tube densimeter), which determines density from the oscillation frequency of a tube in filled with the studied fluid; refractometry, which correlates the refractive index with density; and sound velocity techniques, which use thermodynamic relationships to estimate density from the propagation speed of acoustic waves Figura; Teixeira (2023 e Webster (2023).

As mentioned previously, vibrating tube densimeters are widely employed for HPHT measurements due to their high precision, rapid response, and the minimal amount of sample required. This technique is based on the change in the resonance frequency of a U-shaped tube when filled with the fluid of interest. The fluid's density is determined from the shift in frequency, which is processed by high-resolution electronic evaluation units ALAOUI (2011 e Muñoz Rujas (2018).

In this study, density measurements were performed using an Anton Paar DMA HPM vibrating tube densimeter (VTD), coupled with the mPDS 5 evaluation unit. The operating principle relies on the excitation of the U-shaped tube by electromagnets that induce controlled mechanical oscillations as shown in Figure 10. This U-tube can be assimilated to a tuning fork of total mass m, expressed as:

$$m = m_0 + \rho_f V_i \tag{2.4}$$

where m_0 is the mass of the evacuated tube (under vacuum), V_i is the internal volume of the hollow U-tube and ρ_f is the density of the fluid sample inside the densimeter. When the system is excited in an undamped manner, its mechanical response can be modeled as a mass

oscillating without friction at the end of a spring with stiffness constant K (the stiffness of the tuning fork). The natural frequency of this single-degree-of-freedom oscillator is given by:

$$f = \frac{1}{2\pi}\sqrt{\frac{K}{m}} \tag{2.5}$$

By substituting the mass expression from equation (1.4) into this equation, it is possible to rewrite the expression in terms of the oscillation period τ_f of the VTD filled with the investigated fluid:

$$\tau_f = 2\pi\sqrt{\frac{m_0+\rho_f V_i}{K}} \tag{2.6}$$

From this relationship, the density of the fluid sample can be expressed as a function of the square of the period:

$$\rho_f = \frac{K}{4\pi^2 V_i}\,\tau_f^2 - \frac{m_0}{V_i} \tag{2.7}$$

This equation, commonly referred to as the working equation for a VTD, is typically written as:

$$\rho_f = A\,\tau_f^2 - B \tag{2.8}$$

where A and B are apparatus-specific parameters that depend on temperature and pressure: $A = A(T,p)$ and $B = B(T,p)$. These parameters are determined through calibration, which involves measuring the oscillation periods of the tube filled with two reference fluids of known density.

In this work, the densimeter was calibrated using deionized water (conductivity of 18.2 ± 0.2 mΩ-cm at 298.15 K) and nitrogen (supplied by White Martins/Brazil, with nominal purity of 99.996%) as reference fluids. The calibration procedure followed the approach developed by Lagourette et al. (1992) and applied by Comuñas et al. (2008), assuming that parameter A depends only on temperature, while B depends on temperature and pressure, as mentioned above Comuñas et al. (2008 e Lagourette et al. (1992).

Initially, the cell was evacuated and the oscillation period $\tau_{vacuum}(T)$ was measured at different temperatures. From this, the parameter A(T) was determined using water at 0.1 MPa as the reference fluid, according to the expression:

$$A(T) = \frac{\rho_{water}(T,0.1MPa)}{\tau^2_{water}(T,0.1MPa) - \tau^2_{vacuum}(T)} \quad (2.9)$$

The values obtained for A(T) were adjusted by second-order polynomial regression. With A(T) known, the parameter B(T,P) was calculated based on measurements of the period of the cell filled with water, according to:

$$B(T,P) = A(T) \cdot \tau^2_{water}(T,P) - \rho_{water}(T,P) \quad (2.10)$$

Finally, the density of the fluid under investigation was obtained using the working equation, with parameters A and B applied in equation 2.8.

$$\rho_f = A(T) \cdot \tau^2(T,P) - B(T,P) \quad (2.11)$$

As an additional step in validating the experimental system, density measurements of pure toluene (Sigma-Aldrich/USA; nominal purity of 99.5%) were conducted across the entire temperature range investigated (303.15–468.15 K) and at pressures up to 130 MPa. The experimental results showed excellent agreement with reference values provided by NIST, confirming the accuracy and reliability of the calibration procedure adopted for the high-pressure densimeter. The detailed experimental data for toluene are presented in Table A3 Comuñas et al. (2008 e Valero et al. (2020).

Moreover, the uncertainty analysis was carried out by considering the individual contributions associated with temperature, pressure, and sample composition (Table A1). The combined standard uncertainties were then calculated using the root-sum-square method. A complete description of this procedure and the corresponding results are provided in **Appendix A1**, further supporting the robustness and traceability of the experimental methodology employed in this study.

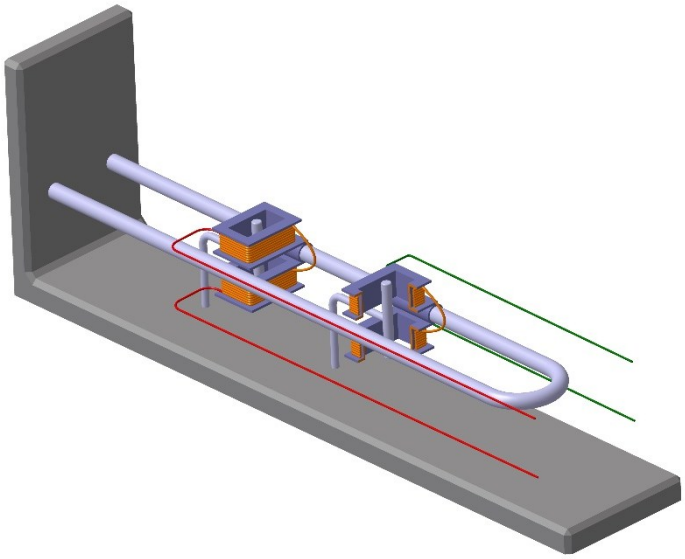

Figure 10 – Schematic of the vibrating U-tube density meter. The tube is excited by an electromagnetic coil (left), and oscillations are detected by piezoelectric sensors (right). Electrical connections are shown in red and green. (Created by the author, 2025)

The experiment begins with the injection of the sample into the high-pressure cell. Initially, the fluid or mixture is transferred to the floating piston cell. Prior to injection, the system is evacuated to remove residual air and ensure complete filling of the lines with the liquid sample. The cell is subsequently connected to the densimeter using stainless steel tubing with a nominal diameter of 1/8”. The system is then purged by injecting the sample at a constant flow rate until the U-shaped tube is completely filled. This purging step is essential to eliminate air bubbles, thereby ensuring reliable measurements. After purging, the system is sealed, and the pressure and temperature parameters are carefully adjusted. The sample remains in the system until thermal and mechanical equilibrium is achieved, as indicated by the stabilization of pressure and temperature readings. Once equilibrium is established, the density measurement is performed.

2.3 Thermodynamic Modeling as a Tool for Complex Systems

Thermodynamic modeling is an indispensable tool for correlating, predicting and understanding the behavior of complex systems, particularly in scenarios where the acquisition of experimental data is limited, costly, or technically unfeasible. The contribution of

thermodynamic models is particularly significant in high-pressure conditions, as experimental data are scarce due to the challenges faced by experiments in these extreme environments, including the high cost of specialized equipment, the need for qualified personnel to ensure safe operations, and the considerable time required for calibration and stabilization of testsOnken et al. (2008). Aspects related to the security and maintenance of the systems also impose additional restrictions.

As previously discussed, (Section 1.4), the investigation of physicochemical properties under extreme conditions is essential for the proper characterization of the systems analyzed in this thesis. Mathematical models Ceriani et al. (2009, 2011, 2013 e Ceriani; Meirelles (2004 e Cunha et al. (2013 e Daridon et al. (2013b e Freitas, S. V. D. et al. (2013 e Freitas, S. V.D. et al. (2013), whether based on physical principles, empirical correlations, or semi-empirical formulations, enable the estimation of equilibrium, transport, and volumetric properties of pure substances and mixtures with good accuracy Ghanbari et al. (2017). When incorporated into computer simulation and optimization tools, these models become especially valuable in the analysis of complex operational scenarios.

The application of these models has proven to be strategic in the chemical and energy sectors, where the diversity of compounds and the severity of operating conditions require robust correlative tools. In addition to enabling reliable extrapolation to conditions not experimentally tested, thermodynamic models contribute to the advancement of scientific knowledge and the development of innovative technologies Wilhelmsen et al. (2017a).

Various approaches can be employed in thermodynamic modeling, including equations of state, group contribution models, empirical correlations, and methods based on the principle of corresponding states Reid et al. (1959). The choice of the most appropriate methodology depends on the nature of the system, the property to be estimated, and the availability of experimental data for validation. These strategies not only complement experimental data but also enhance its practical applicability, enabling the simulation and optimization of industrial processes John M. Prausnitz, Rudiger N. Lichtenthaler (1998).

2.3.1 Correlations

In this study, multiple strategies were employed to correlate, predict, and evaluate the experimental data. These include the use of the Tammann–Tait equation Dymond; Malhotra (1988)

$$(P,T)/(kg\cdot m^{-3}) = \frac{\rho_{Ref}(T)/(kg\cdot m^{-3})}{1-C\cdot\ln\left(\frac{B(T)+P/MPa}{B(T)+P_{Ref}/MPa}\right)} \quad (2.12)$$

where C denotes an adjusted temperature-independent parameter and $B(T)$ is a two-degree polynomial temperature-dependent parameter. The reference pressure P_{Ref} was selected as 0.1 MPa and $\rho_{Ref}(T)$ refers to the density at the reference pressure (P_{Ref}).

It is widely applied in the literature to describe derived properties such as isothermal compressibility and isobaric expansibility, as well as to interpolate data within specific pressure and temperature ranges. Owing to its correlative nature, this equation is effective for accurately fitting volumetric data without requiring direct connections to molecular-level parameters.

Correlative models previously developed for the esters that constitute biodiesel were employed. By applying appropriate combination rules, these models enable the estimation of thermophysical properties of biodiesel, such as density and speed of sound, under a wide range of conditions, including high pressures, as investigated in this thesis. This approach leverages consolidated data available in the literature, facilitating the modeling of complex multicomponent systems based on information from their individual constituents. The models adopted in this study were based on the work of Daridon et al. (2020, 2022), who proposed efficient correlative methodologies for fundamental biodiesel properties, grounded in the compositional profiles of fatty acid esters Daridon (2020, 2022b). Among the numerous correlations proposed to describe thermodynamic properties of biodiesels, Do Carmo, F.R. et al. (2020 e Ceriani et al. (2011, 2013 e Ceriani; Meirelles (2004 e Cunha et al. (2013 e Daridon et al. (2013b e Freitas et al. (2011 e Freitas, S. V. D. et al. (2013 e Freitas, S. V.D. et al. (2013) the method developed by Daridon Daridon (2020, 2022b) was selected because it was specifically designed to operate at very high pressures and focuses on density-related predictions. This method is based on a Murnaghan-type equation, which describes the pressure dependence of both volumetric and acoustic properties. Specifically, it utilizes the molar volume and the product of the speed of sound and the molecular weight raised to a constant power γ (i.e., CM^{γ}):

$$v = A_v(1 + B_v(p - p_{atm}))^{C_v} \quad (2.13)$$

$$cM_{\gamma} = A_{CM\gamma}\left(1 + B_{CM\gamma}(p - p_{atm})\right)^{C_{CM\gamma}} \quad (2.14)$$

The parameters involved in these equations ($A_v, B_v, C_v, A_{CM\gamma}, B_{CM\gamma}, C_{CM\gamma}$), which are temperature-dependent, were determined by regression of available experimental data for pure fatty acid methyl or ethyl esters. In the absence of experimental data, the parameters were estimated using group contribution methods, accounting for the structural characteristics of alkyl chains and ester functional groups. The application of this approach to biodiesel relies on mixing rules that combine the properties of individual components based on their composition.

2.3.2 Equation of state

In addition to empirical correlations, an approach based on more rigorous theoretical foundations was adopted. Among the many equations of state developed, such as cubic equations Peng; Robinson (1976 e Soave (1972 e Van der Waals (1873), modified virial models Benedict et al. (1940 e Lee; Kesler (1975), and perturbed hard-chain approaches SIMNICK et al. (1979), the PC-SAFT (Perturbed Chain–Statistical Associating Fluid Theory) equation was selected in this work. This equation of state Gross; Sadowski (2001b), which is derived from SAFT (Statistical Associating Fluid Theory) allows for the accurate representation of the behavior of associating fluids, enabling the prediction of properties such as liquid–vapor equilibrium, density, and speed of sound based on a limited set of fitted parameters Kontogeorgis et al. (2021).

SAFT theory was originally formulated by Chapman et al. (1989, 1990) and is distinguished by explicitly incorporating associative interactions, such as hydrogen bonding, into the equation of state framework. Based on statistical mechanics, this theory models the Helmholtz free energy as the sum of several contributions: repulsive interactions between hard spheres, dispersion forces, connectivity between chain segments, and specific associations between molecular sites (Prausnitz et al., 1986). This modular structure enables a detailed description of complex systems, including polar solvents and biofuels.

The PC-SAFT equation is an extension of SAFT theory, distinguished by its use of chains of rigid spheres as the reference state instead of isolated spheres. This modification provides greater physical realism in describing systems, particularly those involving elongated molecules or molecules with strong associative interactions. The mathematical formulation of PC-SAFT decomposes the Helmholtz free energy into several distinct contributions, allowing the calculation of thermodynamic properties through partial derivatives of the free energy with respect to temperature, pressure or molar fraction. This versatility makes PC-SAFT a robust

and widely applicable tool for modeling complex mixtures, such as the 1-butanol and biodiesel systems investigated in this thesis.

PC-SAFT equation of state can be expressed as the sum of Helmholtz free energy contributions corresponding to the various interactions present in the system:

$$A = A^{ID} + A^{HC} + A^{disp} + A^{assoc} \tag{2.15}$$

Similarly, the system's compressibility factor can be expressed by the following equation:

$$Z = 1 + Z^{HC} + Z^{disp} + Z^{assoc} \tag{2.16}$$

where the superscripts HC, disp and assoc refer to the contributions of the reference hard chains term, dispersion and association interactions and the compressibility factor of the ideal gas (Z^{ID}) is equal to 1. The equation is usually formulated in terms of the residual property, which represents the deviation from ideal gas behavior ($A^{RES} = A - A^{ID}$), as shown in the following expression for the Helmholtz free energy:

$$A^{RES} = A^{HC} + A^{disp} + A^{assoc} \tag{2.17}$$

Figure 11 presents a schematic representation of each of the contributions, illustrating the stepwise construction of the model: starting from the arrangement of molecules as hard chains, followed by the incorporation of dispersion forces between chain segments, and culminating with the inclusion of specific association effects, such as hydrogen bonding.

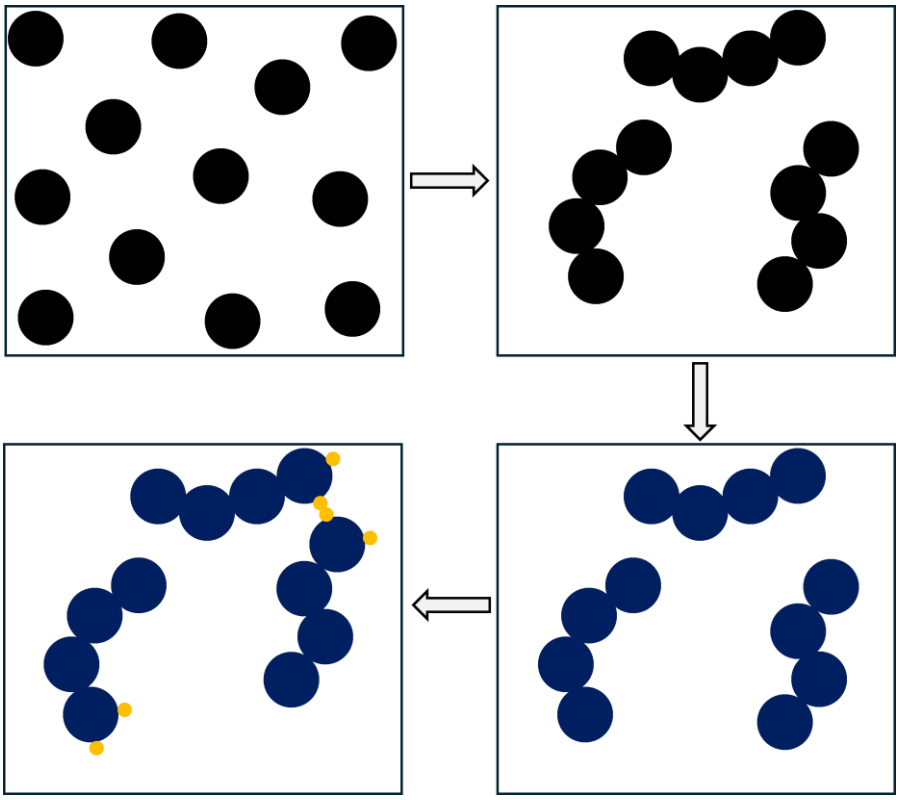

Figure 11 – Visual representation of the PC-SAFT equation of state: rigid spheres interact to form chains, which are subject to dispersive forces and, through association sites, form hydrogen bonds. Source: (Adapted from Avlund (2011)).

The individual contribution of each term was originally defined by Gross and Sadowski Gross; Sadowski (2001c), with the exception of the association term, whose formulation follows the development proposed by Chapman et al. Chapman et al. (1990b). These contributions can be calculated on a molar basis using the following equations:

- Hard chain compressibility term for a mixture (Z^{HC}):

$$Z^{HC} = \bar{m}Z^{HS} - \sum_i x_i(m_i - 1)(g_{ii}^{HS}(d_{ii}))^{-1}\dot{\rho}\frac{\partial g_{ii}^{HS}}{\partial \rho} \tag{2.18}$$

Where: m_i is the chain length of component i and $\bar{m}$ is the average chain length in a mixture of i components with mole fraction x_i ($\bar{m} = \sum_i x_i m_i$). The chain formation assumes that all molecular segments are connected. As indicated by the equation above, this term is related to the average chain length through the hard-sphere contribution. The symbol $\dot{\rho}$ refers to the number density, that is, the total number of molecules per unit volume. g_{ii}^{HS} is the radial

distribution function. Finally, Z^{HS} corresponds to the hard sphere compressibility factor. It is given by the following equation:

$$Z^{HS} = \left(\frac{\zeta_3}{1-\zeta_3} + \frac{3\zeta_1\zeta_2}{\zeta_0(1-\zeta_3)^2} + \frac{(3\zeta_2^3-\zeta_3\zeta_2^3)}{\zeta_0(1-\zeta_3)^3}\right) \tag{2.19}$$

and the associated derivative is:

$$\dot{\rho}\frac{\partial g_{ii}^{HS}}{\partial \dot{\rho}} = \frac{1}{(1-\zeta_3)^2} + \left(\frac{d_i d_j}{d_i+d_j}\right)\left(\frac{3\zeta_2}{(1-\zeta_3)^2} + \frac{6\zeta_2\zeta_3}{(1-\zeta_3)^3}\right) + \left(\frac{d_i d_j}{d_i+d_j}\right)^2\left(\frac{4\zeta_2^2}{(1-\zeta_3)^3} + \frac{6\zeta_2^2\zeta_3}{(1-\zeta_3)^4}\right) \tag{2.20}$$

where ζn is calculated as:

$$\zeta_n = \frac{\pi\dot{\rho}}{6}\sum_i x_i m_i d_i^n \tag{2.21}$$

In this expression, the segment diameter d_i is temperature-dependent and is given by:

$$d_i = \sigma_i\left[1 - 0{,}12\exp\left(-\frac{3\varepsilon_i}{kT}\right)\right] \tag{2.22}$$

where: ε_i and σ_i are the Lennard-Jones-like parameters representing, respectively, the depth of the potential well (scattering energy) and the temperature-independent segment diameter. It is important to note that, although these parameters carry a physical meaning analogous to those in the Lennard-Jones molecular model for spherical particles, the treatment of dispersion in the PC-SAFT equation is based on a modified square-well potential, originally proposed by Chen and Kreglewski Chen; Kreglewski (1977a) In the original square-well potential model, the segment diameter (d_i) is temperature-dependent, and the scattering energy varies with radial distance. In the modified potential used in PC-SAFT, as shown in Equation (2.19), the energy parameter is treated as constant, and the segment diameter depends only on temperature, which significantly reduces the computational effort.

The radial distribution function, $g_{ii}^{HS}(d_{ii})$ in equation 2.18, describes the radial distribution of hard spheres in contact and is expressed as a function of the segment diameter.

- Dispersive contribution

In PC SAFT formalism, the dispersive contribution to the compressibility factor is calculated as follows:

$$Z^{disp} = -2\pi\rho\frac{\partial(\eta I_1)}{\partial\eta}\overline{m^2\varepsilon\sigma^3} - \pi\rho\bar{m}\left[C_1\frac{\partial(\eta I_2)}{\partial\eta} + C_2\eta I_2\right]\overline{m^2\varepsilon^2\sigma^3} \quad (2.23)$$

where: I_1 and I_2 are integrals that can be approximated by power series, as follows:

$$I_1 = \sum_{i=0}^{6} a_i(\bar{m})\eta^i \quad (2.24)$$

$$I_2 = \sum_{i=0}^{6} b_i(\bar{m})\eta^i \quad (2.25)$$

Where $\eta = \zeta_3$ and a_i and b_i are functions of the average chain length $(\bar{m})$ and universal constants, defined as follows:

$$a_i(\bar{m}) = a_{0i} + \frac{\bar{m}-1}{\bar{m}}a_{1i} + \frac{\bar{m}-1}{\bar{m}}\frac{\bar{m}-2}{\bar{m}}a_{2i} \quad (2.26)$$

$$b_i(\bar{m}) = b_{0i} + \frac{\bar{m}-1}{\bar{m}}b_{1i} + \frac{\bar{m}-1}{\bar{m}}\frac{\bar{m}-2}{\bar{m}}b_{2i} \quad (2.27)$$

The constants used in this stage of the calculation were taken directly from the reference in Gross; Sadowski (2001b). The derivatives $\frac{\partial(\eta I_1)}{\partial\eta}$ and $\frac{\partial(\eta I_2)}{\partial\eta}$ also have approximate power series solutions, as follows:

$$\frac{\partial(\eta I_1)}{\partial\eta} = \sum_{j=0}^{6} a_j(\bar{m})(j+1)\eta^j \quad (2.28)$$

$$\frac{\partial(\eta I_2)}{\partial\eta} = \sum_{j=0}^{6} b_j(\bar{m})(j+1)\eta^j \quad (2.29)$$

The constant C_1, which represents an expression of compressibility, is given by:

$$C_1 = \left(1 + Z^{HC} + \dot{\rho}\frac{\partial Z^{HC}}{\partial\dot{\rho}}\right)^{-1} = \left(1 + \bar{m}\frac{8\eta-2\eta^2}{(1-\eta)^4} + (1-\bar{m})\frac{20\eta-27\eta^2+12\eta^3-2\eta^4}{[(1-\eta)(2-\eta)]^2}\right)^{-1} \quad (2.30)$$

$$C_2 = \frac{\partial C_1}{\partial\eta} = -C_1^2\left(\bar{m}\frac{8-4\eta^2+20\eta}{(1-\eta)^5} + (1-\bar{m})\frac{40+12\eta^2+48\eta+2\eta^3}{[(1-\eta)(2-\eta)]^3}\right)^{-1} \quad (2.31)$$

- Associative contribution:

The associating contribution to the compressibility factor was described in the original SAFT theory work by Chapman et al. Chapman et al. (1990b), as follows:

$$Z^{assoc} = \sum_i X_i \frac{\mu_i^{assoc}}{RT} - \frac{a^{assoc}}{RT} \tag{2.32}$$

Since the calculation of the chemical potential ($\frac{\mu_i^{assoc}}{RT}$) nvolves numerous steps, its full description is provided in Appendix A.2. For non-associating systems, the Z^{assoc} term is equal to zero. furthermore, additional contributions can be incorporated into the PC-SAFT framework to improve its predictive capabilities for systems involving specific molecular interactions. One such extension is ePC-SAFT (electrostatic PC-SAFT), which includes terms to account for dipolar, quadrupolar, and general electrostatic interactions between molecules Gross; Vrabec (2006); Held et al. (2014).

- Mixing Rules:

The terms $\overline{m^2\varepsilon^2\sigma^3}$ and $\overline{m^2\varepsilon\sigma^3}$ in Equation (2.23) are given by the following mixing rules:

$$\overline{m^2\varepsilon\sigma^3} = \sum_i \sum_j x_i x_j m_i m_j \left(\frac{\varepsilon_{ij}}{kT}\right) \sigma_{ij}^3 \tag{2.33}$$

$$\overline{m^2\varepsilon^2\sigma^3} = \sum_i \sum_j x_i x_j m_i m_j \left(\frac{\varepsilon_{ij}}{kT}\right)^2 \sigma_{ij}^3 \tag{2.34}$$

Where (ε_{ij}) and (σ_{ij}) are given by:

$$\varepsilon_{ij} = \sqrt{\varepsilon_i \varepsilon_j}\left(1 - k_{ij}\right) \tag{2.35}$$

$$\sigma_{ij} = \frac{1}{2}\left(\sigma_i + \sigma_j\right) \tag{2.36}$$

In these combination rules, only the dispersion energy term incorporates a binary interaction parameter (k_{ij}) similar to those used in classical cubic equations of state. Mixing rules are also provided for cross-association interactions Wolbach; Sandler (1998):

$$\varepsilon^{A_iB_j} = \frac{1}{2}(\varepsilon^{A_iB_i} + \varepsilon^{A_jB_j}) \tag{2.37}$$

$$\kappa^{A_iB_j} = \sqrt{\kappa^{A_iB_i}\kappa^{A_jB_j}}\left(\frac{\sqrt{\sigma_{ii}+\sigma_{jj}}}{\frac{1}{2}(\sigma_{ii}+\sigma_{jj})}\right)^3 \tag{2.38}$$

In these expressions, ε^{AB} and κ^{AB} are pure component parameters associated with the associating term of the compressibility factor, as detailed in Appendix A.2.

SAFT equations of state incorporate the associating term through a square-well potential, as illustrated in Figure 12. This model assumes that association occurs via specific interaction sites located on the molecules; the attractive forces are directed between these specific sites, rather than occurring isotropically as in van der Waals interactions. For two molecules to associate, they must not only be within an appropriate distance (between σ and r^{AB}) but also possess a favorable relative orientation of their interaction sites. Figure 2.10, adapted from Chapman et al. (1990a), schematically illustrates these geometric constraints. Molecular configurations that fail to simultaneously satisfy both the distance and orientation criteria are considered non-associating, whereas those meeting both requirements lead to association

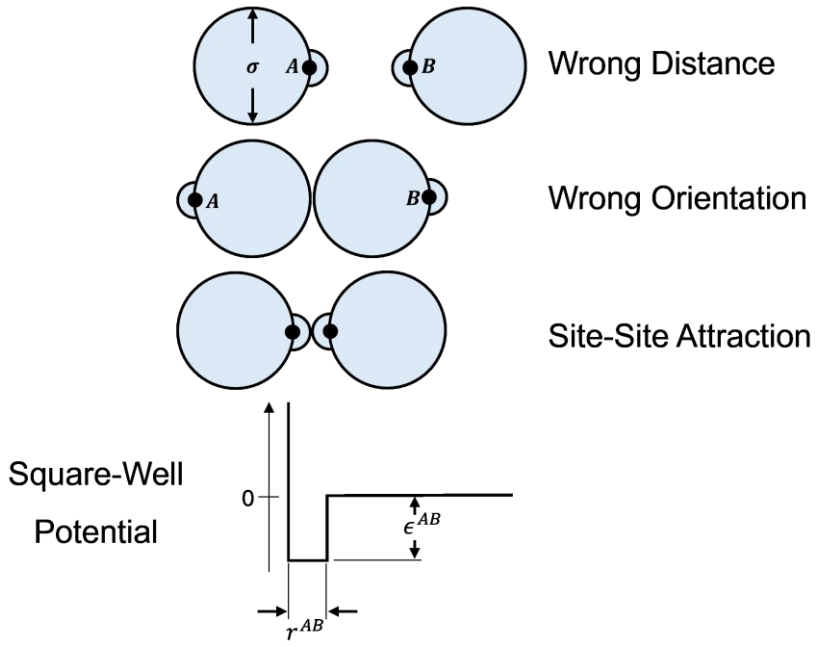

Figure 12 – Schematic representation of the association model via square-well potential within the SAFT equation of state framework. Source: Adapted from Chapman et al. (1990)

The SAFT equation of state association model assumes that molecules can form specific bonds through localized interaction sites, such as those responsible for hydrogen bonding. These interactions are described by a square-well potential characterized by two parameters: the well depth (ε^{AB}), representing the strength of the interaction, and the association volume (κ^{AB}), which relates to the distance and orientation requirements between the sites. The radial term (r^{AB}), typically assumes small values on the order of 10^{-3}.

- Density calculation from PC SAFT:

The PC-SAFT equation of state is formulated in terms of the Helmholtz free energy or, equivalently, the compressibility factor as functions of molecular density and temperature. Therfore, it does not directly yield the mass density at a specified pressure and temperature. To determine the density under these conditions, an iterative numerical procedure is required. In such method, The density is calculated iteratively, starting from the definition of the reduced density $\eta = \zeta_3$, where:

$$\dot{\rho} = \frac{6\eta}{\pi}\left(\sum_i x_i m_i d_i^3\right)^{-1} \tag{2.39}$$

That allows calculating $Z(T, \dot{\rho})$ from PC SAFT formulation (eq. 2.16). Once the compressibility factor (Z), is determined, the pressure is calculated using the conventional form of the equation of state:

$$P = Z\rho RT \tag{2.40}$$

where ρ here should not be confused with $\dot{\rho}$ defined in (2.18) and (2.39), since ρ\rhoρ refers to molar density. These quantities are related by Avogadro's number (N_{AV}) such that $\rho = \frac{\dot{\rho}}{N_{AV}}$. A figure exemplifying the iterative procedure used for calculating ρ is provided in Appendix A2.

The calculation proceeds until the pressure estimated by equation (2.40) matches the experimental pressure at the corresponding density point.

The association sites are defined according to the classification proposed by Huang and Radosz (1990) for associating groups. In the case of the hydroxyl group, although it structurally contains three potential association sites, which correspond to the two lone electron pairs on the oxygen atom and the bonded hydrogen atom, conventional modeling considers only two effective sites: one functioning as a hydrogen bond acceptor and the other as a donorHuang, Stanley H.; Radosz (1990).

Throughout this thesis, the PC-SAFT equation of state was applied in different chapters dedicated to the thermodynamic modeling of systems containing biodiesel and binary mixtures with 1-butanol, under high-pressure conditions and across various temperatures. The approach is based on the evaluation of the Helmholtz free energy and its thermodynamic derivatives, enabling the estimation of volumetric properties such as molar density from the compressibility factor Z, as previously described. For the speed of sound, which depends on compressibility and the derivative of pressure with respect to density, thermodynamic relationships derived from the second derivative of the Helmholtz energy were employed, with adjustments to the residual term. The application of PC-SAFT in this context required not only the appropriate fitting of molecular parameters for biodiesel (considered as a pseudo-component) and 1-butanol, but also careful numerical treatment. A detailed description of the procedures adopted, as well as the results obtained, can be found in the specific chapters dedicated to the modeling of density and speed of sound.

3 ANALYSIS OF BIODIESEL DENSITY AND SPEED OF SOUND AT HIGH PRESSURE: EXPERIMENTAL STUDY, PC-SAFT MODELING, AND EVALUATION OF PREVIOUSLY DEVELOPED MODELS BASED ON FATTY ACID ESTER COMPOSITION

Results published in: *Exploring the Thermophysical Properties of Biodiesel: High-Pressure Density and Speed of Sound Prediction with PC-SAFT and Ester Composition Models*. Fuel 2025, 391, 134707. https://doi.org/10.1016/j.fuel.2025.134707.

3.1 Introduction

As discussed in Chapter 1, biodiesel is a renewable alternative to fossil fuels, with applications in internal combustion engines, particularly in high-pressure injection systems. Under these conditions, properties such as density and speed of sound are crucial for fuel efficiency and safety.

Despite numerous studies on the density and speed of sound of biodiesel, high-pressure data remain scarce. Only seven studies Aitbelale; Abala; et al. (2019 e Aitbelale; Chhiti; et al. (2019 e Bessières et al. (2018 e García-Morales et al. (2024 e Habrioux et al. (2013a, 2023 e Schedemann et al. (2013) have reported density measurements above 100 MPa, while for speed of sound, data exist for just four methyl biodiesels (soybean Habrioux et al. (2013a), rapeseed Habrioux et al. (2013a), sunflower Habrioux et al. (2023), and a blend of palm, rapeseed, and soybean Habrioux et al. (2023)) up to 200 MPa. Thus, this study aims to expand high-pressure data with new biodiesel samples.

This chapter investigates the speed of sound and density of three biodiesels over a pressure range of 0.1 to 200 MPa and temperatures from 293.15 to 373.15 K. The results improve the understanding of biodiesel's thermophysical behavior in high-pressure conditions and its interaction with injection systems. The speed of sound was measured using the pulse-echo technique, and density was determined with a vibrating tube densimeter up to 100 MPa. For pressures from 100 up to 200 MPa, density was estimated using speed of sound and heat capacity data via the Newton-Laplace relation. Isentropic compressibility and acoustic impedance were also derived from these measurements.

Experimental data alone is not sufficient for engineering applications, which often require predictive models capable of estimating thermophysical properties under various conditions. In particular, process simulations and Computational Fluid Dynamics (CFD) studies rely on accurate equations of state (EoS) to model fuel behavior in high-pressure injection systems. Among available models, PC-SAFT has shown potential for predicting biodiesel properties, especially under high pressure. While effective for density Ait Belale et al. (2021 e Aitbelale; Chhiti; et al. (2019 e Aitbelale et al. (2021 e Alves et al. (2024 e García-Morales et al. (2023 e Wang et al. (2018), its accuracy for speed of sound c remains a challenge Lafitte et al. (2006 e Liang et al. (2012) since most EoS models do not match experimental uncertainties (U(c) = 0.3%). Therefore, this study also aims to assess PC-SAFT's ability to predict both density and speed of sound in biodiesels over an extended pressure range.

For predicting density of fatty acid alkyl esters, a Group Contribution Theory (GCT)-based method was developed to correlate molar volume of these components with pressure and temperature, using a Murnaghan-type equation of state F. D. Murnaghan (1924) up to 200 MPa Daridon (2020). This method was later extended to predict biodiesel density based on ester composition using an ideal combination rule. A similar group contribution approach was applied to speed of sound of alkanes and fatty acid alkyl esters, using cM^{γ}, where γ = 0.975 Daridon (2022a). While this method successfully estimated the speed of sound in biodiesel with deviations within uncertainty limits up to 200 MPa Daridon (2022b) using a simple combining rule, it was validated with only four biodiesels Habrioux et al. (2013a, 2023) under pressure up to 200 MPa. To further test its reliability of the method under extreme high pressure, this study expands comparisons to three additional biodiesels, providing new high-pressure data for model validation.

3.2 Experimental measurements.

3.2.1 Materials

The biodiesels investigated in this work were prepared by the transesterification reaction of three vegetable oils: coconut, sucupira, and canola, using methanol (Sigma, molar purity 0.999). For each oil, the molar ratio between oil and alcohol was adjusted to 1:6 to ensure the completion of the reaction. Transesterification was carried out at 333.15 K, using sodium hydroxide as a catalyst in a glass reactor with temperature control and outlets coupled to a condenser to prevent the methanol from evaporating. At the end of the reaction, the product was transferred to a separating funnel, where it was separated from the by-product (glycerol) and

washed with deionized water (conductivity of 18.2 ± 0.2 mΩ-cm, at 298.15 K) to remove residual alcohol, catalyst, and glycerol. The product was then dried to remove excess water, and the water content was checked by Karl-Fischer titration. This procedure was carried out to obtain a water content of less than 0.05% by weight by the limit established by ASTM standard 6751.

The fatty acid methyl ester (FAME) profile analysis was conducted using gas chromatography coupled to mass spectrometry, Agilent instrument model GC-7890B/MSD-5977A. Table 2 details the normalized molar compositions and molar masses of the biodiesels investigated.

Table 2 – Profiles of fatty acid methyl esters in mol% and molar mass M in $\mathrm{g \cdot mol^{-1}}$ for the methyl biodiesels studied in this work.

FAME	molecular formula	biodiesels studied in this work		
		Coconut **(CN)**	Sucupira **(SC)**	Canola **(CN)**
MeC8:0	$C_9H_{18}O_2$	8.48	0.00	0.00
MeC10:0	$C_{11}H_{22}O_2$	7.61	0.00	0.00
MeC12:0	$C_{13}H_{26}O_2$	49.35	0.00	0.00
MeC14:0	$C_{15}H_{30}O_2$	19.98	0.00	0.00
MeC16:0	$C_{17}H_{34}O_2$	8.19	13.22	5.59
MeC18:0	$C_{19}H_{38}O_2$	2.58	4.35	2.44
MeC18:1	$C_{19}H_{36}O_2$	3.81	31.92	71.68
MeC18:2	$C_{19}H_{34}O_2$	0.00	50.51	18.88
MeC20:0	$C_{21}H_{40}O_2$	0.00	0.00	0.51
MeC20:1	$C_{23}H_{46}O_2$	0.00	0.00	0.91
$M/\ g \cdot mol^{-1}$	-	222.95	292.12	295.11

3.2.2 Speed of sound (c) measurement up to 200 MPa

The speed of sound (c) was measured at pressures up to 200 MPa using the pulse-echo technique with a fixed acoustic path length. The experimental apparatus has been detailed in earlier published works Habrioux et al. (2013a, 2018, 2023 e Ndiaye et al. (2012, 2013b) and in the previous chapter of this manuscript. It consists of an immersion ultrasonic sensor

mounted in a high-pressure cell, sealed with a plug that features three high-pressure electrical passages connecting the sensor to a high-voltage pulse generator. The sensor includes a longitudinal ultrasonic wave transducer disk fixed within a hollow stainless-steel cylinder. Two reflectors are positioned facing the transducer at opposite ends of the cylinder, at asymmetric distances from the transducer, creating a difference in acoustic path length ΔL. The speed of sound was determined using a pulse echo method with a double-path length, in which the transmitting transducer emits a high-frequency acoustic pulse (3 MHz), and the time of flight of echoes from the opposite reflectors is recorded. A digital overlap method was employed to measure the time-of-flight difference (Δt), between the two echoes, as described in a previous study Kortbeek et al. (1985 e Muringer et al. (1985).

The high-pressure cell was filled with the biodiesel sample under vacuum to prevent the formation of air bubbles and was subjected to a complete purge. Pressurization was carried out using an external volumetric pump, and the pressure was monitored by two probes: one with a range of 0 to 100 MPa and a standard uncertainty of $u(p) = 0.01$ MPa, and another covering the full range of 0 to 200 MPa, with a standard uncertainty of $u(p) = 0.1$ MPa. The pressure cell was submerged in a thermostatic bath with heat-conducting fluid to maintain isothermal stability during the measurements. The temperature of this fluid was monitored directly with a platinum probe (PT100) in a metal housing, ensuring a standard uncertainty of $u(T) = 0.1\,K$. The combined uncertainty in speed of sound measurements was estimated (Appendix A1) as $U(c) = 0.2\%$ for the 0.1 to 100 MPa range and $U(c) = 0.3\%$ for the 100 to 200 MPa range, corresponding to a 95% level of confidence, following the *Guide to the Expression of Uncertainty in Measurement (GUM)*International Organization for Standardization (2008).

3.2.3 Density measurement up to 100 MPa

The density ρ of biodiesel was measured using an Anton Paar DMA HPM density meter based on the vibrating U-tube principle. The experimental setup primarily consists of the U-tube measuring cell and a pressure generation system comprising a pump and a low-friction high-pressure floating piston cell. Pressure monitoring was performed using a pressure transducer located at the outlet of the U-tube, with a standard uncertainty of $0.03\ MPa$. Thermal regulation of the measuring cell was achieved using a thermostatic bath, which circulated a thermoregulated fluid. The temperature was monitored by a PT100 sensor, providing an

uncertainty of $0.02\,K$ and ensuring the precision required for the experimental conditions. Further details regarding the experimental apparatus and procedure are available in the previous chapter of this manuscript as well as in publications by our team, where the system and methods are described in greater detail Alves et al. (2022, 2024 e Chacón Valero et al. (2022 e Valero et al. (2020, 2021).

Due to the experimental limitations of the equipment, specifically the connections, it was not feasible to obtain direct density measurements at pressures up to 200 MPa, even though the DMA HPM is capable of operating at pressures up to 140 MPa. However, to extend the pressure range to this value, density data were determined from 100 MPa to 200 MPa by integrating the speed of sound values measured within this range. This approach is well-established in literature and has been employed in numerous studies (HABRIOUX et al., 2023; HABRIOUX; NASRI; DARIDON, 2018; NDIAYE et al., 2013a, 2013b; NASRI; DARIDON, 2012). The application of this method relies on the relationship between isentropic κ_s and isothermal κ_T compressibility, along with the Newton-Laplace equation, which correlates the speed of sound with isentropic compressibility. By combining and integrating these relationships, the pressure-induced variation in density can be expressed in terms of speed of sound through the following equation:

$$\rho(p,T) = \rho(p_0,T) + \int_{p_0}^{p} \frac{1}{c^2}\,dp + T \int_{p_0}^{p} \frac{\alpha_p^2}{C_p}\,dp \tag{3.1}$$

where: α_p represents the isobaric thermal expansion and c_p the isobaric specific heat capacity. As shown in Equation (2.1), the expression contains two integrals, with the first being the primary contributor to the density variation with pressure. This term is evaluated by initially fitting a two-dimensional smoothing function to the speed of sound data, followed by the analytical integration of the resulting function. For this adjustment, we employed the function proposed by Ndiaye et al. Ndiaye et al. (2012) for fatty acid esters, the main components of biodiesel. Habrioux et al. Habrioux et al. (2013a, 2023) had previously applied this function to the specific biodiesel compound investigated in this study. It requires nine adjustable parameters, as follows:

$$\frac{1}{c^2} = \frac{A+B_1T+B_2T^2+B_3T^3+C_1p+C_2p^2+C_3p^3}{1+ET+Fp} \tag{3.2}$$

The second integral of Eq. (3.1) was evaluated numerically using a predictor-corrector method, as detailed in the literature Daridon et al. (1998). This procedure requires

initial isobaric heat capacity data (at atmospheric pressure). These values were obtained from a study dedicated to heat capacity measurements in coconut, sucupira, and canola biodiesels Alves, Alanderson Arthu Araújo; Levy; et al. (2025) using a differential scanning calorimeter operating with a 0.2 K/min heating rate.

3.3 Modeling

3.3.1 PC-SAFT equation of state

In this study, the original Perturbed-Chain SAFT (PC-SAFT) equation of state Gross; Sadowski (2001a) was employed to calculate both density and speed of sound of studied biodiesels under high-pressure conditions. This equation is an extension of the SAFT equation of state, initially developed by Chapman et al. Chapman et al. (1989), with significant adaptations. Unlike the conventional SAFT equation, which uses hard spheres as the reference state, the Perturbed-Chain version employs a chain of hard spheres as reference. Additionally, it incorporates the modified square-well potential proposed initially by Chen and Kreglewski Chen; Kreglewski (1977b), enabling a more realistic description of dispersive interactions.

In a previous study Alves et al. (2024), the PC-SAFT equation of state was used to calculate the volumetric properties of soybean and linseed biodiesels by treating them as pseudo-components and assigning specific parameters to each. This approach, which has been extensively utilized in the literature Ait Belale et al. (2021 e Aitbelale; Chhiti; et al. (2019 e Aitbelale et al. (2021 e García-Morales et al. (2023), involved adjusting the parameters of the equation of state, namely, the number of segments (m), segment diameter (σ), and segment energy parameter (ϵ/k), to accurately reproduce density data. Since biodiesel is composed of a mixture of fatty acid alkyl esters that do not form hydrogen bonds, the association parameters were not considered in the fitted PC-SAFT. This approach has been adopted here, but with the consideration of speed of sound data in conjunction with density to adjust the parameters of the equation of state. The parameters were optimized by minimizing an objective function that quantifies the difference between the experimental and predicted values of both density and speed of sound. This approach was initially implemented by Alcantara et al. Alcantara et al. (2018), who utilized exclusively atmospheric pressure data. In this work, all the experimental data were taken into consideration for the adjustment of the equation of state parameters. Specifically, the objective function (OF) was defined as:

$$OF = \sum_{i=1}^{N_\rho} \left(\frac{\rho_{calc,i} - \rho_{exp,i}}{\rho_{exp,i}} \right)^2 + \sum_{j=1}^{N_c} \left(\frac{c_{calc,j} - c_{exp,j}}{c_{exp,j}} \right)^2 \quad (3.3)$$

where N_ρ and N_c denote the number of data points for density and speed of sound, respectively. In agreement with previous works Alves et al. (2024 e Da Costa; De Medeiros; et al. (2024 e Da Costa; Medeiros; et al. (2024), density was directly obtained from the compressibility factor (Z) given by PC-SAFT while the speed of sound was calculated from derivation of the equation of state using the following thermodynamic relations:

$$c = \sqrt{\frac{c_p}{c_v} \left(\frac{\partial P}{\partial \rho} \right)_{T,n}} \quad (3.4)$$

where: c_p and c_v represent the isobaric and isochoric heat capacities, respectively. Ideal gas heat capacity data are required to calculate these properties, as demonstrated in Eqs. (3.5) and (3.6):

$$c_v = -T \left(\frac{\partial^2 a^{RES}}{\partial T^2} \right)_v + c_v^{ideal} \quad (3.5)$$

$$c_p = c_v + \frac{T \alpha_p^2}{\kappa_T \rho} \quad (3.6)$$

Here, a^{RES} denotes the molar residual Helmholtz free energy, while κ_T and α_p represent isothermal compressibility and isobaric thermal expansion, respectively. The superscript "ideal" refers to the properties associated with an ideal gas. As PC-SAFT provides the residual term, the group contribution method proposed by Joback and Reid Joback; Reid (1987) was employed to obtain the thermal capacities of the ideal gas. The application of this method for the calculation of the isobaric heat capacity of biodiesels has been validated previously Alves, Alanderson Arthu Araújo; Levy; et al. (2025 e Do Carmo, F.R. et al. (2020).

3.3.2 Correlations

In previous works, two empirical correlations were proposed to represent the effects of pressure and temperature on the density Daridon (2020) and speed of sound Daridon (2022b)

of pure fatty acid alkyl esters and biodiesel fuels with an uncertainty comparable to the experimental one. For biofuel, these models were extended using combining rules. The models for density and speed of sound were developed separately, considering the differences and limitations of each property. However, a standard methodology for both properties is followed, outlined in the flowchart in Figure 13, illustrating the model development steps.

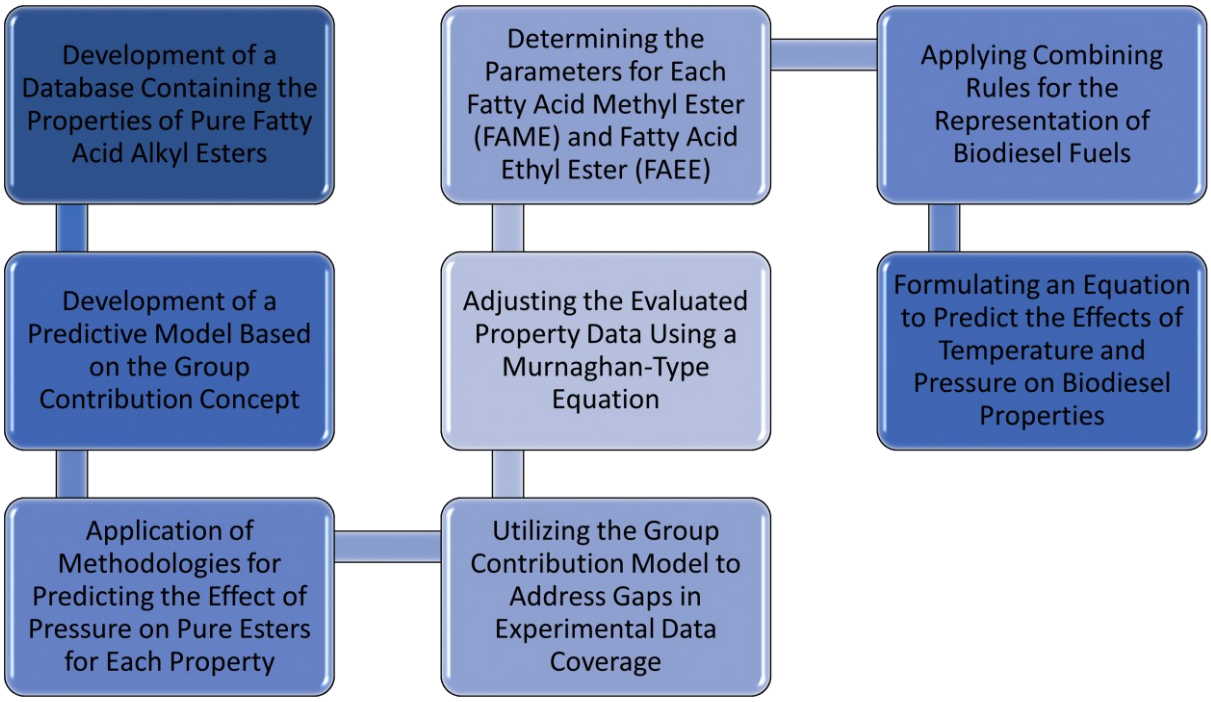

Figure 13 – Flowchart illustrating the standard methodology for developing models to predict the effects of pressure and temperature on the density Daridon (2020) and speed of sound Daridon (2022b) of pure fatty acid alkyl esters and biodiesel fuels. The models for both properties were developed separately. (Created by the author, 2025)

The studies reported Daridon (2020, 2022b) provide predictive methods that were validated against data from the literature for both pure fatty acid alky ester and biodiesels. They use group contribution techniques to predict the densities and sound speeds of fatty acid methyl esters (FAMEs) and fatty acid ethyl esters (FAEEs) found in biodiesel fuels, when experimental data are not available in literature. Based on the experimental data set or group contribution predictions, correlations were developed to represent the effects of pressure and temperature on the properties of each fatty acid ester, ranging from decanoate to lignocerate, using a Murnaghan-type equation F. D. Murnaghan (1924). To describe the influence of pressure and temperature on the speed of sound, the $cM\gamma$ quantity was employed instead of speed of sound. It is defined as the product of the speed of sound and the molecular weight raised to the

previously established power $\gamma = 0.975$ Daridon (2022a). For density, the Murnaghan-type equation was applied directly on density to account for the effect of pressure. The final equations of the model, extended to biodiesel using a mixing rule, are presented in Equations (3.7) and (3.8).

$$c_{Bio} = \frac{A_{cM\gamma,i}\left(1+B_{cM\gamma,i}\cdot\tilde{p}\right)^{C_{cM\gamma,i}{}^{1/\gamma}}}{\sum_i x_i M_i} \tag{3.7}$$

$$\rho_{Bio} = \frac{\sum_i x_i M_i}{A_{v,i}\left(1+B_{v,i}\cdot\tilde{p}\right)^{C_{v,i}}} \tag{3.8}$$

In these expressions, x_i represents the mole fraction of the i-th FAME in biodiesel, M is the molecular weight, and $\tilde{p}$ denotes the relative pressure, defined as $(p - p_{atm})$. The coefficients $A_{cM\gamma,i}$, $B_{cM\gamma,i}$ and, $C_{cM\gamma,i}$, associated with the speed of sound, and $A_{v,i}$, $B_{v,i}$, and $C_{v,i}$, associated with density, are expressed as second-order polynomials of temperature. The coefficients of these polynomials have been reported in previous studies Daridon (2020, 2022b) for each FAME, covering carbon chain lengths ranging from C10:0 to C24:0.

These proposed correlations with their reported parameters can operate over a wide range of conditions: sound speed (c) is predicted for pressures between 0.1 and 150 MPa and temperatures from 293 to 393 K, while density (ρ) is predicted for pressures ranging from 0.1 to 200 MPa and temperatures between 280 and 400 K.

3.4 Results and discussion

A total of 235 experimental sound speed measurements were performed for three biodiesels derived from different oil sources (coconut, sucupira, and canola) across five isotherms, spanning temperatures from $293.15\ K$ to $373.15\ K$ and pressures from $0.1\ MPa$ to $200\ MPa$. These data points are presented in Table 3, which provides experimental sound speed values along with the corresponding pressure and temperature conditions. Densities under the same pressure conditions were also determined, as outlined in Section 3.2.3. However, due to experimental constraints, vibrating tube densimeter measurements were limited to $100\ MPa$. To extend these measurements to $200\ MPa$, the experimental sound speed data were integrated. This procedure requires the adjustments of Equation 3.2 (Section 3.2.3).

Table 4 presents the equation 3.2 adjustable parameters ($A, B_1, B_2, B_3, C_1, C_2, C_3, E$ and F) for each biodiesel studied. Additionally, the Mean Percentage Deviation (MPD), Mean Absolute Percentage Deviation (MAPD), and Maximum Percentage Deviation (MaxPD) are reported, providing metrics to evaluate the quality of the fit between the experimental data and the model. The obtained statistical metrics indicate that the adjustments were satisfactory for each biodiesel, with low deviation values, demonstrating a strong agreement between the experimental data and the calculation of Equation 3.2.

Table 3 – Experimental sound speed data ($\mathrm{m \cdot s^{-1}}$) for coconut, sucupira, and canola biodiesels as a function of pressure (0.1 – 200 MPa)[a] and temperature (293.15 – 373.15 K)[b].

P	T	c	T	c	T	c	T	c	T	c
MPa	K	$m \cdot s^{-1}$	K	$m \cdot s^{-1}$	K	$m \cdot s^{-1}$	K	$m \cdot s^{-1}$	K	$m \cdot s^{-1}$
coconut biodiesel										
0.1	293.15	1357.5	313.15	1284.3	333.15	1212.9	353.15	1144.4	373.15	-
10	293.15	1405.2	313.15	1332.8	333.15	1264.4	353.15	1198.6	373.15	1136.7
20	293.15	1450.5	313.15	1379.6	333.15	1315.3	353.15	1252.9	373.15	1194.4
30	293.15	1491.4	313.15	1424.4	333.15	1361.5	353.15	1302.6	373.15	1246.8
40	293.15	1530.4	313.15	1465.4	333.15	1405.1	353.15	1349.0	373.15	1294.4
50	293.15	1567.6	313.15	1504.7	333.15	1446.4	353.15	1390.8	373.15	1339.3
60	293.15	1603.3	313.15	1542.7	333.15	1484.8	353.15	1432.6	373.15	1381.4
70	293.15	1637.9	313.15	1577.6	333.15	1522.0	353.15	1470.6	373.15	1421.2
80	293.15	1669.4	313.15	1610.9	333.15	1558.1	353.15	1507.0	373.15	1459.2
90	293.15	1700.9	313.15	1644.8	333.15	1591.1	353.15	1542.4	373.15	1494.4
100	293.15	1730.8	313.15	1675.2	333.15	1622.9	353.15	1575.7	373.15	1529.6
120	293.15	1788.3	313.15	1735.0	333.15	1685.6	353.15	1637.7	373.15	1594.6
140	293.15	1842.6	313.15	1790.2	333.15	1743.4	353.15	1698.4	373.15	1654.8
160	293.15	1895.3	313.15	1842.4	333.15	1796.9	353.15	1753.3	373.15	1713.2
180	293.15	-	313.15	1892.4	333.15	1847.2	353.15	1804.8	373.15	1765.6
200	293.15	-	313.15	1937.8	333.15	1895.0	353.15	1853.5	373.15	1815.3
sucupira biodiesel										
0.1	293.15	1422.5	313.15	1349.7	333.15	1281.2	353.15	1215.2	373.15	-
10	293.15	1463.1	313.15	1392.7	333.15	1325.8	353.15	1262.6	373.15	1201.1
20	293.15	1505.1	313.15	1437.7	333.15	1373.5	353.15	1313.3	373.15	1254.7
30	293.15	1545.1	313.15	1479.6	333.15	1417.8	353.15	1359.3	373.15	1303.8
40	293.15	1582.7	313.15	1519.1	333.15	1459.4	353.15	1402.7	373.15	1350.1
50	293.15	1618.2	313.15	1557.1	333.15	1498.7	353.15	1444.1	373.15	1391.7
60	293.15	1651.6	313.15	1592.6	333.15	1536.5	353.15	1482.3	373.15	1432.7
70	293.15	1685.0	313.15	1626.7	333.15	1571.9	353.15	1519.6	373.15	1471.0
80	293.15	1715.9	313.15	1658.7	333.15	1605.5	353.15	1555.4	373.15	1507.6
90	293.15	1744.8	313.15	1692.0	333.15	1638.9	353.15	1588.6	373.15	1543.0
100	293.15	1775.2	313.15	1720.9	333.15	1669.3	353.15	1621.1	373.15	1575.6
120	293.15	1830.7	313.15	1779.0	333.15	1729.3	353.15	1683.3	373.15	1638.9
140	293.15	1882.6	313.15	1832.3	333.15	1784.9	353.15	1739.9	373.15	1698.0
160	293.15	1934.2	313.15	1883.4	333.15	1836.3	353.15	1793.1	373.15	1752.5
180	293.15	-	313.15	1931.1	333.15	1886.0	353.15	1843.4	373.15	1803.6
200	293.15	-	313.15	1976.7	333.15	1933.5	353.15	1891.3	373.15	1852.3
canola biodiesel										

0.1	293.15	1413.9	313.15	1340.8	333.15	1273.3	353.15	1206.6	373.15	1138.3
10	293.15	1458.1	313.15	1388.1	333.15	1322.2	353.15	1258.5	373.15	1198.2
20	293.15	1500.2	313.15	1434.1	333.15	1370.0	353.15	1309.4	373.15	1252.2
30	293.15	1540.9	313.15	1476.3	333.15	1414.4	353.15	1356.8	373.15	1300.9
40	293.15	1578.5	313.15	1516.2	333.15	1456.7	353.15	1399.7	373.15	1347.4
50	293.15	1613.0	313.15	1554.7	333.15	1496.5	353.15	1442.0	373.15	1390.0
60	293.15	1648.4	313.15	1590.0	333.15	1534.9	353.15	1480.4	373.15	1430.6
70	293.15	1682.2	313.15	1623.4	333.15	1570.2	353.15	1517.7	373.15	1469.9
80	293.15	1711.9	313.15	1657.4	333.15	1603.5	353.15	1553.9	373.15	1506.3
90	293.15	1742.8	313.15	1690.3	333.15	1636.2	353.15	1587.8	373.15	1541.9
100	293.15	1771.9	313.15	1718.2	333.15	1668.9	353.15	1620.2	373.15	1574.1
120	293.15	1828.8	313.15	1775.9	333.15	1727.8	353.15	1682.6	373.15	1638.8
140	293.15	1881.6	313.15	1830.0	333.15	1783.0	353.15	1738.8	373.15	1697.9
160	293.15	1930.3	313.15	1881.5	333.15	1835.1	353.15	1792.1	373.15	1751.9
180	293.15	1978.2	313.15	1929.1	333.15	1884.6	353.15	1842.6	373.15	1803.0
200	293.15	2024.7	313.15	1976.3	333.15	1933.6	353.15	1891.3	373.15	1852.1

a: Standard uncertainties u is $u(T) = 0.1K$; *b*: $u(p) = 0.01MPa$ up to $100MPa$, $u(p) = 0.1MPa$ between (100 and 200) MPa and the combined expanded uncertainties U (level of confidence = 0.95) are $U(c) = 0.002c$ up to 100 MPa, $U(c) = 0.003c$ between (100 and 200).

Table 4 – Adjustable parameters of equation 2.2 ($A, B_1, B_2, B_3, C_1, C_2, C_3, E$ and F) for the biodiesels evaluated, accompanied by the statistical adjustment metrics: Mean Percentage Deviation (MPD), Mean Absolute Percentage Deviation (MAPD), and Maximum Percentage Deviation (MaxPD).

parameters (unit)	biodiesels		
	coconut	sucupira	canola
$A\ (s^2 \cdot m^{-2})$	$-8.56280 \cdot 10^{-9}$	$2.91651 \cdot 10^{-8}$	$6.28264 \cdot 10^{-8}$
$B_1(s^2 \cdot m^{-2} \cdot K^{-1})$	$1.28535 \cdot 10^{-9}$	$1.02391 \cdot 10^{-9}$	$7.32912 \cdot 10^{-10}$
$B_2(s^2 \cdot m^{-2} \cdot K^{-2})$	$-1.13700 \cdot 10^{-12}$	$-8.94980 \cdot 10^{-13}$	$4.50023 \cdot 10^{-15}$
$B_3(s^2 \cdot m^{-2} \cdot K^{-3})$	$-4.66050 \cdot 10^{-16}$	$-5.78520 \cdot 10^{-16}$	$-1.10420 \cdot 10^{-15}$
$C_1(s^2 \cdot m^{-2} \cdot MPa^{-1})$	$7.87306 \cdot 10^{-10}$	$5.01513 \cdot 10^{-10}$	$8.03644 \cdot 10^{-10}$
$C_2(s^2 \cdot m^{-2} \cdot MPa^{-2})$	$-1.61330 \cdot 10^{-12}$	$-7.93430 \cdot 10^{-13}$	$-1.65250 \cdot 10^{-12}$
$C_3(s^2 \cdot m^{-2} \cdot MPa^{-3})$	$2.42875.10^{-15}$	$1.33569 \cdot 10^{-15}$	$2.47323 \cdot 10^{-15}$
$E(K^{-1})$	$-1.78483 \cdot 10^{-3}$	$-1.77582 \cdot 10^{-3}$	$-1.70777 \cdot 10^{-3}$
$F(MPa^{-1})$	$4.93964 \cdot 10^{-3}$	$4.08381 \cdot 10^{-3}$	$4.95165 \cdot 10^{-3}$
deviations[a]			
MPD	$6.23 \cdot 10^{-4}$	$-5.52 \cdot 10^{-4}$	$-1.13 \cdot 10^{-4}$
$MAPD$	$3.87 \cdot 10^{-2}$	$5.47 \cdot 10^{-2}$	$4.09 \cdot 10^{-2}$
$MaxPD$	$1.64 \cdot 10^{-1}$	$2.10 \cdot 10^{-1}$	$1.64 \cdot 10^{-1}$

[a] : MPD, Mean Percentage Deviation; MAPD, Mean Absolute Percentage Deviation; MaxPD, Maximum deviation Percentage Deviation.

Table 5 presents the density data measured with the high-pressure vibrating density meter, comprising 294 measurements across nine isotherms, with temperatures ranging from 293.15 K to 373.15 K and pressures from 0.1 MPa to 100 MPa for the same biodiesels.

Additionally, the densities obtained from speed of sound integration (264 density values) were reported in this table, leading to a set of 558 density data, extending the pressure range to 200 MPa. The coupling of the two datasets (sound speed and density) provides a detailed characterization of the thermophysical properties of the evaluated biodiesels and offers deeper insights into their behavior under high-pressure conditions.

Table 5 – Experimental density data ($kg \cdot m^{-3}$) for coconut, sucupira, and canola biodiesels as a function of pressure (0.1-200 MPa) and temperature (293.15-373.15 K).

P	T	ρ	T	ρ	T	ρ	T	ρ	T	ρ
MPa	K	$kg \cdot m^{-3}$	K	$kg \cdot m^{-3}$	K	$kg \cdot m^{-3}$	K	$kg \cdot m^{-3}$	K	$kg \cdot m^{-3}$
coconut biodiesel										
0.1	293.15	870.3	303.15	860.7	313.15	854.9	323.15	846.9	333.15	839.2
10	293.15	876.4	303.15	869.0	313.15	861.5	323.15	854.0	333.15	847.0
20	293.15	882.4	303.15	875.2	313.15	868.1	323.15	860.8	333.15	854.2
30	293.15	887.9	303.15	881.0	313.15	874.0	323.15	867.3	333.15	860.7
40	293.15	893.3	303.15	886.5	313.15	879.7	323.15	873.5	333.15	866.8
50	293.15	898.1	303.15	891.5	313.15	885.1	323.15	879.0	333.15	872.6
60	293.15	903.0	303.15	896.4	313.15	890.2	323.15	884.2	333.15	878.0
70	293.15	907.5	303.15	901.1	313.15	894.8	323.15	889.2	333.15	883.1
80	293.15	911.7	303.15	905.5	313.15	899.5	323.15	894.0	333.15	888.1
90	293.15	915.8	303.15	909.7	313.15	903.9	323.15	898.4	333.15	892.7
100	293.15	919.8	303.15	913.8	313.15	908.1	323.15	902.8	333.15	897.1
110	293.15	923.6	303.15	918.1	313.15	912.7	323.15	907.2	333.15	901.7
120	293.15	927.2	303.15	921.9	313.15	916.6	323.15	911.2	333.15	905.9
130	293.15	930.8	303.15	925.6	313.15	920.3	323.15	915.1	333.15	909.9
140	293.15	934.2	303.15	929.1	313.15	924.0	323.15	918.9	333.15	913.7
150	293.15	937.5	303.15	932.6	313.15	927.5	323.15	922.5	333.15	917.5
160	293.15	940.8	303.15	935.9	313.15	931.0	323.15	926.0	333.15	921.1
170	293.15	943.9	303.15	939.1	313.15	934.3	323.15	929.4	333.15	924.6
180	293.15	946.9	303.15	942.3	313.15	937.5	323.15	932.8	333.15	928.0
190	293.15	-	303.15	945.3	313.15	940.7	323.15	936.0	333.15	931.3
200	293.15	-	303.15	948.3	313.15	943.7	323.15	939.1	333.15	934.5
0.1	343.15	831.2	353.15	823.3	363.15	815.9	373.15	-		
10	343.15	839.1	353.15	831.9	363.15	823.9	373.15	816.3		
20	343.15	846.9	353.15	839.6	363.15	832.0	373.15	824.9		
30	343.15	853.8	353.15	846.8	363.15	839.5	373.15	832.7		
40	343.15	860.1	353.15	853.5	363.15	846.5	373.15	840.0		
50	343.15	866.1	353.15	859.7	363.15	852.9	373.15	846.7		
60	343.15	871.4	353.15	865.4	363.15	859.0	373.15	853.0		
70	343.15	876.7	353.15	871.0	363.15	864.7	373.15	858.9		
80	343.15	881.7	353.15	876.3	363.15	870.1	373.15	864.5		
90	343.15	886.6	353.15	880.9	363.15	875.0	373.15	869.8		
100	343.15	891.3	353.15	885.9	363.15	880.1	373.15	874.8		
110	343.15	896.3	353.15	890.9	363.15	885.7	373.15	880.5		
120	343.15	900.6	353.15	895.3	363.15	890.1	373.15	885.0		
130	343.15	904.7	353.15	899.5	363.15	894.4	373.15	889.4		
140	343.15	908.6	353.15	903.5	363.15	898.5	373.15	893.6		
150	343.15	912.4	353.15	907.5	363.15	902.5	373.15	897.7		
160	343.15	916.1	353.15	911.2	363.15	906.4	373.15	901.6		
170	343.15	919.7	353.15	914.9	363.15	910.1	373.15	905.4		
180	343.15	923.2	353.15	918.4	363.15	913.7	373.15	909.1		
190	343.15	926.6	353.15	921.9	363.15	917.2	373.15	912.7		
200	343.15	929.9	353.15	925.3	363.15	920.7	373.15	916.1		
sucupira biodiesel										
0.1	293.15	896.7	303.15	889.4	313.15	882.4	323.15	874.9	333.15	867.8

10	293.15	902.5	303.15	895.3	313.15	888.6	323.15	881.3	333.15	874.6
20	293.15	908.1	303.15	901.1	313.15	894.5	323.15	887.4	333.15	881.1
30	293.15	913.2	303.15	906.5	313.15	900.1	323.15	893.1	333.15	887.1
40	293.15	917.9	303.15	911.6	313.15	905.2	323.15	898.6	333.15	892.7
50	293.15	922.4	303.15	916.4	313.15	910.2	323.15	903.8	333.15	898.0
60	293.15	926.9	303.15	920.8	313.15	914.9	323.15	908.8	333.15	902.8
70	293.15	931.0	303.15	925.1	313.15	919.3	323.15	913.5	333.15	907.6
80	293.15	935.0	303.15	929.4	313.15	923.7	323.15	917.9	333.15	912.3
90	293.15	938.9	303.15	933.3	313.15	927.6	323.15	922.1	333.15	916.5
100	293.15	942.5	303.15	937.1	313.15	931.5	323.15	926.1	333.15	920.7
110	293.15	946.4	303.15	940.9	313.15	935.5	323.15	930.1	333.15	924.9
120	293.15	950.0	303.15	944.5	313.15	939.2	323.15	933.9	333.15	928.8
130	293.15	953.4	303.15	948.0	313.15	942.8	323.15	937.6	333.15	932.5
140	293.15	956.7	303.15	951.4	313.15	946.3	323.15	941.2	333.15	936.2
150	293.15	959.9	303.15	954.8	313.15	949.7	323.15	944.7	333.15	939.7
160	293.15	963.1	303.15	958.0	313.15	953.0	323.15	948.0	333.15	943.2
170	293.15	966.1	303.15	961.1	313.15	956.2	323.15	951.3	333.15	946.5
180	293.15	969.1	303.15	964.2	313.15	959.3	323.15	954.5	333.15	949.8
190	293.15	-	303.15	967.1	313.15	962.3	323.15	957.6	333.15	952.9
200	293.15	-	303.15	970.1	313.15	965.3	323.15	960.6	333.15	956.0
0.1	343.15	860.5	353.15	853.3	363.15	845.7	373.15	838.45		
10	343.15	867.6	353.15	860.6	363.15	853.6	373.15	846.6		
20	343.15	874.4	353.15	867.6	363.15	860.9	373.15	854.2		
30	343.15	880.6	353.15	874.1	363.15	867.6	373.15	861.1		
40	343.15	886.4	353.15	880.1	363.15	873.9	373.15	867.7		
50	343.15	891.9	353.15	885.9	363.15	879.8	373.15	873.7		
60	343.15	897.0	353.15	891.2	363.15	885.9	373.15	879.5		
70	343.15	902.0	353.15	896.3	363.15	890.6	373.15	884.7		
80	343.15	906.6	353.15	901.1	363.15	895.5	373.15	890.0		
90	343.15	911.2	353.15	905.7	363.15	900.3	373.15	894.8		
100	343.15	915.4	353.15	910.1	363.15	904.8	373.15	899.5		
110	343.15	919.7	353.15	914.6	363.15	909.5	373.15	904.6		
120	343.15	923.7	353.15	918.7	363.15	913.7	373.15	908.9		
130	343.15	927.5	353.15	922.6	363.15	917.8	373.15	913.0		
140	343.15	931.3	353.15	926.4	363.15	921.7	373.15	917.0		
150	343.15	934.9	353.15	930.1	363.15	925.4	373.15	920.8		
160	343.15	938.4	353.15	933.7	363.15	929.1	373.15	924.5		
170	343.15	941.8	353.15	937.2	363.15	932.6	373.15	928.1		
180	343.15	945.1	353.15	940.6	363.15	936.1	373.15	931.6		
190	343.15	948.4	353.15	943.8	363.15	939.4	373.15	935.0		
200	343.15	951.5	353.15	947.0	363.15	942.7	373.15	938.4		
					canola biodiesel					
0.1	293.15	878.8	303.15	871.6	313.15	864.4	323.15	857.4	333.15	849.9
10	293.15	884.6	303.15	877.7	313.15	870.7	323.15	863.8	333.15	856.8
20	293.15	890.0	303.15	883.3	313.15	876.6	323.15	870.0	333.15	863.3
30	293.15	895.1	303.15	888.7	313.15	882.2	323.15	875.7	333.15	869.2
40	293.15	900.0	303.15	893.7	313.15	887.6	323.15	881.1	333.15	874.8
50	293.15	904.6	303.15	898.6	313.15	892.4	323.15	886.3	333.15	880.2
60	293.15	909.1	303.15	903.1	313.15	897.2	323.15	891.3	333.15	885.3
70	293.15	913.3	303.15	907.4	313.15	901.6	323.15	895.8	333.15	890.1
80	293.15	917.3	303.15	911.6	313.15	906.0	323.15	900.3	333.15	894.6
90	293.15	921.3	303.15	915.7	313.15	910.1	323.15	904.5	333.15	899.0
100	293.15	924.9	303.15	919.5	313.15	914.0	323.15	908.6	333.15	903.2
110	293.15	928.5	303.15	923.2	313.15	917.9	323.15	912.5	333.15	907.2
120	293.15	932.1	303.15	926.9	313.15	921.6	323.15	916.4	333.15	911.2
130	293.15	935.5	303.15	930.4	313.15	925.2	323.15	920.1	333.15	915.0
140	293.15	938.8	303.15	933.8	313.15	928.7	323.15	923.7	333.15	918.7
150	293.15	942.0	303.15	937.1	313.15	932.1	323.15	927.2	333.15	922.2
160	293.15	945.1	303.15	940.3	313.15	935.4	323.15	930.6	333.15	925.7
170	293.15	948.1	303.15	943.4	313.15	938.6	323.15	933.8	333.15	929.1

180	293.15	951.1	303.15	946.4	313.15	941.7	323.15	937.0	333.15	932.3
190	293.15	954.0	303.15	949.4	313.15	944.8	323.15	940.1	333.15	935.5
200	293.15	956.8	303.15	952.3	313.15	947.7	323.15	943.2	333.15	938.6
0.1	343.15	842.9	353.15	835.1	363.15	827.9	373.15	820.5		
10	343.15	849.6	353.15	842.8	363.15	835.8	373.15	828.7		
20	343.15	856.3	353.15	849.7	363.15	843.1	373.15	836.4		
30	343.15	862.6	353.15	856.2	363.15	849.8	373.15	843.4		
40	343.15	868.5	353.15	862.3	363.15	856.2	373.15	850.0		
50	343.15	874.0	353.15	868.1	363.15	862.0	373.15	856.2		
60	343.15	879.2	353.15	873.4	363.15	867.6	373.15	861.9		
70	343.15	884.2	353.15	878.5	363.15	872.9	373.15	867.3		
80	343.15	889.0	353.15	883.3	363.15	877.8	373.15	872.5		
90	343.15	893.4	353.15	888.0	363.15	882.6	373.15	877.4		
100	343.15	897.7	353.15	892.5	363.15	887.2	373.15	882.1		
110	343.15	902.0	353.15	896.7	363.15	891.6	373.15	886.6		
120	343.15	906.0	353.15	900.9	363.15	895.8	373.15	890.9		
130	343.15	909.9	353.15	904.9	363.15	899.9	373.15	895.0		
140	343.15	913.7	353.15	908.7	363.15	903.8	373.15	899.0		
150	343.15	917.3	353.15	912.4	363.15	907.6	373.15	902.9		
160	343.15	920.9	353.15	916.1	363.15	911.3	373.15	906.7		
170	343.15	924.3	353.15	919.6	363.15	914.9	373.15	910.3		
180	343.15	927.6	353.15	923.0	363.15	918.4	373.15	913.8		
190	343.15	930.9	353.15	926.3	363.15	921.7	373.15	917.2		
200	343.15	934.0	353.15	929.5	363.15	925.0	373.15	920.6		

a Standard uncertainties u are $u(T) = 0.1\ K$ and $u(p) = 0.003\ MPa$; and the combined expanded uncertainties U (level of confidence = 0.95) are $U(\rho) = 0.001\rho$ up to 100 MPa and $U(\rho) = 0.002\rho$ between (100 and 200) MPa.

Obtaining experimental values for density and speed of sound enables the calculation of two critical acoustic properties for the injection process in diesel engines: isentropic compressibility (κ_s) and acoustic impedance (Z). These properties were determined using the following relationships:

$$\kappa_s = \frac{1}{\rho \cdot c^2} \tag{3.9}$$

$$Z = \rho \cdot c \tag{3.10}$$

These derived acoustic properties were calculated under all experimental pressure and temperature conditions, comprehensively characterizing the biodiesels analyzed. This data were reported in **Tables B1 and B2**, with graphical representations of the property behaviors shown in **Figure B1**, illustrating their variations concerning pressure and temperature. These **Tables B1–B2** and **Figure B1** are provided in Appendix B: Complementary Material to Chapter 3. The results provide essential insights into the behavior of these fuels in injection systems, significantly contributing to developing strategies for optimizing diesel engine performance. The acoustic impedance of the biodiesel represents its resistance to the propagation of sound waves. On the other hand, isentropic compressibility quantifies the volumetric variation of

biodiesel under pressure changes at constant entropy, directly influencing the propagation of acoustic waves. This property is significant for assessing performance in high-pressure injection systems.

A literature review was performed to identify data on the thermophysical properties of biodiesel derived from the same oil sources evaluated in this study. Among the studies reviewed, Tat and Van Gerpen Tat; Van Gerpen (2003b) stand out, as they reported values for density, speed of sound, and isentropic bulk modulus for biodiesel and its primary constituents (pure esters). Their study covered a temperature range of 20 to 100°C (293.15 to 373.15 K) and pressures up to 32.5 MPa. Notably, canola biodiesel was among the oilseeds analyzed, allowing for a direct comparison with the experimental data obtained in this work. The mean absolute percentage deviations (MAPD) observed were 0.23% for density and 0.37% for speed of sound, indicating excellent agreement between the experimental results and previously reported literature values, despite differences in the fatty acid methyl ester profiles of the two canola biodiesels compared. Experimental data for coconut biodiesel are scarce in the literature, with most studies focusing on density and viscosity and speed of sound under atmospheric pressure conditions Feitosa et al. (2010 e Mesquita et al. (2014). A comparison between the available data and the values obtained in this study under similar conditions revealed a deviation of only 0.10% for density Feitosa et al. (2010 e Mesquita et al. (2014). A comparison of the atmospheric speed of sound in coconut oil-based biodiesel was not made due to significant differences in composition between the biodiesel studied here and that reported in the literature. Notably, the laurate content was absent in the literature's biodiesel. At high pressures, the literature is limited to studies on pure esters, common components in coconut biodiesel's ester profile Żarska et al. (2014a). Thermophysical property values are more frequently reported for other biodiesel sources, such as palm, rapeseed, soybean, animal fat, linseed, corn, and grape seed. No data on these properties was found in the literature for sucupira biodiesel, highlighting the novelty of the current study.

The thermophysical data obtained from experiments were used to evaluate the effectiveness of the PC-SAFT multiparametric equation of state, along with two correlations developed to predict the impact of pressure on the density and speed of sound of biodiesels. Although the PC-SAFT equation has been explored in our previous studies, earlier investigations were limited to modeling density (ALVES, ALANDERSON ARTHUARAÚJO et al., 2024; DA COSTA; DE MEDEIROS; et al., 2024) or density and vapor pressure Da Costa; Medeiros; et al. (2024). As detailed in Section 3.2.3, the present work extends this analysis by incorporating the evaluation of parameters by simultaneous optimization of density and sound

speed. The resulting parameters from this approach are provided in **Table B3** in Appendix B. The outcomes of the statistical evaluation are summarized in Table 6, which presents the MPD (Mean Percentage Deviation), MAPD (Mean Absolute Percentage Deviation), and MaxPD (Maximum Percentage Deviation) values for each property, biodiesel, and model analyzed in this study. It is important to note that in these comparisons, the equation of state PC-SAFT was used to calculate density and sound speed after optimizing its parameters based on the experimental data tested. The purpose of the comparison is therefore to assess the equation's ability to describe simultaneously density and sound speed, specifically the volume and its derivative with respect to pressure. In contrast, correlations were used as proposed by Daridon Daridon (2020, 2022b). Consequently, the comparisons with the values provided by these correlations aim to evaluate their predictive capability. The correlations Daridon (2020, 2022b) consistently outperform PC-SAFT across all evaluated properties. Their MAPD values are significantly lower, achieving an average accuracy improvement of threefold for density, twelvefold for speed of sound, tenfold for isentropic compressibility, and sevenfold for acoustic impedance. Furthermore, all properties' average MPD values are closer to zero, indicating reduced bias in the predictions. A notable advantage is the consistently lower MaxPD values, reflecting greater precision and reduced variability compared to PC-SAFT. These results underscore the reliability of Daridon's correlations. The goal of these correlations was to develop models capable of predicting density and sound speed under pressure, including high-pressure conditions, with an uncertainty comparable to experimental measurements. It appears that this is indeed the case for the three biodiesels investigated here, and the models are valuable up to 200 MPa.

Figures 14 and 15 present graphs comparing the experimental sound speed and density values with those calculated using the PC-SAFT and correlations. In these graphs, the PC-SAFT model is represented by gray circles. In contrast, the values obtained from the tested correlations are depicted by white, orange, and yellow circles, corresponding to coconut, sucupira, and canola biodiesels, respectively. The continuous black line represents perfect agreement, where the experimental values match the calculated data. The dotted lines indicate a ±1% uncertainty margin (adopted value).

In general, both models exhibit good agreement with the experimental data, with the points lying close to the line of perfect agreement and within the adopted 1% margins. However, two key trends can be observed across the graphs. At low sound speeds, between 1100 m/s and 1300 m/s (as seen for coconut biodiesel), the PC-SAFT model tends to overestimate the experimental values, with the points positioned above the line of agreement.

The model underestimates higher sound speeds, between 1700 m/s and 1900 m/s, with the points falling below the agreement line.

An opposite behavior is observed in the density graph of Figure 15, where the PC-SAFT model underestimates the experimental values at low densities and overestimates them at high densities. Compared to that observed for the speed of sound, this inverse pattern suggests that the model faces similar challenges in capturing the influence of pressure on volumetric properties of biodiesels. These trends indicate that the PC-SAFT model overestimates the compressibility of biodiesel at high pressures. Since the tests were conducted after optimizing the parameters based on adjustments to both density and sound speed data, this behavior cannot be rectified simply by further parameter adjustments. A more comprehensive enhancement of the equation is necessary to better represent the effects of pressure on the thermophysical properties of biodiesel when using this type of model.

Table 6 – Results of the comparative analysis between the data obtained by the PC-SAFT equation of state and the models studied Daridon (2020) and Daridon (2022b), with the MPD (Mean Percentage Deviation), MAPD (Mean Absolute Percentage Deviation), and MaxPD (Maximum Percentage Deviation) values for each biodiesel property and model evaluated in this study.

Statistics	PC-SAFT				Models Daridon (2020) Daridon (2022b)			
	ρ	c	κ_s	Z	ρ	c	κ_s	Z
	coconut biodiesel							
MPD^a	-0.35	-1.21	2.98	-1.56	-0.16	0.18	-0.18	0.01
$MAPD^b$	0.67	2.26	4.61	2.24	0.16	0.21	0.39	0.20
$MaxPD^c$	1.92	5.29	11.99	5.72	0.50	0.56	1.08	0.57
	sucupira biodiesel							
MPD^a	-0.09	-0.61	1.44	-0.71	-0.13	0.17	-0.22	0.05
$MAPD^b$	0.66	1.89	3.59	1.69	0.13	0.18	0.30	0.16
$MaxPD^c$	1.91	4.16	7.12	3.58	0.23	0.81	1.64	0.81
	canola biodiesel							
MPD^a	-0.04	-0.69	1.56	-0.74	-0.34	-0.09	0.53	-0.43
$MAPD^b$	0.63	1.92	3.67	1.73	0.34	0.13	0.53	0.43
$MaxPD^c$	1.73	3.90	7.79	3.72	0.39	0.30	0.93	0.63
	Overall							
MPD^a	-0.16	-0.83	1.99	-1.00	-0.21	0.08	0.04	-0.13
$\boldsymbol{MAPD^b}$	**0.65**	**2.03**	**3.96**	**1.89**	**0.21**	**0.17**	**0.41**	**0.27**

$MaxPD^c$	1.85	4.45	8.97	4.34	0.38	0.56	1.22	0.67

a: Mean Percentage Deviation (MPD); b: Mean Absolute Percentage Deviation (MAPD); c: maximum percentage deviation (MaxPD).

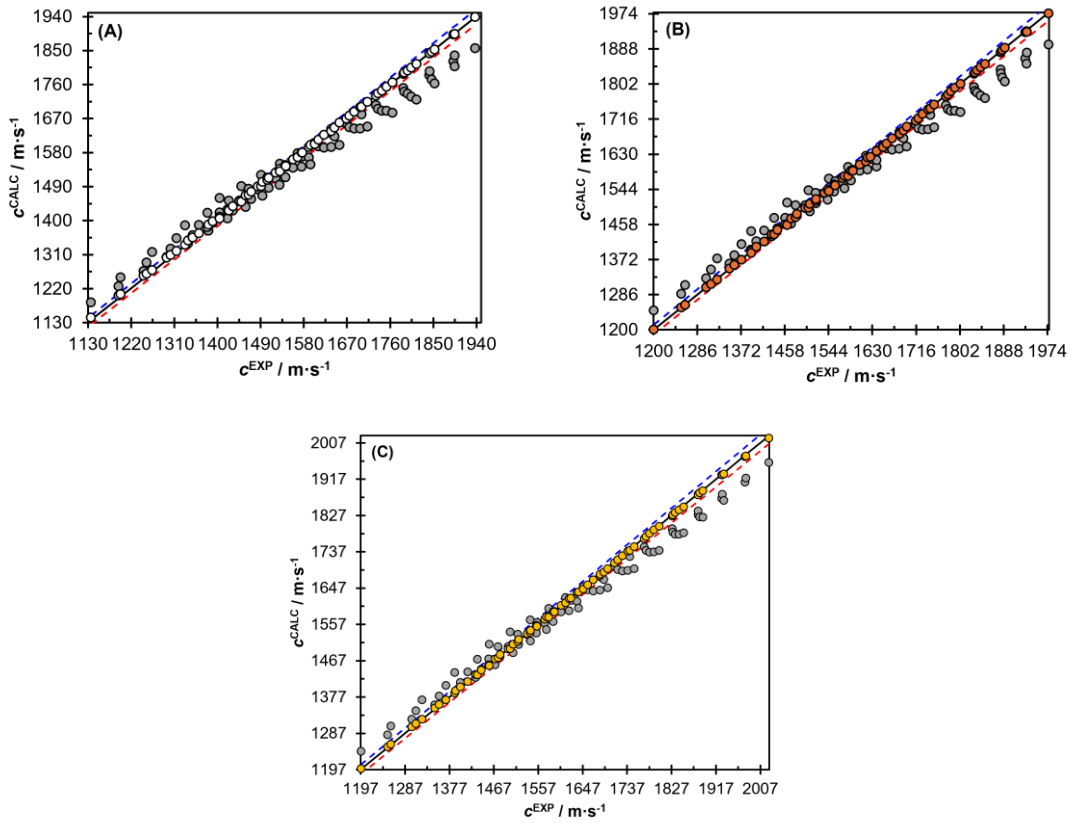

Figure 14 – Graph comparing the experimental values of the speed of sound (c^{EXP}) with the calculated values (c^{CALC}) using the PC-SAFT (gray circles) and Daridon (white (A), orange (B), and yellow (C) circles, representing coconut, sucupira, and canola biodiesels, respectively) models. The continuous black line indicates perfect agreement, where the experimental values coincide with the experimental data. The dotted lines represent arbitrary uncertainties of plus or minus 1%, providing a margin of error for the experimental data.

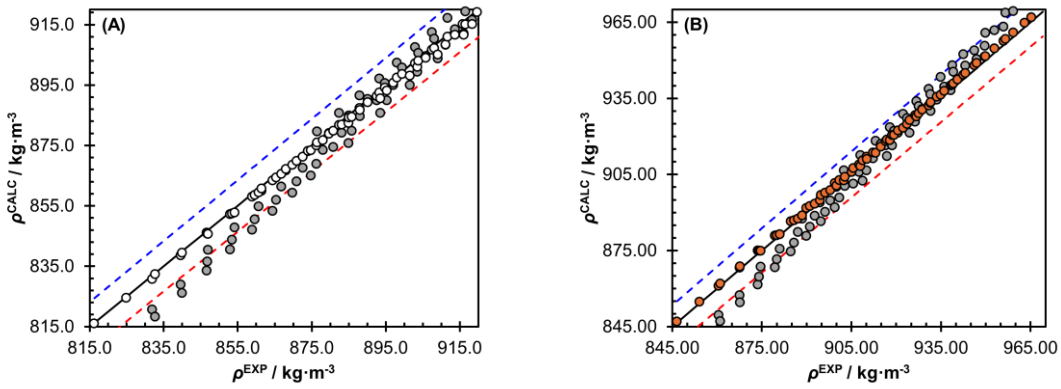

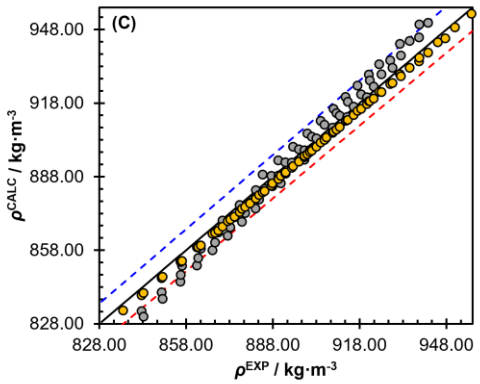

Figure 15 – Graph comparing the experimental values of the density (ρ^{EXP}) with the calculated values (ρ^{CALC}) using the PC-SAFT (gray circles) and Daridon (white (A), orange (B), and yellow (C) circles, representing coconut, sucupira, and canola biodiesels, respectively) models. The continuous black line indicates perfect agreement, where the experimental values coincide with the experimental data. The dotted lines represent arbitrary uncertainties of plus or minus 1%, providing a margin of error for the experimental data. (Created by the author, 2025)

Figure 16 presents the deviations of the thermophysical properties ($\rho, c, \kappa_s, and\ Z$) as a function of pressure for temperatures of 313 K and 353 K, enabling an analysis of the combined effects of temperature and pressure. The graphs depict the relative deviations relative to the expanded uncertainties for each evaluated property. Overall, the results are consistent with the findings presented in Table 6, demonstrating that Daridon's correlations show good agreement with experimental results. The deviations remain within the expected experimental uncertainties, regardless of the pressure conditions investigated. However, these correlations are currently limited to biodiesel alone and are not applicable for determining the thermophysical properties of diesel-biodiesel blends or biodiesel mixed with gases such as air, nitrogen, CO_2, or oxygen. This information is crucial for accurately describing the effect of blending diesel with biodiesels or injection and combustion processes. Initial efforts have been made to extend these correlations to fatty acid methyl ester + hydrocarbons mixtures Bazile et al. (2024 e Daridon et al. (2023) but further development is still needed to extend it to biodiesels + petrodiesels blends. Although calculations based on the PC-SAFT equation of state may exhibit slightly higher deviations compared to certain specific correlations in representing thermophysical data, this methodology stands out for its theoretical robustness and its ability to derive a wide range of thermodynamic properties for systems under varying temperature and pressure conditions using the adjusted parameters. With the obtained parameter set, deviations from experimental data remain below 5%, highlighting the model's strong agreement with the data. Furthermore, PC-SAFT enables predictive analyses in commercial software Ayad et al. (2018 e Chen; Kreglewski (1977b e Da Costa; Medeiros; et al. (2024), allowing the prediction

of mixture effects with diesel or light gases without requiring additional experimental data. This establishes PC-SAFT as a versatile and powerful tool for practical engineering applications.

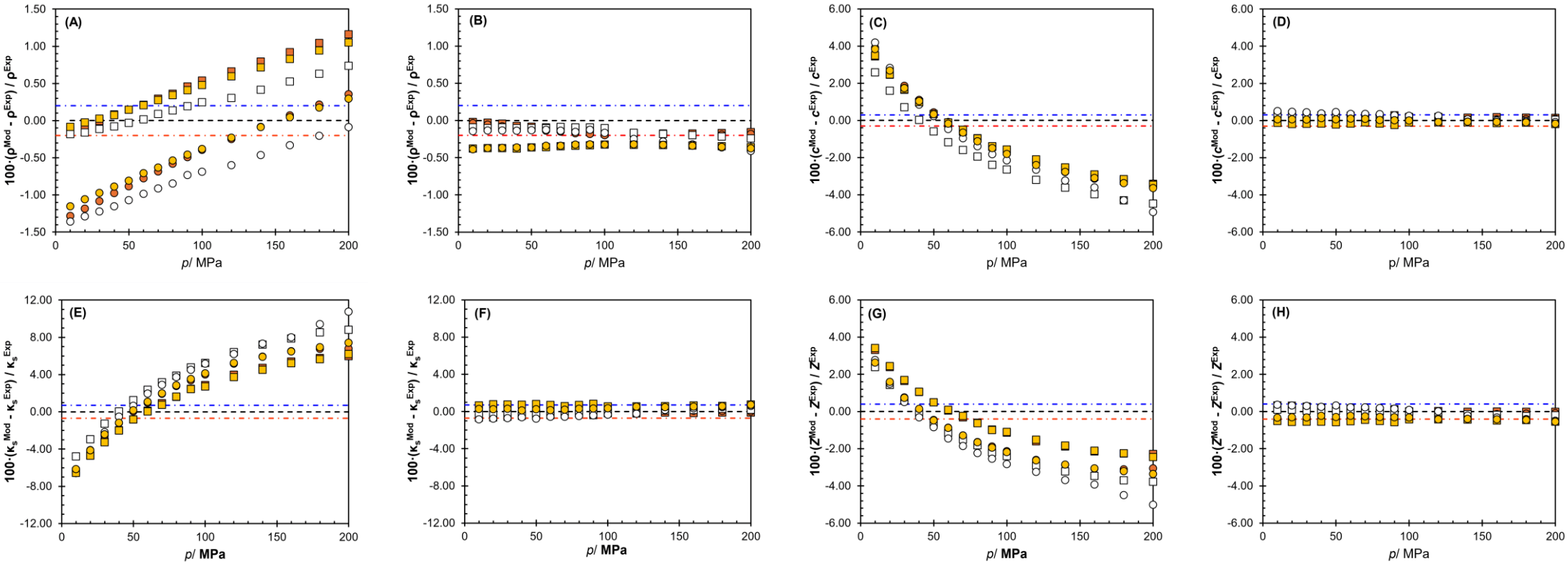

Figure 16 – Deviations between experimental data and the values predicted by the models studied for density, speed of sound, isentropic compressibility, and acoustic impedance. The white symbols represent coconut biodiesel, the orange ones sucupira biodiesel and the yellow one's canola biodiesel. The (■) indicates data at 313 K, while the (●) represents 353 K. Graphs A, C, E, and G refer to the PC-SAFT equation, and graphs B, D, F, and H are based on Daridon's models. The black dotted line indicates the zero deviation, while the red and blue dashed and dotted lines represent the uncertainties associated with each property: 0.2 for ρ, 0.3 for c, 0.7 for , and 0.4 for Z. (Created by the author, 2025)

3.5 Conclusion

Speed of sound and density measurements were conducted on three methyl biodiesels derived from coconut, sucupira, and canola oils, covering pressures up to $200\ MPa$ and temperatures between 293.15 and $373.15\ K$. The experimental data generated 235 new speed of sound points and 558 density values. From these properties, isentropic compressibility and acoustic impedance were determined, offering essential insights into biodiesel's thermodynamic and acoustic behavior, with direct implications for optimizing the performance of injection systems in diesel engines. Various models were evaluated to predict the studied properties (ρ, c, κ_s and Z). The PC-SAFT equation of state was applied, combining experimental density and speed of sound data to obtain a new set of parameters for each biodiesel studied. Additionally, two correlations (Daridon Daridon (2020, 2022b)) were tested to predict the thermophysical properties of methyl biodiesel up to 200 MPa based on fatty acid methyl ester composition. These correlations Daridon (2020, 2022b) generally outperformed PC-SAFT, with significantly lower mean absolute percentage deviations (MAPD) from experimental data. For density, the MAPD observed was three times higher with PC-SAFT than with the correlation proposed by Daridon for density Daridon (2020) (0.65/0.21). This difference was even higher for speed of sound with deviations obtained with PC SAFT twelve times greater than those obtained with the correlation developed specifically for speed of sound (2.03/0.17). Despite the larger deviations observed with the PC-SAFT equation compared to the specific correlations, the deviations remain acceptable, and the state equation can still be used to describe the thermodynamic behavior of biodiesels.

4 EXPERIMENTAL STUDY OF THE ISOBARIC HEAT CAPACITY OF DIFFERENT BIODIESELS AND EVALUATION OF A CORRESPONDING STATES MODEL DEVELOPED FOR PURE ESTERS, APPLIED TO BIODIESEL USING MIXING RULES

Results published in: *Biodiesel Isobaric Heat Capacity: A Comprehensive Assessment through Experimental Evaluation and Prediction with a Corresponding States Model*. Fuel 2025, 379, 13300. https://doi.org/10.1016/j.fuel.2024.133003.

4.1 Introduction

In the previous chapter of this thesis, the density and speed of sound of three different biodiesels were investigated through both experimental and modeling approaches, considering each biodiesel in its pseudo-pure state. Within this context, heat capacity was employed to support the extrapolation of density data up to 200 MPa.

In the present chapter (Chapter 3), the focus shifts to a detailed investigation of heat capacity, expanding the analysis to a broader range of biodiesels. The heat capacities of the three biodiesels previously studied are now complemented by experimental data obtained for seven additional biodiesels, using the Differential Scanning Calorimetry (DSC) technique. In addition, various values available in the literature were incorporated Dzida (2007 e Habrioux et al. (2013a, 2023 e De Lima et al. (2011 e Narváez et al. (2008 e Pauly et al. (2014), enabling the construction of an extensive database on the heat capacity (C_p) of biodiesels. This database encompasses 22 biodiesel types within the temperature range of 282 to 425 K and comprises a total of 460 data points.

With this comprehensive database, it was possible to analyze the behavior of heat capacity as a function of temperature at atmospheric pressure and the feedstock origin of the biodiesel. Furthermore, this study explores the applicability of a model based on the principle of corresponding states to predict the heat capacity of the constituent esters of biodiesel. Various methodologies were evaluated for representing this property, including the application of mixing rules and the adjustment of binary interaction parameters. Although originally developed for pure esters, the model was extended to biodiesel, which is, by definition, a complex mixture of esters. The objective was to assess the model's robustness in predicting the

heat capacity of multicomponent mixtures, while also investigating potential limitations and the need for adjustments to better capture the compositional diversity of the biodiesels studied.

Heat capacity not only influences the thermal behavior but also shapes process design and combustion efficiency, which are fundamental aspects for advancing the effectiveness and sustainability of biodiesel as an energy source Bogatishcheva et al. (2017a e Villazón-León; Bonilla-Petriciolet; Tapia-Picazo, J. C.; et al. (2024). Therefore, knowledge of heat capacity in addition to density, viscosity, and speed of sound is essential for optimizing the injection process in a diesel engine when using biodiesel from different raw materials.

While a vast database is available for density, viscosity, and speed of sound for biodiesel, there is a limited one on heat capacity. For the ester components of biodiesel in its pure state, there is a significant amount of data at both atmospheric Agafonova et al. (2011 e Bogatishcheva et al. (2017b, 2019 e Dzida et al. (2013 e Liu et al. (2019 e Van Miltenburg; Oonk (2005 e Pauly et al. (2014 e Żarska et al. (2022) and high pressures Liu et al. (2015, 2016, 2017 e Su et al. (2018). However, the number of studies reporting specific data on the heat capacity of biodiesel is small. Studies such as Narvárez et al. Narváez et al. (2008) and Habrioux et al. Habrioux et al. (2013a, 2023) have reported C_P data for more common methyl biodiesels, including palm, soy, rapeseed, and sunflower. Pauly et al. Pauly et al. (2014) presented innovative data on palm, soy, and sunflower biodiesel blends. Dzida and Prusakiewicz Dzida; Prusakiewicz (2008) reported data on three commercial fuels, including biodiesel, and used other properties to calculate heat capacity at high pressures. Lima et al. De Lima et al. (2011) also provided data on ethyl biodiesels derived from palm, coconut, castor, and animal fat.

As previously highlighted, one of the main objectives of this study was to expand the existing database on the heat capacity of various methyl biodiesels derived from different feedstocks, including palm, soybean, canola, coconut, cotton, sucupira, grape seed, corn, and sesame, all of which were analyzed throughout this thesis.

Furthermore, in relation to the other objective of this work, the investigating C_P modeling is essential for gaining a deeper understanding of biodiesel's thermal characteristics. Using modeling approaches allows for the prediction of C_P variation under different operating conditions. Such modeling yields valuable insights into the thermal properties, serving as a cornerstone for ongoing innovation in pursuing sustainable energy alternatives. An illustrative example is the application of Computational Fluid Dynamics (CFD), a powerful tool for simulating processes in internal combustion engines. CFD provides pertinent information at lower operating costs and in a shorter time than experimental methods. However, ensuring the accuracy of CFD simulations necessitates exact input data on the thermophysical properties of

biodiesel Azad et al. (2016 e Do Carmo, F.R. et al. (2020 e Ismail et al. (2012 e Nancarrow et al. (2015 e Villazón-León; Bonilla-Petriciolet; Tapia-Picazo, J. C.; et al. (2024).

Given this context, do Carmo et al. Do Carmo, F.R. et al. (2020) conducted a rigorous model evaluation procedure for the prediction of the C_P of Fatty Acid Methyl Ester (FAME) and Fatty Acid Ethyl Ester (FAEE) type esters. A total of eight models were evaluated, incorporating concepts such as group contribution (CG) Ceriani et al. (2009 e Kolská et al. (2008 e Růžička; Domalski (1993a, 1993b e Zábranský; Růžička (2004, 2005) and the principle of corresponding states (PEC) Bondi (1966 e Reid et al. (1987, 1959). In the same study, do Carmo et al. proposed a new corresponding states model to estimate the isobaric heat capacities of fatty acid esters. They concluded that the developed model showed greater precision than the others evaluated, demonstrating thermodynamic consistency through procedures tested by the authors Do Carmo, F.R. et al. (2020). The good predictive capability of the model they proposed for pure esters motivated us to attempt to extend this model to predict the heat capacity of biodiesels.

4.2 Experimental measurements

4.2.1 Materials

A homogeneous transesterification reaction employing methanol (Sigma, molar fraction purity 0.999) was carried out to produce the biodiesels investigated in this work. The molar ratio of oil to alcohol was kept at 1:6. Refer to the methodology outlined elsewhere Nogueira et al. (2010, 2012a, 2015a) for comprehensive details. The fatty acid methyl ester (FAME) profile analysis was conducted through gas chromatography coupled to mass spectrometry, utilizing an Agilent instrument model GC-7890B/MSD-5977A. All the biodiesels evaluated had an ester content of more than 97.0% by mass, meeting the quality criteria established by the ASTM D6751 specification for biodiesel, which defines a minimum requirement of 96.5% by mass of esters to be considered biodiesel. Molar compositions and molar masses of the investigated biodiesels are detailed in Table 7. It can be observed that most biodiesel has a molar mass ranging between 285 and 295 g/mol, except for coconut biodiesel. This is because of the predominantly composition of unsaturated fatty acids with long chains, such as monounsaturated MeC18:1 (M=296.5 g.mol^{-1}) and polyunsaturated MeC18:2 (M=294.5 g.mol^{-1}) fatty acid methyl esters. However, coconut biodiesel triglycerides are primarily composed of saturated fatty acids Bezard et al. (1971), with over 90% of its fatty acids having

a medium-chain length, i.e., methyl laurate (M=214.3 g.mol^{-1}), caprate (M=186.3 g.mol^{-1}), and even caprylate (M=158.2 g.mol^{-1}) fatty acid methyl esters.

Table 7 – Profiles of fatty acid methyl esters (FAME) in mol% and molar mass (M) in g/mol for the studied methyl biodiesels. FAME refers to the esters present in the profile of each biodiesel, and each acronym represents a different biodiesel.

FAME	biodiesels studied in this work (acronyms)[a]									
	CC	**SC**	**GS**	**CT**	**SS**	**PL1**	**CR**	**PL2**	**CN**	**SB**
MeC8:0	8.48	0.00	0.00	0.00	0.00	0.00	0.00	0.00	0.00	0.00
MeC10:0	7.61	0.00	0.00	0.00	0.00	0.00	0.00	0.13	0.00	0.03
MeC12:0	49.35	0.00	0.00	0.00	0.00	0.00	0.00	0.20	0.00	0.00
MeC14:0	19.98	0.00	0.00	0.57	0.00	0.00	0.00	1.15	0.00	0.09
MeC16:0	8.19	13.22	6.62	0.34	16.72	30.69	13.92	41.71	5.59	3.96
MeC16:1	0.00	0.00	0.00	25.76	0.00	0.00	0.00	0.28	0.00	0.51
MeC18:0	2.58	4.35	4.32	3.13	4.64	4.06	0.00	3.70	2.44	1.60
MeC18:1	3.81	31.92	28.79	20.06	39.09	56.64	36.62	41.07	71.68	57.12
MeC18:2	0.00	50.51	59.97	50.15	39.06	8.61	48.66	11.20	18.88	34.82
MeC18:3	0.00	0.00	0.30	0.00	0.00	0.00	0.80	0.00	0.00	0.00
MeC20:0	0.00	0.00	0.00	0.00	0.49	0.00	0.00	0.28	0.51	0.41
MeC20:1	0.00	0.00	0.00	0.00	0.00	0.00	0.00	0.14	0.91	1.02
MeC22:0	0.00	0.00	0.00	0.00	0.00	0.00	0.00	0.06	0.00	0.20
MeC22:1	0.00	0.00	0.00	0.00	0.00	0.00	0.00	0.02	0.00	0.05
MeC24:0	0.00	0.00	0.00	0.00	0.00	0.00	0.00	0.06	0.00	0.20
M/g.mol^{-1}	222.95	292.12	293.63	287.92	291.59	288.41	291.85	284.69	295.11	295.29

[a] CoConut (CC), SuCupira (SC), Grape Seed (GS), CoTton (CT), CoRn (CR), SaSame (SS), PaLm 1 (PL1), CaNola (CN), SoyBean (SB), PaLm 2 (PL2).

4.2.2 Differential Scanning Calorimetry (DSC) Measurements

The calorimetric analyses were performed using the Micro DSC 7 evo microcalorimeter (SETARAM). Operating under atmospheric pressure, this device captures calorimetric signals that depict the differential heat exchange between two distinct cells. The sample under analysis is placed in one cell house, while the other is either empty or filled with a reference fluid.

Each cell is outfitted with flat flow meters that span the entire programmed temperature range, exhibiting sensitivity ranging from 0.02 μW to 0.002 μW and covering

temperatures from 228 K to 393 K. To counteract parasitic effects, the two flow meters are strategically placed in opposition within each cell.

The detailed uncertainty assessment process is outlined in another study (Pauly et al. Pauly et al. (2014)), wherein the expanded uncertainties, with a confidence level of 0.95 (k = 2), were determined as 0.01 K and 0.005 mW based on estimates provided by the calorimeter manufacturer, 0.0001 g from the balance manufacturer. The uncertainty of the heat capacity of the reference fluid used (n-decane) is 0.3% for the temperature below 313 K and 0.5% above Pauly et al. (2014 e Zábranský et al. (2010). Combining these different sources of uncertainty using a quadratic propagation approach leads to a relatively combined expanded uncertainty $U_r(C_p) = 1\%$, with a confidence level of 0.95 (k = 2).

4.3 Modeling

4.3.1 Predictive Model for Isobaric Heat Capacity (C_p)

This study aims to assess the predictive capability of a model Do Carmo, F.R. et al. (2020) rooted in the corresponding state's theory for isobaric heat capacity. While the original model was developed for pure fatty acid alkyl esters, this research focuses on its extension to biodiesels, i.e., mixtures of fatty acid alkyl esters. The model under analysis is based on the equation proposed by Poling, Prausnitz, and O'Connell Reid et al. (1987) but has been improved to predict the molar heat capacity C_P of pure esters involved in biodiesel composition. It takes the following form:

$$\frac{C_{Pm}-C_{Pm}^{IG}}{R} = 1.586 + \frac{0.49}{1-T_r} + \omega \cdot \left[4.3164 + 5.5558\frac{(1-T_r)^{1/3}}{T_r} + \frac{5.0610\cdot 10^{-2}}{1-T_r}\right] \quad (4.1)$$

Here T_r is the reduced temperature (T/T_C), ω is the acentric factor while R in the equation stands for the ideal gas constant. The critical temperature (T_C) and acentric factor (ω) values were obtained from Evangelista et al. (2018) and are listed in **Table C2** (Appendix C) for all fatty acid methyl esters involved in methyl biodiesels. Finally, C_{Pm}^{IG} is the heat capacity of ideal gas. It is obtained using the Joback and Reid method Joback; Reid (1987), as recommended by the model's authors Do Carmo, F.R. et al. (2020).

4.3.2 Methodology for Calculating Heat Capacity and Critical Properties

As discussed in the previous section and as indicated by Equation 4.1, determining the molar heat capacity of a pure component using a corresponding state method necessitates knowledge of critical properties, the acentric factor, and the molar mass of the compound in question. However, these properties are not defined in the case of mixtures. Therefore, a strategy must be develop to adapt the method for use with mixtures. For that purpose, two distinct approaches were explored for predicting biodiesel C_P from their fatty acid alkyl esters profile.

The first one is to apply a combination rule directly to heat capacity. This could be referred to as an internal combining rule. A simple additive combination was retained since biodiesel fuels comprise fatty acid alkyl ester with alkyl chain lengths ranging from 9 to 25 carbons. Assuming that the mixture excess heat capacity is negligible, biodiesel molar heat capacity ($C_{P,bio}$) is related to the values of the pure components according to the following linear combination:

$$C_{P,bio} = \sum_{i=1}^{n} x_i \cdot C_{P\,i} \tag{4.2}$$

where x_i is the mole fraction of compound i, and C_{Pi} is the molar heat capacity of pure esters estimated based on their critical property values. **Tables C3 and C4** (Appendix C) give C_{Pi} values for each ester found in biodiesel for the temperature range studied here (T = 293 to 393 K).

The second approach involves characterizing biodiesel as a pseudo-component and using mixing rules to determine its pseudo-critical temperature ($T_{c,bio}$) and its acentric factor (ω_{bio}). This methodology relies on the critical properties of the individual components as the basis for our analysis and does not require knowledge of the heat capacity of pure components. It could be referred to as an external combining rule.

We applied mixing rules to obtain the critical properties based on the methodologies proposed by do Carmo et al. Do Carmo; Evangelista; Fernandes, Fabiano A. N.; et al. (2015a), equations 4.3-4.7. The equations follow the guidelines indicated by Chueh and Prausnitz Chueh; Prausnitz (1967) and Spencer and Danner Spencer; Danner (1973).

$$\omega_{bio} = \sum_{i}^{n} x_i \cdot \omega_i \tag{4.3}$$

$$T_{c,bio} = \sum_{i}^{n} \sum_{j}^{n} \frac{x_i \cdot x_j \cdot V_{c,ij}^{1/4} \cdot T_{c,ij}}{V_{c,bio}^{1/4}} \tag{4.4}$$

with:

$$V_{C,bio} = \sum_i^n \sum_j^n x_i \cdot x_j \cdot V_{c,ij} \quad (4.5)$$

$$T_{c,ij} = \left(T_{c,i} \cdot T_{c,j}\right)^{1/2}\left(1 - k_{ij}\right) \quad (4.6)$$

$$V_{c,ij} = \frac{\left(V_{c,i}^{1/3} + V_{c,j}^{1/3}\right)^3}{8} \quad (4.7)$$

In the given equations, the variables are defined as follows: n denotes the number of ester components in biodiesel and $V_{c,i}$ stands for the critical volume of pure component i. The values of $V_{c,i}$ for all the FAME ranging from methyl caprylate to methyl lignocerate have been included in **Table C2** (Appendix C) along with $T_{c,i}$ and M_i. The binary interaction parameter k_{ij} was added in equation 4.6 to account for the asymmetry between i and j components. Its value is set to zero for a component belonging to the same chemical family and with a slight difference in chain length, as usual in biodiesel fuels.

To improve understanding of the procedures adopted in this work, we present a schematic flowchart in Figure 17. This diagram summarizes steps taken during the study methodology, providing a more precise and comprehensive view of the work.

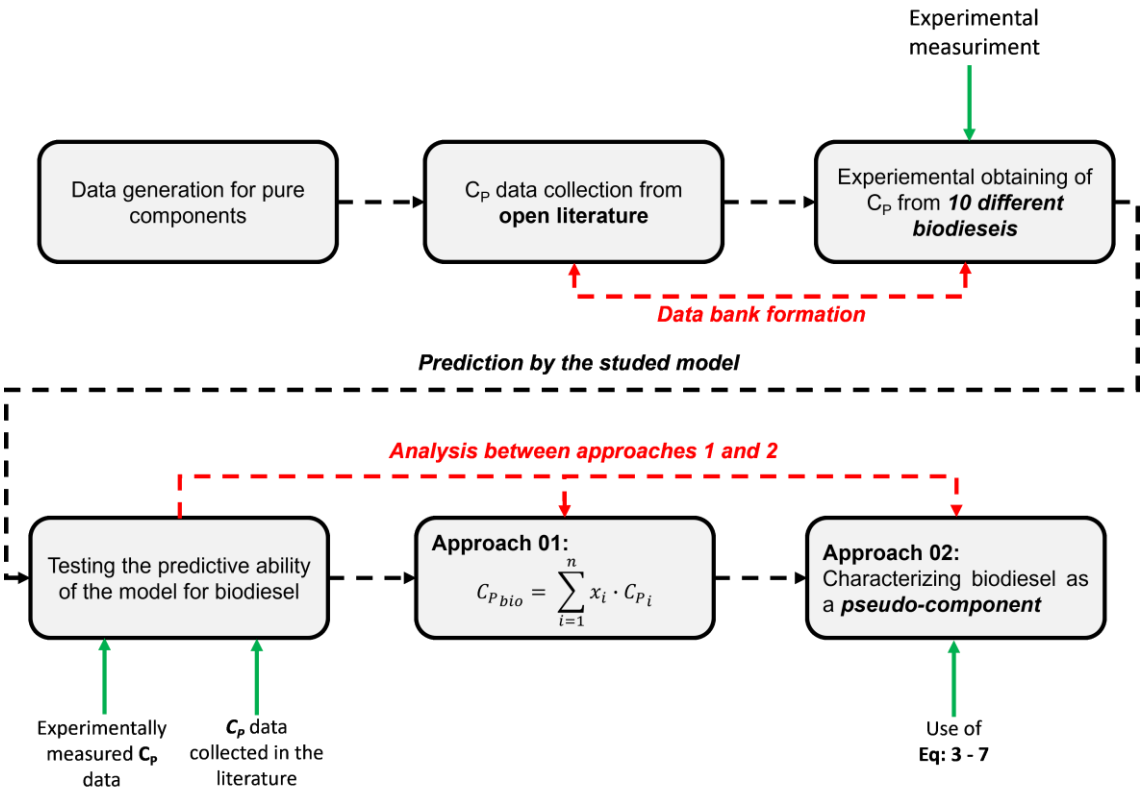

Figure 17 – Flowchart of the methodology used in this work, which includes the creation of

the evaluated model, the formation of the database, the statistical evaluation of the model, and the use of methodologies with different approaches to applying the model. (Created by the author, 2025)

In assessing the model's performance, we utilize two statistical parameters: mean percentage deviation (MPD) and mean absolute percentage deviation (MAPD). They are outlined in Equations (4.8) and (4.9) below.

$$\mathrm{MPD} = \frac{1}{\mathrm{N_{data}}} \sum_{\mathrm{i=1}}^{\mathrm{N_{data}}} \frac{\mathrm{C_{P_i}^{CALC}} - \mathrm{C_{P_i}^{EXP}}}{\mathrm{C_{P_i}^{EXP}}} \times 100 \tag{4.8}$$

$$MAPD = \frac{1}{N_{data}} \sum_{i=1}^{N_{data}} \left| \frac{C_{P_i}^{CALC} - C_{P_i}^{EXP}}{C_{P_i}^{EXP}} \right| \times 100 \tag{4.9}$$

4.4 Results and discussion

4.4.1 Experimental Measurements of Isobaric Heat Capacity (C_P) for Biodiesels Studied

The molar heat capacities of ten different biodiesels were measured for temperatures ranging from 297 to 387 K at atmospheric pressure, as shown in Table 8. It is also given in this table the second-order polynomial ($C_P = a_0 + a_1 T + a_2 T^2$) parameters used for interpolated heat capacity data for the whole temperature range. The observed (R^2) values greater than 0.999 show that such a second-order polynomial is enough to fit C_P data within this limited temperature range.

When analyzing the relationship between heat capacity and temperature in Figure 18, it is notable that sucupira (SC) and soybean (SB) biodiesels exhibit similar behavior in response to temperature variations. The curves display comparable slopes, implying a consistent thermal behavior pattern. This similarity has been observed with most biodiesels, except those produced from coconut oil feedstock. Furthermore, it is essential to emphasize that the ester profile influences the heat capacity values of biodiesels. For instance, upon observing Figure 18, it can be seen that sucupira (SC) exhibits a lower molar thermal capacity compared to Soybean (SB) biodiesel, which contains esters with higher molecular weights.

Table 8 – Experimental data on Isobaric Heat Capacity (C_P) or different biodiesels at various temperatures (T) and parameters of second-degree polynomial equations ($C_P = a_0 + a_1 T + a_2 T^2$) fitted to experimental data.

T/K	Isobaric heat capacity (C_P) for biodieseis studied* / ($J \cdot mol^{-1} \cdot K^{-1}$)									
	CC	**SC**	**GS**	**CT**	**SS**	**PL1**	**CR**	**PL2**	**CN**	**SB**
297.91	460.1	575.8	583.8	580.9	585.4	590.1	592.3	593.2	593.6	595.6
307.79	464.7	583.1	591.2	588.2	592.2	596.6	599.5	600.2	601.1	602.9
317.66	469.5	591.0	598.1	595.8	600.0	604.0	607.3	607.3	608.8	610.6
327.54	475.0	599.1	605.0	602.8	608.2	612.0	615.3	615.2	617.0	617.4
337.42	480.5	607.2	613.4	610.5	616.7	619.9	623.5	622.1	625.2	625.4
347.29	485.8	615.1	621.4	618.1	625.1	626.6	632.1	629.5	633.0	633.0
357.17	491.2	623.5	630.2	625.8	633.7	633.5	641.1	638.1	640.7	640.9
367.05	496.9	632.8	639.4	633.6	642.8	641.7	650.8	647.3	649.1	649.5
376.92	503.7	641.8	649.4	641.6	651.6	651.6	660.4	655.5	657.3	657.8
386.80	510.1	650.8	658.5	649.5	662.0	659.5	669.6	663.3	665.7	667.7
Parameters	$C_P = a_0 + a_1 T + a_2 T^2$									
	CC	**SC**	**GS**	**CT**	**SS**	**PL1**	**CR**	**PL2**	**CN**	**SB**
a_0	415.852	452.773	570.736	405.693	490.661	470.831	518.680	488.109	390.821	505.010
$a_1/10^2$	-16.869	8.075	-56.831	44.697	-10.121	10.714	-23.692	1.283	57.868	-7.636
$a_2/10^4$	10.646	11.151	20.581	4.742	14.073	9.834	16.238	11.410	3.407	12.813
R^2	0.999	0.999	0.999	0.999	0.999	0.999	0.999	0.999	0.999	0.999

[a] SuCupira (SC), Grape Seed (GS), CoRn (CR), CoConut (CC), CaNola (CN), SaSame (SS), CoTton (CT) PaLm 1 (PL1), SoyBean (SB), and PaLm 2 (PL2).

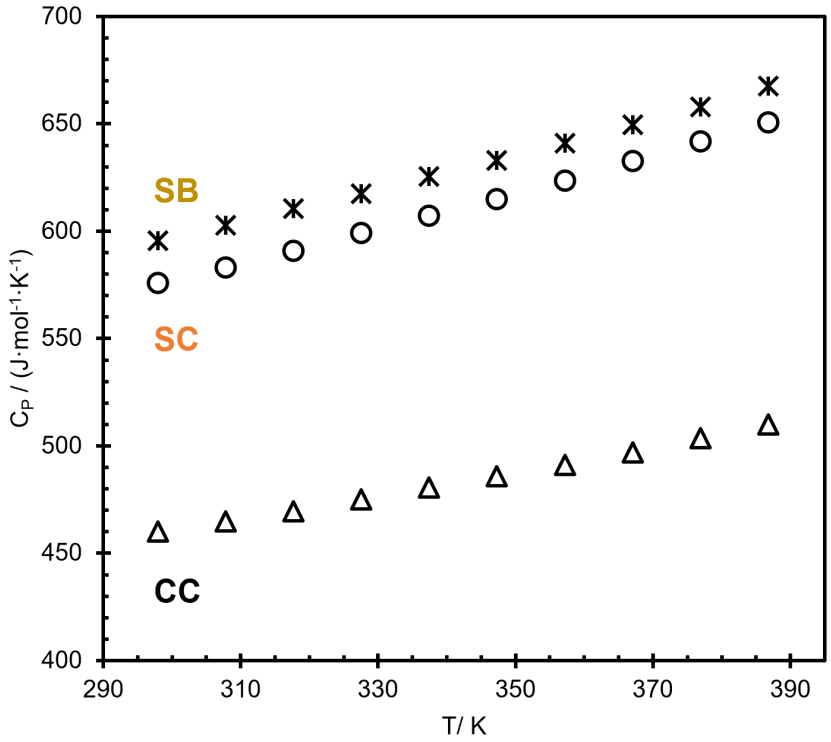

Figure 18 – Comparison of isobaric molar heat capacity (C_P) as a function of temperature (T) for three different biodiesels: (∗) soybean (SB) biodiesel, (○) sucupira (SC) biodiesel, and (△) coconut (CC) biodiesel. (Created by the author, 2025)

The difference between coconut (CC) and soybean (SB) biodiesels is remarkably noticeable, with a mean absolute percentage deviation (MAPD) of 23%. This deviation, of the same order of magnitude as the molar mass deviation between the two biodiesels, decreases drastically when the specific heat capacity is considered instead of the molar mass. In this case, the mean absolute deviation between the heat capacities decreases to only 2%.

4.4.2 Evaluation of the Prediction of the Heat Capacity of Biodiesel

As discussed in Section 4.3.2, we have employed two methodologies based on internal or external combining rules to acquire biodiesel heat capacities. The objective here is to compare whether both approaches have the same predictive capacities and assess whether the incorporation of a mixing rule influences the quality of the results compared with those obtained for pure components. It also aims to determine whether incorporating binary interaction parameters (k_{ij}) influences the results of external combinations.

Figure 19 illustrates the disparities between the experimental data and the model-calculated values for each of the investigated approaches for biodiesel: canola (CN) biodiesel. Notably, the results obtained from the two methods are consistent when k_{ij} is set to zero for all

i-j interactions. To compare the predictive capacities of the model for mixtures (biodiesel) with the results obtained for pure fatty acid alkyl esters, the deviations between calculated and experimental values Ndiaye et al. (2013c) for pure methyl oleate (MeC18:1) were added to Figure 19. This compound was chosen as it represents the main component of canola biodiesel (71.7 mol%). As depicted in Figure 19 (blue square symbols), the deviation observed for this component is of the same magnitude (around 1% on average) as those found for canola biodiesel. The deviation curves appear nearly parallel in the figure. This finding shows that the primary source of error in heat capacity prediction for biodiesel results from pure component prediction rather than from the combining rules that can be used interchangeably.

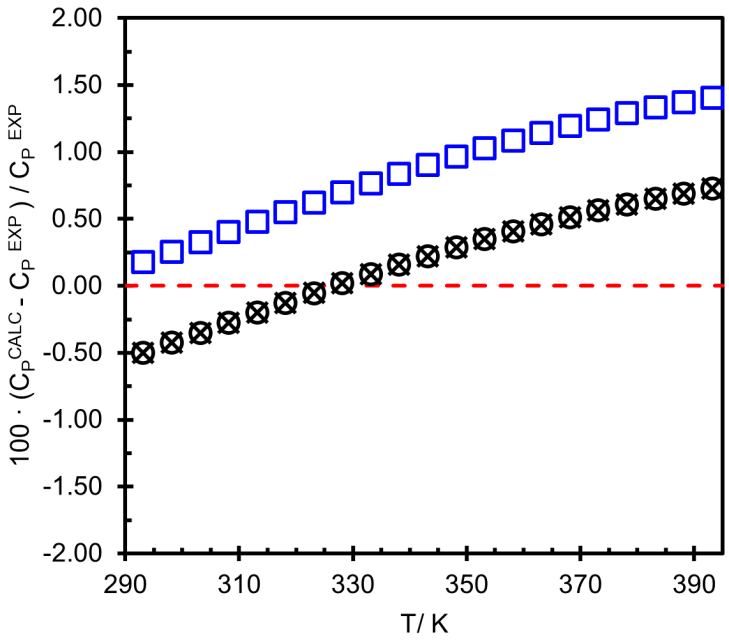

Figure 19 – Relative deviations between calculated and experimental isobaric heat capacity vs. canola (CN) biodiesel temperature. (×) deviations using approach 1 (eq. 2), (○) deviations using approach 2 (eq. 3 – 8) with k_{ij} = 0.0, and (□) deviation from experimental data Ndiaye et al. (2013c) for pure methyl oleate (MeC18:1).

Significant deviations between the two approaches were not observed throughout all the biodiesels investigated, as summarized in Table 9. This figure shows the disparities between the heat capacities calculated by both methods and the experimental data. Biodiesels derived from different raw materials – sucupira, grape seed, corn, coconut, canola, sesame, cotton, palm, soybean, and sunflower, obtained experimentally in this work and from literature – were considered to assess the predictive capacity of the methods under investigation. The data sources can be found in **Table C1** in Appendix C: Complementary Material to Chapter 4.

However, it is worth noting that only a few studies were conducted to provide biodiesel experimental heat capacities. The uncertainty of the reported data is often not specified in these publications. Sometimes, the heat capacity (C_p) is not provided as experimental data but rather through correlations.

Although additional datasets are available, as in the study by Dzida and Prusakiewicz Dzida; Prusakiewicz (2008), heat capacity data from these sets are not included in **Table C1**. This is attributed to the need for more information on the FAME (fatty acid methyl esters) profile for these biodiesel fuels. Similarly, the study by de Lima et al. De Lima et al. (2011) provides information on six biodiesels with different FAEE (fatty acid ethyl esters) profiles. However, only three of these datasets were added to our database due to difficulties in obtaining coherent heat capacity values from the equations provided by the authors to correlate their experimental data. The comparative tests also incorporated the biofuels' heat capacity data from blending palm, rapeseed, and soy biodiesels Dzida et al. (2013 e Van Miltenburg; Oonk (2005). The statistical analysis presented in Table 9 refers to evaluating the model's capacities on twelve biodiesels from the literature and another ten biodiesels produced in this work. The fatty acid alkyl ester profiles of each biodiesel, normalized to 100, are summarized in Table 1 for those obtained experimentally in this study and **Table C5** for the biodiesels found in the literature. The complete database comprises 460 data points from 22 biodiesels, with the majority belonging to the FAME (methyl esters) category and a few to FAEE (ethyl esters). This database under atmospheric pressure encompasses a wide temperature range, from 282 to 425 K.

Table 9 – Statistical results (MAPD and MPD) for model prediction of isobaric heat capacity (C_P) data from the literature and experimental using approaches 1 (Eq. 4.2) and 2 (Eq. 4.3 – 4.7), with k_{ij} = 0.0.

Ref.	soucer biodiesel	acronym[a]	statistical parameter			
			Approach 01		Approach 02	
			MAPD	*MPD*	*MAPD*	*MPD*
FAME						
This work	Sesame	SS	0.177	-0.177	0.182	-0.182
This work	Soybean	SB	0.359	-0.359	0.361	-0.361
This work	Canola	CN	0.365	0.182	0.365	0.181
Habrioux et al. (2023)	PL + RS + SB[b]	MB-PRS	0.357	-0.357	0.366	-0.366
This work	grape seed	GS	0.389	0.331	0.388	0.329
Habrioux et al. (2023)	sunflower	MB-SF	0.426	0.401	0.423	0.397
This work	Palm	PL1	0.743	-0.743	0.750	-0.750
This work	Coton	CT	0.916	-0.916	0.920	-0.920

This work	coconut	CC	0.829	-0.829	0.936	-0.936
Pauly et al. (2014)	PL + RS + SB[b]	B1	0.961	0.961	0.956	0.956
This work	sucupira	SC	1.282	1.282	1.279	1.279
Pauly et al. (2014)	PL + RS + SB[b]	B2	1.301	1.301	1.296	1.296
Pauly et al. (2014)	rapeseed	BR	1.349	1.334	1.345	1.329
Pauly et al. (2014)	soybean	BS	1.620	1.620	1.615	1.615
Habrioux et al. (2013a)	rapeseed	R	1.686	-1.686	1.691	-1.691
This work	Corn	CR	1.719	-1.719	1.722	-1.722
Habrioux et al. (2013a)	soybean	S	2.282	-2.282	2.287	-2.287
This work	palm	PL2	2.565	-2.565	2.576	-2.576
Narváez et al. (2008)	palm	TG	5.498	5.264	5.490	5.253
FAEE						
De Lima et al. (2011)	coconut	CCN	2.741	3.016	2.644	2.958
De Lima et al. (2011)	palm	PLN	16.353	16.353	16.341	16.341
De Lima et al. (2011)	castor	CAN	20.410	-20.288	20.420	-20.300

[a] Acronym assigned by the reference.
[b] PL + RS + BB: mixture between palm biodiesel, rapeseed, and soybean.

Figure 19 and Table 9 show that the two approaches are equivalent. Adding a mixing rule does not bring about any significant deviation in the model from what was previously obtained for pure components. The deviation shown in Table 9 reveals that most of the mean deviations calculated for each biodiesel fall within a mean absolute percentage deviation (MAPD) lower than 2%. In particular, the model exhibits excellent agreement with the experimental data obtained for sesame biodiesel (SS), with the lowest MAPD of 0.18%. Palm biodiesel (TG) and (PL2) show the most significant discrepancies, with MAPDs of 5.49% and 2.57%, respectively.

Interestingly, the two highest deviations observed were FAME-type biodiesels originating from palm oil. However, a third palm biodiesel (PL1) was included in our dataset and exhibited a deviation of 0.743%, ranking 7th in terms of lowest MAPD among the 22 biodiesels evaluated. This difference could be attributed to impurities not considered in the normalized fatty acid profile. Finally, the mean percentage deviation (MPD) measures the model's relative accuracy concerning the observed data, indicating the systematic deviation between predictions and actual data regarding underestimation or overestimation. A comprehensive analysis of MPD values reported for methyl biodiesels reveals a variation between positive and negative values, indicating a non-systematic model deviation. These analyses underscore the remarkable robustness of the model in predicting C_P of biodiesels.

Figure 20 illustrates the relative deviations between the experimental C_P values and the model predictions for all the analyzed biodiesel samples. The analysis underscores the consistency and reliability of the model, as no significant systematic deviations are observed. This suggests that the model does not consistently underestimate or overestimate the thermal capacity of the studied biodiesels.

When analyzing deviations for ethyl biodiesel, we observed a smaller number of works carried out to evaluate the heat capacity of these biodiesels. This scarcity could be attributed to the limited availability of biodiesels produced with ethanol Verma; Sharma (2016). We identified only one reference providing heat capacity data for this specific biodiesel De Lima et al. (2011). Unfortunately, the data values were not directly reported in this work but in correlations with a R^2 lower than 0.9. We observed significant deviations (greater than 10%) in the model predictions from these correlations. One probable reason for these higher errors may be linked to the fact that the reported experimental values are significantly lower compared to the values observed for the primary components, C18:1 and C18:2 found in ethyl biodiesels. This is not realistic. Moreover, equations selected for the correlation of these experimental data, which consist of a logarithmic equation, have poor correlation coefficients. Consequently, the significant deviation found for these systems cannot be attributed to the predictive capacities of the model but rather to the inconsistency of data.

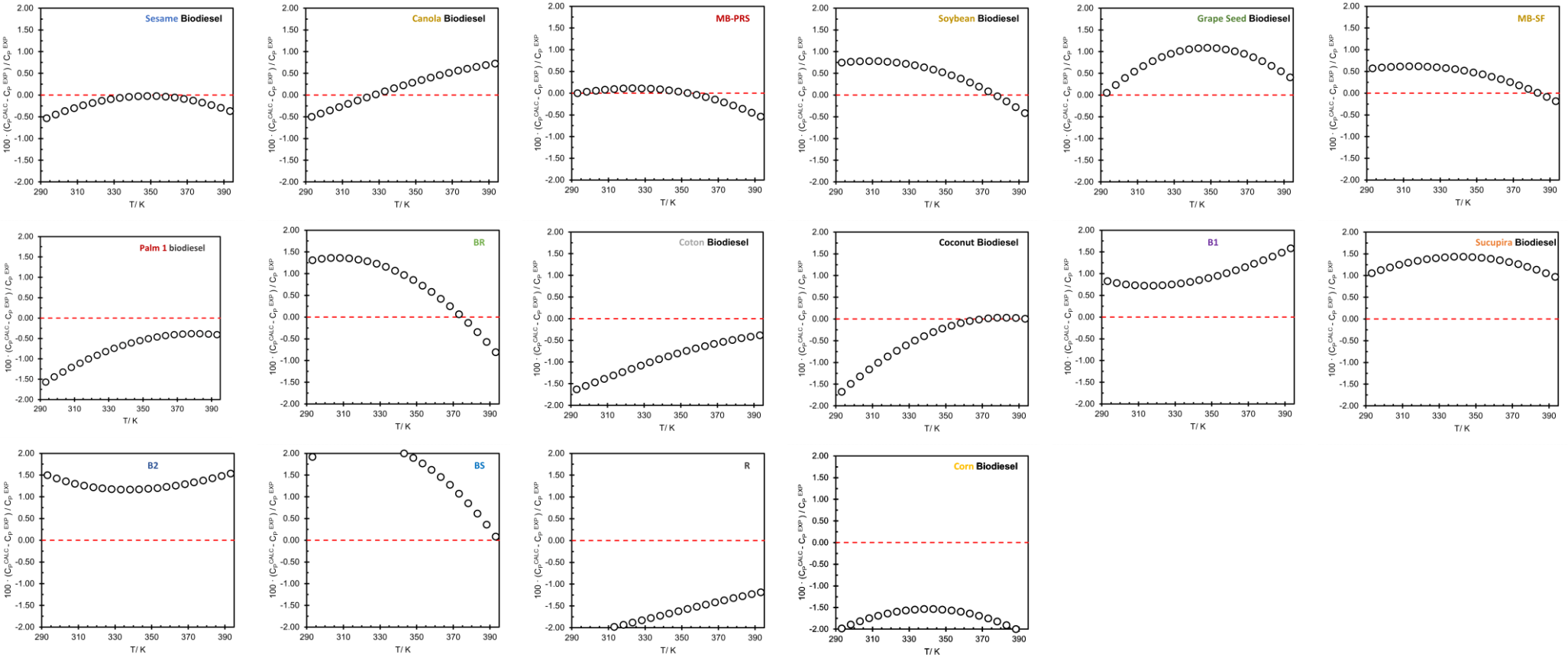

Figure 20 – Percentage deviation between calculated and experimental isobaric heat capacity (C_P) predictions versus temperature (T) for methyl biodiesels obtained in this work and from the literature using Approach 2 Eq. 4.3 – 4.7 ($k_{ij} = 0$). This is to observe the unsystematic behavior of the model. (Created by the author, 2025)

Including a new experimental data set for measurements of biodiesels is valuable information. Having a comprehensive database facilitated an extensive comparison between the model estimates considering k_{ij} equals zero and adjusted k_{ij} for all the data sets. For that purpose, a simple correlation was proposed to evaluate the binary interaction parameter k_{ij} between two fatty acid alkyl esters "*i*" and "*j*", as a function only of their critical temperatures and a single adjustable parameter k :

$$k_{ij} = k\frac{|T_{c,i}-T_{c,j}|}{T_{c,i}+T_{c,j}} \tag{4.10}$$

This expression, which considers the asymmetry between "*i*" and "*j*", yields a matrix k_{ij} representing the different binary interactions between biodiesel components without requiring specific adjustments for each binary mixture for which data are unavailable. After optimization, the value of $k = -3.7$ was obtained. However, Table 10 demonstrates that inserting this parameter into the model has a minor impact. The adjustment's impact is not prominent, revealing subtle variations in the model's performance and overall, achieving a reduction of 0.042% compared to the unadjusted model, with an overall deviation of 1.27%. Although some biodiesels display more significant changes, emphasizing the influence of k_{ij} on prediction accuracy, the overall variation remains modest. This outcome can be interpreted in connection with the predominant presence of ester in biodiesel composition. Esters, derived from fatty acids and alcohols, typically share closely related chemical structures, leading to relatively weak intermolecular interactions. The balancing act of van der Waals forces and dipole-dipole interactions between these esters tends to result in a k_{ij} value close to zero. Additionally, factors such as the mixture's composition, the similarity in polarity among the esters, and the specific temperature and pressure conditions may collectively contribute to the limited influence of k_{ij}.

In conclusion, this comparison between the use (or not) of the binary interaction parameters is reported in Table 10. It suggests that the proposed model does not require binary interaction parameters (k_{ij}) in the combining rule for predicting the heat capacity of methyl biodiesel. Without k_{ij}, the model for methyl biodiesels achieves an overall MAPD close to 1.3% from experimental data subject to uncertainty of 1%. These results are considered highly satisfactory, particularly considering that the model, initially designed for pure esters, demonstrates an overall performance of 0.9% for FAMEs, with an accuracy of 0.8% for

saturated esters and 1.0% for unsaturated esters, as reported by do Carmo et al. Do Carmo, F.R. et al. (2020). This consistent accuracy across various biodiesels derived from different oil sources underscores the versatility and robustness of the model in predicting the isobaric thermal capacity of these alternative fuels. However, it is essential to note that due to the limited amount of reliable data for ethyl biodiesel, it was impossible to address a conclusion for ethyl biodiesels. Nevertheless, no objective reason could lead to worse predictions in such systems than in methyl biodiesels.

It is important to note that there are no specific C_P prediction models for biodiesel, nor is there any literature that applies existing models to this biofuel. Clique ou toque aqui para inserir o texto. Recently, Villazón-León et al. Villazón-León; Bonilla-Petriciolet; Tapia-Picazo, J.C.; et al. (2024) proposed a model that exploits the synergy between group contributions and artificial neural networks, using an extensive database consisting of 22,715 experimental net heat capacity values for 441 different compounds, including esters. An important comparison made in this work was between the model's predictions and those obtained using Aspen Plus® process simulation software, widely used in industry worldwide. Villazon-León et al. reported that, for esters, Aspen Plus® shows deviations of 2.33%. In comparison, the results of our study demonstrate that the evaluated model is relevant and performs better, with an average relative absolute deviation of 0.86% for esters (as reported by do Carmo et al.) and 1.27% for biodiesels, highlighting its applicability and accuracy.

Table 10 – Statistical results for predicting the isobaric thermal capacity model (C_P) for all data considering adjusted k_{ij} ($k_{ij} \neq 0$) and difference between the same methodology using $k_{ij} = 0$ and adjusted ($k_{ij} \neq 0$).

Ref.	biodieseis studied	soucer biodiesel	$k_{ij} \neq 0$	$Variation\ MAPD$
			$MAPD$	$(k_{ij} = 0) - (k_{ij} \neq 0)$
This work	SS	sessame	0.129	0.053
Habrioux et al. (2023)	MB-PRS	PL + RS + SB[b]	0.143	0.223
This work	SB	soybean	0.261	0.100
This work	CN	canola	0.400	-0.035
This work	CC	coconut	0.436	0.500
This work	PL1	palm	0.455	0.295
This work	GS	grape seed	0.471	-0.083
Habrioux et al. (2023)	MB-SF	sunflower	0.554	-0.131
This work	CT	coton	0.682	0.238
Pauly et al. (2014)	B1	PL + RS + SB[b]	1.169	-0.214

This work	SC	sucupira	1.467	-0.188
Pauly et al. (2014)	B2	PL + RS + SB[b]	1.471	-0.175
Pauly et al. (2014)	BR	rapeseed	1.495	-0.150
Habrioux et al. (2013a)	R	rapeseed	1.532	0.158
This work	CR	corn	1.554	0.168
Pauly et al. (2014)	BS	soybean	1.833	-0.218
Habrioux et al. (2013a)	S	soybean	2.080	0.207
This work	PL2	palm	2.194	0.382
Narváez et al. (2008)	TG	palm	5.820	-0.330
Overall (FAME)	-	-	**1.270**	**-0.042**
De Lima et al. (2011)	coconut	CCN	3.851	0.893
De Lima et al. (2011)	palm	PLN	16.829	0.488
De Lima et al. (2011)	castor	CAN	20.198	-0.222
Overall (FAEE)	**-**	**-**	**13.626**	**+0.386**

4.5 Conclusion

In this study, we conducted experimental measurements of the isobaric heat capacity at various temperatures for 10 different biodiesels encompassing various oil sources. These measurements were carried out using Differential Scanning Calorimetry (DSC). Additionally, we augmented this data by including information from the open literature on these properties for 12 more biodiesels, resulting in a comprehensive database of 22 biodiesels covering a variety of oil sources and temperatures. These data were utilized to assess a predictive model based on the concept of corresponding states initially developed for esters, and the critical properties of these compounds were used as input parameters. This marks the first application of this model to biodiesel, which, by definition, is a mixture of esters. Within this context, we evaluated two methodologies for determining the heat capacity of biodiesel using the proposed model. The first approach treated biodiesel as a pseudo-component to derive its critical properties, with k_{ij}varying between 0 and an adjusted value. The second methodology involved a direct mixing rule between the C_P value of the pure ester (estimated by the model) and the biodiesel composition.

With an Overall Absolute Mean Percentage Deviation (MAPD) of 1.27% for biodiesels, the model showed no systematic deviations in its predictions. Minimal differences indicated a low dependence on the mixing rule. Additionally, modest variations were recorded even with k_{ij} adjustments, a reduction of 0.042 in the mean absolute percentage deviation of the property C_P, considering all the values in the database. These variations can be attributed to

the prevalence of ester-ester bonds in biodiesel, as esters often share related chemical structures, resulting in weak intermolecular interactions. Consequently, the balance of van der Waals forces and dipole-dipole interactions between these esters leads to k_{ij} values close to zero.

The results of this study suggest that the isobaric heat capacity prediction model is equally effective when applied to biodiesel. The model's versatility and practical applicability, evidenced by its successful extension to different types of biodiesels, underline its robustness. The significance of isobaric heat capacity data lies in its contribution to a deeper understanding of biodiesel's thermal behavior, providing valuable information for optimizing industrial processes and practical applications.

5 EXPERIMENTAL DETERMINATION AND ANALYSIS OF THE DENSITY BEHAVIOR OF 1-BUTANOL + BIODIESEL BLENDS AT HIGH PRESSURES: CONTRIBUTION TO THE UNDERSTANDING OF ALTERNATIVE FUEL SYSTEMS

Results published in: *Investigating the thermophysical properties of the 1-butanol + biodiesel system: the impact of pressure on volumetric characteristics*. Fuel 2024, 371, 132076. https://doi.org/10.1016/j.fuel.2024.132076.

5.1 Introduction

This chapter marks the beginning of the investigation into biodiesel and butanol blends, with the primary objective of understanding how the addition of this alcohol influences the properties of the resulting biofuel, focusing initially on density. The study of biodiesel blended with alcohol is essential for advancing their application as viable and sustainable alternatives to fossil fuels. Among the various alcohols, butanol has been widely recognized in the literature for its significant potential in fuel formulations Killol et al. (2019b e Kuszewski et al. (2023 e Thakkar et al. (2021b e Zheng et al. (2016b). Its unique physicochemical characteristics make it a particularly promising component in this context. To enhance the understanding of butanol and biodiesel mixtures and their practical use in internal combustion engines, it is crucial to evaluate their behavior under different operating conditions, especially under high-pressure and high-temperature (HPHT) conditions, as emphasized in previous research Razzaq et al. (2020 e Vargas-Ibáñez et al. (2020a e Wang et al. (2022 e Zaharin et al. (2017a).

Many environmental problems result from applications of fossil fuels and the harmful gases they produce, such as CO_2, NO_x, and CO. Several research projects seek to replace or reduce the utilization of these materials Aljaafari et al. (2022 e Canabarro et al. (2023 e Habrioux et al. (2013b). Consequently, alternative fuels are a growing area of research, mainly focused on developing biodiesel, aiming to reduce dependence on fossil fuels and mitigate harmful environmental impacts Erdiwansyah et al. (2019 e Payri et al. (2011a e Tamilselvan et al. (2017 e Żarska et al. (2014b).

Biodiesel is a class of ester-based materials produced from renewable sources. It is considered a potential substitute for fossil fuels for several reasons. Its biodegradability and various renewable production methods are key advantages Habrioux et al. (2013a). These

materials could be produced through a transesterification reaction of animal fats or vegetable oils along with an alcohol Pratas et al. (2011). Another highlight is the direct application of these materials in the cycle of diesel engines with minimal modifications needed Hoang et al. (2021).

While biodiesel applications offer numerous advantages, significant challenges arise due to its competition with the food industry and the associated high production costs. These factors could hinder its effective adoption as a replacement for fossil fuels (FERREIRA et al., 2021; MANSIR et al., 2018; ZAMBRANO et al., 2016). Another disadvantage is related to the fluidity of biodiesels in low-temperature operational conditions, which could be affected by their high viscosity and density Hazrat et al. (2020). This issue can be circumvented by several means, with one of the most attractive being the use of biodiesel + short/medium chain alcohol blend for property regulation Ait Belale et al. (2021 e Aitbelale et al. (2021 e Ferreira et al. (2021 e Kuszewski et al. (2023 e Wang et al. (2015c).

Evaluating biodiesel and alcohol mixtures is essential for understanding and enhancing their applications as fossil fuel alternatives. Butanol, is recognized in the literature as an excellent alcohol for such mixtures Killol et al. (2019b e Kuszewski et al. (2023 e Thakkar et al. (2021b e Zheng et al. (2016b). Therefore, to enhance our understanding of butanol + biodiesel blends and their effective engine applications, it is imperative to assess their properties under various operational conditions, particularly under high-pressure and high-temperature (HP-HT) conditions, as previously documented in the literature Razzaq et al. (2020 e Vargas-Ibáñez et al. (2020a e Wang et al. (2022 e Zaharin et al. (2017a).

The ability to correlate and predict volumetric behavior under HP-HT conditions is of significant interest due to the high cost and frequent inaccessibility of experimental data. Equations such as Tammann–Tait Dymond; Malhotra (1988) for correlation and PC-SAFT Chapman et al. (1990a) for prediction provide robust and reliable mathematical methods for describing fluid behavior under high pressure and high-temperature conditions. Utilizing these equations allows for extracting valuable information, such as derivative properties, regarding substance properties in extreme conditions without costly experiments. Furthermore, modeling offers the flexibility to explore various scenarios and compositions, contributing to a comprehensive understanding of substance behavior in challenging conditions.

The Tammann-Tait equation was widely used to represent volumetric properties of biofuel systems Ait Belale et al. (2021 e Aitbelale et al. (2021 e Alves et al. (2022 e Gülüm; Bilgin (2017 e Ivaniš et al. (2016a, 2016b) but its application is limited to correlating density data as a function of pressure and temperature Aitbelale; Chhiti; et al. (2019). Biofuel can

behave as self-associating compounds, and in mixtures with alcohols, the predictive capability of classic cubic equations of state could be limited. Therefore, a more robust model should be applied when dealing with such compounds. For that purpose, the Perturbed-Chain Statistical Association Fluid Theory equation of state (PC-SAFT EOS) is a suitable choice, as it yields favorable results for such systems Ait Belale et al. (2021 e Aitbelale; Chhiti; et al. (2019 e Aitbelale et al. (2021) requiring only a set of 5 parameters.

In this context, our study investigated the impact of adding 1-butanol to biodiesel, focusing on examining its density under high pressures and deriving associated properties. Experimental density data were collected for mixtures of 1-butanol with two different biodiesels: Linseed and soybean methyl biodiesel over a temperature range of $293.15\ to\ 373.15\ K$, up to a pressure of $100\ MPa$. Subsequently, we analyzed excess properties to identify deviations from ideal behavior. We correlated the data using the Tait and PC-SAFT (Perturbed Chain - Statistical Associating Fluid Theory) equations to observe their capability, considering their theoretical and statistical differences. We demonstrated the wide applicability of the parameters of the Tammann-Tait equation in deriving properties such as isothermal compressibility and isobaric thermal expansivity. Additionally, we applied the density data obtained by PC-SAFT EoS to derive these properties, aiming to highlight distinctions between the two approaches and evaluate the derivation of properties using this equation.

5.2 Experimental section

5.2.1 Materials

Linseed and soybean methyl biodiesel were produced through a homogeneous transesterification reaction using methanol, following the methodology described elsewhere Mesquita et al. (2014 e Nogueira et al. (2010, 2012a, 2015a). Table 11 reports the molecular formula, the CAS number, and the molecular weight ($g \cdot mol^{-1}$) of 1-butanol and fatty acid methyl esters present in linseed and soybean biodiesels along with the profiles of fatty acid methyl esters. Table 5.2 presents information about physiochemistry characterizations, with the acid number ($mg\ KOH/g$), kinematic viscosity at 40°C (mm^2/s), density at 15°C (kg/m^3), and mass fractions (w_i) of biodiesels.

Table 11 – Molecular Formula, CAS Number, and Molecular Weight of Pure Components and Biodiesel Composition in Mass Fraction w_i

Name	molecular formula	molecular weight ($g \cdot mol^{-1}$)	CAS Reg. No.	w_i linseed	w_i soy
methyl linolate	$C_{19}H_{34}O_2$	294.472	112-63-0	0.536	0.497
methyl oleate	$C_{19}H_{36}O_2$	296.488	112-62-9	0.420	0.320
methyl stearate	$C_{19}H_{38}O_2$	298.504	112-61-8	0.001	0.046
methyl palmitate	$C_{17}H_{34}O_2$	270.451	112-39-0	0.043	0.122
1-butanol[a]	$C_4H_{10}O$	74.122	71-36-3	-	-

[a]Supplier: Sigma-Aldrich [purity (w/w) >99.8 %].

Table 12 Physiochemistry Characterizations for Sample of Biodiesel Used in This Paper

tests for biodiesel	physiochemistry characterizations		
	acid number ($mg\ KOH/g$)	kinematic viscosity at $40°C$ (mm^2/s)	density at $15°C$ (kg/m^3)
method ASTM[a]	D664	D445	D1298
limit ASTM[a] D6751	Max 0.5	1.9-6.0	860-900
linseed biodiesel[b]	0.08	4.051	897.2
soybean biodiesel[b]	0.09	5.016	899.3

[a]American Society for Testing and Materials; [b]$Yield\ (wt\ \%) > 99.0$.

5.2.2 Mixtures Preparation

All binary 1-butanol + biodiesel mixtures were prepared by gravimetry using an electronic analytical scale (Shimadzu, model AY220) with a precision of ±0.0001 g. These samples were then loaded into a low-friction, high-pressure floating piston transfer cylinder from Vinci Technologies/France, equipped with an internal mixing ring to ensure complete sample homogenization. This experimental setup could reach a maximum pressure and temperature of 100 MPa and 473.15 K, respectively. The estimated standard uncertainties for molar fraction were lower than $u_c(x_{\text{butanol}}) = 4 \cdot 10^{-5}$, for all mixture.

5.2.3 Experimental Procedure

The density (ρ) measurements were carried out using the Anton Paar DMA HPM densimeter, whose operating principle and experimental configuration were previously

described in Chapter 1. For completeness, it is important to emphasize that the pressure was measured with a standard uncertainty of 0.03 MPa using an Omega pressure transducer positioned at the U-tube outlet, while the temperature was monitored via a PT100 sensor with an uncertainty of 0.02 K. The expanded uncertainty associated with the high-pressure and high-temperature density measurements was evaluated by propagating the standard uncertainties of temperature, pressure, and reference fluid density as shown in **Appendix D**, resulting in a maximum value of $U(\rho) = 0.93\ kg \cdot m^{-3}$ at a 95% confidence level (coverage factor $k = 2$). Prior to measurements with binary mixtures, the system was validated using toluene (Sigma-Aldrich, 99.5% purity), yielding an average deviation of 0.07% when compared to reference data Valero et al. (2020).

5.3 Modeling

5.3.1 Correlating Experimental Density Data at High-Pressure and High-Temperature

Density correlation against pressure and temperature was carried out using the Tammann-Tait equation, defined in equation (5.1), with temperature-dependent parameters, in the following form as reported in the literature Ait Belale et al. (2021 e Aitbelale et al. (2021 e Alves et al. (2022 e Ivaniš et al. (2016a, 2016b):

$$(P,T)/(kg \cdot m^{-3}) = \frac{\rho_{Ref}(T)/(kg \cdot m^{-3})}{1 - C \cdot \ln\left(\frac{B(T)+P/MPa}{B(T)+P_{Ref}/MPa}\right)} \tag{5.1}$$

where C denotes an adjusted temperature-independent parameter and $B(T)$ is a two-degree polynomial temperature-dependent parameter, as defined in equation (5.2). The reference pressure P_{Ref} was selected as 0.1 MPa and $\rho_{Ref}(T)$ refers to the density at the reference pressure (P_{Ref}), as expressed as a function of temperature in equation (5.3).

$$\mathrm{B}(T) = b_0 + b_1 \cdot T + b_2 \cdot T^2 \tag{5.2}$$

$$\rho_{Ref} = a_0 + a_1 \cdot T + a_2 \cdot T^2 \tag{5.3}$$

where a_0, a_1, a_2 and b_0, b_1, b_2 were adjusted based on density data, in addition to the parameter C.

Since the composition is not considered in the Tammann-Tait correlation, these parameters were determined for each 1-butanol + biodiesel mixture studied in this work. The

mean absolute percentage deviation was calculated to evaluate the accuracy of the correlation with the estimated parameters Alves et al. (2022 e Ivaniš et al. (2016a, 2016b).

5.3.2 Derived Properties Calculated from the Modified Tamman-Tait Equation

Isothermal compressibility (κ_T) and isobaric thermal expansibility (α_P) were calculated from the Tamman-Tait equation using the fitted parameters. These properties could be helpful for industrial and academic applications Sas et al. (2021).

Isothermal compressibility was calculated from equations 5.4 and 5.5 Alves et al. (2022 e Ilić Pajić et al. (2020 e Ivaniš et al. (2016a, 2016b e Sas et al. (2021):

$$\kappa_T = \frac{1}{\rho} \cdot \left(\frac{\partial \rho}{\partial P}\right)_T \tag{5.4}$$

$$\kappa_T = \frac{C}{\left(1 - C \cdot ln\left(\frac{B(T)+P}{B(T)+P_{ref}}\right)\right) \cdot (B(T)+P)} \tag{5.5}$$

Similarly, isobaric thermal expansivity (α_P) is obtained for equations 5.6 and 5.7 Alves et al. (2022 e Ilić Pajić et al. (2020 e Ivaniš et al. (2016a, 2016b e Sas et al. (2021):

$$\alpha_P = -\frac{1}{\rho} \cdot \left(\frac{\partial \rho}{\partial T}\right)_P \tag{5.6}$$

$$\alpha_P = -\frac{a_1 + 2 \cdot a_2 \cdot T}{\rho_{Ref}} - \frac{C \cdot (P_{Ref} - P)}{(B(T)+P) \cdot (B(T)+P_{Ref})} \cdot \frac{b_1 + 2 \cdot b_2 \cdot T}{\left(1 - C \cdot ln\left(\frac{B(T)+P}{B(T)+P_{Ref}}\right)\right)} \tag{5.7}$$

where: equations 5.5 and 5.7 are derivations of equations 5.1 – 5.3.

5.3.3 PC-SAFT Modeling

The Perturbed-Chain Statistical Associating Fluid Theory (PC-SAFT) is a widely used equation of state developed by Gross and Sadowski Gross; Sadowski (2001c), which is based on the SAFT theory proposed by Chapman *et al.* Chapman et al. (1990a). The PC-SAFT equation of state can be written in terms of the compressibility factor as follows in equation 5.8:

$$Z = 1 + Z^{HC} + Z^{DISP} + Z^{ASSOC} \tag{5.8}$$

In this expression, the compressibility factor is denoted as a contribution of four terms: the ideal gas contribution ($Z = 1$); the hard-chain contribution (Z^{HC}), which correspond to hard chain molecules with no attractive interactions and serves as the reference fluid; the contribution from dispersion forces (Z^{DISP}), which is based on the Lennard-Jones parameters for the dispersion energy; and the contribution due to association (Z^{ASSOC}) for associating fluids.

A detailed equation description can be found elsewhere Chapman et al. (1990a e Gross; Sadowski (2001c, 2002a, 2002b). Each contribution necessitates a set of parameters for pure compounds: the hard-chain contribution requires a parameter to describe the number of segments in a chain (m); the dispersive contribution uses the Lennard-Jones parameters for the dispersion energy (ε) and the segment diameter (σ); the association term requires a parameter for the energy of association (ϵ^{AB}/k), and another for the effective volume of association between two association sites (κ_{AB}). These parameters are unique for each molecule and must be obtained through experimental data Gross; Sadowski (2001c). In this study, we considered 1-butanol, with an associating scheme described as 2B, following the nomenclature proposed by Huang and Radosz (HUANG; RADOSZ, 1990), consisting of one donor and one acceptor site. To apply the equation of state to mixtures, we used the Berthelot-Lorentz combining rule, which involves a single binary interaction parameter (k_{ij}) to correct dispersive interactions Gross; Sadowski (2002b e Wolbach; Sandler (1997).

The parameters for 1-butanol utilized in this research were derived from the experimental data collected in this study, considering the component's behavior in its pure form. They were compared with relevant references with a similar methodology Ait Belale et al. (2021 e Grenner et al. (2007 e Gross; Sadowski (2002b). The regression process minimizes the objective function described in equation 5.9.

$$OF = \sum_{i=1}^{N_P} \left(\frac{\rho_{calc} - \rho_{exp}}{\rho_{exp}} \right)^2 \tag{5.9}$$

where the subscript *calc* is for data obtained through the PC-SAFT equation and *exp* is for experimental values. The minimization through density data was successfully used for such purposes Ait Belale et al. (2021 e Aitbelale; Chhiti; et al. (2019 e Aitbelale et al. (2021 e García-Morales et al. (2023 e Mohammadkhani et al. (2018 e Mokhtari et al. (2023). To minimize the objective function, the Differential Evolution algorithm Storn; Price (1997) was used. This methodology proposes a global minimization over a wide interval of possible candidates for each variable.

For biodiesels, we employed a PC-SAFT approach conducted by García-Morales et al. García-Morales et al. (2023) for FAME beef tallow mixture and Ait Belale et al. Aitbelale; Chhiti; et al. (2019) for soybean biodiesel. In this approach, biodiesel was treated as a pseudo-component, and its parameters (m, σ, and ε/k) were optimized using onlydensity data.

After completing the adjustments of the PC-SAFT parameters for the 1-butanol and biodiesel components, it is possible to extend the model to anticipate the behavior of the binary mixture made up of these elements. This extension of the model involves incorporating the binary interaction parameters (k_{ij}), which characterize the reciprocal influences between the 1-butanol and biodiesel molecules in the mixture.

5.4 Results and discussion

5.4.1 Density Measurements in Butanol, Biodiesel, and Butanol + Biodiesel Mixture Densities at High Pressure and High Temperature

The following nomenclature was used in the designation of 1-butanol+biodiesel blends: "But 5", "But 10", etc. Here, "But" refers to 1-butanol followed by its volumetric percentage $\phi_{butanol}\%$ in the mixture, for example, "But 5" corresponds to 5% vol of 1-butanol in the mixture. Table 13 provides a list of the mixtures investigated studied in this work. However, the composition of the blends is also given in terms of mass $w_{butanol}$ and mole x_{butano} fractions in this table.

Table 13 – Mixtures Composition

Acronyms used for nomenclature	$\phi_{butanol}$ $vol/vol\ (20°C)$	$w_{butanol}$ $mass/mass$	$x_{butanol}$ mol/mol
	But	But	But
But 0	0.00	0.00	0.00
But 5	0.05	0.04	0.15
But 13	0.13	0.12	0.35
But 22	0.22	0.20	0.50
But 34	0.34	0.32	0.65
But 61	0.61	0.59	0.85
But 100	1.00	1.00	1.00

The operational conditions investigated in this study included a pressure range of 0.10 – 100 MPa and a temperature range of 293.15 – 373.15 K. Tables 14, 15, and 16 present the reported density data for 1-butanol and mixtures of 1-butanol and biodiesel (linseed and soybean).

For experimental validation purposes, a comparison was conducted. When comparing the results obtained in this study for pure 1-butanol experimental density data with previously published literature data Ait Belale et al. (2021 e Safarov et al. (2015 e Torín-Ollarves et al. (2017), the mean absolute percentage deviation (MAPD) was 0.06%. This value agrees with the estimated uncertainty in density measurement. Additionally, Figure 21 illustrates the relative deviation between our experimental density data and the literature results for pure 1-butanol.

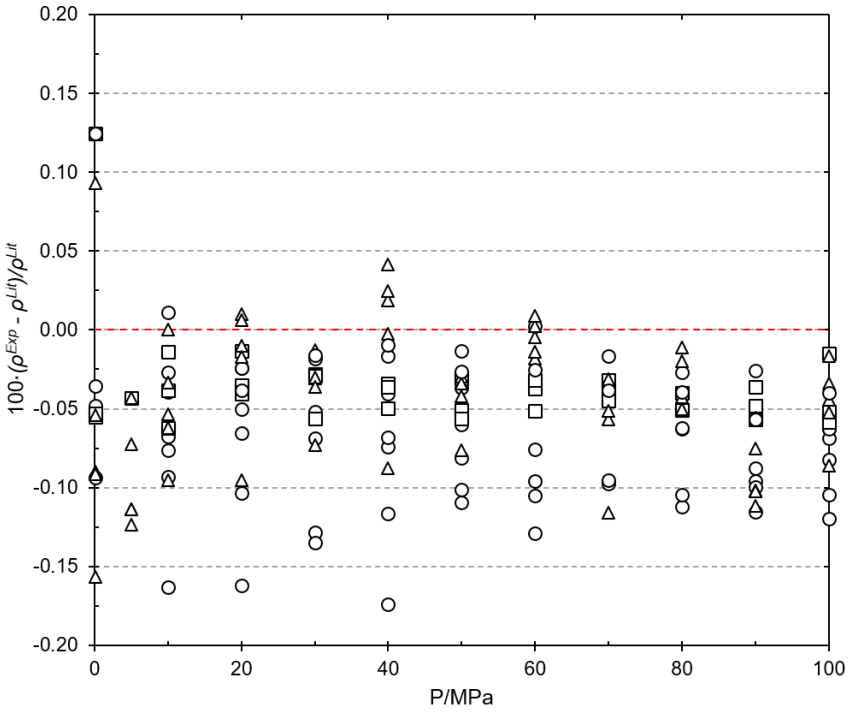

Figure 21 – Relative deviations between the experimental density data, which were determined in this paper for pure 1-butanol, and the literature values for 1-butanol as a function of experimental pressure at various temperatures. Literature data: (□) Tórin-Ollarves et al. 2012 Torín-Ollarves et al. (2017), (○) Ait Belale et al. 2021 Ait Belale et al. (2021), (Δ) Safarov et al. 2015 Safarov et al. (2015). (Created by the author, 2024)

Figure 22 illustrates the change in density as a function of the molar fraction of butanol along the studied isobars. It can be observed that the system containing soy biodiesel exhibited higher density values than the systems containing linseed biodiesel. This disparity is likely related to the distinct mass percentages of esters present in their compositions, emphasizing the direct influence of chemical composition on the system's density. The results observed regarding variations in pressure (P), temperature (T), and composition align with

findings in the literature from previous studies on a blend of 1-butanol with other biodiesels Ait Belale et al. (2021 e Cano-Gómez et al. (2017).

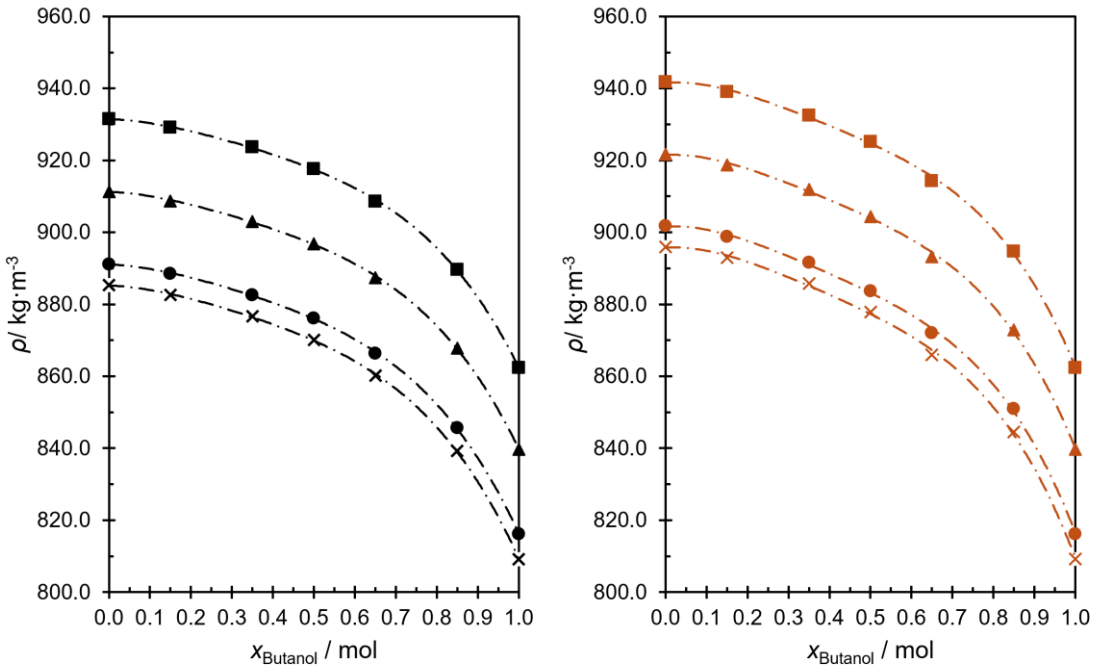

Figure 22 – Density values (ρ) as a function of butanol mole fraction (x_{But}) at temperature $T = 293.15\ K$ and pressures 0.1(×, cross), 10 (●, circle), 50 (▲, triangle) and 100 (■, square) MPa. The dotted line is a polynomial fit. Graphs with black symbols represent the blends of the system with linseed biodiesel, while those with brown symbols represent the system with soybean biodiesel. (Created by the author, 2024)

In a previous investigation reported by Barabás Barabás; Todoruţ (2009) on ethanol and biodiesel blends at atmospheric pressure, positive excess volumes were identified, reaching a maximum of approximately 0.4 $cm^3 \cdot mol^{-1}$ at a temperature of 333.15 K. Additionally, Vargas-Ibáñez et al. Vargas-Ibáñez et al. (2020b, 2022a) performed measurements on blends of biodiesels with hexanol, octanol, and their isomers, finding volumes of around 0.2 $cm^3 \cdot mol^{-1}$. These two findings suggest a minor deviation from ideal solutions' volumetric behavior. However, for butanol and biodiesel blends, Ait Belale et al. Ait Belale et al. (2021 e Aitbelale et al. (2021) found excess volume values that can reach V_m^E = 8-9 $cm^3 \cdot mol^{-1}$, revealing a significant deviation from ideal behavior in this system. The values reported by Ait Belale et al. Ait Belale et al. (2021 e Aitbelale et al. (2021) appear twenty times higher than those calculated by either Barabás Barabás; Todoruţ (2009) or Vargas-Ibáñez et al. Vargas-Ibáñez et al. (2020b, 2022a). The significant difference in volumetric behaviors observed in butanol + biodiesel by

Ait Belale et al. Ait Belale et al. (2021 e Aitbelale et al. (2021) with other alcohol + biodiesel systems cannot be explained simply by the difference between the alcohols considered in the mixtures. We conducted a detailed study of the excess volumes through calculations derived from our density measurements, as detailed in equation 5.10:

$$V_m^E = \frac{\sum_i x_i M_i}{\rho} - \sum_i x_i \frac{M_i}{\rho_i} \tag{5.10}$$

where M_i is the molecular weight, x_i is the molar fraction, and ρ_i is the density of pure (alcohol) or pseudo (biodiesel) component i.

In agreement with the investigations carried out by Barabás Barabás; Todoruţ (2009) and Vargas-Ibáñez et al., Vargas-Ibáñez et al. (2020b, 2022a) a minimal relative excess volume (0.15%) was found from our density measurements. However, as shown in Figure 23, the excess values calculated were in the same order as the expended uncertainty associated with excess volume calculated from the propagation of density measurements for both mixtures and pure components. This makes the precise interpretation of excess volume results, particularly the curve's S-shape, questionable. For this reason, density measurements at atmospheric pressure were repeated using a more accurate device: the Anton Paar SVM 3000. This apparatus provides more digits for the measurement of the oscillation period.

Consequently, a lower expanded uncertainty ($U(\rho) = 0.5\ kg \cdot m^{-3}$) than with the DMA HPM, on the other hand, its operation is limited to atmospheric pressure. The density values obtained with this second densimeter can be found in the supporting information (**Table D2**, in **Appendix D**), and the excess values derived from these measurements were compared to those obtained from the high-pressure densimeter in Figure 24. It can be seen in this figure that there is an excellent agreement between the two excess volume data sets, with the error bars overlapping. However, as expected, the shape of the excess curve obtained from the SVM 3000 densimeter appears smoother and more regular. These curves were plotted for different isotherms in Figure 24. It can be noted that the excess volumes move from positive to negative values as the temperature of isotherms increases. In all cases, the excess values are very low (around 0.3) and the same order of magnitude of Barabás Barabás; Todoruţ (2009) and Vargas-Ibáñez et al. Vargas-Ibáñez et al. (2020b, 2022a). However, it is incomparably smaller than those reported by Ait Belale et al. Ait Belale et al. (2021 e Aitbelale et al. (2021) with Butanol. There is not enough variation in biodiesel compositions to induce changes in interactions between butanol and biodiesel molecules that could explain such a significant difference.

The nearly ideal behavior observed in this type of system shows that there is no cross-association between associative alcohols and non-associative biodiesels. The alcohol molecules associate with each other exactly as they do in their pure state. This agrees with our recent work Alves, Alanderson Arthu Araújo; Medeiros; et al. (2025), where it was shown that molecular interactions in similar mixtures lead to minimal excess volumes due to weak interactions between alcohol and ester groups.

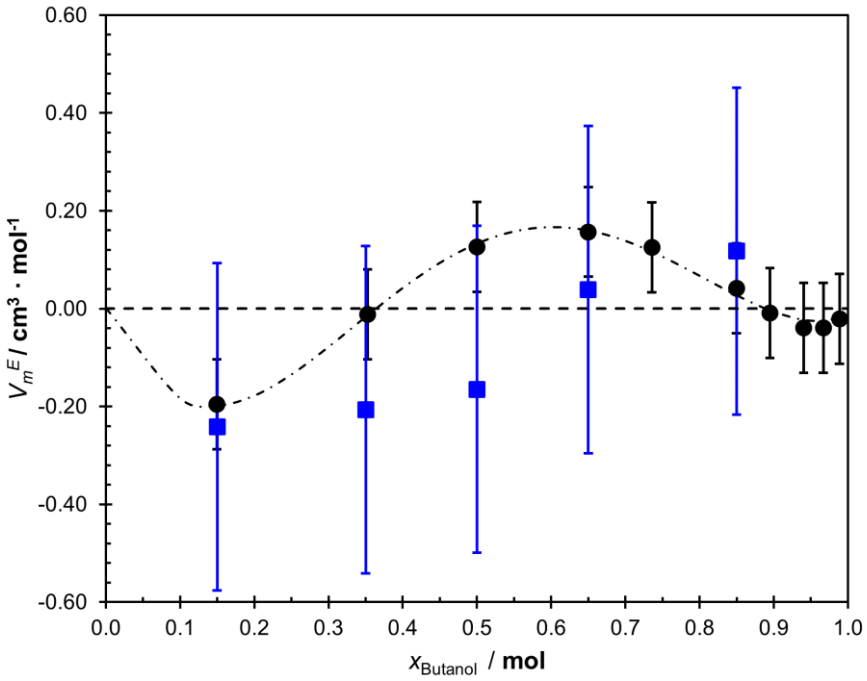

Figure 23 – Comparison between excess volumes obtained by DMA HPM (●, black circle) and Anton Paar SVM 3000, atmospheric pressure (■, blue square), at temperature T = 353.15 K. Error bars indicate the maximum expanded uncertainty corresponding to a 95% confidence level for each equipment. (Created by the author, 2024)

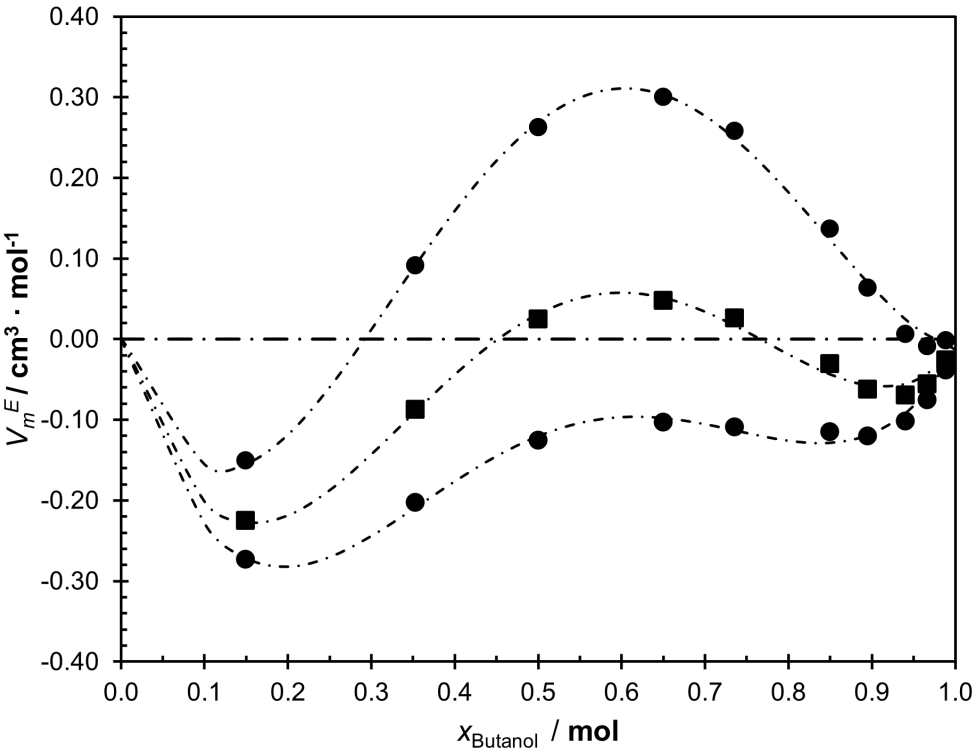

Figure 24 – Excess molar volume as a function of the molar fraction of 1-butanol for the 1-butanol + linseed biodiesel system at temperature (●) T = 293.15 K, (■) T = 333.15 K, and (■, lower) T = 373.15 K and pressure 0.1 MPa. Error bars indicate expanded uncertainty corresponding to a 95% confidence level. (Created by the author, 2024)

Table 14 – Experimental Density Data (ρ) 1-Butanol (But 100), as Function of Temperature (T) and Pressure (P)[a].

T/K	293.15	313.15	333.15	353.15	373.15
$P/\ MPa$			**But 100**		
0.1[b]	809.9	794.4	778.3	761.2	743.1
5	812.8	797.9	781.9	765.4	747.4
10	816.2	801.7	786.2	770.1	752.7
20	822.7	808.8	794.1	778.8	762.5
30	828.8	815.3	801.2	786.7	771.2
40	834.4	821.3	807.8	793.8	779.1
50	839.7	827.0	813.9	800.4	786.3
60	844.7	832.4	819.7	806.7	793.0
70	849.5	837.5	825.2	812.4	799.4
80	854.0	842.3	830.3	818.0	805.3
90	858.3	846.8	835.2	823.1	810.8
100	862.4	851.3	839.8	828.2	816.0

[a] The standard uncertainties are $u(T) = 0.02\,K$, $u(P) = 0.03\,MPa$, and $u(x_i) = 4 \cdot 10^{-5}$. Expanded uncertainty $U\,(\rho) = 0.002\rho$ (0.95 confidence level); [b] Data was obtained using a densimeter at atmospheric pressure.

Table 15 – Experimental Density Data (ρ) Blending 1-Butanol with Linseed Biodiesel, 0, 5, 13, 22, 34, and 61 ϕ_{But}, as Function of Temperature (T) and Pressure (P)[a].

T/K	293.15	313.15	333.15	353.15	373.15	T/K	293.15	313.15	333.15	353.15	373.15
$P/\ MPa$			**But 0**			$P/\ MPa$			**But 5**		
0.1[b]	886.6	872.2	857.6	843.1	828.8	0.1[b]	883.9	869.3	854.5	839.8	825.2
5	888.3	874.0	859.6	845.5	831.1	5	885.6	871.3	856.7	842.3	827.6
10	891.1	877.1	863.1	849.0	835.3	10	888.5	874.5	860.2	845.9	831.8
20	896.7	883.1	869.5	856.3	842.9	20	894.1	880.5	866.8	853.3	839.6
30	901.8	888.7	875.6	862.7	849.9	30	899.2	886.1	872.9	859.8	846.7
40	906.7	893.9	881.2	868.8	856.5	40	904.1	891.4	878.6	865.9	853.3
50	911.3	898.9	886.6	874.5	862.6	50	908.7	896.4	883.9	871.7	859.4
60	915.6	903.6	891.6	879.9	868.3	60	913.1	901.1	889.0	877.1	865.2
70	919.9	908.1	896.4	885.1	873.8	70	917.4	905.6	893.9	882.3	870.7
80	924.0	912.4	901.0	889.9	878.9	80	921.5	910.0	898.5	887.2	875.9
90	927.8	916.6	905.4	894.5	883.8	90	925.4	914.1	902.9	891.8	880.9
100	931.5	920.5	909.7	898.9	888.4	100	929.1	918.1	907.0	896.3	885.6
$P/\ MPa$			**But 13**			$P/\ MPa$			**But 22**		
0.1[b]	877.3	862.5	847.5	832.3	817.1	0.1[b]	870.5	855.6	840.3	824.8	809.1
5	879.7	865.3	850.5	835.6	820.3	5	873.2	858.7	843.7	828.5	812.8
10	882.6	868.5	854.0	839.3	824.7	10	876.2	861.9	847.3	832.3	817.3
20	888.2	874.5	860.7	846.7	832.6	20	881.8	868.1	854.0	839.8	825.4
30	893.4	880.2	866.8	853.4	839.9	30	887.1	873.8	860.2	846.7	832.8
40	898.3	885.6	872.6	859.6	846.6	40	892.1	879.3	866.1	852.9	839.7
50	903.0	890.6	878.0	865.5	852.8	50	896.8	884.3	871.6	858.9	846.1
60	907.4	895.5	883.2	871.0	858.8	60	901.2	889.2	876.9	864.5	852.1
70	911.8	900.0	888.1	876.2	864.3	70	905.7	893.9	881.8	869.8	857.8
80	915.9	904.4	892.9	881.2	869.6	80	909.9	898.2	886.7	874.9	863.1
90	919.9	908.6	897.2	885.9	874.6	90	913.9	902.5	891.1	879.6	868.2
100	923.6	912.6	901.4	890.4	879.5	100	917.7	906.5	895.4	884.1	873.0
$P/\ MPa$			**But 34**			$P/\ MPa$			**But 61**		
0.1[b]	861.1	845.9	830.4	814.5	798.2	0.1[b]	840.6	825.2	809.4	792.7	775.4
5	863.3	848.6	833.4	817.8	801.8	5	842.5	827.7	812.1	795.7	778.8
10	866.3	851.9	837.0	821.9	806.4	10	845.7	831.2	815.9	800.2	783.7
20	872.1	858.2	843.9	829.4	814.8	20	851.8	838.0	823.3	808.1	792.6
30	877.5	864.1	850.3	836.5	822.4	30	857.4	844.1	830.0	815.4	800.6
40	882.6	869.6	856.3	842.9	829.5	40	862.8	849.8	836.2	822.2	808.1
50	887.4	874.8	861.9	849.0	836.0	50	867.8	855.2	842.0	828.5	814.9
60	891.9	879.8	867.2	854.7	842.1	60	872.6	860.4	847.6	834.5	821.3
70	896.5	884.5	872.3	860.1	848.0	70	877.1	865.2	852.8	840.2	827.5
80	900.7	888.9	877.2	865.3	853.4	80	881.5	869.8	857.6	845.4	833.1
90	904.8	893.2	881.7	870.1	858.6	90	885.7	874.2	862.3	850.4	838.4
100	908.6	897.3	886.3	874.6	863.4	100	889.7	878.5	866.9	855.2	843.5

[a] The standard uncertainties are $u(T) = 0.02\,K$, $u(P) = 0.03\,MPa$, and $u(x_i) = 4 \cdot 10^{-5}$. Expanded uncertainty $U\ (\rho) = 0.002\rho$ (0.95 confidence level).; [b] Data was obtained using a densimeter at atmospheric pressure.

Table 16 – Experimental Density Data (ρ) Blending 1-Butanol with Soybean Biodiesel 0, 5, 13, 22, 34, and 61 ϕ_{But}, as Function of Temperature (T) and Pressure (P)[a].

T/K	293.15	313.15	333.15	353.15	373.15	T/K	293.15	313.15	333.15	353.15	373.15
P/MPa			**But 0**			P/MPa			**But 5**		
0.1[b]	895.7	881.3	866.5	852.1	837.0	0.1[b]	891.8	877.2	862.3	847.6	832.0
5	898.9	884.6	870.2	855.8	841.3	5	895.9	881.5	867.0	852.3	837.6
10	901.7	887.6	873.5	859.6	845.7	10	898.7	884.6	870.3	855.9	841.5
20	907.1	893.5	879.9	866.3	852.9	20	904.1	890.5	876.8	863.0	849.2
30	912.2	899.0	885.8	872.9	860.2	30	909.2	896.1	882.8	869.5	856.2
40	917.0	904.2	891.4	878.8	866.6	40	914.1	901.3	888.4	875.6	862.7
50	921.7	909.1	896.7	884.5	872.7	50	918.7	906.3	893.8	881.3	868.9
60	926.0	913.8	901.7	889.9	878.4	60	923.2	911.0	898.8	886.7	874.7
70	930.2	918.3	906.6	894.9	883.6	70	927.4	915.5	903.6	891.8	880.3
80	934.2	922.5	911.0	899.9	889.0	80	931.4	919.8	908.2	896.7	885.3
90	938.0	926.8	915.4	904.3	893.7	90	935.3	923.9	912.5	901.4	890.3
100	941.8	930.6	919.6	908.8	898.3	100	939.1	927.9	916.8	905.8	895.1
P/MPa			**But 13**			P/MPa			**But 22**		
0.1[b]	885.0	870.2	855.1	840.0	823.8	0.1[b]	878.3	863.4	848.1	832.5	816.1
5	888.7	874.1	859.3	844.3	828.8	5	881.1	866.4	851.4	836.1	820.6
10	891.6	877.4	862.8	847.9	832.9	10	884.0	869.6	854.9	840.0	824.8
20	897.1	883.3	869.4	855.3	841.0	20	889.6	875.8	861.7	847.4	832.8
30	902.3	889.1	875.6	861.8	847.9	30	894.9	881.5	867.9	854.1	840.3
40	907.2	894.4	881.3	868.0	854.6	40	899.9	886.9	873.7	860.4	847.1
50	911.9	899.4	886.7	873.8	860.9	50	904.7	892.0	879.2	866.3	853.4
60	916.4	904.2	891.8	879.3	866.8	60	909.2	896.8	884.4	871.9	859.4
70	920.7	908.7	896.6	884.6	872.7	70	913.5	901.5	889.3	877.1	865.1
80	924.7	913.1	901.3	889.5	877.6	80	917.6	905.8	894.0	882.2	870.4
90	928.7	917.1	905.7	894.4	882.8	90	921.6	910.0	898.5	886.9	875.5
100	932.5	921.3	910.0	898.9	887.6	100	925.3	914.0	902.7	891.4	880.3
P/MPa			**But 34**			P/MPa			**But 61**		
0.1[b]	868.9	853.7	838.2	822.2	805.6	0.1[b]	845.4	830.2	814.3	797.7	780.6
5	871.0	856.3	841.3	825.9	810.2	5	847.7	832.8	817.1	800.7	783.6
10	874.0	859.6	844.9	829.9	814.4	10	850.9	836.2	820.9	805.1	788.5
20	879.7	865.9	851.8	837.4	822.7	20	857.0	842.9	828.2	813.0	797.3
30	885.1	871.7	858.1	844.3	830.3	30	862.6	849.0	834.9	820.4	805.4
40	890.2	877.2	864.0	850.7	837.2	40	867.9	854.7	841.1	827.1	812.8
50	895.1	882.4	869.6	856.7	843.7	50	872.9	860.2	846.9	833.4	819.6
60	899.7	887.3	874.9	862.4	849.8	60	877.7	865.2	852.4	839.4	825.9
70	904.1	892.0	879.9	867.7	855.6	70	882.3	870.1	857.5	844.9	832.0
80	908.2	896.5	884.6	872.8	861.0	80	886.6	874.7	862.5	850.2	837.6
90	912.2	900.7	889.2	877.6	866.1	90	890.8	879.1	867.3	855.2	842.9
100	915.5	904.2	892.8	881.5	870.2	100	894.7	883.3	871.7	859.9	848.0

[a] The standard uncertainties are $u(T) = 0.02\,K$, $u(P) = 0.03\,MPa$, and $u(x_i) = 4 \cdot 10^{-5}$. Expanded uncertainty $U(\rho) = 0.002\rho$ (0.95 confidence level); [b] Data was obtained using a densimeter at atmospheric pressure.

5.4.2 Correlation and Derivation of Density Data

The density data were first correlated using the Tammann–Tait equation, as described in Section 5.3.1. Table 5.7 displays the adjusted parameters (a_0, a_1, and a_2; b_0, b_1, b_2; and C) of the modified Tammann–Tait equation (equations 5.4−5.7) for the butanol, the biodiesels, and the blends of different compositions. With these fitted parameters, an excellent agreement was observed between experimental density data and the Tammann–Tait equation calculations, with a maximum absolute average deviation of only 0.011%. The adjustment algorithm used was the Levenberg-Marquardt algorithm Moré (1978), widely used for this type of situation in various systems, with the aim of minimizing the square of the difference between the densities.

Using these parameters, it was consequently possible to calculate the isothermal compressibility (κ_T) and the isobaric thermal expansivity (α_P). The methodology for obtaining isothermal compressibility uncertainties was based on Monte Carlo analysis, as proposed by Daridon and Bazile Daridon; Bazile (2018). This paper presents a computational method for estimating compressibility and its uncertainty, using density measurements taken from atmospheric pressure up to 100 MPa. A detailed evaluation of equations for adjusting density data and calculating isothermal compressibility was performed. Subsequently, a numerical method was proposed for estimating isothermal compressibility and its uncertainty, employing a Monte Carlo procedure based on a limited number of experimental density data points. This procedure involves generating multiple random samples of the density data and applying them to the model to calculate a distribution of compressibility values, from which the uncertainty is determined.

For this procedure, their combined standard uncertainties were considered. This approach involves randomly perturbing the density data. The procedure first generated 5000 sets of perturbed density data, with each set randomly adjusted using Tait's equation of state to derive compressibility for each random set. Consequently, 5000 compressibility values were obtained for each data point. In the subsequent phase, average standard deviations were calculated over the compressibility distribution to determine the standard uncertainty of this property. This robust methodology guarantees the reliable derivation of uncertainty associated ($U(\kappa_T)$) with this property Daridon; Bazile (2018). The values obtained are reported in **Table D3-D6** in **Appendix D**, which provides additional information for this chapter Finally, some references have described various advantages of Monte Carlo simulation Coleman; Steele (1995 e Papadopoulos; Yeung (2001). This method is capable of handling both small and large

uncertainties in the input quantities, eliminating the need for complex partial differentiations to determine the sensitivity coefficients. Additionally, it automatically manages input covariances or dependencies Coleman; Steele (1995). Compared to conventional methods for obtaining uncertainty, such as those described in (Guide to the expression of the uncertainty in measurement) ISO/GUM JCGM (2008), Monte Carlo simulation offers similar uncertainty values for properties Chen; Chen (2016).

Table 17 – Modified Tammann–Tait Equation Adjustable Parameters for 1-Butanol + Biodiesel (Linseed and Soy) Mixtures Studied Here.

parameters	blends But %					
	But 0	*But 5*	*But 13*	*But 22*	*But 34*	*But 61*
	linseed biodiesel					
a_0	1101.075	1079.357	1053.779	1042.158	1012.365	961.111
$a_1/10^{-3}$	-741.230	-616.335	-482.860	-441.093	-308.963	-95.371
a_2 / 10^{-6}	17.074	-187.383	-414.409	-496.952	-718.117	-1092.872
b_0	453.975	449.625	428.546	430.723	371.008	342.204
b_1 / 10^{-3}	-1577.331	-1537.885	-1402.354	-1416.353	-1077.309	-94.224
b_2 /10^{-6}	1523.219	1444.777	1221.044	1231.251	728.314	644.067
C /10^{-3}	83.577	84.385	85.476	86.385	87.117	85.542
$MAPD^a$	0.007	0.007	0.006	0.005	0.001	0.008
parameters	*But 0*	*But 5*	*But 13*	*But 22*	*But 34*	*But 61*
	soybean biodiesel					
a_0	1088.753	1068.722	1062.194	1053.865	1031.673	975.792
$a_1/10^{-3}$	-602.710	-485.603	-471.126	-460.917	-379.360	-152.101
a_2 / 10^{-6}	-189.141	-390.322	-445.776	-472.110	-607.140	-1009.005
b_0	373.702	387.198	446.923	436.343	417.966	342.204
b_1 / 10^{-3}	-1008.142	-1089.740	-1467.221	-1411.918	-1338.425	-1114.585
b_2 /10^{-6}	626.825	729.354	1283.278	1200.787	1102.479	810.813
C /10^{-3}	87.028	86.848	86.521	87.348	85.985	86.807
$MAPD^a$	0.011	0.007	0.008	0.005	0.010	0.007

[a] $\mathrm{MAPD} = \frac{1}{\mathrm{N_{data}}}\sum_{\mathrm{i-1}}^{\mathrm{N_{data}}}\left|\frac{\rho_{\mathrm{i}}^{\mathrm{Calc}}-\rho_{\mathrm{i}}^{\mathrm{Exp}}}{\rho_{\mathrm{i}}^{\mathrm{Exp}}}\right| \times 100$;. Unit parameters: $\mathrm{a_0}$ $(\mathrm{kg\cdot m^{-3}})$, $\mathrm{a_1}$ $(\mathrm{kg\cdot m^{-3}\cdot K^{-1}})$, $\mathrm{a_2}$ $(\mathrm{kg\cdot m^{-3}\cdot K^{-2}})$, $\mathrm{b_0}$ (MPa), $\mathrm{b_1}$ $(\mathrm{MPa\cdot K^{-1}})$, $\mathrm{b_2}$ $(\mathrm{MPa\cdot K^{-2}})$.

Figure 25 illustrates the influence of pressure on isothermal compressibility (κ_T) behavior in all the analyzed blends of 1-butanol + linseed biodiesel, particularly under high pressure and temperature conditions. Further information can be found in **Figure D1**, which presents the graphical analysis corresponding to the system with soy biodiesel. Additionally,

the effect of butanol content on the compressibility of butanol + biodiesel blends was shown in Figure 26, where κ_T values along with their expanded uncertainties were plotted as a function of volume fraction of butanol ϕ_{But}. This ideal quantity is defined in equation 5.11:

$$\phi_{But} = \frac{x_{But} M_{But}}{\rho_{But} \sum_i x_i \frac{M_i}{\rho_i}} \tag{5.11}$$

The choice of this quantity as the abscissa in this graph, instead of the molar fraction, aims to facilitate comparison with the isothermal compressibility of an ideal solution, which is defined in equation 5.12 as a linear combination of the isothermal compressibilities of the pure components:

$$\kappa_T^{id} = \sum_i \phi_i \kappa_{T,i} \tag{5.12}$$

Upon examining the error bars associated with the data points in Figure 26, it becomes apparent that the estimated uncertainty, (κ_T) in determining κ_T is significant compared to the deviation from ideal behavior, characterized by a straight line in this graph. This significant uncertainty compared to the excess property is typical for a derivative property, especially given that the conditions correspond to the extremes of the working range, here at 0.1 and 100 MPa. However, despite this significant uncertainty, the excess compressibility $(\kappa_T^E = \kappa_T - \kappa_T^{id})$ shows a regular pattern in the graph of Figure 27, where it was plotted against the mole fraction for two isobars, 0.1 MPa and 100 MPa.

Observations from this figure indicate a decrease in excess compressibility with increasing pressure, suggesting a reduction in the system's excess compressibility when the system becomes denser. Under atmospheric conditions, the relative excess compressibility can reach up to 1.5%. By comparing this value to the 0.15% obtained for the excess volume under the same conditions, it becomes evident that mixing effects are ten times more sensitive to the derivative of volume concerning pressure than to the volume itself. This behavior has implications for other derivative properties, mainly acoustic properties, closely linked to the medium's compressibility through which waves propagate. Therefore, it can be anticipated that acoustic properties will exhibit higher excess properties compared to excess volume due to their dependency on compressibility.

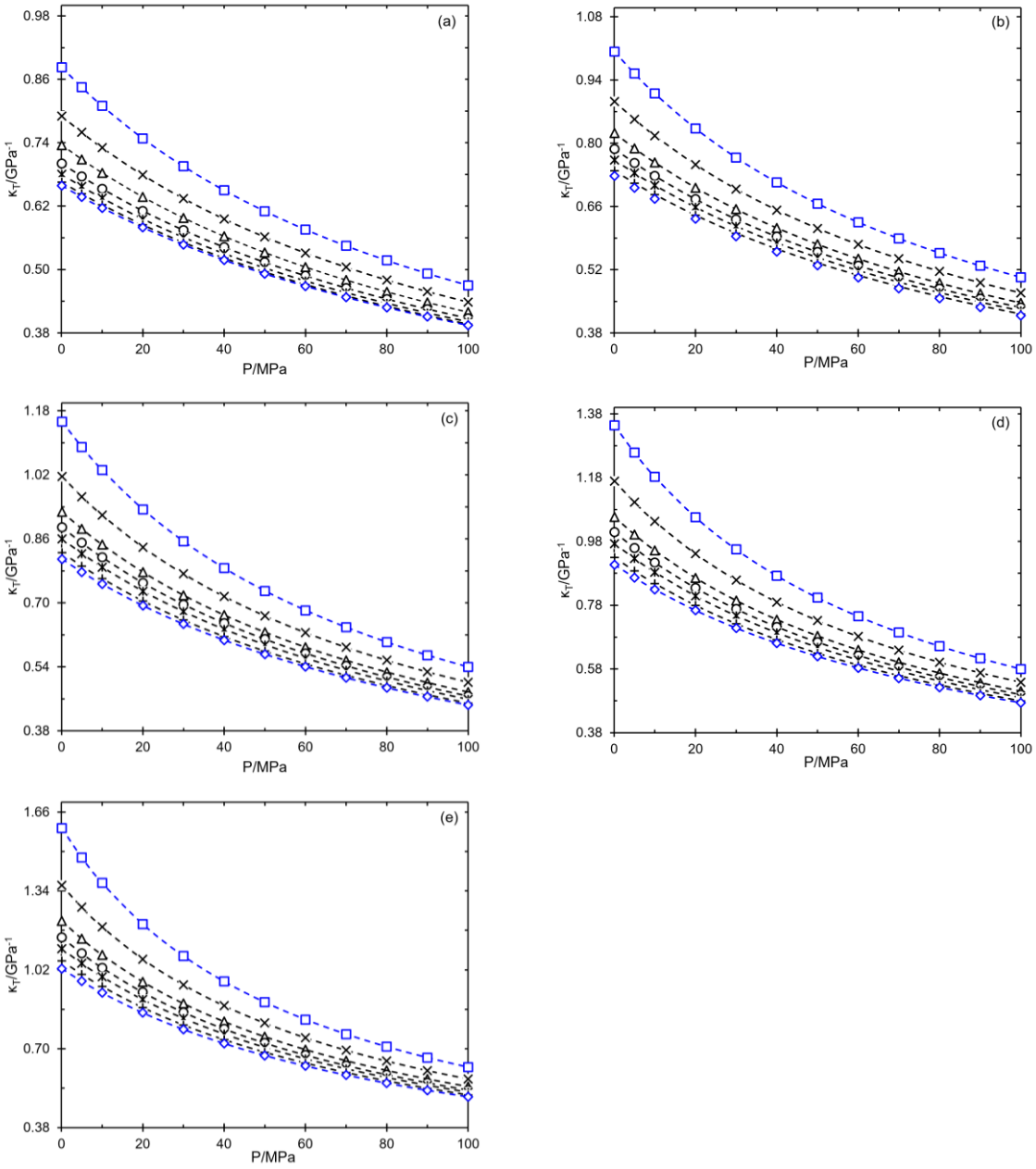

Figure 25 – Isothermal compressibility (κ_T) as a function of pressure for 1-butanol and linseed biodiesel blends. Each symbol refers to a mixture, where: (◇, blue diamond) But 0, (+, black plus signal) But 5, (∗, black asterisk) But 13, (○, open black circle) But 22, (△, black open triangle) But 34, (×, black cross) But 61, and (□, blue open square) But 100. The isothermal graphs presented are respectively: (a) 293.15 K, (b) 313.15 K, (c) 333.15 K, (d) 353.15 K, (e) 373.15 K. The dotted line is a guide for the eyes. (Created by the author, 2024)

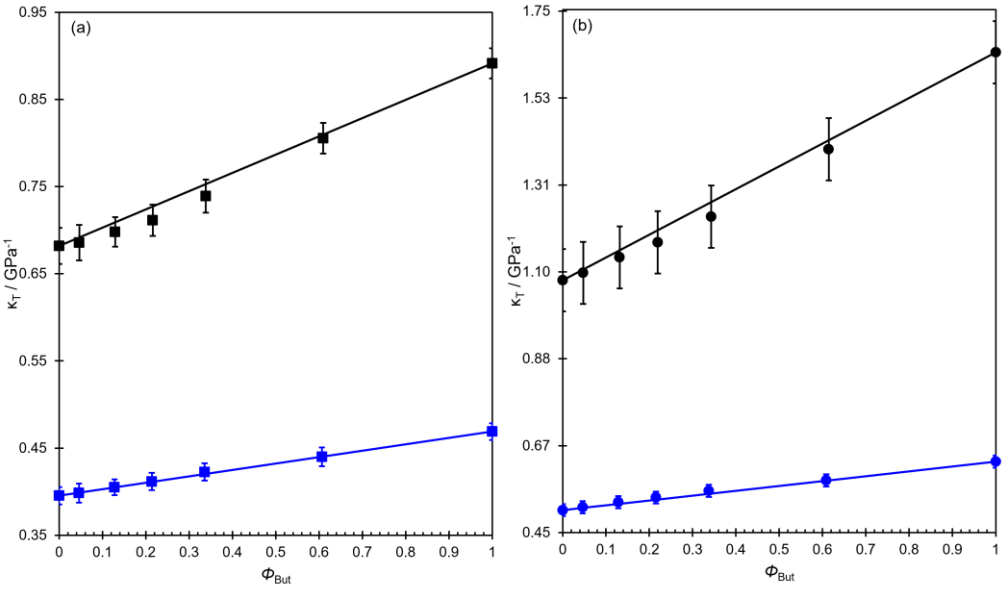

Figure 26 – Isothermal compressibility as a function of the volume fraction of 1-butanol (ϕ_{But}) in 1-butanol and linseed biodiesel blends at temperatures of: $T = 293.15\,K$ (a), $T = 393.15\,K$ (b), and pressure, P: (■, black square), $0.1\,MPa$; (■, blue square), $100\,MPa$. Straight lines, ideal behavior. Error bars indicate the expanded uncertainty corresponding to a 95% confidence level.

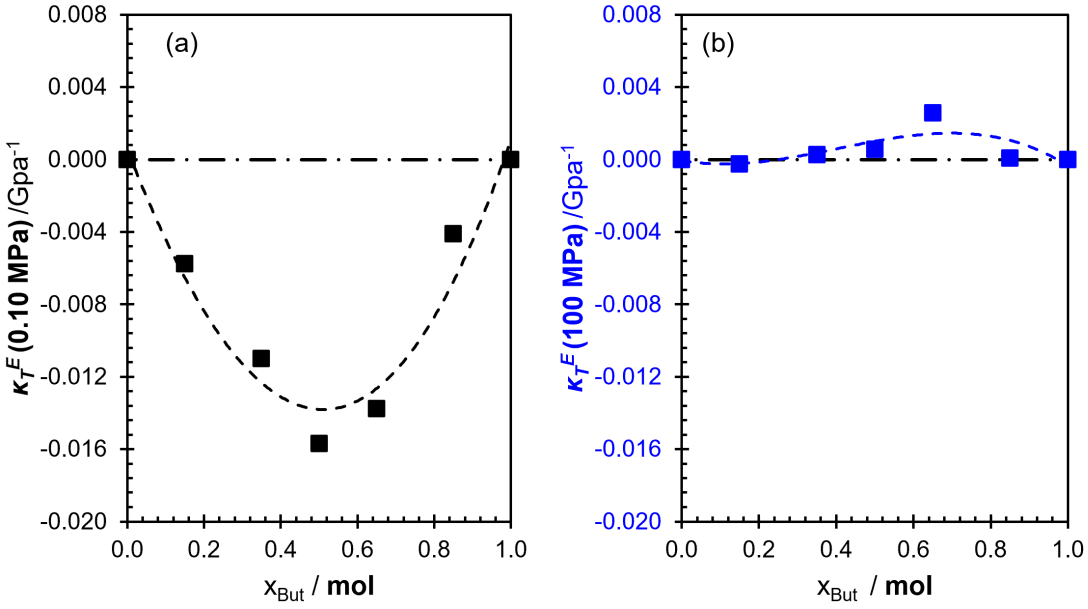

.

Figure 27 – Excess isothermal compressibility (κ_T^E) as a function of the molar fraction of 1-butanol (x_{But}) in 1-butanol and linseed biodiesel blends at temperature $T = 293.15\,K$ and pressure, P: (■, black square), $0.1\,MPa$; (■, blue square), $100\,MPa$. Dotted line polynomial fit. (Created by the author, 2024)

The isobaric thermal expansivity (α_P) for the 1-butanol and the linseed biodiesel blends were plotted in Figure 28 as a function of pressure for different isotherms for different

mixtures. Our research group demonstrated that an inversion point was also observed Ait Belale et al. (2021 e Aitbelale et al. (2021 e Alves et al. (2022 e Ivaniš et al. (2016a, 2016b). At this crossover point, the isobaric thermal expansivity becomes independent of temperature, i.e., $(\partial \alpha_P / \partial T) = 0$. As the biodiesel content increases, the isotherms tend to converge. When the composition reaches But 5 (with the highest biodiesel content), an intersection between the isotherms becomes apparent. This phenomenon was observed by Ait Belale et al. Ait Belale et al. (2021 e Aitbelale et al. (2021) for biodiesel and alcohols (1-butanol and 2-butanol) mixtures. Notably, α_P of biodiesels derived from grape seed, sunflower, corn, linseed, and waste oil is documented in the literature to exhibit an inversion point within the range of $30 - 50\,MPa$ Alves et al. (2022 e Ivaniš et al. (2016a, 2016b e Prieto et al. (2015). In a previous study carried out by our research group with blends of petro-diesel and biodiesel Alves et al. (2022), we observed this inversion point in all the combinations evaluated. This suggests that the occurrence of the inversion point in all blend proportions may be associated with the nature of the bonds formed between the compounds. While in mixtures of low-polar compounds (petro-diesel and biodiesel) this point appeared in all mixture proportions, in the mixture alcohol + biodiesel, it only appeared as biodiesel was added to alcohol but not in pure alcohol. This behavior may be linked to the reduction in the concentration of hydrogen bonds coming from the alcohol. All calculated values of the derived properties, along with their corresponding graphs, are presented in **Appendix D**.

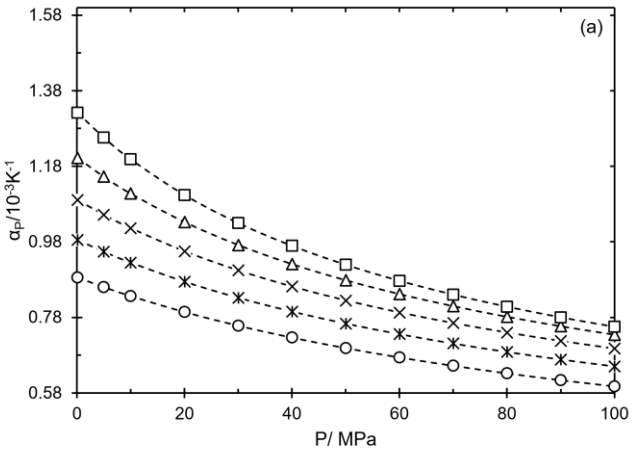

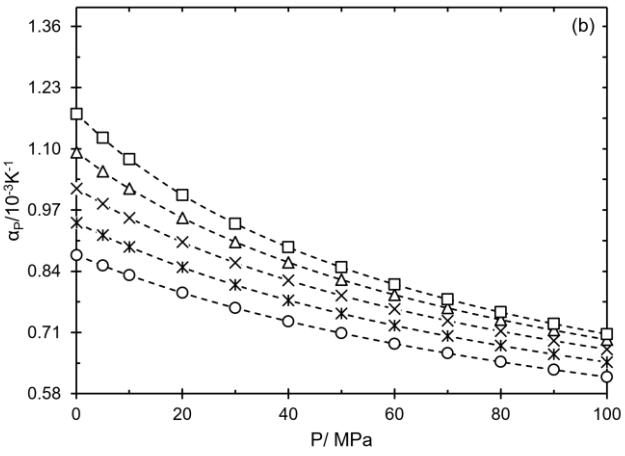

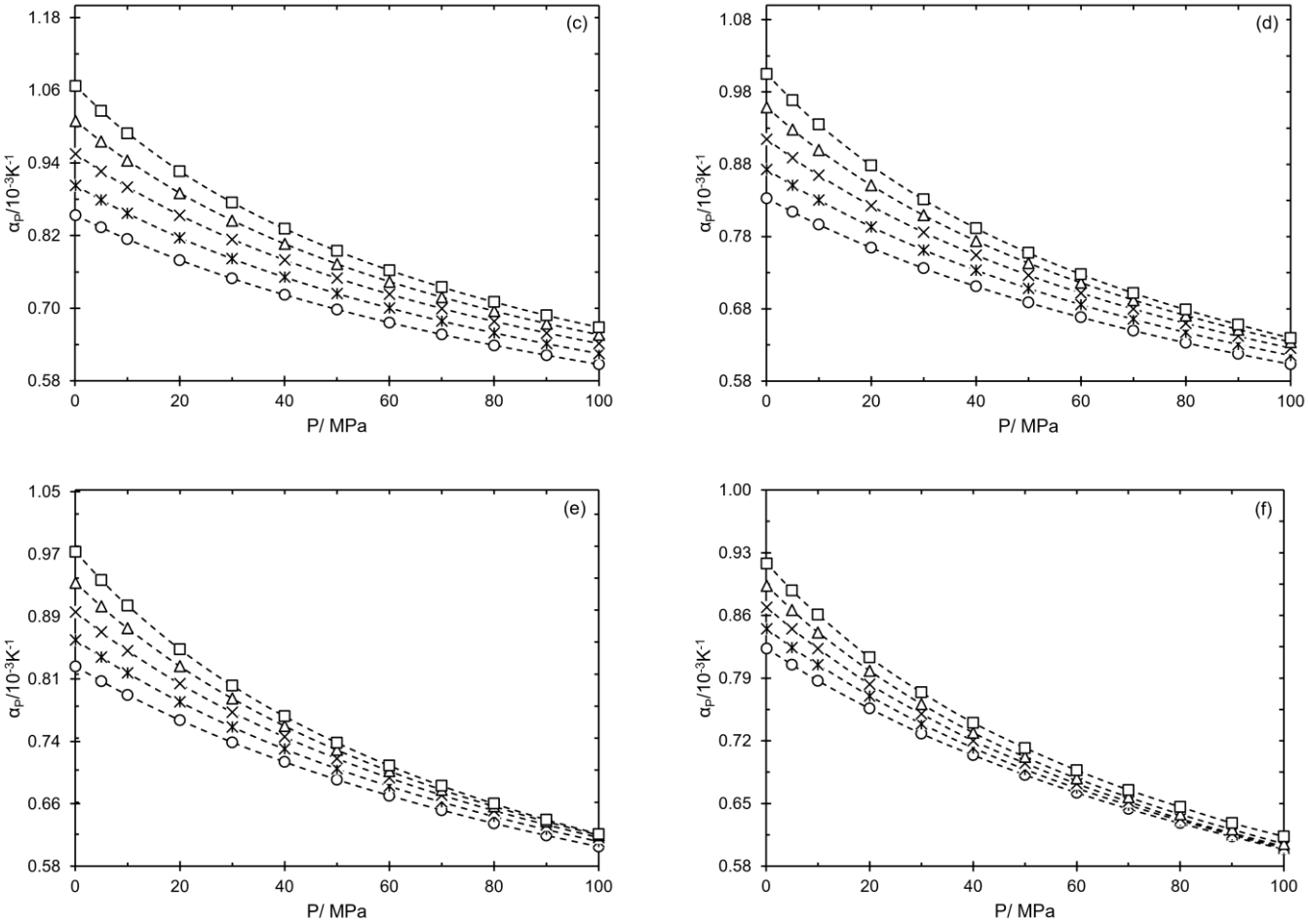

Figure 28 – Isobaric thermal expansivities (α_P) as a function of pressure for different 1-butanol and biodiesel blends. Symbols and dotted lines represent isobaric thermal expansivities. Each symbol means a temperature isotherm, and all graphs have a fixed composition. 373.15 K (□, black open square), 353.15 K (△, black open triangle), 333.15 K(×, black cross), 313.15 K(∗,black asterisk), and 293.15 K (○, black solid circle). (a) But 100; (b) But 61; (c) But 34; (d) But 22; (e) But 13; (f) But 5. The dotted line is a guide for the eyes. (Created by the author, 2024)

5.4.3 PC-SAFT EoS

The density data of 1-butanol and biodiesels were first correlated using the PC-SAFT equation of state, as described in Section 5.3.3. In Table 18, the parameters obtained for 1-butanol agree with those documented in the literature, validating our approach of fitting the equation of state to the data, a procedure similar to that used in another article by the research group but for a different alcohol (methanol) Da Costa; De Medeiros; et al. (2024). Some articles Ait Belale et al. (2021 e Aitbelale; Chhiti; et al. (2019 e Aitbelale et al. (2021) present PC-SAFT modeling for the volumetric behavior of biofuel systems, utilizing an approach like those discussed for 1-butanol, where the association parameter is considered. However, since

biodiesel is composed of a mixture of fatty acid alkyl esters and their molecules do not form hydrogen bonds, the association parameters were not considered in this work for biodiesels. This methodology is similar to the one used by García-Morales et al. García-Morales et al. (2023). Thus, for biodiesels, the PC-SAFT equation requires only three parameters: the segment number (m), the segment diameter (σ), and the segment energy parameter (ε/k). Table 19 compares the parameters derived from this study and those reported in the literature for two other biodiesels. The mean absolute percentage deviation for the studied biodiesels was 0.10% for linseed biodiesel and 0.12% for soy biodiesel, respectively, as shown in Table 19. These results closely resemble those obtained for the FAME-beef tallow mixture García-Morales et al. (2023) (MAPD = 0.11%) and soybean biodiesel Aitbelale; Chhiti; et al. (2019) (MAPD = 0.10%).

Table 18 – Pure Component (1-Butanol) Parameters for PC-SAFT Equation of State**.**

1-butanol parameters							References
m_i	σ_i (Å)	ε_i/k (K)	κ_{AB_i}	ε_i^{AB}/k (K)	T range / K	$MAPD^a$	
3.269	3.376	243.22	0.019	2349.91	283-503	0.34	Grenner et al. (2007)
3.667	3.220	213.03	0.040	2298.34	298-393	0.10	Ait Belale et al. (2021)
2.751	3.614	259.59	0.007	2544.60	184-563	1.63	Gross; Sadowski (2002b)
2.843	**3.550**	**253.94**	**0.001**	**3178.87**	**293-373**	**0.07**	**This Work**

[a] $\text{MAPD} = \frac{1}{\text{N}_{\text{data}}} \sum_{\text{i}-1}^{\text{N}_{\text{data}}} \left| \frac{\rho_{\text{i}}^{\text{Calc}} - \rho_{\text{i}}^{\text{Exp}}}{\rho_{\text{i}}^{\text{Exp}}} \right| \times 100$;

Table 19 – PC-SAFT parameters obtained in this work and data from the literature on biodiesel.

biodiesel/ source	**biodiesel parameters**					References
	$MM(g \cdot mol^{-1})$	m_i	σ_i (Å)	ε_i/k (K)	$MAPD^a$	
SOB (soybean)	265.1	9.601	3.566	281.298	0.10	Aitbelale; Chhiti; et al. (2019)
FAME mixture (beef Tallow)	281.0	12.890	3.257	241.350	0.11	García-Morales et al. (2023)
linseed	**294.2**	**11.278**	**3.495**	**271.511**	0.10	**T**his **W**ork
soybean	**291.9**	**11.412**	**3.457**	**269.867**	**0.12**	**T**his **W**ork

[a] $\text{MAPD} = \frac{1}{\text{N}_{\text{data}}} \sum_{\text{i}-1}^{\text{N}_{\text{data}}} \left| \frac{\rho_{\text{i}}^{\text{Calc}} - \rho_{\text{i}}^{\text{Exp}}}{\rho_{\text{i}}^{\text{Exp}}} \right| \times 100$

The combination rule was applied to mixtures of butanol and biodiesel, incorporating a temperature-independent binary interaction parameter (k_{ij}) to account for cross-interactions between butanol, which exhibits molecular association due to its hydroxyl group, and biodiesel, treated as a non-associative pseudo-component. The model considered the association between butanol molecules, while biodiesel molecules were modeled as non-associative, reflecting the absence of functional groups promoting significant association. The adjusted k_{ij} parameter was used to capture cross-interactions between the associative component (butanol) and the non-associative component (biodiesel), resulting in values of -0.03474 for linseed biodiesel and -0.03561 for soy biodiesel, which is justified by the similarity in the ester profiles of these biofuels. Table 20 presents the mean percentage deviations between the experimental densities and those predicted by the PC-SAFT equation, considering the constant parameters shown in Tables 18 and 19, both with adjusted k_{ij} and with ($k_{ij} = 0$). As expected, the inclusion of the adjusted k_{ij} parameter reduces the errors, although the predictive capability of the PC-SAFT equation remains remarkable, showing an overall average deviation of just 0.33% even without k_{ij} adjustment.

Figure 29 illustrates the deviations between the experimental data and density calculated by the PC-SAFT equation of state for both blends studied.

Table 20 – Mean Average Percentage Deviations between the experimental densities and those predicted by the PC-SAFT EoS. For 1-Butanol + Biodiesel (Linseed and Soy) Mixtures Studied Here.

Blends But + Bio / approaches k_{ij}	**But 5**	**But 13**	**But 22**	**But 34**	**But 61**
biodiesel linseed			***MAPD***		
$k_{ij} = 0$	0.243	0.354	0.410	0.370	0.296
$k_{ij} = -0.03474$	0.176	0.168	0.130	0.102	0.217
biodiesel soybean			***MAPD***		
$k_{ij} = 0$	0.195	0.151	0.382	0.492	0.416
$k_{ij} = -0.03561$	0.268	0.338	0.107	0.106	0.105

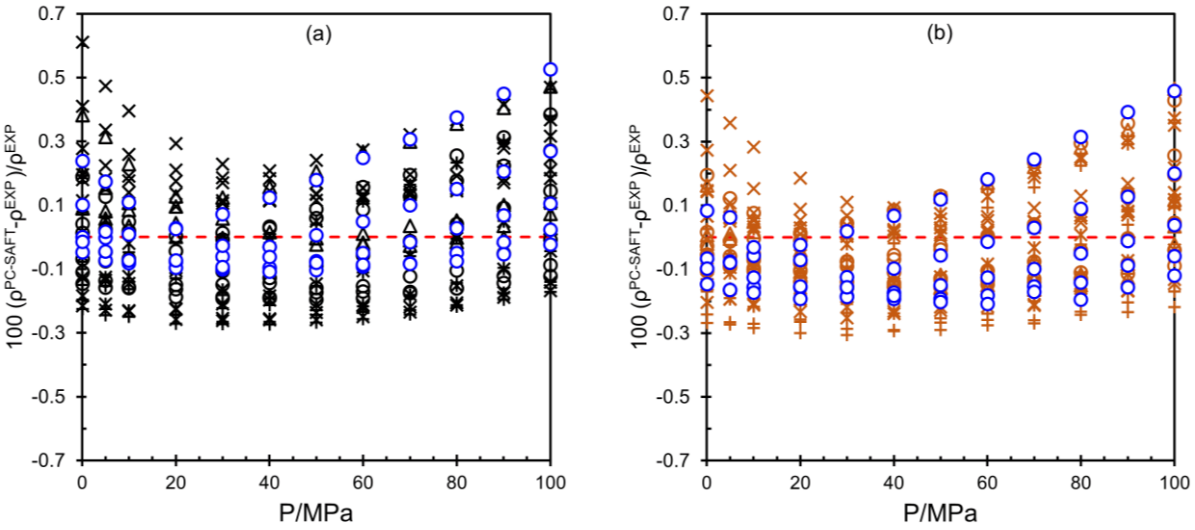

Figure 29 – Residuals for density calculations of the 1-butanol + biodiesel blends systems by the PC-SAFT EoS as a pressure function Where: (○, blue open circle) But 0, (+, plus signal) But 5, (∗, asterisk) But 13, (○, open circle) But 22, (△, open triangle) But 34, and (×, cross) But 61. Graphs with black symbols (a) represent the blends of the system with linseed biodiesel, while those with brown symbols (b) represent the system with soybean biodiesel, both at different temperatures. (Created by the author, 2024)

5.4.4 Tammann-Tait correlation

As expected, the Tammann-Tait equation with temperature-dependent parameters yielded very good fits to the experimental data, justifying its use in the previous section to obtain derivatives of density concerning either pressure or temperature. This favorable outcome comes at the cost of the number of adjustable parameters: seven for each mixture. Additionally, it can only be employed to correlate measurements for a specific mixture. Under no circumstances it can be utilized to predict density beyond the experimental temperature and pressure range, nor can it be used to calculate the volumetric properties of a mixture whose composition has not been experimentally investigated. On the contrary, the PC-SAFT equation can predict the volumetric behavior of a mixture of compositions for which no experimental data is available since it requires only one binary interaction to describe the blending effect. Despite this single adjusted parameter, the densities calculated in 1-butanol+biodiesel with the equation state remained highly satisfactory.

Figure 30 compares experimental and calculated densities using PC-SAFT for blends (But 22) of 1-butanol and biodiesel from linseed and soybeans. The results demonstrate outstanding agreement between measured and predicted densities across various pressure and

temperature values. Specifically, for this system, the MAPD between experiment and calculation is 0.130% and 0.107% for PC-SAFT linseed and soybean, respectively.

About the maximum deviations (maximum APD, Absolute Percentage Deviation) of the compounds shown in Figure 30, values of 0.018% and 0.020% were recorded for the Tammann-Tait equation, while using the PC-SAFT model, the maximum deviations were 0.384% and 0.429% for linseed and soy, respectively. Although the data obtained using the PC-SAFT EoS model proved to be slightly larger and more dispersed than the Tammann-Tait equation, it is essential to note the significant difference in the number of parameters involved between the two methods. Nevertheless, the fact that the Tammann-Tait equation demonstrates an excellent fit to the experimental data underscores the quality of the data obtained in this study.

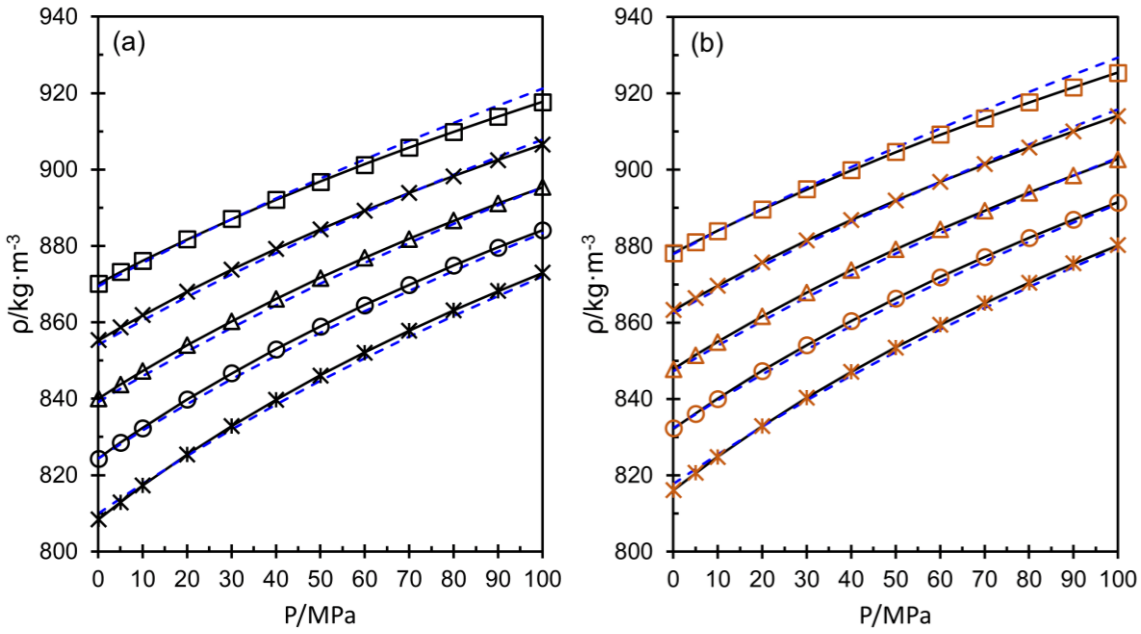

Figure 30 – Experimental density (ρ) as a function of pressure for 1-butanol and biodiesel blends. Each symbol means a temperature isotherm: 293.15 K (□, black open square), 313.15 K (×, black cross), 333.15 K (△, black open triangle), 353.15 K (○, solid black circle), and 353.15 K (*, black asterisk). The graph on the black symbols refers to blend But 22 for linseed biodiesel; on the brown symbols, the same blend for soybean biodiesel. Modeling: (−,continuous black line) corresponds to the fit of Tammann–Tait, and (---, blue dashed lines) represent the data obtained by PC-SAFT. (Created by the author, 2024)

The Tammann-Tait correlation and the PC-SAFT equation of state can be employed to determine isothermal compressibility and isobaric thermal expansion by deriving the density calculated from the equation. For this purpose, a methodology from the literature was used

García-Morales et al. (2023). As mentioned earlier, while the adjusted PC-SAFT equation demonstrates an acceptable average deviation for density, it inadequately represents the effect of pressure on the derived volumetric properties, as depicted in Figures 31 and 32. Consequently, it yields a poor representation of compressibility and expansivity compared to that obtained using the Tammann-Tait equation adjustment. The results obtained in this comparison align closely with those reported by Gracía-Morales et al. García-Morales et al. (2023), albeit for mixtures of alkanes and biodiesel.

In Figure 31, the comparison illustrates the compressibility behaviors of two mixtures (But 5 and But 61), as well as pure 1-butanol (But 100). Similar trends regarding pressure and temperature between the two methodologies (Tammann-Tait and PC-SAFT), albeit with notable disparities in κ_T. The mean absolute percentage deviation (MAPD) reaches 7.2%, with relative point deviations nearing 20%. To enhance clarity, the graphs for expansivity are juxtaposed rather than overlaid, facilitating visualization. Regarding isobaric thermal expansivity, Figure 32 presents a similar comparative analysis for the same systems (But 5, But 61 and But 100.

When observing the graphs of Figure 31, it is evident that the PC-SAFT EoS did not accurately represent the compressibility of 1-butanol+biodiesel systems. An illustrative example is the inversion observed in the isotherms when analyzing pairs (a) - (d). However, it is important to highlight a key point, as reported in the literature for both associative and non-associative compounds: in certain instances, the data obtained by PC-SAFT successfully captures the general trends observed for each property, as demonstrated in Figures 31 and 32. This phenomenon has been documented by Llovell and Vega Llovell; Vega (2006), who validated the calculation of several key thermodynamic properties for N-alkanes and a 1-alkanol from SAFT equation of state.

Previous studies have underscored the challenges in accurately representing second-order derivative properties using SAFT-type equations, a topic also discussed in this paper Diamantonis; Economou (2011 e Llovell; Vega (2006 e Mao et al. (2023 e Wilhelmsen et al. (2017b). Apart from properties like κ_T and α_P, others such as thermal capacities, speed of sound, and Joule-Thomson coefficients also pose difficulties due to their second-order derivative nature Diamantonis; Economou (2011). The analysis of mixtures, as addressed in this study, introduces further complexity to the accurate multiparametric modeling of fluid behavior under high-pressure and temperature conditions, particularly for compound mixtures encompassing both associative and non-associative fluids.

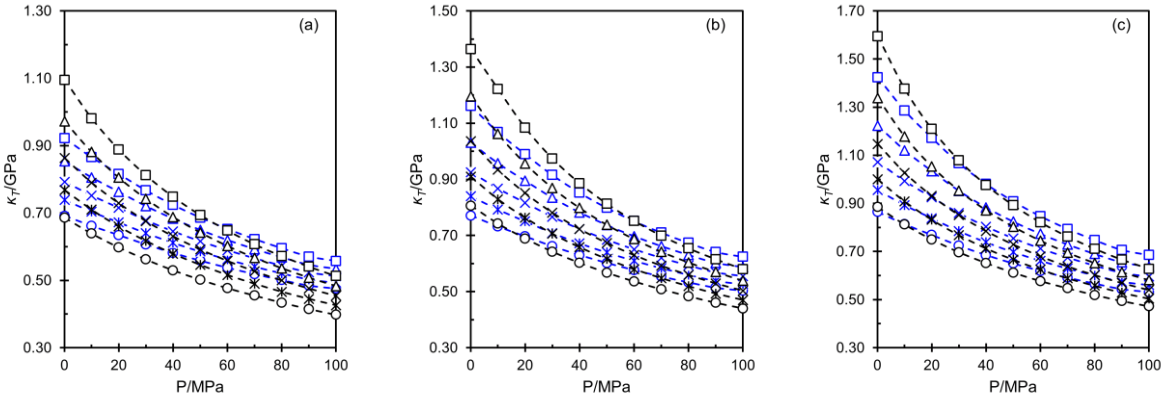

Figure 31 – Comparison of the Isothermal compressibility (κ_T) for mixtures of 1-butanol and linseed biodiesel, obtained using the Tammann Tait equation (represented by the black symbols) and PC-SAFT equation (represented by the blue symbols) as a function of pressure. The graphs illustrate the differences and similarities in the properties of the two thermodynamic models. Each symbol refers to the temperature: 293.15 K (□, black open square) 313.15 K, (×, black cross) 333.15 K, (△, black open triangle) 353.15 K, (○, open black circle) 373.15 K, (∗, black asterisk). Dashed lines are for visual guidance. (a), (b) and (c) represent data for But 5, But 61, and But 100 mixtures. (Created by the author, 2024)

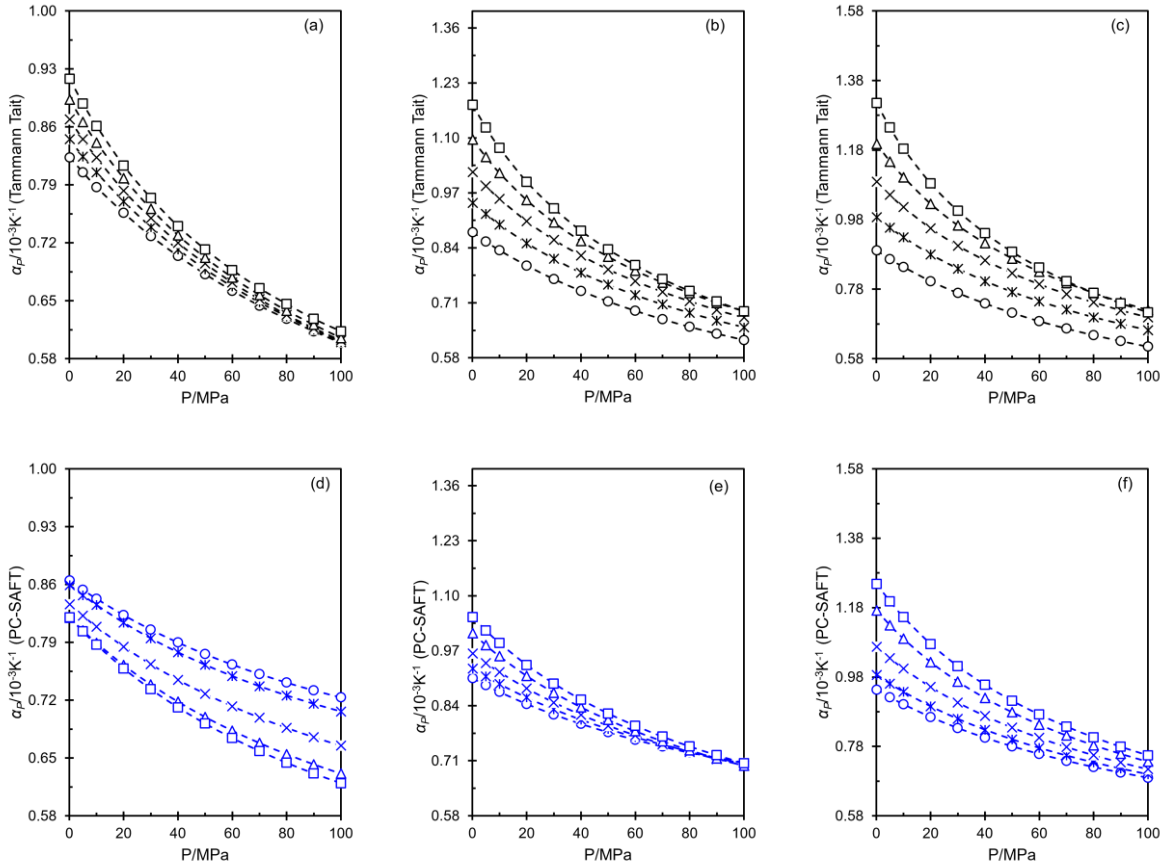

Figure 32 – Comparison of the isobaric thermal expansivities (α_P) for mixtures of 1-butanol and linseed biodiesel, obtained using the Tammann-Tait equation (represented by the black symbols) and PC-SAFT equation (represented by the blue symbols), as a function of pressure.

The graphs illustrate the differences and similarities in the properties of the two thermodynamic models. Each symbol refers to temperature, where: 293.15 K (□, black open square) 313.15 K, (×, black cross) 333.15 K, (△, black open triangle) 353.15 K, (○, open black circle) 373.15 K, (∗, black asterisk). Dashed lines are for visual guidance. (a), (b), and (c) are respectively the But 5, But 61 and But 100 mixtures obtained by Tammann-Tait; (d), (e), and (f) are respectively the But 5, But 61 and But 100 mixtures obtained by PC-SAFT. (Created by the author, 2024)

5.5 Conclusions

Density measurements were conducted within binary mixtures comprising 1-butanol and either linseed or soy methyl biodiesel at pressures up to 100.0 MPa and temperatures spanning from 293.15 to 373.15 K. These measurements yielded a total of 720 new experimental density data points. The calculated excess volume for the two binary systems revealed minimal deviation from ideal behavior, with a maximum deviation of 0.15% of the total volume. This indicates that despite the inherent complexity introduced by associative compounds in biodiesels, the volumetric behavior of 1-butanol + methyl biodiesel closely resembles that of an ideal solution. The nearly ideal behavior observed in this type of system shows that there is no cross-association between associative alcohols and non-associative biodiesels. The alcohol molecules associate with each other exactly as they do in their pure state. This finding contradicts a prior study Ait Belale et al. (2021) on a similar system involving the binary mixture of butanol and biodiesel derived from cooking oil. The densities of the studied systems were correlated using the Tammann-Tait and PC-SAFT equations, resulting in maximum deviations of MAPD = 0.01% and MAPD = 0.49%, respectively, for the 1-butanol + biodiesel mixture. Derived properties such as isothermal compressibility κ_T and isobaric thermal expansivity α_P were calculated using fitted Tammann-Tait equation, and obtained data were compared with the predictions of PC-SAFT equation of state. While the PC-SAFT equation of state reliably represented the behavior of density, it predicted a distinct behavior for the derived properties compared to that obtained by the Tammann-Tait equation.

6 EXPERIMENTAL DETERMINATION AND ANALYSIS OF THE SPEED OF SOUND IN 1-BUTANOL + BIODIESEL MIXTURES AT HIGH PRESSURES: A CONTRIBUTION TO THE UNDERSTANDING OF ALTERNATIVE FUEL SYSTEMS

Results: Manuscript Under Review.

6.1 Introduction

Chapter 3 of this thesis investigated the density and speed of sound properties of three biodiesels derived from canola, sucupira, and coconut oils, with experimental data collected under pressures of up to 200 MPa. These results not only provided valuable insight into the thermophysical behavior of biofuels but also served as a foundation for evaluating thermodynamic models aimed at predicting these properties. Subsequently, Chapter 5 presented an experimental study on the density of binary mixtures of 1-butanol with biodiesels produced from soybean and linseed oils, emphasizing the effects of alcohol addiction on volumetric properties.

Continuing this line of research, the main objective of this chapter is to experimentally investigate the speed of sound in mixtures of 1-butanol with biodiesels derived from canola and sucupira, thereby expanding the available database for systems of this type. Despite the change in feedstock compared to Chapter 5, the experimental data for the pseudopure biodiesels characterized in Chapter 3 were used as a reference. The analysis was conducted under various pressure and temperature conditions, with a particular focus on the influence of 1-butanol incorporation on the acoustic properties of the mixtures.

The literature has shown increasing interest in the combination of medium-chain alcohols with biodiesel, driven by biodiesel's potential as a renewable alternative to fossil fuels and the role of 1-butanol as a promising additive capable of significantly altering the physical and chemical properties of the fuel Kuszewski et al. (2023 e Rakopoulos et al. (2010 e Wang et al. (2015a).

In this context, this study presents experimental data on the speed of sound in mixtures of 1-butanol with canola and sucupira biodiesels under pressures of up to 100 MPa. Measurements were performed for molar compositions ranging from 0 to 1 in 1-butanol, at temperatures of 293.15 K, 313.15 K, and 333.15 K.

In addition to experimental characterization, this study aims to evaluate the applicability of previously proposed empirical correlations for predicting the speed of sound in complex mixtures. Properties such as the relative deviation with respect to the additive behavior speed of sound (c^{Rmix}, relative deviation with respect to the additive behavior speed of sound) and the product of the speed of sound and the molar mass raised to a constant power (cM^{γ}, with γ=0.975) were analyzed. The latter has proven effective in describing the speed of sound using group contribution techniques for long chain n-alkanes Daridon (2022a) and fatty acid methyl esters (FAMEs) Daridon (2022b). Previous studies indicate that cM^{γ} follows a simple additivity rule in terms of mole fraction for alkane–alkane Khasanshin et al. (2009, 2010, 2014) and FAME–FAME mixtures Daridon et al. (2023), with behavior close to ideal even in hybrid systems such as n-alkane + methyl oleate, showing reduced deviations Daridon et al. (2023).

Motivated by these findings, this chapter aims to assess the applicability of the empirical approach to mixtures containing alcohol and biodiesel. The cM^{γ},values were determined for the systems studied under different pressure conditions, with the objective of identifying an appropriate combination rule for these binary systems.

Finally, the experimental data were used to evaluate the predictive capability of the PC-SAFT equation of state in describing the speed of sound in the studied mixtures. The model was applied without any adjustment of binary interaction parameters, using molecular parameters previously determined for the pure components. The comparison between experimental and calculated values allowed for an assessment of the suitability of PC-SAFT for systems involving associative components, such as 1-butanol, in combination with the biodiesels analyzed in this work.

6.2 Experimental measurements.

6.2.1 Materials

The biodiesels investigated in this study were synthesized following the procedure described in Chapter 2, Section 2.2, via the transesterification reaction of sucupira and canola oils with methanol (Sigma, molar purity 0.999). The process was conducted under the same experimental conditions and purification protocols previously established, ensuring a water content of less than 0.05% by mass, in compliance with ASTM D6751. Further details, including the compositional profile of these biodiesels, can be found in Chapter 2 of this thesis.

The binary mixtures of 1-butanol and biodiesel were prepared gravimetrically using an electronic analytical balance with a precision of ±0.0001 g. Mixtures were prepared with

mass fractions of 0, 20, 40, 60, 80, and 100% 1-butanol. The 1-butanol used (Thermo Scientific, purity 0.999) was utilized without further purification. The maximum standard uncertainties estimated for the compositions of the mixtures were less than $u_c(x_{\text{butanol}}) = 4 \cdot 10^{-5}$, calculated on a molar basis from the conversion of the respective mass fractions.

6.2.2 Speed of sound (c) measurement

The speed of sound was measured using the pulse-echo technique in a high-pressure cell, as described in Chapter 1, Section 1.5.2. In this study, measurements were conducted for pressures up to 100 MPa and temperatures of 293.15 K, 313.15 K, and 333.15 K. The experimental system features an immersion ultrasonic sensor coupled with a high-voltage pulse generator operating at 3 MHz. The speed of sound was determined using the time-of-flight method, accounting for the difference in acoustic path between two asymmetrically positioned reflectors. The experimental apparatus and calibration procedures adhere to protocols established in previous studies. The measuring cell was filled under vacuum to eliminate the presence of bubbles and was maintained in a thermostatic bath to ensure thermal stability. The pressure was controlled by an external volumetric pump and monitored by a sensor with a standard uncertainty of 0.01 MPa in the range of 0-100 MPa. The temperature was recorded using a PT100 probe, ensuring a standard uncertainty of 0.1 K.

6.3 Modeling

6.3.1 PC-SAFT Modeling

In Chapters 3 and 5 of this thesis, the PC-SAFT equation of state was applied to calculate the density and speed of sound at high pressures for three biodiesels (coconut, sucupira, and canola) and to estimate the density, also at high pressures, of mixtures of 1-butanol with two biodiesels (linseed and soybean), respectively. In this chapter, the same equation of state is applied once again, this time with the objective of calculating the speed of sound at high pressures for mixtures of 1-butanol with two additional biodiesels, sucupira and canola, which were previously investigated in Chapter 3.

The methodology adopted for applying the PC-SAFT equation is similar to that described in Chapter 3, involving the adjustment of the model's fundamental parameters, namely: the number of segments (m), the segment diameter (σ), and the segment energy parameter (ε/k). As in previous chapter and litterature (AIT BELALE *et al.*, 2021; ALVES,

ALANDERSON ARTHU ARAÚJO *et al.*, 2024; ARAÚJO ALVES *et al.*, 2025; GARCÍA-MORALES *et al.*, 2023)*et al., 2025; GARCÍA-MORALES et al., 2023)*, biodiesels were modeled as mixtures of fatty acid alkyl esters that do not exhibit hydrogen bonding. Therefore, the association parameters were disregarded. Conversely, for 1-butanol, which is capable of forming hydrogen bonds, the association term was included in the model, as was done in Section 5.3.3 of Chapter 5, dedicated to the study of 1-butanol/biodiesel blends.

However, there is an important methodological difference compared to Chapter 5. While that study was limited to the analysis of density at high pressures, using only this property to fit the equation of state parameters, the present chapter calibrates the parameters based on both experimental density data (obtained in Chapter 5) and speed of sound data (obtained in this chapter), all at high pressures. The parameters were optimized by minimizing an objective function that quantifies the discrepancy between the experimental and predicted values of both properties. The mathematical expression used for this optimization is presented in Equation 3.3.

In summary, the parameters used for the biodiesels studied in this chapter (sucupira and canola) were the same as those obtained in Chapter 3, as the compounds are the same. In contrast, for 1-butanol, new parameter sets were derived from the simultaneous consideration of density and speed of sound data, the latter being experimentally determined in this chapter.

6.4 Results and discussion

6.4.1 Speed of sound

The speed of sound in the liquid mixtures under study was measured at temperatures of 293.15 K, 313.15 K, and 333.15 K, across pressure ranges from atmospheric pressure to 100 MPa, with increments of 10 MPa. The values obtained as a function of pressure and temperature for both systems are presented in Table 21. The speed of sound data for the two pure biodiesels are not included in this table, as they were already provided in Chapter 3. However, the measurements performed on pure 1-butanol are included in the last column of the table. These experimental data for pure 1-butanol were compared with values available in the literature Dávila et al. (2016 e Dzida (2020 e Plantier et al. (2002 e Wilson; Bradley (1964) as shown in Figure 33, to validate both the reagent and the experimental apparatus used in this study.

The average absolute deviation between the experimentally measured data and the values reported in the literature was only 0.18%, demonstrating excellent agreement between the datasets. This low deviation confirms the reliability of the measurements and the suitability of the equipment for determining the speed of sound under high-pressure conditions.

As presented in Chapter 3 of this thesis, experimental data on the speed of sound in biodiesel under high pressures are quite limited Araújo Alves et al. (2025 e Habrioux et al. (2013a, 2023). Even more scarce are studies addressing the speed of sound in biodiesel-butanol blends under these conditions. To the best of our knowledge, only one study in literature reports sound speed data for blends involving biodiesel and isobutanol (an isomer of 1-butanol), evaluating the effects of pressure and temperature up to a limit of 25 MPa. However, there are no records in the literature of sound velocity measurements for biodiesel blends with 1-butanol in the pressure ranges evaluated in this study. The available data for isobutanol is relevant due to its consistency, the scarcity of reported values in the literature, and the near absence of experimental information at pressures above 0.1 MPa.

Table 21 – Experimental Speed of Sound (c) Blending 1-Butanol with Biodiesel (Canola and Sucupira), as Function of Composition (x_1) Temperature (T) and Pressure (p)[a].

x_1/mol		0.50	0.73	0.86	0.94	0.50	0.72	0.86	0.94	1.00
$w_1/mass$		0.20	0.40	0.60	0.80	0.20	0.40	0.60	0.80	1.00
p/MPa	T/K	Canola biodiesel				Sucupira biodiesel				1-But
0.1	293.15	1372.7	1338.9	1310.0	1283.7	1378.5	1343.2	1313.2	1285.7	1258.2
10	293.15	1419.9	1387.9	1360.4	1336.0	1425.0	1392.4	1363.7	1337.7	1313.3
20	293.15	1464.0	1433.6	1407.6	1384.4	1468.2	1437.2	1410.4	1386.2	1363.0
30	293.15	1505.1	1476.3	1452.0	1430.3	1509.9	1480.3	1454.6	1431.5	1409.6
40	293.15	1544.4	1516.5	1493.0	1472.4	1548.6	1520.0	1495.4	1473.6	1453.4
50	293.15	1581.1	1554.5	1531.6	1511.6	1584.9	1557.4	1533.9	1513.1	1493.5
60	293.15	1615.7	1590.0	1568.9	1550.1	1620.6	1594.1	1571.1	1550.7	1531.9
70	293.15	1650.0	1624.6	1603.7	1585.4	1653.7	1627.9	1605.8	1586.4	1568.3
80	293.15	1682.3	1657.5	1636.6	1618.9	1685.5	1660.6	1639.6	1621.1	1603.9
90	293.15	1712.5	1688.5	1668.7	1652.0	1715.3	1691.3	1671.2	1653.6	1637.4
100	293.15	1742.1	1718.9	1700.1	1683.7	1745.2	1721.4	1701.8	1684.6	1668.1
0.1	313.15	1300.6	1267.0	1238.3	1213.2	1306.3	1271.2	1241.7	1215.5	1190.4
10	313.15	1350.8	1319.6	1292.8	1269.2	1355.7	1324.0	1296.1	1270.9	1247.6
20	313.15	1397.4	1368.0	1343.6	1322.0	1402.2	1372.3	1346.4	1323.2	1301.5
30	313.15	1441.8	1413.4	1389.7	1369.2	1446.1	1417.5	1392.5	1370.5	1350.9
40	313.15	1482.8	1456.1	1433.9	1414.4	1486.9	1459.9	1436.6	1415.7	1395.8
50	313.15	1521.7	1495.6	1474.2	1455.9	1525.3	1499.1	1476.8	1457.2	1439.0
60	313.15	1559.2	1533.7	1512.5	1494.6	1562.8	1537.2	1515.2	1496.0	1479.0
70	313.15	1594.1	1569.9	1549.6	1532.2	1597.2	1572.7	1551.8	1533.5	1516.9
80	313.15	1627.4	1603.6	1584.3	1568.1	1629.9	1606.4	1586.7	1569.7	1554.0
90	313.15	1659.9	1636.6	1618.0	1602.3	1663.0	1639.7	1620.3	1603.4	1587.7
100	313.15	1691.1	1668.9	1650.4	1634.3	1694.2	1671.7	1652.4	1635.4	1619.4
0.1	333.15	1230.6	1196.5	1168.7	1145.3	1236.8	1201.2	1171.9	1147.0	1124.9

10	333.15	1284.4	1253.4	1227.4	1205.4	1289.6	1258.3	1230.8	1207.0	1186.5
20	333.15	1334.7	1305.6	1281.4	1261.1	1339.3	1309.9	1284.4	1262.5	1243.8
30	333.15	1381.2	1353.9	1331.2	1312.1	1385.0	1357.4	1333.8	1313.5	1296.0
40	333.15	1424.5	1398.3	1376.9	1359.1	1428.1	1401.6	1379.1	1360.0	1344.1
50	333.15	1465.7	1440.5	1419.8	1402.3	1468.5	1443.2	1421.6	1403.1	1387.3
60	333.15	1503.9	1479.5	1460.1	1444.2	1507.3	1482.9	1462.4	1445.2	1430.8
70	333.15	1541.0	1517.3	1498.1	1482.4	1543.9	1520.2	1500.1	1483.3	1469.8
80	333.15	1576.2	1553.6	1534.8	1519.3	1578.5	1555.8	1536.5	1520.2	1506.8
90	333.15	1609.0	1587.3	1569.8	1555.2	1612.3	1590.1	1571.5	1555.8	1542.6
100	333.15	1641.1	1619.5	1602.4	1588.5	1643.7	1622.2	1604.1	1589.1	1577.1

a: Standard uncertainties u is $u(T) = 0.1K$; $u(p) = 0.01MPa$ up to $100MPa$, the combined expanded uncertainties U (level of confidence = 0.95) are $U(c) = 0.002c$ up to 100 MPa. *b:* Data for biodiesel in its pseudo-pure state ($x_1 = 0$) can be found in Chapter 2 or in the referenced publication Araújo Alves et al. (2025).

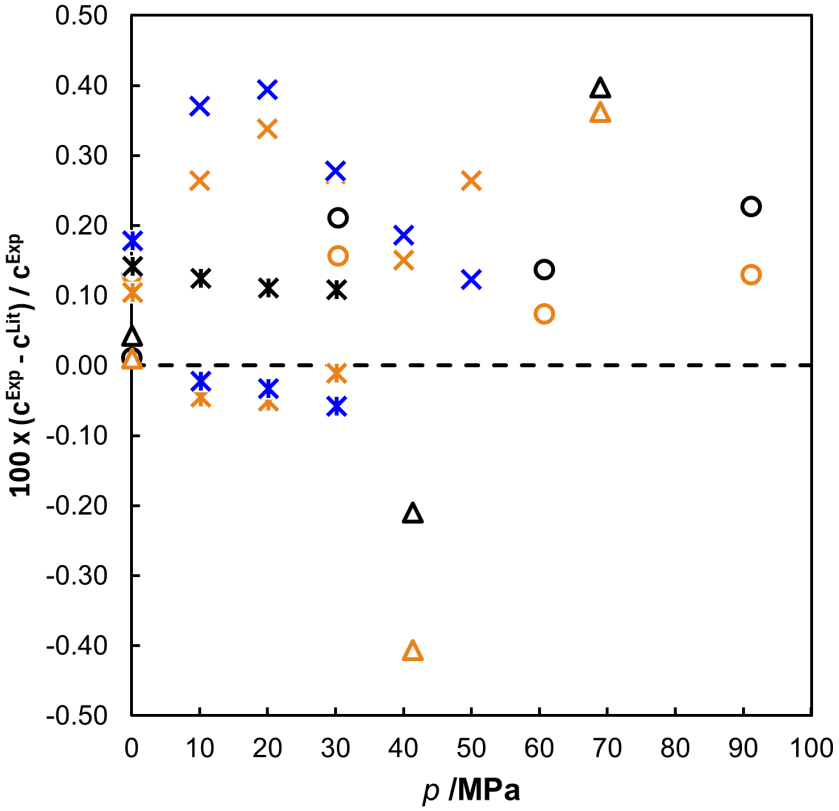

Figure 33 – Relative deviations between the experimental speed of sound data, which were determined in this paper for pure 1-butanol, and the literature values for 1-butanol as a function of experimental pressure at various temperatures. Literature data: (×) Plantier et al. (2002), (○) Dzida (2020), (Δ) Wilson; Bradley (1964), and (∗) Dávila et al. (2016). The symbols with black colors refer to the temperatures of 293.15 K, Orange 313.15 K and Blue 333.15 K. (Created by the author, 2025)

The behavior observed for mixtures of 1-butanol and biodiesel reveals a monotonic decrease in the speed of sound with increasing alcohol mole fraction in both systems, as illustrated in Figure 34. Notably, this reduction in sound speed does not follow a linear trend

with respect to the molar fraction of butanol in the mixture. However, this non-linearity cannot be attributed to deviations from ideality as the speed of sound in ideal mixtures does not obey a simple additive combining rule based on molar fractions. Several factors must be considered to better understand the phenomenon, but primarily, the non-linear behavior arises from the functional form of the Newton-Laplace equation (Equation 6.1), which relates the speed of sound to the density (ρ) and isentropic compressibility (κ_s) of the system, properties that do not vary linearly with molar fraction.

$$c = \frac{1}{\sqrt{\rho \kappa_S}} \tag{6.1}$$

Another factor that may contribute to the observed behavior is the molecular asymmetry between 1-butanol and biodiesel. Studies conducted by Daridon with mixtures of alkane + fatty acid methyl ester (FAME), such as n-hexane + methyl oleate and n-decane + methyl oleate, showed that the deviation from sound speed additivity on a mole fraction basis tends to be more pronounced when there is a significant difference in the length of the carbon chain between the components. This tendency was more pronounced in the system containing n-hexane, due to the greater structural asymmetry compared to the system containing n-decane.

To better assess the deviation from the ideal additive behavior of the speed of sound, several authors have employed the change upon mixing, denoted as c^{mix}, and defined by the expression:

$$c^{mix} = c - \sum_i x_i c_i \tag{6.2}$$

where c is the speed of sound in the mixture, x_i and c_i are the mole fraction and the speed of sound of the pure component *i*, respectively.

In the present study, however, we favor the use of the relative deviation with respect to the additive behavior. This approach provides a more consistent basis for comparing deviations across different binary systems:

$$c^{Rmix} = \frac{c^{mix}}{\sum_i x_i c_i} \tag{6.3}$$

The values of this quantity, calculated for both binary mixtures, are presented in Figures 35 for two isobars: 0.1 and 100 MPa at 293 K. To facilitate comparison, both binary systems are plotted on the same figures. From this figure, it is evident that the two biodiesels exhibit similar mixing behavior in the presence of 1-butanol. It can also be observed that the deviation from additive behavior becomes more pronounced at lower pressures for a given

temperature. In other words, the deviation decreases as the system becomes denser and less compressible.

It is important to note that in a previous study (Chapter 5 of this thesis Alves et al. (2024)), the density of these mixtures (1-butanol + linseed biodiesel and +1-butanol soy biodiesel) was investigated in volumetric terms. The results showed a very small deviation from ideality, with a maximum excess volume of only 0.15%, which suggests a behavior close to ideal for this property.

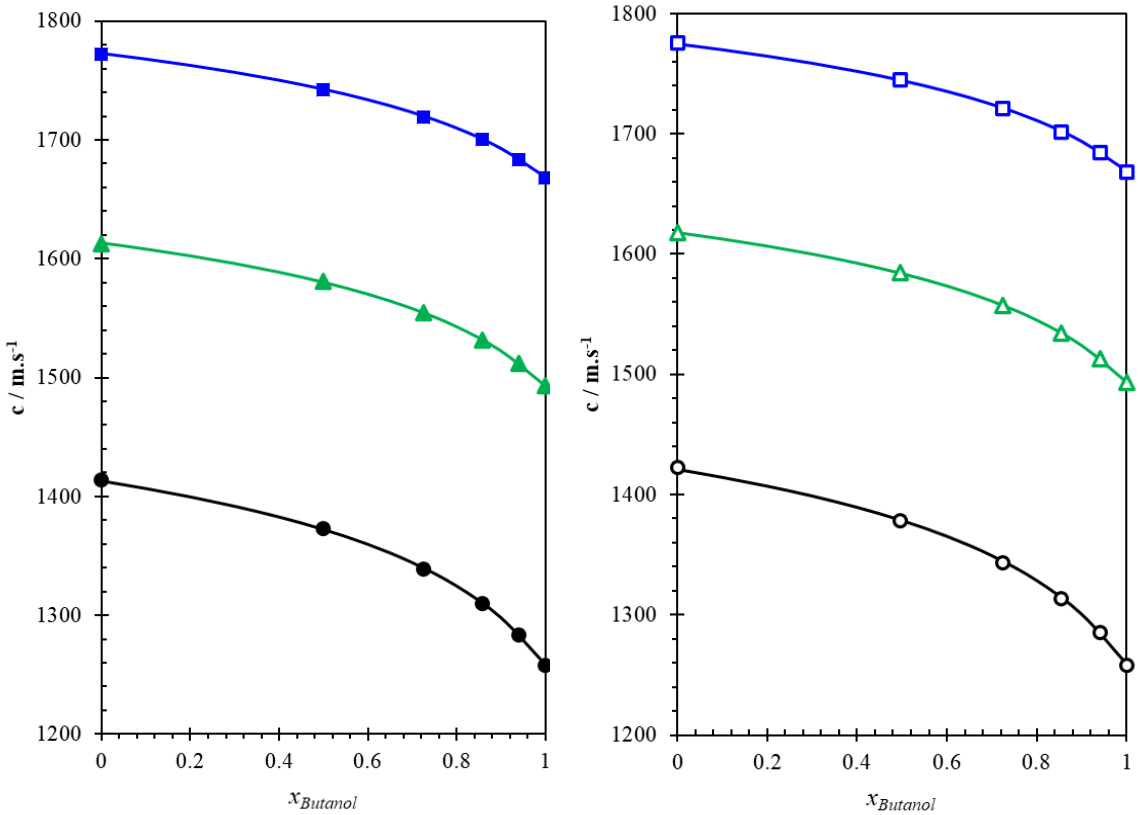

Figure 34 – Speed of sound c as a function 1-butanol molar fraction $x_{Butanol}$ at temperature $T = 293.15$ K and at various pressures p: ●, 0.1 MPa; ▲, 50 MPa; ■, 100 MPa. The solid symbols represent the blends of the 1-butanol + canola biodiesel system (a), while the hollow symbols correspond to the 1-butanol + sucupira biodiesel system (b). Solid lines are given by the proposed combining rule (eq. 6.10). (Created by the author, 2025)

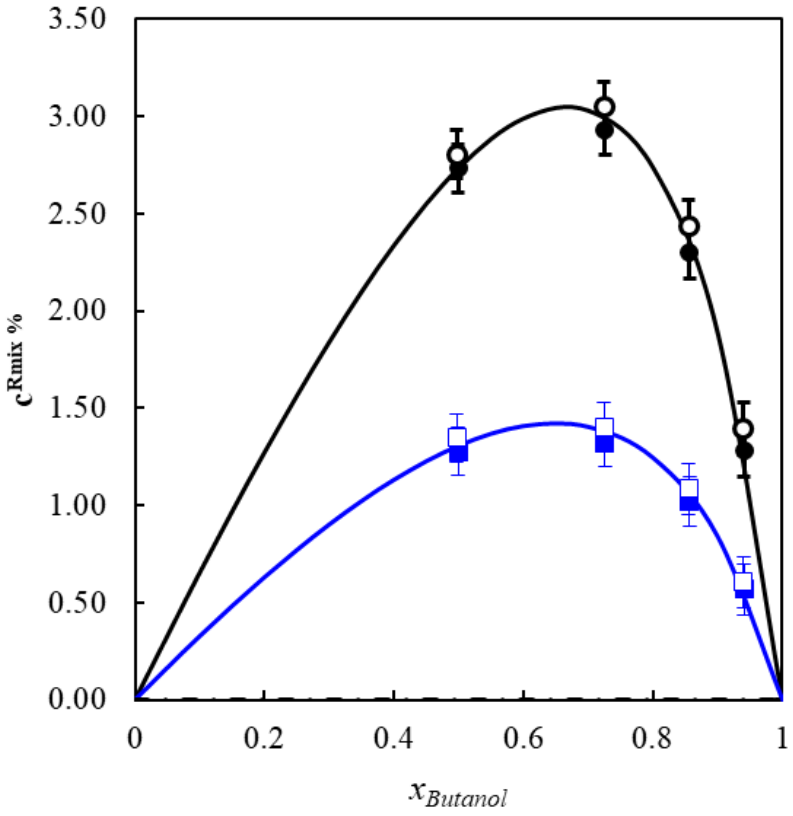

Figure 35 – Relative change of speed of sound along mixing: c^{Rmix} (in percentage) as a function 1-butanol molar fraction $x_{Butanol}$ at temperature T = 293.15 K and at two pressures p: ●, 0.1 MPa; ■, 100 MPa. The solid symbols represent the blends of the 1-butanol +canola system, while the hollow symbols correspond to the 1-butanol +sucupira system (b). Solid lines are given by the proposed combining rule (eq. 6.10). (Created by the author, 2025)

Analysis of the excess property of the speed of sound (c^E) is a widely used approach for investigating intermolecular interactions in liquid mixtures. The ideal sound speed can be calculated from expressions based on isentropic compressibility and the density of the components, as described in the literature. However, this type of calculation has important limitations. As reported by Daridon et al. Daridon et al. (2022, 2023) in their work, the combination of various thermophysical properties in its calculation, such as molar mass, isobaric heat capacity, density and its derivatives: isobaric expansion and compressibility for both pure components, can propagate significant uncertainties.

Given these limitations, an alternative approach was adopted using the $cM\gamma$ parameter, proposed in literature as an empirical way of describing the behavior of the speed of sound in binary mixtures. This parameter is defined as the product of the speed of sound and the average molar mass of the mixture, raised to a constant γ, which has been determined to provide good agreement with group additivity rules in the heavy alkane (above

n-C10) Daridon (2022a). For butanol + biodiesel blends, the property derived from this product raised to a constant power was evaluated. Mathematically, the $cM\gamma$ quantity is defined by means of a power transformation applied to the product of the speed of sound (c) and the average molar mass of the mixture, as shown in Equation 6.4:

$$cM_\gamma = (c\sum_i x_i M_i)^\gamma \tag{6.4}$$

In this equation, c represents the speed of sound in the mixture, x_i and M_i are, respectively, the molar fraction and molar mass of component i, and γ is an exponent adjusted empirically to maximize the linearity of the property with the composition. For this study, γ=0.975 was used, a value previously reported in the literature to correctly represent Alkanes and FAME systems.

To examine the behavior of the $cM\gamma$ property as a function of composition, its values were plotted against the butanol mole fraction in Figure 36. To highlight any deviations from molar additivity, the quantities cM_γ^{mix} and $cM\gamma^{Rmix}$ as defined by Equations 6.5 and 6.6, have been calculated:

$$cM_\gamma^{mix} = cM_\gamma - \sum_i x_i cM_{\gamma,i} \tag{6.5}$$

$$cM_\gamma^{Rmix} = \frac{cM_\gamma^{mix}}{\sum_i x_i cM_{\gamma,i}} \tag{6.6}$$

In both blends studied (canola biodiesel and sucupira biodiesel with butanol) at atmospheric pressure, the $cM\gamma$ parameter exhibits in Figure 36 an almost linear behavior with respect to the molar fraction of butanol. At first glance, this trend suggests near-linear behavior, as no significant deviations are apparent from the direct representation of $cM\gamma$ as a fonction of $x_{butanol}$. However, by considering the relative quantity $cM\gamma^{Rmix}$, which expresses the deviation of the mixture from the expected additive value, it becomes possible to identify and quantify small deviations from additivity in the system more sensitively. The calculated values of $cM\gamma^{Rmix}$ were plotted in Figures 37 and 38 respectively for two isobars :0.1 and 100 MPa at one temperature: 293.15 K and for two isotherms: 293.15 and 33.15 K at atmospheric pressure.

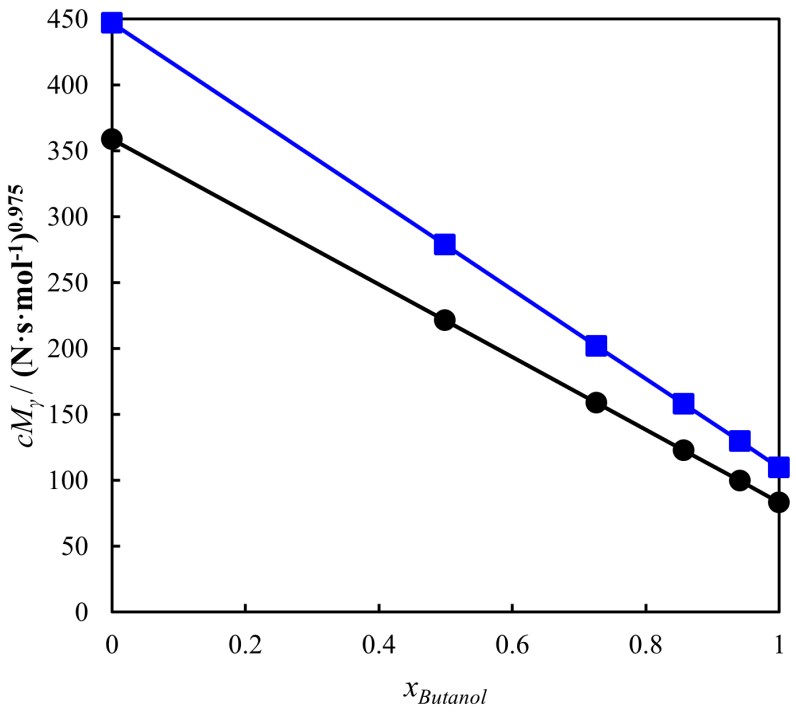

Figure 36 – Product of the speed of sound and the molar mass raised to a constant power (cM_γ) with γ=0.975 as a function of the molar fraction of butanol ($x_{Butanol}$) at temperature T = 293,15 K and pressures of ●, 0.1 MPa e ■, 100 MPa. symbols represent the experimental values, and the solid line corresponds to the prediction based on the simple additivity rule. (Created by the author, 2025)

Evaluation of Figures 37 and 38 reveals systematic negative deviations across the entire composition range at atmospheric pressure (0.1 MPa) for both temperatures, indicating the presence of interactions between the components. In contrast, at 100 MPa, the deviations are close to zero, although small fluctuations remain evident. Figure 39 presents both c^{Rmix} and $cM\gamma^{Rmix}$ on the same graph for the binary system 1-butanol + canola biodiesel at 293.15 K and atmospheric pressure. It can be observed in this figure that the deviation from additivity is approximately ten times smaller for $cM\gamma^{Rmx}$ than for c^{Rmix}.

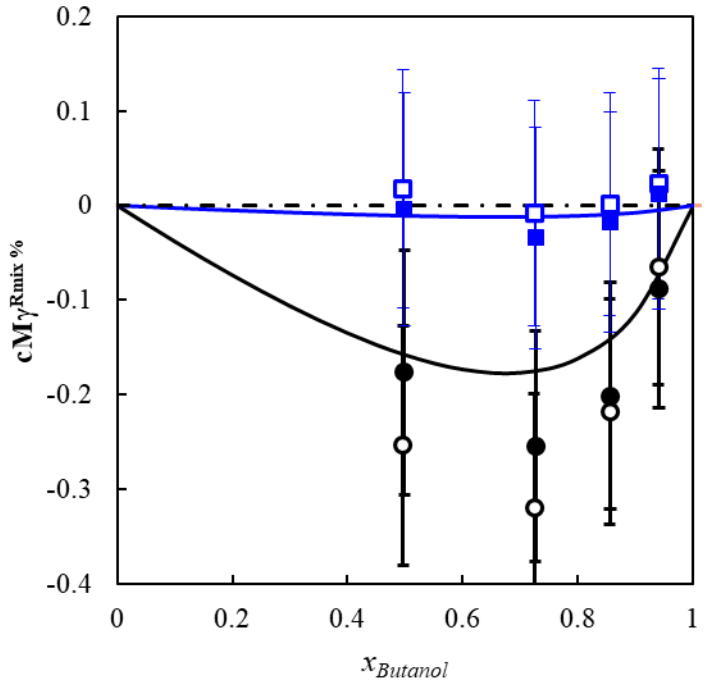

Figure 37 – Relative change of $cM\gamma$ along mixing : $cM\gamma^{Rmix}$ (in percentage) as a function 1-butanol molar fraction $x_{Butanol}$ at temperature $T = 293.15$ K and at two pressures p: ●, 0.1 MPa; ■, 100 MPa. The solid symbols represent the blends of the 1-butanol +canola biodiesel system, while the hollow symbols correspond to the 1-butanol +sucupira biodiesel system (b). Solid lines are given by the proposed combining rule (eq. 6.10). (Created by the author, 2025)

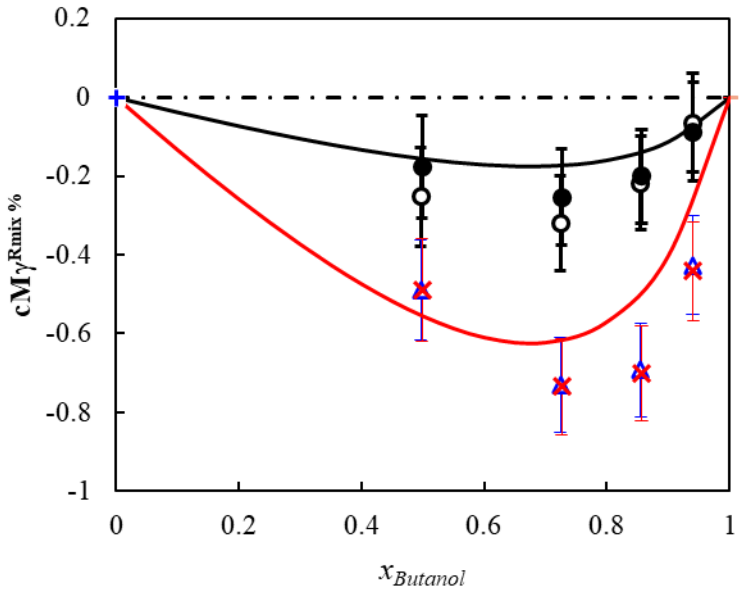

Figure 38 – Relative change of $cM\gamma$ along mixing : $cM\gamma^{Rmix}$ (in percentage) as a function 1-butanol molar fraction $x_{Butanol}$ at atmospheric pressure and two temperatures: ●, $T = 293.15$ K ; ×, Δ, 333.15 K. The solid symbols represent the blends of the 1-butanol +canola system, while the hollow symbols correspond to the 1-butanol +sucupira system (b). Solid lines are given by the proposed combining rule (eq. 6.10). (Created by the author, 2025)

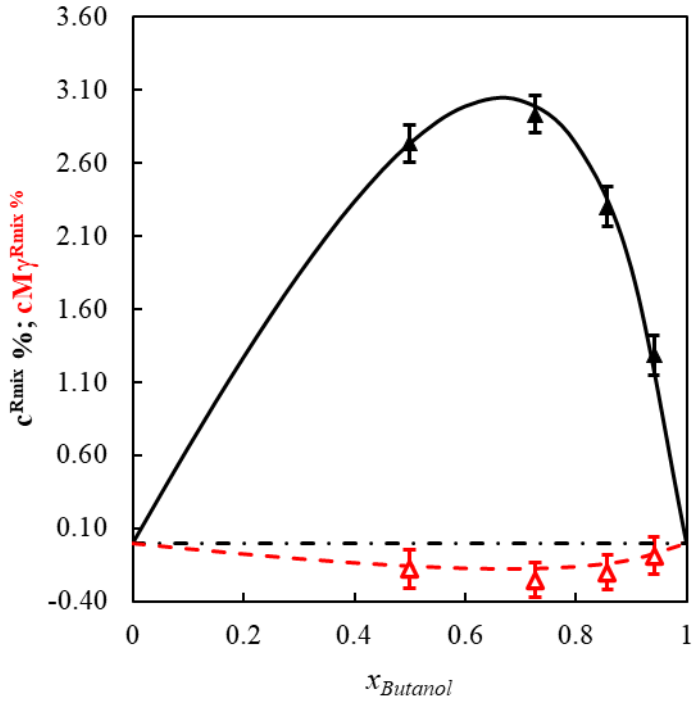

Figure 39 – Relative change upon mixing in percentage for speed of sound: c^{Rmix} and for $cM\gamma$: $cM\gamma^{Rmix}$ (as a function 1-butanol molar fraction $x_{Butanol}$ 1-butanol +canola biodiesel at atmospheric pressure and at temperature T = 293.15 K. The solid symbols ▲ represents c^{Rmix} while the hollow symbols Δ correspond to $cM\gamma^{Rmix}$. Solid and dashed lines are obtained by the proposed combining rule (eq. 6.10).

The inclusion of error bars in the different graphs strengthens this interpretation: although the deviations are small, they exceed the uncertainty limits for some compositions, particularly at high pressures. Additionally, a tendency for these deviations to increase with rising temperature at atmospheric pressure was observed. At a temperature of 333.15 K, for instance, the deviations reached values close to -0.75% relative to the additive behavior, nearly doubling the deviations observed at lower temperatures, as illustrated in Figure 38. Thus, even though the $cM\gamma$ quantity exhibits an apparently linear behavior, the analysis of relative deviations along with their corresponding uncertainties reveals nuances in the thermophysical behavior of the system. This suggests the need for careful consideration and potential correction, as such variations should not be overlooked. It is worth noting that the data presented in this figure pertains to the system containing canola biodiesel. Similar results were observed for the system with sucupira biodiesel.

As shown in Figures 37 and 38, which depict the behavior of the blends with the two different biodiesels, the deviation from additivity follows the same trend with respect to both pressure and temperature for both mixtures. This suggests that the deviations can be

described by a single correlation. Furthermore, the nearly symmetric bell-shaped profile observed for these mixtures when representing $cM\gamma^{mix}$ instead of $cM\gamma^{Rmix}$indicates that $cM\gamma^{mix}$ can be represented using a one-parameter Margules-type equation:

$$cM\gamma^{mix} = Ax_{butanol}(1 - x_{butanol}) \tag{6.7}$$

where parameter A exhibits a strong decrease with increasing pressure and a and linear increase with temperature. Therefore, to correlate $cM\gamma^{mix}$ with the mole fraction, temperature, and pressure, the following expression was employed:

$$cM\gamma^{mix} = A_0(1 + \mathrm{a}(\mathrm{T} - \mathrm{T}_0))\exp\left(-\frac{p-p_0}{b}\right)x_{butanol}(1 - x_{butanol}) \tag{6.8}$$

where $T_0 = 293.15\ K$, p_0 is set to atmospheric pressure and the three parameters A_0, a, b were adjusted to fit the $cM\gamma^{mix}$ values of both the binary systems investigated by minimizing the following objective function:

$$F_{obj} = \sum_{i_{exp}=1}^{N_{exp}}\left(cM\gamma_{cal}^{mix} - cM\gamma_{i_{exp}}^{mix}\right)^2 \tag{6.9}$$

The obtained parameters were reported in Table 22. From these parameters the speed of sound in binary mixtures can be calculated for any composition between $x_{Butanol} = 0$ and 1 and for pressure between 0 and 100 MPa in the temperature range 293.15 -333.15 K using the following expression:

$$c = \frac{\left(\sum_i x_i\, cM_{\gamma,i} + x_1x_2A_0(1+\mathrm{a}(\mathrm{T}-\mathrm{T}_0))\exp\left(-\frac{p-p_0}{b}\right)\right)^{1/\gamma}}{\sum_i x_iM_i} \tag{6.10}$$

where $cM_{\gamma,i}$ for pure butanol and biodiesels were correlated in both pressure and temperature using a Murnaghan type equation F. D. Murnaghan (1924):

$$cM_{\gamma,i} = A_{cM\gamma,i}\left(1 + B_{cM\gamma,i}\cdot\tilde{p}\right)^{C_{cM\gamma,i}} \tag{6.11}$$

where parameters $A_{cM\gamma,i}$, $B_{cM\gamma,i}$ and $C_{cM\gamma,i}$ are all a function of temperature according to the following relationships:

$$A_{cM\gamma,i} = a_{0,i} + a_{1,i}T + \frac{a_{-1,i}}{T} \quad (6.12)$$

$$B_{cM\gamma,i} = b_{0,i} + b_{1,i}T + b_{2,i}T^2 \quad (6.13)$$

$$C_{cM\gamma,i} = c_{0,i} + c_{1,i}T + c_{2,i}T^2 \quad (6.14)$$

The nine parameters of these equations were determined by regression of the experimental speed of sound data presented in Table 21 for 1-butanol and from Chapter 3 for pure biodiesels up to 200 MPa. The resulting values are provided in Table 23.

Table 22 – Parameters A_0, a and b of eq 6.8 for correlating $cM\gamma^{mix}$ as a function of molar fraction, temperature and pressure for both systems investigated with $\gamma = 0.975$ and where the units are K for the temperature T, MPa for pressure p, kg.mol^{-1} for molecular weight M and m.s^{-1} for speed of sound c

systems	A_0	$a \times 10^3$	b
1 Butanol + Canola biodiesel 1 Butanol + Sucpira biodiesel	-1.393	54.68	40.62

Table 23 – Parameters of Murnaghan type equation F. D. Murnaghan (1924) for pure 1-butanol and biodiesels used in eqs. 6.11 – 6.14 with $\gamma = 0.975$ and where the units are K for the temperature T, MPa for pressure p, kg.mol^{-1} for molecular weight M and m.s^{-1} for speed of sound c.

system	a_0	$a_1 \times 10^3$	a_{-1}	$b_0 \times 10^3$	$b_1 \times 10^6$	$b_2 \times 10^9$	$c_0 \times 10^3$	$c_1 \times 10^6$	$c_2 \times 10^9$
1-Butanol	140.0961	-206.3336	1077.7530	31.9103	-199.1300	470.1210	293.3263	-43.2340	405.4140
Canola	508.7000	-701.5000	16300.0000	12.0800	-70.7300	217.8000	420.8000	-755.6000	1377.0000
Sucupira	435.7803	-592.2491	27832.2600	4.0347	-23.0880	143.2630	463.1776	-963.3900	1653.6200

The performance of the proposed model (Eq. 6.10) with parameters reported in Tables 22 and 23 was evaluated by comparing the calculated values of speed of sound with the experimental data. The statistical analysis of the deviations for both binary systems is summarized in Table 24. For comparison, the deviations obtained using the Murnaghan correlations for pure components were also included in the table to highlight the influence of the mixing rule on the overall deviations, relative to those arising solely from the adjustment of pure component values. In addition, Figure 40 illustrates the deviations between the experimental and calculated speed of sound values as a function of the butanol mole fraction, for three extreme conditions (T=293.15 K, p=0.1 MPa; T=293.15 K, p=100 MPa; T=333.15 K, p=0.1 MPa).

As noted from table 24 and observed in Figure 40, the values calculated using the proposed correlation, based on the combination of Eqs. (6.10) and (6.11) exhibit excellent agreement with experimental measurements. The maximum deviations are 0.16% for the 1-butanol +canola system and 0.26% for the 1-butanol +sucupira system, both of which with an mean average percentage deviation of 0.06 % that fall below the expanded experimental uncertainty. Moreover, model accuracy does not deteriorate with increasing pressure; on the contrary, the average deviation decreases as pressure rises.

These findings confirm that the speed of sound in 1-butanol + biodiesel mixtures can be reliably correlated using the proposed mixing rule. This approach requires only the speed of sound of the pure components and three adjustable parameters. The model was developed using experimental data up to 100 MPa. However, since the parameters for the pure components were fitted using data up to 200 MPa and the exponential pressure-dependent term ($\exp(-(p - p_0)/b)$ approaches unity before 100 MPa, the model can be extended to 200 MPa with an uncertainty comparable to that of experimental measurements. Furthermore, by comparing the deviations observed for the pure components with those obtained for the mixtures, it can be noted that the use of the mixing rule does not lead to an increase in the average deviation and results in only a slight increase in the maximum deviation, on the order of 0.03% compared to that observed for the pure components.

Since the mixing rule does not distinguish between the two types of biodiesels used in this study, it is reasonable to expect that it could be applied to 1-butanol + biodiesel mixtures derived from other feedstocks. Nevertheless, to extend the predictive capability of the model to broader applications, such as 1-butanol + other biodiesels or mixtures involving other alcohols like methanol, additional experimental validation is required. This is particularly important, as the present study was limited to correlation rather than full prediction.

Table 24 – Statistical characteristics (Mean Percentage Deviation, Mean Average Percentage Deviation, Maximum Percentage Deviation) for the prediction of speed of sound in pure and binary systems up to 100MPa using eqs. 6.10 – 6.14 with parameters given in Tables 22 and 23.

System	MPD	MAPD	MaxPD
1-Butanol + Canola biodiesel	-0.025	0.056	0.16
1-Butanol + Sucupira biodiesel	0.020	0.053	0.26
Pure 1-Butanol	0.010	0.045	0.13
Pure Canola biodiesel	-0.0013	0.049	0.12
Pure Sucupira biodiesel	0.0007	0.054	0.22

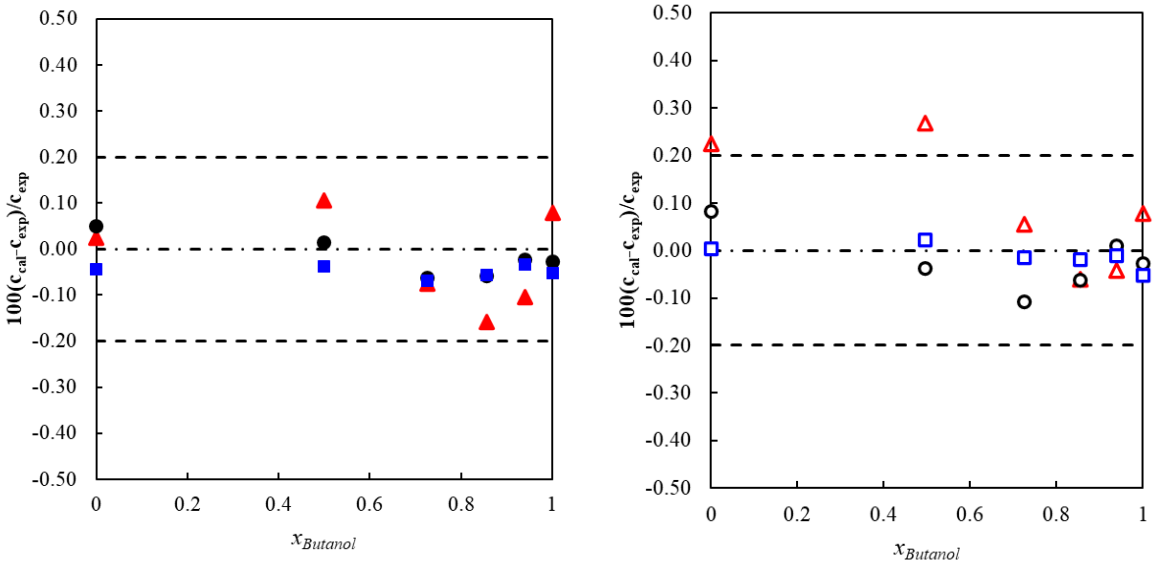

Figure 40 – Percentage deviations between the predictions of the proposed method and the experimental speed of sound data for 1-Butanol + Canola biodiesel (a) and 1-Butanol + Sucupira biodiesel (b), ●○, p=0.1 MPa, T=293.15 K; ■□, p=100 MPa, T=293.15 K; ▲△, p=0.1 MPa, T=333.15 K. The dashed line corresponds to the expanded uncertainty U(c). (Created by the author, 2025)

6.4.2 PC-SAFT EoS

The experimental speed of sound data for 1-butanol, as well as for canola and sucupira biodiesels, were calculated using the PC-SAFT equation of state, as described in Section 6.3.1. For 1-butanol, the molecular parameters were optimized based on a combined dataset of experimental density and speed of sound measurements under high-pressure conditions. The parameters obtained from this fitting procedure are presented in Table 25. The MAPD values obtained were 0.17% for density and 2.05% for speed of sound, indicating good agreement between the calculated and experimental results.

For comparison purposes, Table 25 also includes the parameters previously obtained in Chapter 5, where the fitting was performed using only density data. A comparison between the two parameter sets shows that the differences are minor and are attributed to the inclusion of speed of sound as a second fitting property. As expected, this inclusion led to a slight increase in the deviation for predicted density, in exchange for a more robust and comprehensive representation of the system's thermodynamic behavior.

Using the newly fitted parameters, the density and speed of sound of 1-butanol were calculated at different pressures and temperatures. Figure 41 presents the results for the speed

of sound as a function of pressure for three isotherms: 293.15 K, 313.15 K, and 333.15 K. The main graph (a) shows a direct comparison between the experimental data and the values predicted by the PC-SAFT equation of state, while the inset graph (a.a) displays the corresponding relative deviations as a function of pressure. The density values calculated for 1-butanol using the updated parameter set are provided in **Appendix E, Figure E1**.

With regard to biodiesels, the molecular parameters used were the same as those presented in Chapter 3, since both the samples and the experimental data used in this section are identical. The evaluation of the performance of the PC-SAFT equation of state for biodiesels, treated as pure pseudocompounds, is detailed in that chapter. The MAPD values obtained were 1.895% for sucupira biodiesel and 1.924% for canola biodiesel.

Table 25 – Pure Component (1-Butanol) Parameters for PC-SAFT Equation of State**.**

1-butanol parameters

m_i	σ_i (Å)	ε_i/k (K)	κ_{AB_i}	ε_i^{AB}/k (K)	[a]T - ρ/ K	[a]T - c/ K	$MAPD$ (ρ)	$MAPD$ (c)	Ref.
2.843	3.550	253.94	0.001	3178.87	293-373	-	0.07	-	Chapter 3[b]
3.139	3.423	248.38	0.008	2320.08	293-373	293-333	0.17	2.05	This Work

[a]: Range of temperature. [b]Alves et al. (2024)

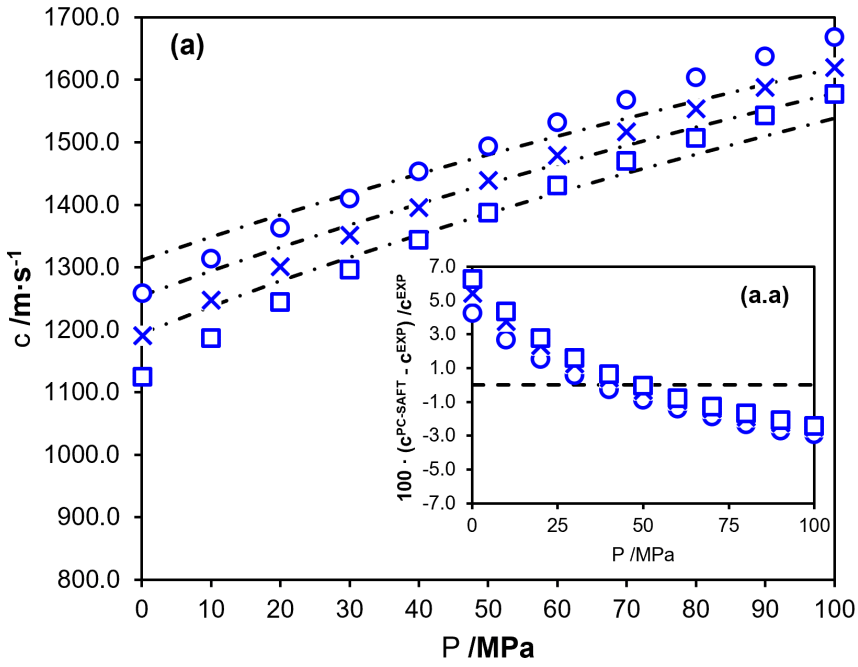

Figure 41 – Sound speed as a function of pressure for three isotherms: (○) 293,15 K, (×) 313,15 K e (□) 333,15 K. Graph (a) shows the comparison between the experimental data (symbols) and the values estimated by the PC-SAFT equation of state (dotted lines). Graph (a.a) shows

the corresponding relative deviations as a function of pressure, for the same conditions. (Created by the author, 2025)

In addition, for pure 1-butanol, the results obtained with the new set of parameters yielded an MPD of 0.232%, a MAPD of 2.055%, and a MaxPD of 6.267%, as also shown in Figure 42. These values reinforce the quality of the fit and demonstrate the capability of the PC-SAFT equation of state to represent acoustic properties across a wide pressure range.

For modeling the binary mixtures of 1-butanol with canola and sucupira biodiesels, no adjustable binary interaction parameter was used, setting $k_{ij} = 0$. Cross-interactions between components were estimated solely using the classical Lorentz-Berthelot combining rules. Additionally, no cross-association was considered, since only one component (1-butanol) exhibits associative behavior. This methodological choice aims to evaluate the predictive capability of the PC-SAFT equation of state based solely on pure component parameters, without specific adjustments for the mixtures, thereby enhancing the model's generality and independence.

Table 26 presents the MPD, MAPD, and MaxPD values between the experimental and calculated data for the speed of sound, using the molecular parameters previously determined for the pure components based on the simultaneous fitting of density and speed of sound at high pressures (see Chapter 3 and Section 6.3.1). For the 1-butanol + canola biodiesel and 1-butanol + sucupira biodiesel mixtures, the MAPD values were 2.050% and 1.989%, with corresponding MaxPD values of 6.732% and 7.043%, respectively. The MPD values were 0.425% for the canola blend and −0.153% for the sucupira blend, indicating a slight tendency to overestimate and underestimate the speed of sound, respectively, but without any pronounced systematic bias.

In comparative terms, the results obtained for the pure systems demonstrate similar performance of the model. For 1-butanol, the MAPD was 2.055% and the MaxPD was 6.267%, with an MPD of 0.232%. For the pure biodiesels, the deviations were similarly low, with MAPD values of 2.044% for canola and 1.993% for sucupira, and MaxPD values of 5.284% and 5.077%, respectively. The MPD values for biodiesels indicate a slight tendency of the model to underestimate the speed of sound, at −0.298% for canola and −0.243% for sucupira. These results remain within the range of excellent model performance, especially considering that the biodiesels were treated as pure pseudocompounds.

The comparison between pure systems and mixtures shows that the PC-SAFT equation of state, even without the inclusion of binary interaction parameters $k_{ij} = 0$, predicts

the speed of sound in the studied mixtures with good accuracy. Figure 42 presents the percentage deviations between the PC-SAFT predicted values and the experimental data for blends of 1-butanol with canola biodiesel (a) and sucupira biodiesel (b) as a function of the 1-butanol mole fraction, under three different conditions: T=293.15 K, p=0.1 MPa; T=293.15 K, p=100 MPa; T=333.15 K, p=0.1 MPa. It is observed that under low pressure (0.1 MPa), the deviations are systematically positive and increase with the mole fraction of 1-butanol, indicating that the model overestimates the speed of sound in butanol-rich mixtures near atmospheric pressure. In contrast, at high pressure (100 MPa), the deviations are negative and remain nearly constant across the compositional range, suggesting a slight underestimation of the experimental values by the model under these conditions.

Table 26 – Statistical characteristics (Mean Percentage Deviation, Mean Average Percentage Deviation, Maximum Percentage Deviation) values for the speed of sound in binary mixtures of 1-butanol with canola and sucupira biodiesels, calculated using PC-SAFT with parameters fitted to pure components (no binary interaction parameters) with parameters given in Table 6.5 and Chapter 3.

System	MPD	MAPD	MaxPD
1-Butanol + Canola biodiesel	0.425	2.050	6.732
1-Butanol + Sucupira biodiesel	-0.153	1.989	7.043
Pure 1-Butanol	0.232	2.055	6.267
[a]Pure Canola biodiesel	-0.298	2.044	5.284
[a]Pure Sucupira biodiesel	-0.243	1.993	5.077

a.data referring to chapter 3 of this thesis T = (293.15 K, 313.15 K and 333.15 K).

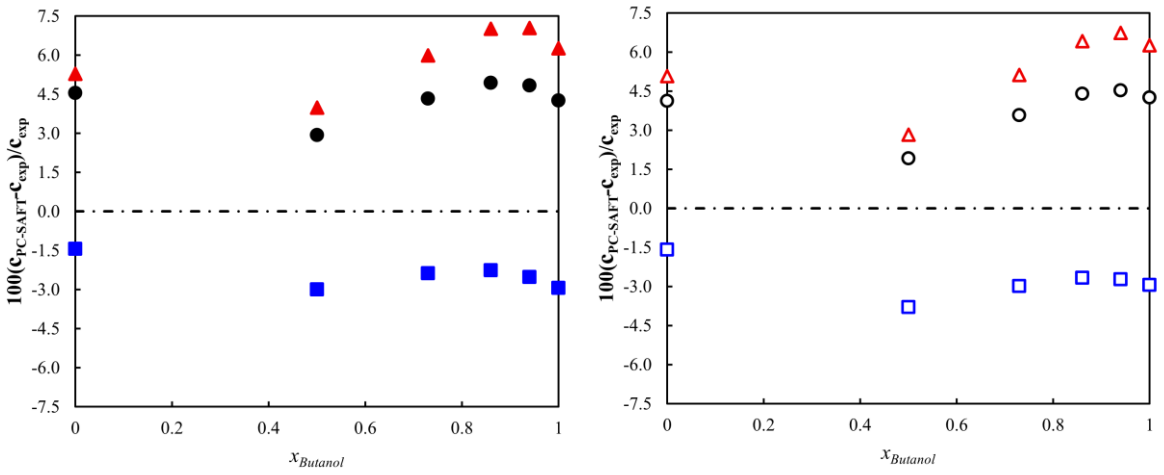

Figure 42 – Percentage deviations between the predictions of the PC-SAFT method and the experimental speed of sound data for 1-Butanol + Canola biodiesel (a) and 1-Butanol + Sucupira biodiesel (b), ●○, p=0.1 MPa, T=293.15 K; ■□, p=100 MPa, T=293.15 K; ▲△, p=0.1 MPa, T=333.15 K. (Created by the author, 2025)

6.5 Conclusions

Experimental measurements of the speed of sound were carried out for binary systems composed of 1-butanol and two biodiesels derived from canola and sucupira oils, at temperatures of 293.15 K, 313.15 K, and 333.15 K, and at pressures of up to 100 MPa. Based on these data, the behavior of the quantity $cM\gamma$ was analyzed, showing a decreasing linear trend with an increasing 1-butanol mole fraction, which suggests an approximately additive behavior. However, the relative deviations $cM\gamma^{Rmix}$ revealed interactions, with systematically negative values reaching up to approximately -0.75% at 333.15 K and 0.1 MPa. It was observed that these deviations increase with temperature and decrease with pressure, becoming practically zero at 100 MPa. To describe the influence of composition on the speed of sound, a combination rule was proposed based on the behavior of $cM\gamma$, capable of predicting the speed of sound in the studied mixtures with errors compatible with experimental uncertainty, regardless of temperature and pressure conditions. This approach proved effective in representing the impact of 1-butanol addition on the thermophysical properties of binary systems, contributing to the development of fuel formulations with higher renewable content. In addition, experimental data were used to evaluate the performance of the PC-SAFT equation of state in predicting the speed of sound in the studied mixtures, employing the molecular parameters previously fitted in Chapter 3 of this thesis. The results showed that, even in the absence of binary interaction parameters, the model was able to satisfactorily reproduce the experimental data, reinforcing its applicability to systems containing biodiesels with different ester compositions. This study expands upon the work previously conducted by Daridon Daridon (2022b), extending the validity of the proposed approach to new biodiesel sources and making a significant contribution to the understanding of the thermophysical behavior of biodiesel/alcohol blends under high-pressure and high-temperature conditions.

7 ADVANCED CHARACTERIZATION OF DIESEL–BIODIESEL BINARY BLENDS: A COMPLEMENTARY STUDY ON THEIR DISTILLATION PROFILES AND THERMOPHYSICAL BEHAVIOR

Results published in: *Distillation Analysis of Diesel-Biodiesel Mixtures: A Comparative Study with ASTM Norms, Experimental Data, and Novel Correlations* Fuel 2025, 383, 133864. https://doi.org/10.1016/j.fuel.2024.133864.

7.1 Introduction

The growing global search for sustainable alternatives to fossil fuels has driven research into biodiesel, a renewable fuel capable of reducing pollutant emissions and mitigating environmental impacts. Chapters 3 and 4 of this thesis present a detailed study on the density, speed of sound, and heat capacity of biodiesel, contributing to a better understanding of its thermophysical properties under real operating conditions. Although the central focus of this work lies in the investigation of these properties for pure biofuels and their mixtures with alcohols under high-pressure conditions, the widespread use of diesel and biodiesel blends in the industrial and transport sectors supports the inclusion of a complementary study addressing the behavior of such combinations.

Several studies have explored the fundamental properties of diesel and biodiesel blends Bukkarapu et al. (2018 e Ellappan; Rajendran (2021 e Malik et al. (2021 e Moradi et al. (2013 e Nogueira et al. (2012b e Parente et al. (2011 e Payri et al. (2011b e Silitonga, A. S. et al. (2013 e Tat; Van Gerpen (2000 e Ulusoy et al. (2018 e Vargas-Ibáñez et al. (2022b e Yamane et al. (2001 e Zaharin et al. (2017b e Zvirin et al. (1998). In a recent study conducted by our group, the high-pressure density of diesel and biodiesel blends produced from three different feedstocks was investigated, contributing to the expansion of available data under conditions closer to real operational environments Alves et al. (2022).

Despite the high practical relevance of these mixtures, properties such as the distillation curve remain underexplored in scientific literature, which highlights the importance of a study with this focus. Biodiesel and petroleum diesel can be blended in any proportion and are widely employed in compression ignition engines Silitonga, A.S. et al. (2013 e Tat; Van Gerpen (2000). However, these fuels exhibit significant differences in chemical composition, volatility, and flow behavior Smith et al. (2008). Therefore, a thorough understanding of their

physicochemical properties is essential for the proper design and operation of engineering processes.

The addition of biodiesel to diesel has become a common practice in several countries, aiming to promote the use of more sustainable fuels Wirawan et al. (2024). Among the fundamental properties for characterizing these blends, the distillation curve stands out due to its relevance in defining volatility and the technical performance of automotive fuels Leonardo et al. (2020) This curve provides information on the boiling range of the mixtures and is widely used in the motor fuel industry Kosychova L. et al. n.d (2015), allowing the analysis of changes in the distillation profile as the biodiesel content increases (PAULAUSKIENE, BUCAS and LAUKINAITE, 2019).

Several contributions have sought to address the gaps in distillation studies. Smagala et al. (2013) Smagala et al. (2013) investigated the distillation curves of fuels derived from Fischer-Tropsch synthesis, while Smith, Ott and Bruno (2008) Smith et al. (2008) analyzed commercial biodiesel and petroleum diesel. Aleme e Barbeira (2012) Aleme; Barbeira (2012) evaluated blends with soybean biodiesel in different proportions, both with pure diesel and S500 diesel. Aburudyna et al. (2015) Aburudyna et al. (2015) studied mixtures containing up to 35% biodiesel, highlighting its impact on the distillation profile. More recently, Hidegh et al. (2023) Hidegh et al. (2023) investigated various physicochemical properties, including the distillation curve, for coconut, palm and waste oil biodiesels, as well as their blends with diesel in proportions of 25%, 50% and 75%. McCormick et al. (2024) McCormick et al. (2024) also evaluated distillation curves and key properties of biodiesel blends with both conventional and hydroprocessed diesel, contributing to the technical understanding of these combinations.

Other studies have addressed alternative biofuels and drop-in fuels. Kurczyński et al. (2023) Kurczyński et al. (2023) observed that blends with babassu biodiesel exhibited a more favorable distillation profile compared to those with canola biodiesel. Bullermann et al. (2024b) Bullermann et al. (2024) evaluated mixtures containing oxymethylene ether (OME) and identified distillation curves that differ significantly from those of standard marine diesel (MAD), emphasizing the implications for performance and fuel handling. Furthermore, Niculescu, Năstase e Clenci (2022) Niculescu et al. (2022) proposed the use of gas chromatography as an alternative to vacuum distillation for determining distillation curves, offering a practical solution for laboratories with limited infrastructure.

Given the scarcity of experimental data on diesel and biodiesel blends, this study aims to address this gap by providing detailed distillation data for three biodiesel blend systems (derived from grape seed, corn, and linseed) with low-sulfur diesel (S10). Volumetric

compositions of 20%, 40%, 60%, and 80% biodiesel were investigated, along with the extremes of 0% and 100%, thereby covering the full range of possible blends. Additionally, properties crucial to fuel characterization, such as density, viscosity, refractive index, cetane number, and flash point, were meticulously evaluated following the stringent standards of the American Society for Testing and Materials (ASTM). This approach allows for precise comparisons with standard specifications; a topic rarely explored in literature. As a key contribution, this work proposes two new correlations addressing the lack of distillation models applicable to biodiesel and its blends with diesel. Based on the probability distribution function and the models of Riazi and Daubert Riazi; Daubert (1987), these new models were calibrated using experimental distillation curve data. The first correlation developed enables the calculation of distillation temperatures at 10%, 50%, and 90% of the distilled volume of biodiesel, critical parameters for biofuel specification. The second correlation was designed to model the distillation curve of diesel and biodiesel blends, offering a novel and essential contribution to the field.

7.2 Experimental sections

7.2.1 Materials

Three biodiesel samples used in this work (grape seed, corn, and linseed) were provided by Núcleo de Análise e Desenvolvimento de Processos (NADP, Fortaleza, Brazil). Diesel S10 (10 mg/kg of sulfur) was supplied by Lubrificantes e Derivados de Petróleo do Nordeste (Petrobras LUBNOR, Fortaleza, Brazil), with a molar mass of 205.06 g/mol, with a hydrocarbon profile shown in Figure 43 (a).

The methyl ester composition of biodiesel samples was determined by gas chromatography using a CG Thermos Ultra chromatograph and a flame ionization detector. The analyses used an OV-1 capillary column of 0.25 μm film thickness, 0.25 mm inner diameter, 30 m length, and helium as a carrier gas at a constant pressure of 100 kPa. The oven temperature varied from 323.15 to 503.15 K at a heating rate of 10 K/min. The temperature of the injector and detector was 523.15 K. All analyses were carried out in duplicate, and the deviation between analyses was lower than 3%. Figure 43 (b) displays chromatographic profiles for grape seed, corn, and linseed biodiesels.

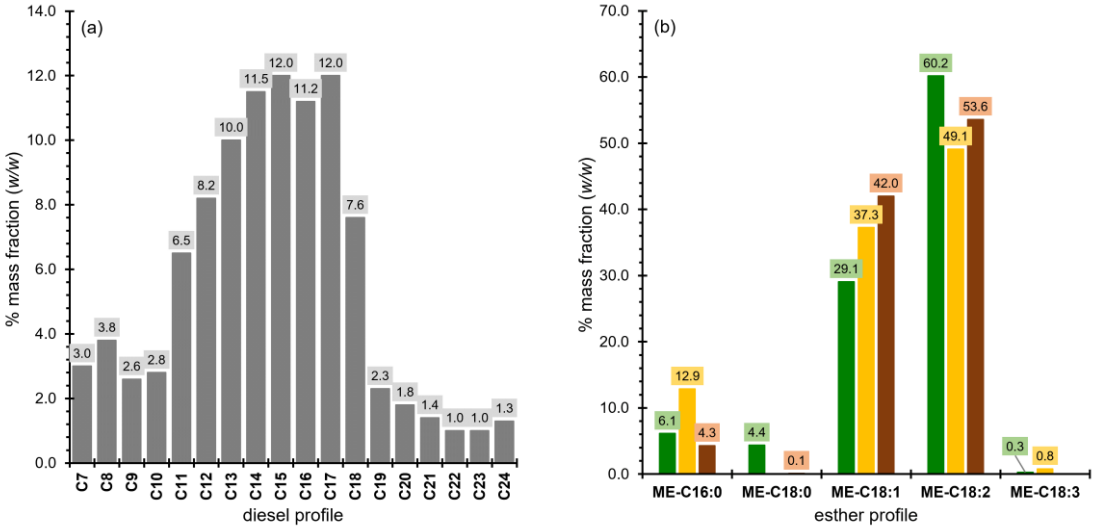

Figure 43 – Hydrocarbon profile of diesel and the three biodiesels studied in this work as a function of mass fractions. (a) Hydrocarbon diesel profile represented by gray bars. (b) Fatty Acid Methyl Esters (FAME) profile of Grape seed (green bar), Corn (yellow bar), and Linseed (brown bar) biodiesels. (Created by the author, 2025)

7.2.2 Apparatus and Procedure

To comprehensively investigate the properties of biodiesel, diesel, and their mixture, we conducted an experimental study utilizing a suite of advanced instrumentation tailored for precise characterization. Specifically, we employed five different apparatus, each meticulously selected to assess specific properties with high accuracy and reliability.

The instrumentation utilized in this study comprised the following:

- **Diana 700:** Dedicated to the precise measurement of boiling temperatures.
- **SVM 3000:** Employed to determine dynamic viscosity and kinematic viscosity, ensuring comprehensive fluid characterization.
- **DSA 5000:** Utilized for the density measurement, providing insights into volumetric properties.
- **Abbemat 300:** Instrumentation utilized to assess refractive index, crucial for understanding optical characteristics.
- **PMA 500:** Dedicated to determining flashpoint, a pivotal parameter in assessing safety and combustion properties.

Utilizing this array of advanced instrumentation, we thoroughly investigated the properties of biodiesel, diesel, and their blend, providing a nuanced understanding essential for high-impact scientific inquiry and technological advancement. **Table F1** of the information

support contains illustrations and brief technical descriptions of each equipment used in this study. These descriptions provide essential details on the characteristics and functionalities of the instruments, allowing a clear understanding of the experimental methods and conditions applied.

7.2.2.1 Distillation

Distillation curves (boiling temperature as a function of recovery volume) atmospheric pressure were obtained using an automatic Anton Paar Diana 700 distiller. Diesel S10 and biodiesel samples (grape seed, corn, and linseed) were distilled individually, according to standard test ASTM D1078 ASTM International (2011). Diesel-biodiesel blends were prepared under agitation in the 0.2 to 0.8 (v/v), with a step of 0.2 [in percent 20, 40, 60, and 80% (v/v)]. These compositions were applied to all experiments performed in this paper. Distillation of mixtures was carried out following the standard test ASTM D86 ASTM International (2018). Diana 700 is an automated D86 analyzer with a temperature resolution of 0.1 °C and sample volume scanning to a resolution of 0.01 mL.

For the distillation procedure, 100 mL of each liquid sample, pure or blended, was transferred to a specific distillation flask equipped with a thermocouple sensor and heated. The condensed phase was collected in a cooling chamber (13 to 18 °C), and the recovered volume was measured with a digital contact image sensor. Distillation curves were described after measuring the final residue volume according to the results screen.

7.2.2.2 Density and viscosity

Density (ρ), dynamic viscosity (η), and kinematic viscosity (ν) data for all samples studied were obtained using viscodensimeter Anton Paar SVM 3000 (for viscosities) and DSA 5000 (for density) at atmospheric pressure. Before DSA analyses, a calibration procedure was conducted using deionized water (with a conductivity of 18.2 ± 0.2 mΩcm at 25 °C) and dry air.

Density was determined using the U-tube principle, while viscosity was determined using a cell rotating at a constant speed, both filled with the sample volume. Following the analyses, standard uncertainties of ±0.0005 g/cm³ for density, 0.01 °C for temperature, and ±0.002 mPa·s for viscosity were observed.

7.2.2.3 Refractive Index

The refractive index (n) was determined using an Anton Paar Abbemat 300 refractometer. Before measurements, the equipment was calibrated using ultrapure deionized water, with a conductivity of 18.2 ± 0.2 mΩcm at 25 °C, following the standard procedures recommended by the manufacturer. All readings were performed at temperatures of 20 °C, using a wavelength of 589 nm, with a reported uncertainty of ±0.0001 and a temperature accuracy of ±0.05 °C. The tests were conducted in duplicate, ensuring the reliability of the results.

It is essential to highlight that the method used follows the guidelines of ASTM method D1218. This method is recognized as a reference to the refractive index for clear and transparent liquids. Using a specific wavelength of 589.3 nanometers at a standard temperature of 20°C, the ASTM D1218 method establishes rigorous criteria for evaluating whether diesel meets the quality requirements.

7.2.2.4 Flashpoint

The flashpoints of biodiesel (grape seed, linseed, and corn) and diesel S10 were measured on the Anton Paar PMA 500, a closed cup flashpoint analyzer Pensky-Martens, to determine the flashpoint following ASTM D93 standards. The automated analyzer has a flashpoint measurement range of 20 °C to 410 °C, a block heating system according to the established standard (ASTM), and an agitation system that reaches up to 500 RPM. Only the compounds without mixtures were evaluated in these tests to identify whether the fuels were within the imposed standards.

7.2.3 Cetane index calculation

ASTM D975 defines the cetane number (CN) as a measure of diesel fuel's ability to self-ignite under compression. The higher the cetane number, the more efficiently the diesel ignites under compression. ASTM D613

As the EN ISO 5165 and ASTM D613 protocol specify, CN can only be calculated if experimental equipment is available. Therefore, the cetane index (CCI) can replaced it. Despite its estimated character, CCI also provides information about ignition delays in diesel

engines Vera-Rozo et al. (2022). It is much cheaper to determine than the engine-based cetane number, but its accuracy is limited to a specific fuel from which the equation was based. Two ASTM methods are available for computing the cetane index: D 4737 (**Equations F1 – F6**) and D 976 (**Equations F7 – F9**).

As previously noted, the equations presented do not apply to fuels other than petroleum. Therefore, Vera-Rozo et al. Vera-Rozo et al. (2022) readjusted the parameters outlined in ASTM D 4737 specifically for biodiesel, as shown in Equations **F10 – F15**.

7.2.4 ASTM specification for biodiesel and diesel

The American Society for Testing and Materials (ASTM) is an international organization that develops and publishes technical standards for various materials, products, systems, and services. **Table F2 (in in Appendix F)** summarizes some specifications regarding diesel and biodiesel.

We will analyze various properties to determine how adding biodiesel affects fuel conformity. Specifically, we will examine how adding biodiesel affects each property from the ASTM specifications for different fuel compositions (diesel + biodiesel). The objective is to assess the extent to which the blends meet the ASTM D975 standard criteria, which applies to diesel fuel without restrictions on engine operation.

7.2.5 Experimental Uncertainties

The treatment of uncertainties in this work was carried out using different approaches to ensure the reliability of the experimental data. Uncertainties were classified as Type A and Type B, in accordance with the recommendations of the *Guide to the Expression of Uncertainty in Measurement* (GUM).

Type A uncertainties were applied to the flash point and distillation data (ebullition temperature) and were obtained through multiple measurements under identical experimental conditions. The experiments were conducted using the previously described PMA 500 and Diana 700 equipment. These uncertainties were derived from statistical methods, specifically through the calculation of the standard deviation of repeated measurements. The standard uncertainty was determined based on the distribution of the values obtained, reflecting the

intrinsic variability of the measurement process and providing a quantitative assessment of the repeatability of the results.

For other properties, such as refractive index, density, and viscosity, Type B uncertainties were considered, which are based on non-statistical sources. These include information from instrument manufacturers' specifications, calibrations performed with certified standards, and the characteristics of the reagents used. The expanded uncertainty for density, for example, was calculated by considering uncertainties associated with the measurement temperature, the oscillation periods of the densimeter, and the density of the reference fluid, ensuring that all potential sources of error were accounted for and properly combined. This procedure was conducted with a 95% confidence level, adopting a coverage factor of $k = 2$, ensuring that the uncertainty interval adequately reflects the reliability of the experimental data. The maximum value of the expanded uncertainty was based on the largest variation observed during the measurements, ensuring that the uncertainty estimate remained conservative. Similarly, the calculation of uncertainty for the refractive index and viscosity properties followed the same methodological rigor. All obtained uncertainties for the measured properties are summarized in **Table F1 in Appendix F**.

7.3 Modeling the distillation curve

7.3.1 Biodiesel distillation temperatures (T_{10}, T_{50}, T_{90})

The methodology developed by Riazi and Daubert Riazi; Daubert (1987) represents a fundamental approach to modeling fuel distillation. Initially designed for hydrocarbons, it relies on characterizing substances' thermodynamic properties, enabling the prediction of boiling temperatures and the construction of distillation curves.

However, the methodology must be adapted because of the diversity of compounds, such as biodiesel, which varies in composition and molecular properties from hydrocarbons. The Riazi and Daubert Riazi; Daubert (1987) method was tailored to suit the specific biodiesel requirements in this study.

For this reason, biodiesel's kinematic viscosity and density were used to consider the distinctive molecular characteristics of biodiesel. These properties are highly informative and for many industrial applications. Equation 7.1 represents the generic model proposed by Riazi and Daubert:

$$\theta = a \cdot \theta_1^b \cdot \theta_2^c \quad (7.1)$$

where: θ_1, the kinematic viscosity (υ) of biodiesel, measures the liquid's resistance to flow and characterizes the molecular energy, influenced by molecular interactions. It is directly related to the flow characteristics of biodiesel. θ_2, the density (ρ) of biodiesel measures the compactness of the molecules within the liquid and represents the molecular size, influenced by the size of the molecules and the proximity between them.

Vera Rozo et al. Vera-Rozo et al. (2022) developed a correlation using data for 14 different biodiesel sources, including 10%, 50%, and 90% distillate volume temperatures. These data are used to regulate norms for characterizing biodiesel distillation.

The adapted methodology enabled us to establish correlations between biodiesel's kinematic viscosity and density properties and the temperatures at which 10%, 50%, and 90% of the volume is distilled. This approach effectively captured the variations among different samples, providing a robust tool for characterizing the biodiesel distillation process based on its molecular properties. The equations of the resulting model are represented by the following expressions (Equations 7.2 – 7.4).

$$T_{10} = a \cdot \upsilon_{40°}^b \cdot \left(\frac{\rho_{15°}}{999}\right)^c \quad (7.2)$$

$$T_{50} = a \cdot \upsilon_{40°}^b \cdot \left(\frac{\rho_{15°}}{999}\right)^c \quad (7.3)$$

$$T_{90} = a \cdot \upsilon_{40°}^b \cdot \left(\frac{\rho_{15°}}{999}\right)^c \quad (7.4)$$

where: T10, T50, and T90 represent the temperatures (in K) at which 10%, 50%, and 90% of the volume is distilled; parameters a, b, and c are adjusted using the least squares methodology, widely applied in the literature to optimization; ν denotes the kinematic viscosity of biodiesel (in mm^2/s), at T = 40°C; ρ represents the density of biodiesel (in kg/m^3), at T = 15°C; and, the constant 999 refers to the density of water at 15°C to represent the relative density.

7.3.2 Distillation curve for diesel and biodiesel mixture

A methodology like that described for biodiesel was adopted to obtain the distillation curve for the diesel and biodiesel mixtures. However, unlike the previous approach, complete distillation curve data covered the entire mixture distillation.

It is important to note that the previous methodology relied on two properties, i.e., biodiesel's kinematic viscosity and density. Nevertheless, different properties were considered for diesel and biodiesel blends: the relative density was maintained, and the boiling temperature was estimated from the pseudo-pure components. This adaptation adds a layer to the modeling, considering the interaction between specific components of the mixture, thereby contributing to a more accurate representation of the molecular properties of the combination of diesel and biodiesel throughout the distillation process. Furthermore, this approach can be interpreted as a correction of the boiling temperature for an "ideal solution," considering the unique characteristics of the mixture, as presented in Equation 7.5:

$$T_i^{mix} = \phi_i \cdot T_i^{Diesel} + (1 - \phi_i) \cdot T_i^{Biodiesel} \quad (7.5)$$

where: T_i^{mix}, T_i^{Diesel}, and $T_i^{Biodiesel}$ represent the temperature (in K), in a distillate volume "i", for diesel-biodiesel mixtures, diesel, and biodiesel, respectively; ϕ denotes the volumetric fraction, representing the volumetric proportion of each component in the mixture. It should be observed that the previous one keeps a close relationship with the one proposed by Riazi e Daubert Riazi; Daubert (1987) but with a second-degree polynomial parametrization, as shown in Equations 7.6 – 7.9. This modification incorporates more parameters, leading to a more detailed characterization of the distillation curve.

The amount of data available in the literature for this system needs to be increased. The grape biodiesel data collected in this work was added to enhance the correlation set and the data from Hidegh et al. Hidegh et al. (2023). The data for corn and linseed biodiesels were utilized to assess the accuracy of the correlation. The initial bubble point (IBP) data was not considered in the fit because of the significant differences between the biodiesels. The equation governing the model is presented below in Equation 7.9, which describes the temperatures in a distillate volume "i" for the diesel and biodiesel blend, T_i:

$$D(x_D) = d_2 x_D^2 + d_1 x_D + d_0 \quad (7.6)$$

$$E(x_D) = e_2 x_D^2 + e_1 x_D + e_0 \quad (7.7)$$

$$F(x_D) = f_2 x_D^2 + f_1 x_D + f_0 \quad (7.8)$$

$$T_i = D(x_D) \cdot T_i^{mix^{E(x_D)}} \cdot \left(\frac{\rho_{15°}}{999}\right)^{F(x_D)} \quad (7.9)$$

where: x_D denotes the distillate volume fraction; "$E\ (x_D)$", "$F(x_D)$", and "$G(x_D)$" are functions of the distillate volume fraction and involve nine parameters adjusted using the least squares methodology. These parameters were adjusted based on experimental data on diesel and biodiesel blends, with the above data.

7.4 Results and discussion

7.4.1 Distillation curves for diesel, biodiesel, and blends of 20, 40, 60, and 80% diesel + biodiesel

Figure 44 presents the distillation curves for biodiesel (grape seed, linseed, and corn) in mixtures with diesel for a volumetric composition ranging from 0% to 100% as a function of the recovered volume percentage. As biodiesel content increases, the distillation curves shift towards higher temperatures, indicating a change in the mixture's volatility. This volatility alteration influences droplets' evaporation during the spraying process and the formation of droplets (atomization) during combustion Cerinski et al. (2020 e Hidegh et al. (2023).

A significant difference is observed between biodiesel and diesel distillation curves. The curve remains relatively flat for biodiesel throughout most of the distillation (% volume recovered), as observed by Lovestead et al. Lovestead et al. (2010) and Hidegh et al. Hidegh et al. (2023). The three biodiesels studied (grape seed, linseed, and corn) exhibit similar mass compositions, with more than 87% of esters containing 19 carbons in their chains, resulting in similar boiling points.

On the other hand, diesel exhibits a steeper slope in the curves, as previously observed Hidegh et al. (2023 e Hosseinifar; Shahverdi (2021 e Lovestead et al. (2010). This behavior could be attributed to the variation in its hydrocarbon profile. **Table F3 (Appendix F)** shows the boiling temperatures of the hydrocarbons and esters present in diesel and biodiesel, offering a valuable reference for comprehending the distillation properties of these systems.

It is essential to note that depending on the plant source, which typically determines the properties of biodiesel, there may be variations in the distillation curves, leading to

differences compared to diesel. For example, Hidegh et al. Hidegh et al. (2023) analyzed three types of biodiesels derived from different sources: palm, coconut, and a mixture of sunflower and rapeseed. They found a significant variation in the distillation curves of coconut biodiesel and its blends. This variation was attributed to the composition of triglycerides in coconut oil, which mainly consist of saturated fatty acids Bezard et al. (1971), with more than 90% of the fatty acids being of medium chain length, such as methyl caprylate and methyl laurate.

An analysis conducted by McCormick et al. McCormick et al. (2024) focused on the differences between the T90 and T10 boiling points (T90 - T10), a crucial indicator of the slope of the distillation curve. This characteristic is fundamental as it provides low boiling temperature components that ensure easy cold starting and the deactivation of the diesel oxidation catalyst (DOC) to regenerate the particulate filter Lakkireddy et al. (2024). McCormick et al. McCormick et al. (2024) observed that conventional petroleum diesel exhibits a wide boiling range, with a T90 - T10 difference of 100 °C or more. Their study examined biodiesel blends with traditional and renewable diesel derived from hydroprocessing. The results revealed differences of approximately 15 °C for biodiesel, 26 °C for renewable diesel, and 100 °C for conventional diesel, respectively.

In addition, Smagala et al. Smagala et al. (2013) reported T90 - T10 values for different types of diesel. In the present study, a T90 - T10 difference of 137 °C and a T50 - T10 difference of 79 °C were observed for diesel. For biodiesels, the differences were 5 °C, 8 °C, and 6 °C for grape, corn, and linseed, respectively. A graph illustrating the temperature differences (T90 - T10 and T50 - T10) for the three diesel and biodiesel systems is shown in Figure F1 in the supplementary material. As expected, there was a reduction in these differences with the addition of biodiesel, showing similar values among the three systems analyzed.

The distillation phenomenon yields crucial information on mixtures' volatility and boiling point characteristics, thereby significantly enhancing our understanding of fuels' thermal behavior and evaporation. This data is indispensable for optimizing production processes, formulating fuels, and ensuring adequate performance under various operating conditions. The experimental boiling temperature values for all systems are presented in **Tables F4 – F6 in Appendix F**.

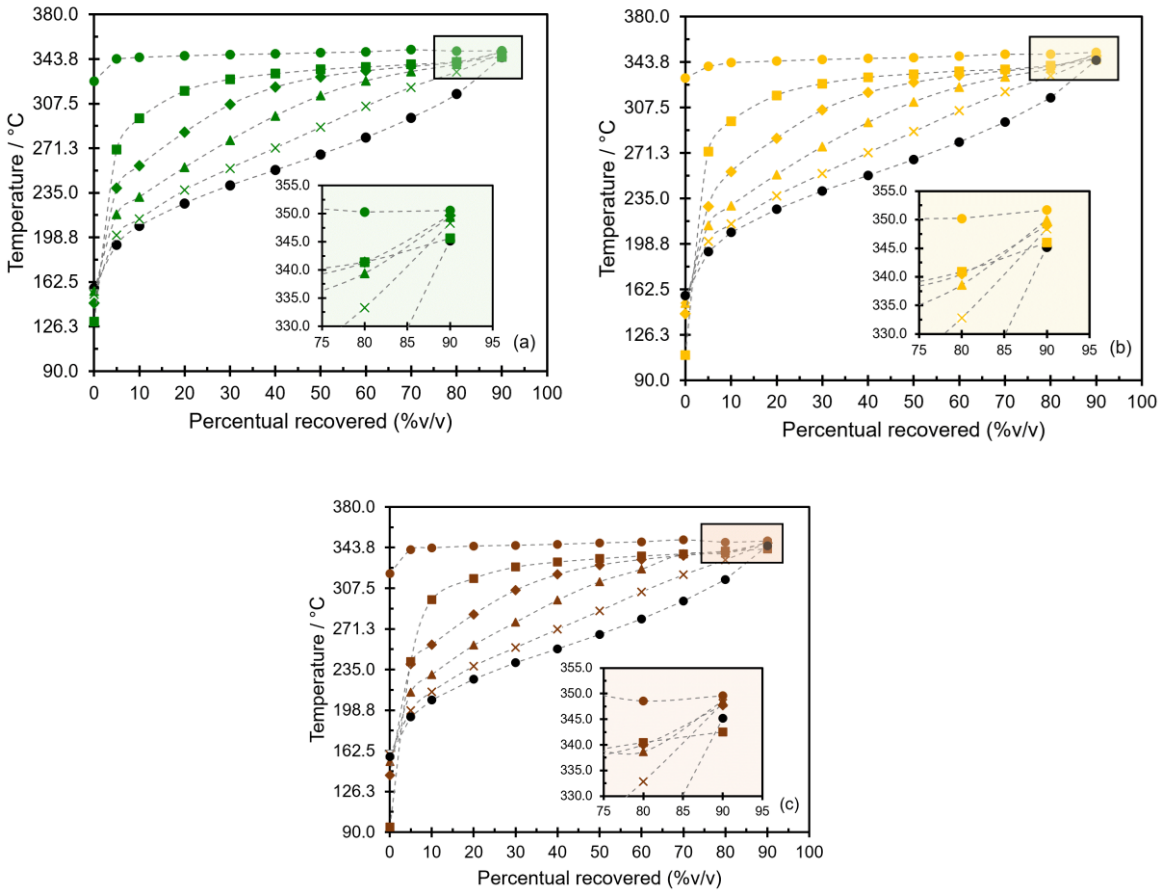

Figure 44 – Distillation curves for diesel, biodiesel, and diesel + biodiesel mixtures. (●, circle) 0% Biodiesel, (×, cross) 20% Biodiesel, (▲, triangle) 40% Biodiesel, (◆, diamond) 60% Biodiesel, (■, square) 80% Biodiesel, and (●, circle) 100%. Graph (a) refers to diesel + grape seed biodiesel, (b) refers to diesel + corn biodiesel, and (c) refers to diesel + linseed biodiesel. Repeatability for T_{10}, T_{50}, and T_{90} is ±0.2−2 °C. (Created by the author, 2025)

7.4.2 Comparison with regulatory norms

This study represents a comprehensive approach, beginning with comparative analyses between the properties of these blends and the standards established by ASTM (American Society for Testing and Materials). The objective of this analysis is not only to comprehend the intrinsic characteristics of diesel-biodiesel blends but also to evaluate their compliance with internationally recognized standards. Our research group published many papers regarding the effect of temperature and pressure on physicochemical properties Alves et al. (2022 e Mesquita et al. (2011, 2014 e Nogueira et al. (2015b e Parente et al. (2011).

Figures 45, 46, and 47 depict the density, viscosity, and refractive index of the volumetric compositions of biodiesel alongside their respective limits established by ASTM.

Upon analyzing these properties of the pseudo-pure compounds, it is observed that all of them meet the limits imposed by ASTM.

Regarding density, the diesel-biodiesel blend meets the limits set for diesel, even for compositions with up to 37% biodiesel. This finding aligns with a study conducted by Silitonga et al. Silitonga, A.S. et al. (2013), wherein blends containing up to 30% biodiesel meet the requirements in terms of density and viscosity. Other literature also presents similar results that support those obtained Koohshekan et al. (2023 e McCormick et al. (2024 e Samuel et al. (2019). The density behavior mirrors that of diesel, remaining within the parameters imposed by the standard.

Regarding kinematic viscosity, numerous studies have reported data on this property for biodiesel blends in various proportions Alptekin; Canakci (2008 e Bukkarapu et al. (2018 e Moradi et al. (2013). Our data indicate a behavior similar to that of diesel up to a composition range of 0.67 - 0.76 biodiesel, presenting viscosities at 40°C within the limits of ASTM D975. This finding is consistent with data from Moradi et al. Moradi et al. (2013), who analyzed diesel blends with biodiesel from soy, canola, sunflower, tallow, and waste oil, observing that a composition of 0.80 already exhibits behavior outside the diesel specifications for biodiesel from tallow and waste oil. Variations in properties can depend on the vegetable source studied, resulting in different values.

It is important to note that in both analyses (ASTM D975 and ASTM D6751), all the percentages comply with the requirements established for the upper limit for ASTM D6751.

Although ASTM D 975 does not establish specific limits for the refractive index of diesel, this analysis's results are valuable in providing insights into the fuel's transparency and quality.

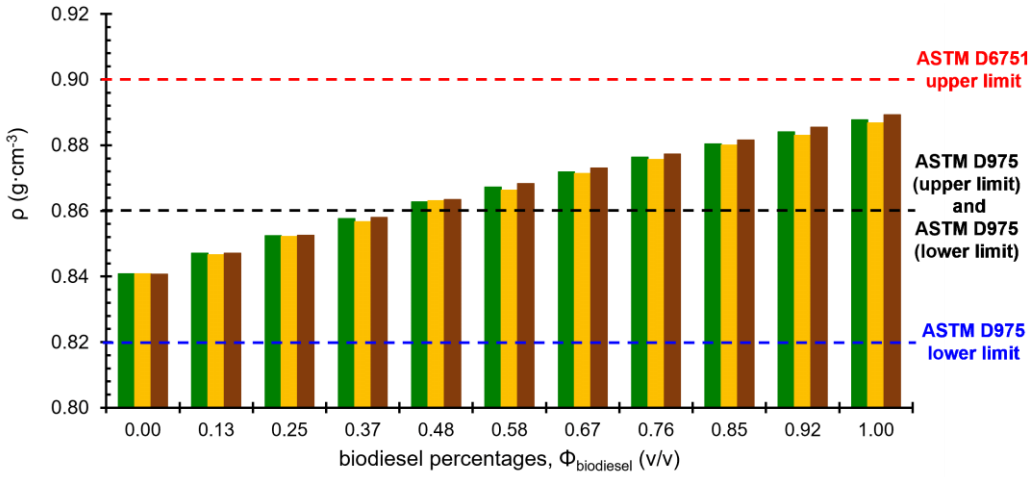

Figure 45 – Density (ρ) values about the volumetric composition of biodiesel ($\phi_{biodiesel}$). The dotted lines correspond to the limits imposed by ASTM. Bars: green (grape seed biodiesel), yellow (corn biodiesel), brown (linseed biodiesel). (Created by the author, 2025)

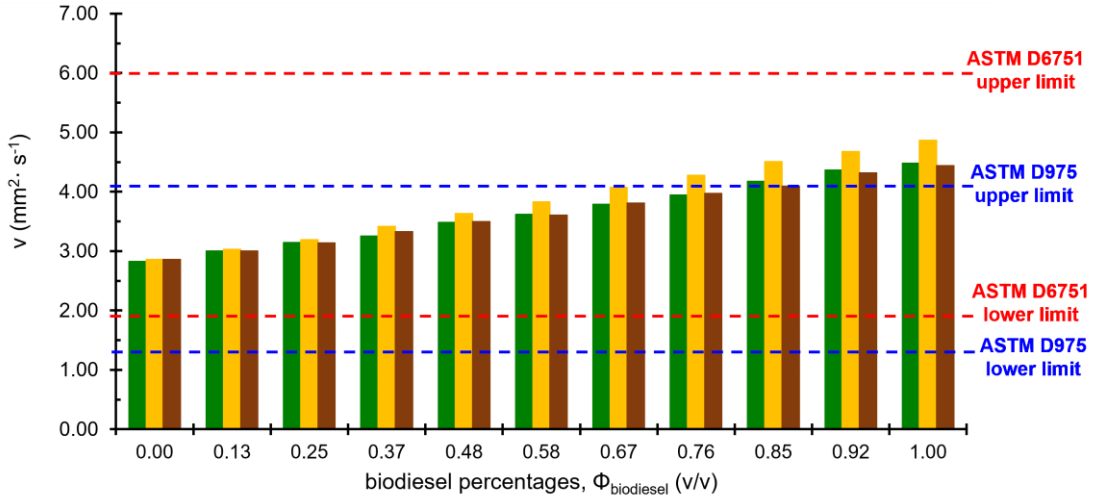

Figure 46 – Kinematic viscosity (ν) values about the volumetric composition of biodiesel ($\phi_{biodiesel}$). The dotted lines correspond to the limits imposed by ASTM. Bars: green (grape seed biodiesel), yellow (corn biodiesel), brown (linseed biodiesel).

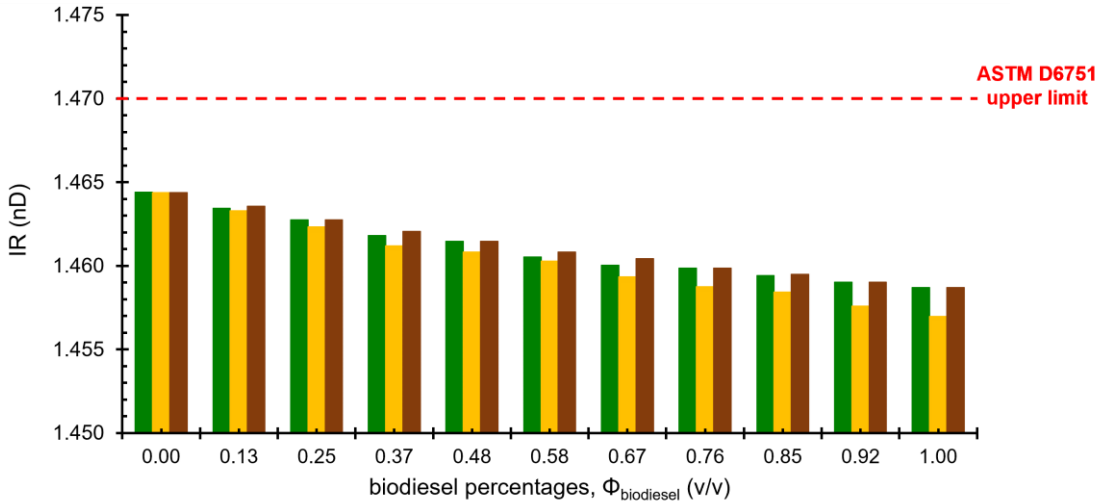

Figure 47 – Refractive index (IR) values about the volumetric composition of biodiesel ($\phi_{biodiesel}$). The dotted lines correspond to the limits imposed by ASTM. Bars predominantly: green (grape seed biodiesel), yellow (corn biodiesel), brown (linseed biodiesel). (Created by the author, 2025)

Following the essential analyses for a complete characterization of biodiesel and diesel, we evaluated the flashpoint of the pseudo-pure compounds. A fuel's flashpoint is the lowest temperature at which it will ignite and produce a flame when exposed to a spark or flame. The flashpoints of diesel and biodiesel can vary depending on their chemical composition. Still, in general, the flashpoint of biodiesel is slightly higher than that of conventional diesel fuels.

The flashpoint of petroleum diesel fuel typically ranges from 52°C to 96°C, while the flashpoint of biodiesel made from vegetable oils or animal fats generally is around 130°C to 170°C. However, the exact flashpoint of a particular fuel can vary depending on the specific feedstock and production process used to create it. For the three biodiesels studied in this work, it is observed that the flashpoint values did not vary so much, probably because of the similarity between the ester profiles shown in Figure 48.

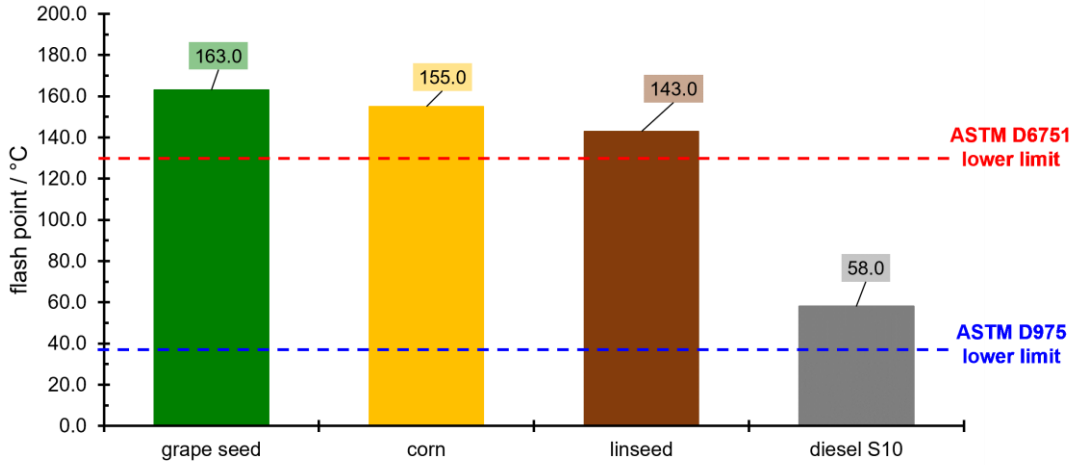

Figure 48 – Flashpoints relative to fuels. Bars: green (grape seed biodiesel), yellow (corn biodiesel), brown (linseed biodiesel), and gray (diesel S10). (Created by the author, 2025)

It is worth noting that the flashpoint is a crucial safety consideration when handling and storing fuels, as a lower flashpoint means that the fuel is more volatile and has a higher risk of catching fire or exploding. Following proper handling and storage procedures for all fuels, including diesel and biodiesel, is essential. Another important characterization is the biodiesel acidity index, which offers insights into the oil's condition and product quality. The values obtained for grape seed, corn, and linseed were 0.11, 0.24, and 0.08, respectively. These values are below the limit set at 0.5 $mgKOH \cdot g^{-1}$ (**presented in Table F2, in Appendix F**). These properties are crucial as they offer Elevated acidity levels that can lead to corrosion in both storage tanks and engines Vieira et al. (2021).

Figures 49 and 50 illustrate how distillation curves vary on diesel + biodiesel blends as a function of volumetric composition, compared to the distillation curves specification established by ASTM.

In the case of diesel, the specifications cover distillation temperatures of 10%, 50%, and 90%. As for biodiesel, the specifications only focus on the distillation temperature of 90%. The results indicate that both fuels (diesel and biodiesel) fully comply with the specifications of ASTM in all the analyses. Furthermore, it can be observed in Figure 50 that the diesel + biodiesel blends meet the distillation curve specifications in all the compositions evaluated.

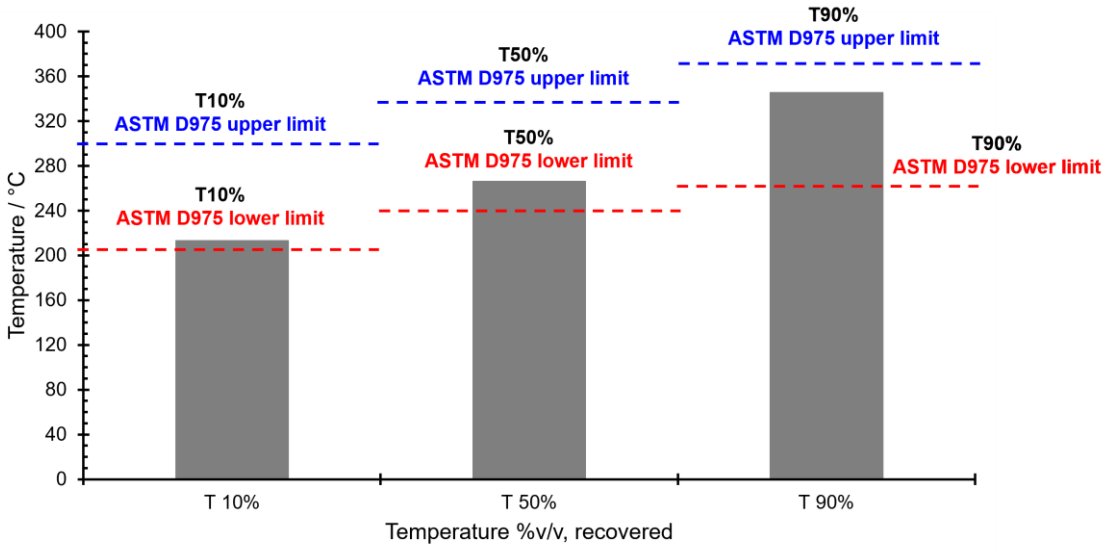

Figure 49 – Distillation temperature values for diesel (T_{10}, T_{50}, and T_{90}). The dotted lines correspond to the limits imposed by ASTM. (Created by the author, 2025)

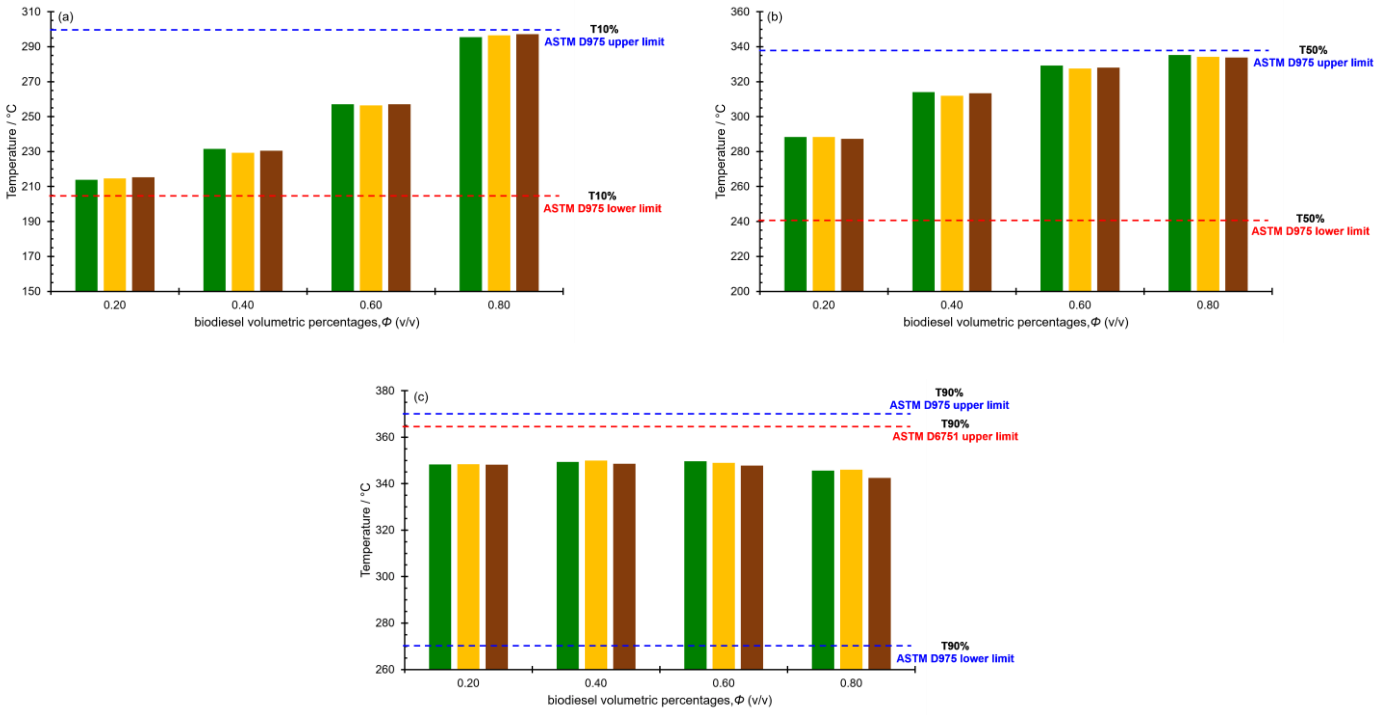

Figure 50 – Distillation temperature values for biodiesel and its mixtures. The dotted lines correspond to the limits imposed by ASTM. Bars: green (grape seed biodiesel), yellow (corn biodiesel), brown (linseed biodiesel), and gray (diesel S10). Where: (a) Temperature at 10% distilled volume, (b) Temperature at 50% distilled volume, and (c) Temperature at 90% distilled volume. (Created by the author, 2025)

As introduced in Section 7.2.3, the Cetane Index (CCI) was obtained as a calculated quantity designed to approximate the Cetane Number (CN). Three different methodologies

were used to carry out these calculations, all based on distillation temperatures. Two of them refer to calculating the CCI for diesel, as expressed in **equations F1 to F9**, following the ASTM D976 and ASTM D4737 standards. In the case of biodiesel, an adaptation of ASTM D4737 proposed by Vera Rozo et al. Vera-Rozo et al. (2022) was adopted, as shown in **equations F10 to F15**.

Figures 51 and 52 display the cetane indices for the biodiesel samples (grape seed, corn, and linseed) and diesel (S10) studied here. The difference between diesel ASTM specifications (D976 and D4737) for cetane indices could be negligible (50.23 against 50.05), both reaching compliance with the specifications. Only corn biodiesel is within the cetane number limit imposed by ASTM for biodiesels. Nevertheless, because of the indirect nature of the methodology used, an error bar of 6.9% of the biodiesel CCI value was added, representing the maximum uncertainty established by the model proposed by Vera Rozo et al. Vera-Rozo et al. (2022). Considering this uncertainty, the biodiesels remain close to the limits established by ASTM.

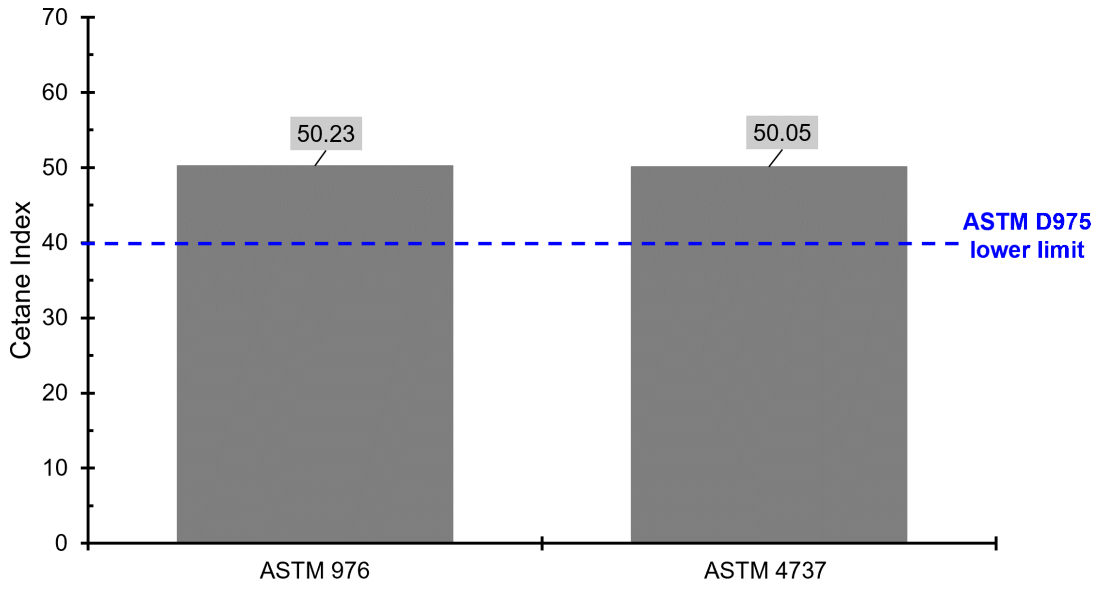

Figure 51 – Cetane indexes for diesel, according to ASTM D976 and ASTM D4737. (Created by the author, 2025)

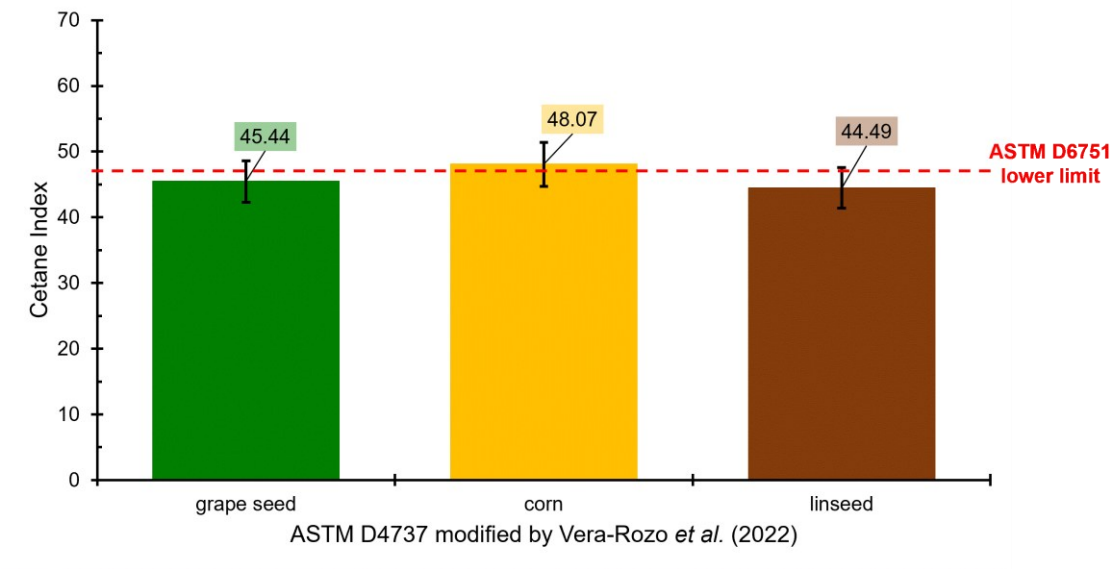

Figure 52 – Cetane index for biodiesel, according to Modified ASTM D4737. (Created by the author, 2025)

7.4.3 Correlation for distillation temperatures (T_{10}, T_{50}, T_{90})

As presented in Section 6.3.1, a correlation was developed for distillation temperatures (T_{10}, T_{50}, and T_{90}) using the relative density and the kinematic viscosity as input parameters. Experimental data was collected from the literature for 26 biodiesels from various sources Bachler et al. (2010 e Benjumea et al. (2008 e Berman et al. (2011 e Candeia et al. (2009 e Giakoumis (2013 e Hidegh et al. (2023), including rice bran, fish oil, soybeans, waste cooking oil, and castor beans, among other oilseeds. In addition, simulated distillation data available in the study developed by Bachler et al. Bachler et al. (2010) was included. This database was used to validate this correlation. The biodiesel density data at 15°C ranged from 871.6 to 924.4 kg/m^3, while the kinematic viscosity at 40°C from 4.1 to 15.2 mm^2/s. These data are available in **Table F7 (in Appendix F)**. It is worth mentioning that some literature data found in the literature were not included in the database because of the absence of information on density and viscosity Aleme; Barbeira (2012 e Anitescu; Bruno (2012b e Lovestead et al. (2010).

Table F8 displays the adjusted parameters of Equations 7.2 to 7.4 for different pseudopure biodiesels obtained from the correlation dataset Vera-Rozo et al. (2022), as shown in the Supplementary material file. Figures 53 to 55 illustrate the absolute relative deviations between predicted by and experimental data values for temperatures at 10%, 50%, and 90% distillate volume. It is important to note that the data available for T_{10} (10 biodiesels from

various sources) is smaller than for T_{50} and T_{90} (26 biodiesels from multiple sources), which may influence deviation analysis.

These figures used the following acronyms for biodiesel oil sources: LinSeed (LS1 and LS2), CoRn (CR), Grape Seed (GS), PaLm (PME, PL1 and PL2), Waste Cooking (WCO and WC), SunFlower (SF1 and SF2), CaSTor (CST1 and CST2), CaNola (CN), Beef Tallow (BT), Croton (CRT), FiSh (FS), JaTropha (JT), KaRanja (KR), LarD (LD), RaPeseed (RP), Rice Bran (RB), SoyBean (SB1 and SB2).

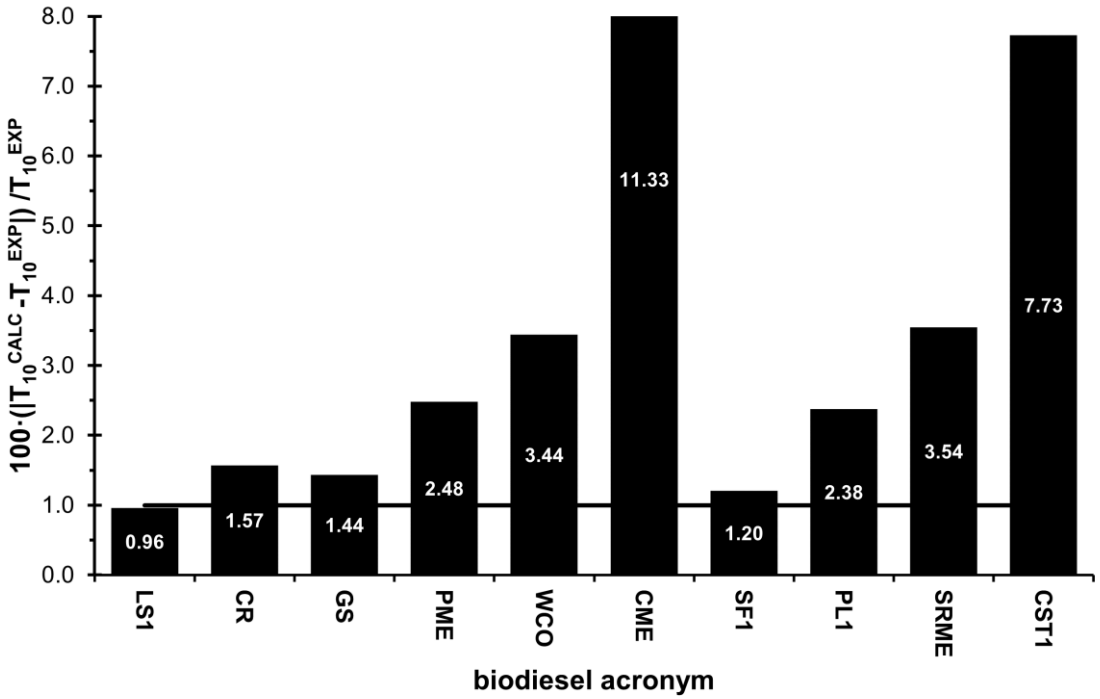

Figure 53 – Absolute relative percentage deviations for the 10% distillate volume temperature for various biodiesels from different oil sources. The solid black line represents the average of the deviations. (Created by the author, 2025)

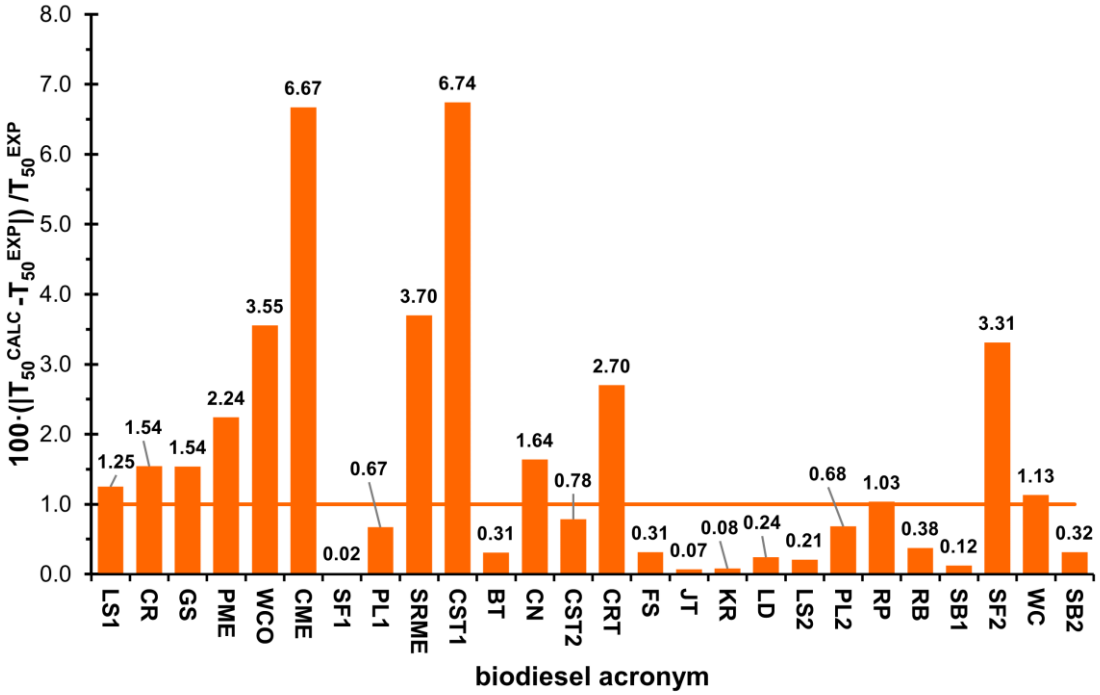

Figure 54 – Absolute relative percentage deviations for the 50% distillate volume temperature for various biodiesels from different oil sources. The solid orange line represents the average of the deviations. (Created by the author, 2025)

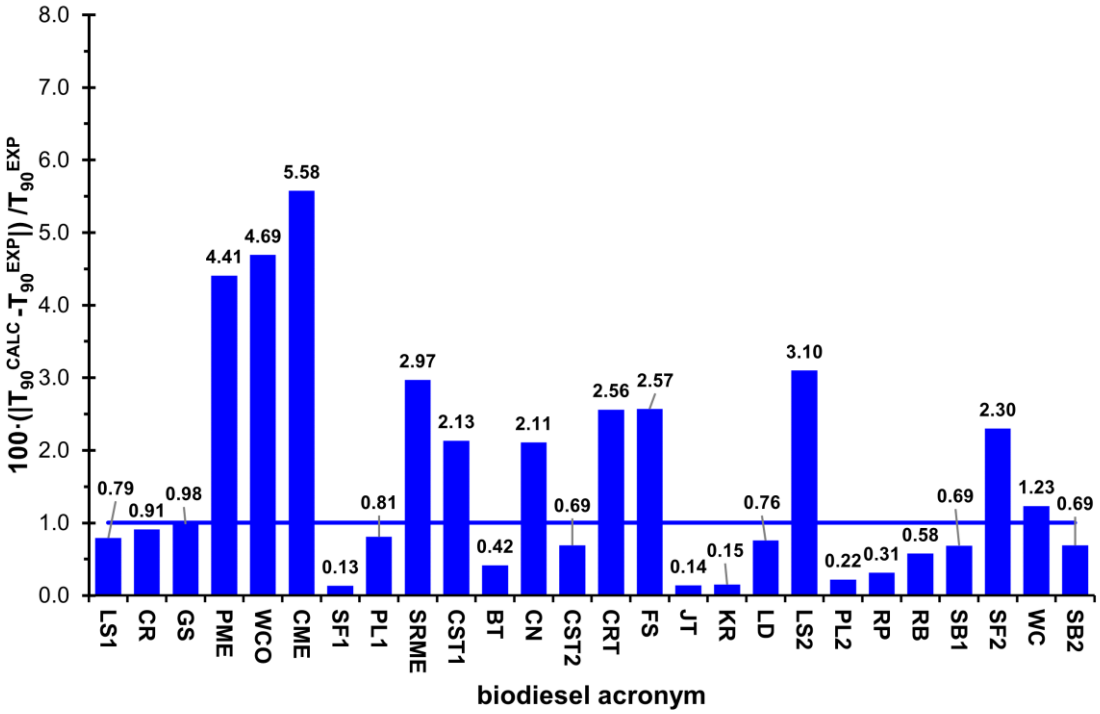

Figure 55 – Absolute relative percentage deviations for the 90% distillate volume temperature for various biodiesels from different oil sources. The solid blue line represents the average of the deviations. (Created by the author, 2025)

Generally, reasonable accuracy was observed for T_{10}, T_{50}, and $T_{90,}$ with average deviations (MAPD) of 3.61%, 1.59%, and 1.61%, respectively. The most significant deviations were observed for castor bean (CST) and coconut (CME)-based biodiesels, which have significantly different properties than other biodiesels. CST biodiesel mainly comprises methyl ricinoleate ($C_{19}H_{36}O_3$), representing around 80-90% of its total content. This composition results in characteristics such as high viscosity and high density. In contrast, CME biodiesel exhibits the opposite properties, with low viscosity and low density, due to smaller esters in its composition, such as methyl caprylate ($C_9H_{18}O_2$) and methyl laurate ($C_{13}H_{26}O_2$).

7.4.4 Distillation curve for diesel and biodiesel mixture

As discussed in Section 7.3.2, the distillation curve for the diesel-biodiesel blend was determined using a methodology like that used for pure biodiesel but extended to encompass the full distillation range. This methodology considered the blend's relative density, and the boiling temperature estimated from the pseudo-pure components. The parameters derived from the correlation set, which are used in equations 7.6 to 7.9, are detailed in **Table F9**. The parametrization applied the boiling temperatures square difference minimization for each distillate volume, with an MAPD deviation of 1.06% for the Hidegh et al. Hidegh et al. (2023) data and 1.08% for the grape biodiesel data presented in this work (correlation/parameterization set), as illustrated in Figure 56 corn and linseed biodiesels determined here, and the data reported by McCormick et al.McCormick et al. (2024) for blend diesel + soy biodiesel (test/validation set). The dotted lines highlight the errors at the temperatures defined by the ASTM D975 standard specifications (T_{10}, T_{50}, and T_{90}). The results reveal a maximum average absolute relative deviation of 1.33%, 0.62%, and 1.02% for the temperatures corresponding to 10%, 50%, and 90% of the distilled volume, respectively, demonstrating good accuracy of the data used for validation.

When examining the blends of diesel and biodiesel, deviations of 1.46%, 1.25%, 1.06%, 0.83%, and 0.82% were observed for the proportions of 20%, 40%, 60%, 80%, and 90%, respectively, as shown in Figure 56. The sharp decrease in deviations after the 60% ratio, from 1.06% to 0.83% (80%) and 0.82% (90%), can be attributed to variations in the central boiling temperature. These variations may arise due to the specific characteristics of the fuel and the type of oilseed used in biodiesel production, as the composition can vary significantly. For instance, coconut oil is primarily composed of the short-chain ester methyl laurate, while linseed oil, used in this study, has methyl linoleate as its main component.

In addition, another possible explanation for the decrease in deviations is the reduction in boiling temperature differences between the intervals of 10% to 50% and 50% to 90% of the distillate volume, as the biodiesel content increases. This issue is discussed in more detail in Section 7.4.1, where a progressive decrease in temperature variations is observed with increasing biodiesel concentration in the blend (**Figure F1**), resulting in behavior approaching linearity in blends with 100% biodiesel, as shown in Figure 44, after the first 5% of distilled volume.

The data provided by Aburudyna et al. Aburudyna et al. (2015) was tested to obtain the distillation curves using the parameters from the correlation proposed in this work. Aburudyna et al. Aburudyna et al. (2015) examined the impact of adding biodiesel on the properties of the blend, including the distillation profile, evaluating additions of up to 35% biodiesel and presenting the distillation curve at 0, 5, 10, 50, 90, and 95% distillate volume. The proposed correlation achieved an average relative absolute deviation of 3.10% across all data points. Specifically, for the temperatures corresponding to 10%, 50%, and 90% of the distilled volume, the deviations were 2.96% for T_{10}, 4.71% for T_{50}, and 1.74% for T_{90}, indicating a higher deviation at the central distillation temperature. For both the blends measured in this study (corn and linseed biodiesel) and those obtained by Aburudyna et al. Aburudyna et al. (2015), no systematic behavior was observed about the different blends evaluated.

This analysis demonstrates the efficiency of the proposed correlation for calculating the distillation curves of diesel and biodiesel blends, reinforcing the developed methodology's applicability for different compositions. It is important to highlight the limited availability of experimental data for this property, which may result in inaccuracies for some specific types of biodiesels.

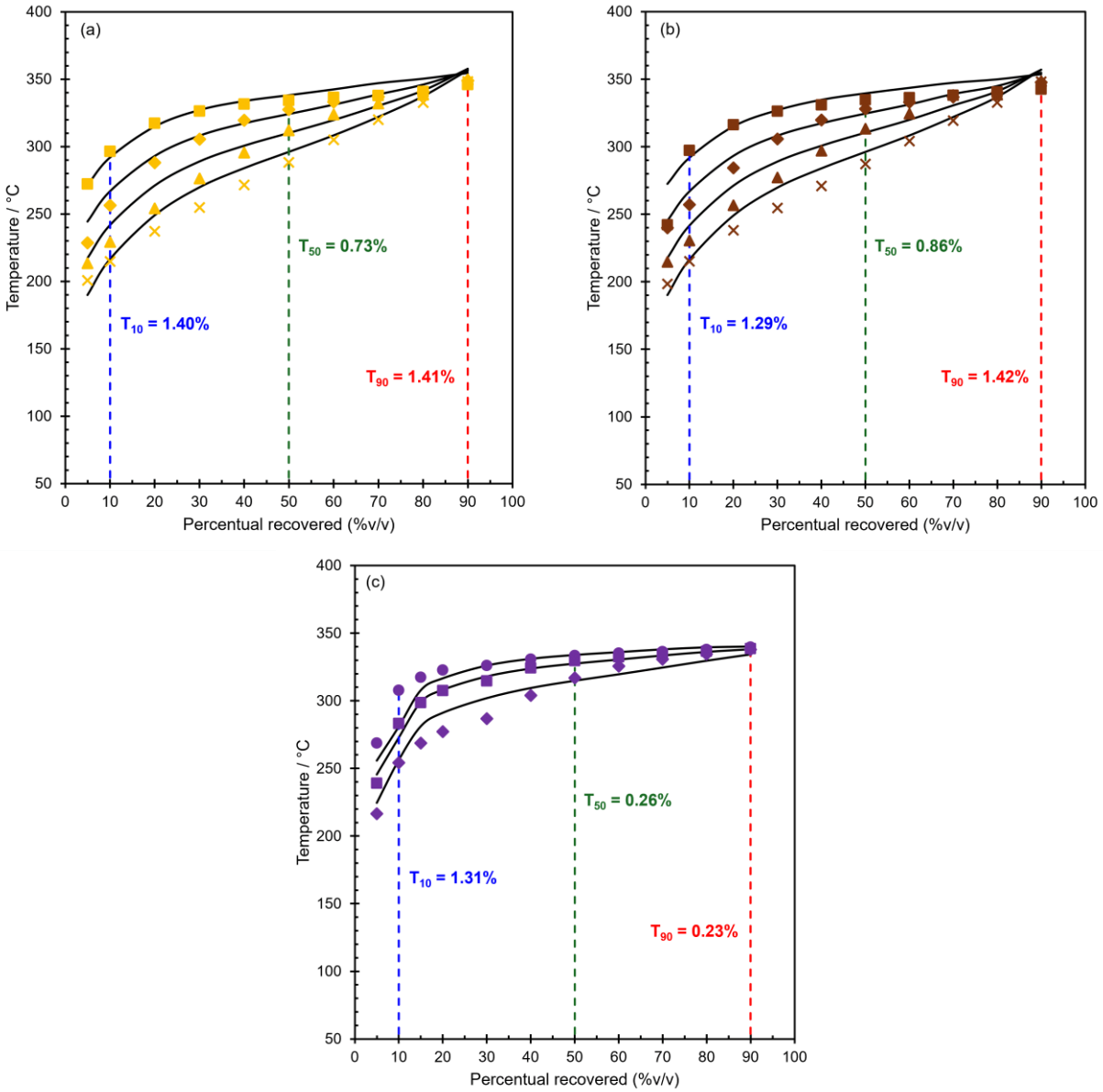

Figure 56 – Distillation curves for diesel + biodiesel. Where: (×, cross) 20% Biodiesel, (▲, triangle) 40% Biodiesel, (◆, diamond) 60% Biodiesel, and (■, square) 80%, and (●, circle) 90% Biodiesel. Solid lines represent the data obtained by the proposed correlation. (a) diesel + corn biodiesel, (b) diesel + linseed biodiesel, and (c) diesel + soybean biodiesel, reported in McCormick et al. McCormick et al. (2024). (Created by the author, 2025)

7.5 Conclusion

This study analyzed the distillation curves of diesel and biodiesel blends involving three types of biodiesels derived from grape seed, corn, and linseed. The analysis encompassed 207 experimental distillation points for the diesel + biodiesel system. A comparative study of the fundamental properties of the fuels was conducted, including density, viscosity, refractive index, flashpoint, acidity index, and cetane index, by ASTM D 975 and D 6751 standards. Two

correlations were proposed based on the Riazi model: the first to calculate the distillation temperatures of biodiesel at 10%, 50%, and 90% of the distilled volume, which are essential for specifying biofuel, and the second to model the distillation curve of the diesel + biodiesel blend.

Distillation curves were obtained for blends containing 20%, 40%, 60%, and 80% biodiesel in diesel. It was observed that adding biodiesel to the blends shifts the distillation curves to higher temperatures, indicating a change in the blend's volatility. This variation influences the evaporation of droplets during the spraying process and the formation of droplets during combustion. Moreover, a notable difference was observed in the behavior of the pseudo-pure curves of biodiesels compared to the diesel curve, attributed to the differing chemical nature of the compounds; biodiesel consists of ester mixtures, while diesel comprises hydrocarbons. The three types of biodiesels studied exhibited similar mass compositions, with more than 87% of esters containing 19 carbons in their chains, resulting in comparable boiling points.

Compared with the ASTM D 975 standard, which sets the specifications for conventional petroleum diesel (density at 15°C between 0.82 and 0.86 g/cm³ and kinematic viscosity at 40°C between 1.3 and 4.1 mm²/s), it was found that for the diesel + biodiesel blends studied, up to a volumetric content of 37% biodiesel, the density remained within the established limits. Additionally, the kinematic viscosity fell within the 67 - 76% range, indicating compliance with the diesel specifications for these properties.

Two correlations were proposed: one for biodiesel and the other for diesel + biodiesel blends. It's worth noting that no existing models or correlations were suitable for this blend, given the limited available data. For biodiesel, a correlation was developed utilizing relative density and kinematic viscosity as input parameters to compute distillation temperatures at 10%, 50%, and 90% of the distilled volume, resulting in deviations of 3.61%, 1.59%, and 1.61%, respectively. Regarding the diesel + biodiesel blends, a small dataset was employed, yielding deviations of 1.46%, 1.25%, 1.06%, and 0.82% for the proportions of 20%, 40%, 60%, and 80%, respectively, with no systematic deviations observed concerning the increase in biodiesel content in the blend.

The findings of this study represent a significant contribution to understanding the properties and behavior of diesel and biodiesel blends, laying the groundwork for future research and development in the field of biofuels.

8 GENERAL CONCLUSION

This thesis presents comprehensive experimental and modeling research on the thermophysical properties of biodiesels and their blends with alcohols and diesel, addressing critical knowledge gaps in density, speed of sound, isobaric heat capacity, and distillation behavior across broad ranges of temperature and pressure.

Studies on pseudo-pure biodiesels demonstrated the reliability of experimental measurements of density and speed of sound up to 200 MPa, from which key derived properties, such as isentropic compressibility and acoustic impedance, were obtained. The predictive capability of the PC-SAFT equation of state was assessed, along with specific correlations based on ester composition, the latter achieving superior accuracy.

The determination of isobaric heat capacity using Differential Scanning Calorimetry (DSC), together with literature data for 22 biodiesels, confirmed the applicability of a predictive model based on the principle of corresponding states. This represents the first successful extension of the model to biodiesel, providing robust and accurate predictions and establishing a new approach for describing its thermal behavior.

In the context of biodiesel–alcohol systems, measurements of density and speed of sound revealed near-ideal volumetric behavior and acoustic trends, with only minor deviations from additivity, which decreased at high pressures and increased with temperature. A new combination rule proposed for predicting sound velocity proved consistent under all conditions studied, offering practical value for future formulations of renewable fuel blends.

Finally, the study of diesel–biodiesel mixture distillation provided new experimental data and correlations capable of predicting the evaporation behavior of both pure biodiesel and its mixtures with diesel. These results clarified the influence of biodiesel addition on volatility and droplet formation processes, which are critical for combustion efficiency. The proposed correlations address the lack of adequate models for these systems, enhancing predictive capability for industrial applications.

Overall, this thesis expands the experimental database of thermophysical properties of biodiesel and its blends while proposing and validating predictive models and correlations. The results provide a deeper understanding of the thermal, acoustic, and phase behavior of biodiesel-based fuels, offering insights that can inform the design of more efficient combustion systems, optimize industrial processes, and guide the development of future renewable fuel formulations.

REFERENCES

ABURUDYNA, A. et al. Impact of biodiesel addition on distillation characteristics and cetane index of diesel fuels. **Journal of Energy Engineering**, v. 141, n. 2, 2015. Disponível em: https://doi.org/10.1061/(ASCE)EY.1943-7897.0000244. Acesso em: 10 jun. 2025.

AGAFONOVA, L. E.; VARUSHCHENKO, R. M.; DRUZHININA, A. I.; POLYAKOVA, O. V.; KOLESOV, Y. S. Heat capacity, saturation vapor pressure, and thermodynamic functions of ethyl esters of C3–C5 and C18 carboxylic acids. **Russian Journal of Physical Chemistry A**, v. 85, n. 9, p. 1516–1527, 2011.

AIT BELALE, R.; M'HAMDI ALAOUI, F. E.; CHHITI, Y. *et al.* Study on the thermophysical properties of waste cooking oil biodiesel fuel blends with 1-butanol. **Fuel**, v. 287, p. 119540, 2021.

AITBELALE, R.; ABALA, I.; M'HAMDI ALAOUI, F. E. *et al.* Characterization and determination of thermodynamic properties of waste cooking oil biodiesel: experimental, correlation and modeling density over a wide temperature range up to 393.15 K and pressure up to 140 MPa. **Fluid Phase Equilibria**, v. 497, p. 87–96, 2019.

AITBELALE, R.; ACHAK, M.; CHHITI, Y. *et al.* Effects of 2-butanol addition on waste cooking oil biodiesel density: an updated experimental measurement and thermodynamic modeling study. **Journal of Chemical & Engineering Data**, v. 66, n. 8, p. 3123–3141, 2021.

AITBELALE, R.; CHHITI, Y.; ALAOUI, F. E. M. *et al.* High-pressure soybean oil biodiesel density: experimental measurements, correlation by Tait equation, and perturbed chain SAFT (PC-SAFT) modeling. **Journal of Chemical & Engineering Data**, v. 64, n. 9, p. 3994–4004, 2019.

ALAGUMALAI, A. Internal combustion engines: progress and prospects. **Renewable and Sustainable Energy Reviews**, v. 38, p. 561–571, 2014.

ALAOUI, F. E. M. **Investigación experimental de propiedades termodinámicas de entalpía de mezcla y densidad en sistemas multicomponentes de aditivos oxigenados e hidrocarburos en biocombustibles de bajo impacto ambiental**. 2011. Tese (Doutorado em Ingeniería Electromecánica) – Universidad de Burgos, Burgos, 2011.

ALCANTARA, M. L.; DE CARVALHO, M. L.; ÁLVAREZ, V. H. *et al.* High pressure vapor-liquid equilibria for binary carbon dioxide and protic ionic liquid based on ethanolamines + butanoic acid. **Fluid Phase Equilibria**, v. 460, p. 162–174, 2018.

ALEME, H. G.; BARBEIRA, P. J. S. Determination of biodiesel content in diesel using distillation curves and multivariate calibration. **Energy & Fuels**, v. 26, n. 9, p. 5769–5774, 2012.

ALJAAFARI, A.; FATTAH, I. M. R.; JAHIRUL, M. I. *et al.* Biodiesel emissions: a state-of-the-art review on health and environmental impacts. **Energies**, v. 15, n. 17, 2022.

ALPTEKIN, E.; CANAKCI, M. Determination of the density and the viscosities of biodiesel–diesel fuel blends. **Renewable Energy**, v. 33, n. 12, p. 2623–2630, 2008.

ALVES, A. A. A.; ALVES, R. S.; DE MEDEIROS, P. Y. G. *et al.* Distillation analysis of diesel-biodiesel mixtures: a comparative study with ASTM norms, experimental data, and novel correlations. **Fuel**, v. 383, p. 133864, 2025.

ALVES, A. A. A.; ARAÚJO ALVES, A. A.; LEVY, H. M. *et al.* Biodiesel isobaric heat capacity: a comprehensive assessment through experimental evaluation and prediction with a corresponding states model. **Fuel**, v. 379, p. 133003, 2025.

ALVES, A. A. A.; ARAÚJO ALVES, A. A.; MEDEIROS, H. A. D. *et al.* Viscosity and density of binary mixtures of methyl hexanoate + alcohols (C3, C4, and C5) at different temperatures and atmospheric pressure. **Journal of Molecular Liquids**, p. 128034, 2025.

ALVES, A. A. A.; DA COSTA, M. F. L.; DE MEDEIROS, L. H. G. *et al.* Investigating the thermophysical properties of the 1-butanol + biodiesel system: the impact of pressure on volumetric characteristics. **Fuel**, v. 371, p. 132076, 2024.

ALVES, A. A. A.; DE MEDEIROS, L. H. G.; FEITOSA, F. X.; DE SANT'ANA, H. B. Thermodynamic properties of biodiesel and petrodiesel blends at high pressure and high temperature and a new model for density prediction. **Journal of Chemical & Engineering Data**, v. 67, n. 3, p. 607–621, 2022.

ANITESCU, G.; BRUNO, T. J. Biodiesel fuels from supercritical fluid processing: quality evaluation with the advanced distillation curve method and cetane numbers. **Energy & Fuels**, v. 26, n. 8, p. 5256–5264, 2012b.

ANITESCU, G.; BRUNO, T. J. Liquid biofuels: fluid properties to optimize feedstock selection, processing, refining/blending, storage/transportation, and combustion. **Energy & Fuels**, v. 26, n. 1, p. 324–348, 2012a.

ARAÚJO ALVES, A. A.; LEAL DA COSTA, M. F.; BAZILE, J.-P. *et al.* Exploring the thermophysical properties of biodiesel: high-pressure density and speed of sound prediction with PC-SAFT and ester composition models. **Fuel**, v. 391, p. 134707, 2025.

ASTM INTERNATIONAL. ASTM D1078: standard test method for distillation range of volatile organic liquids. West Conshohocken, PA, 2011.

ASTM INTERNATIONAL. ASTM D86: standard test method for distillation of petroleum products and liquid fuels at atmospheric pressure. West Conshohocken, PA, 2018.

AYAD, A.; NEGADI, A.; MUTELET, F. Carbon dioxide solubilities in tricyanomethanide-based ionic liquids: measurements and PC-SAFT modeling. **Fluid Phase Equilibria**, v. 469, p. 48–55, 2018.

AZAD, A. K.; RASUL, M. G.; KHAN, M. M. K.; SHARMA, S. C.; BHUIYA, M. M. K. Recent development of biodiesel combustion strategies and modelling for compression ignition engines. **Renewable and Sustainable Energy Reviews**, v. 56, p. 1068–1086, 2016.

BACHLER, C.; SCHOBER, S.; MITTELBACH, M. Simulated distillation for biofuel analysis. **Energy & Fuels**, v. 24, n. 3, p. 2086–2090, 2010.

BAIJU, B.; NAIK, M. K.; DAS, L. M. A comparative evaluation of compression ignition engine characteristics using methyl and ethyl esters of Karanja oil. **Renewable Energy**, v. 34, n. 6, p. 1616–1621, 2009.

BAIRD, Z. S.; UUSI-KYYNY, P.; POKKI, J. P.; PEDEGERT, E.; ALOPAEUS, V. Vapor pressures, densities, and PC-SAFT parameters for 11 bio-compounds. **International Journal of Thermophysics**, v. 40, n. 11, 2019.

BARABÁS, I.; TODORUŢ, A. I. **Key fuel properties of biodiesel-diesel fuel-ethanol blends**. Warrendale: SAE International, 2009. (SAE Technical Paper 2009-01-1810).

BAZILE, J.-P.; NASRI, D.; DARIDON, J.-L. Speed of sound in hydrocarbon–fatty acid methyl ester blends: experimental investigation and combining rule development. **Journal of Chemical & Engineering Data**, v. 69, n. 9, p. 2949–2958, 2024.

BAZILE, J.-P.; NASRI, D.; DARIDON, J.-L. Speed of sound, density, and derivative properties of tris(2-ethylhexyl) trimellitate under high pressure. **Journal of Chemical & Engineering Data**, v. 62, n. 5, p. 1708–1715, 2017.

BENEDICT, M.; WEBB, G. B.; RUBIN, L. C. An empirical equation for thermodynamic properties of light hydrocarbons and their mixtures I: methane, ethane, propane and n-butane. **The Journal of Chemical Physics**, v. 8, n. 4, p. 334–345, 1940.

BENJUMEA, P.; AGUDELO, J.; AGUDELO, A. Basic properties of palm oil biodiesel–diesel blends. **Fuel**, v. 87, n. 10–11, p. 2069–2075, 2008.

BERMAN, P.; NIZRI, S.; WIESMAN, Z. Castor oil biodiesel and its blends as alternative fuel. **Biomass and Bioenergy**, v. 35, n. 7, p. 2861–2866, 2011.

BESSIÈRES, D.; BAZILE, J.-P.; TANH, X. N. T.; GARCÍA-CUADRA, F.; ACIEN, F. G. Thermophysical behavior of three algal biodiesels over wide ranges of pressure and temperature. **Fuel**, v. 233, p. 497–503, 2018.

BEZARD, J.; BUGAUT, M.; CLEMENT, G. Triglyceride composition of coconut oil. **Journal of the American Oil Chemists' Society**, v. 48, p. 134–139, 1971.

BOGATISHCHEVA, N. S.; FAIZULLIN, M. Z.; NIKITIN, E. D. Heat capacities and thermal diffusivities of n-alkane acid ethyl esters—biodiesel fuel components. **Russian Journal of Physical Chemistry A**, v. 91, n. 9, p. 1647–1653, 2017.

BOGATISHCHEVA, N. S.; FAIZULLIN, M. Z.; NIKITIN, E. D. Heat capacities and thermal diffusivities of some n-alkanoic acid methyl esters. **The Journal of Chemical Thermodynamics**, v. 130, p. 33–37, 2019.

BONDI, A. Estimation of heat capacity of liquids. **Industrial & Engineering Chemistry Fundamentals**, v. 5, n. 4, p. 442–449, 1966.

BOUDY, F.; SEERS, P. Impact of physical properties of biodiesel on the injection process in a common-rail direct injection system. **Energy Conversion and Management**, v. 50, n. 12, p. 2905–2912, 2009.

BUKKARAPU, K. R.; KRISHNASAMY, A. A critical review on available models to predict engine fuel properties of biodiesel. **Renewable and Sustainable Energy Reviews**, v. 155, p. 111925, 2022.

BUKKARAPU, K. R.; RAHUL, T. S.; KUNDLA, S.; VARDHAN, G. V. Effects of blending on the properties of diesel and palm biodiesel. **IOP Conference Series: Materials Science and Engineering**, v. 330, p. 012092, 2018.

BULLERMANN, J.; MEYER, N. C.; KRAFFT, A.; WIRZ, F. Comparison of fuel properties of alternative drop-in fuels with standard marine diesel and the effects of their blends. **Fuel**, v. 357, 2024.

CANABARRO, N. I.; SILVA-ORTIZ, P.; NOGUEIRA, L. A. H. *et al.* Sustainability assessment of ethanol and biodiesel production in Argentina, Brazil, Colombia, and Guatemala. **Renewable and Sustainable Energy Reviews**, v. 171, 2023.

CANDEIA, R. A.; SILVA, M. C. D.; CARVALHO FILHO, J. R. *et al.* Influence of soybean biodiesel content on basic properties of biodiesel–diesel blends. **Fuel**, v. 88, n. 4, p. 738–743, 2009.

CANO-GÓMEZ, J. J.; IGLESIAS-SILVA, G. A.; RIVAS, P.; DÍAZ-OVALLE, C. O.; DE JESÚS CERINO-CÓRDOVA, F. Densities and viscosities for binary liquid mixtures of biodiesel + 1-butanol, + isobutyl alcohol, or + 2-butanol from 293.15 to 333.15 K at 0.1 MPa. **Journal of Chemical & Engineering Data**, v. 62, n. 10, p. 3391–3400, 2017.

CARMO, F. R. do; DA SILVA, M. R. L.; ALVES, A. A. A.; EVANGELISTA, N. S. A new method for predicting the isobaric heat capacity of biodiesel-related esters based on the corresponding states principle. **Fluid Phase Equilibria**, v. 509, p. 112467, 2020.

CARMO, F. R. do; EVANGELISTA, N. S.; FERNANDES, F. A. N.; DE SANT'ANA, H. B. Evaluation of optimal methods for critical properties and acentric factor of biodiesel compounds with their application on Soave-Redlich-Kwong and Peng-Robinson equations of state. **Journal of Chemical & Engineering Data**, v. 60, n. 11, p. 3358–3381, 2015.

CERIANI, R.; GANI, R.; LIU, Y. A. Prediction of vapor pressure and heats of vaporization of edible oil/fat compounds by group contribution. **Fluid Phase Equilibria**, v. 337, p. 53–59, 2013.

CERIANI, R.; GANI, R.; MEIRELLES, A. J. A. Prediction of heat capacities and heats of vaporization of organic liquids by group contribution methods. **Fluid Phase Equilibria**, v. 283, n. 1–2, p. 49–55, 2009.

CERIANI, R.; GONÇALVES, C. B.; COUTINHO, J. A. P. Prediction of viscosities of fatty compounds and biodiesel by group contribution. **Energy & Fuels**, v. 25, n. 8, p. 3712–3717, 2011.

CERIANI, R.; MEIRELLES, A. J. A. Predicting vapor–liquid equilibria of fatty systems. **Fluid Phase Equilibria**, v. 215, n. 2, p. 227–236, 2004.

CERINSKI, D.; VUJANOVIĆ, M.; PETRANOVIĆ, Z. *et al.* Numerical analysis of fuel injection configuration on nitrogen oxides formation in a jet engine combustion chamber. **Energy Conversion and Management**, v. 220, p. 112862, 2020.

CHACÓN VALERO, A. M.; ALVES, C. A.; DE MEDEIROS, P. Y. G.; FEITOSA, F. X.; DE SANT'ANA, H. B. Density and volumetric behavior of ternary CO_2 + n-decane + n-butylcyclohexane mixtures at high pressure and high temperature. **Journal of Chemical & Engineering Data**, v. 67, n. 6, p. 1397–1405, 2022.

CHAPMAN, W. G.; GUBBINS, K. E.; JACKSON, G.; RADOSZ, M. New reference equation of state for associating liquids. **Industrial & Engineering Chemistry Research**, v. 29, n. 8, p. 1709–1721, 1990.

CHAPMAN, W. G.; GUBBINS, K. E.; JACKSON, G.; RADOSZ, M. SAFT: equation-of-state solution model for associating fluids. **Fluid Phase Equilibria**, v. 52, p. 31–38, 1989.

CHEN, A.; CHEN, C. Comparison of GUM and Monte Carlo methods for evaluating measurement uncertainty of perspiration measurement systems. **Measurement**, v. 87, p. 27–37, 2016.

CHEN, S. S.; KREGLEWSKI, A. Applications of the augmented van der Waals theory of fluids: I. pure fluids. **Berichte der Bunsengesellschaft für physikalische Chemie**, v. 81, n. 10, p. 1048–1052, 1977.

CHUEH, P. L.; PRAUSNITZ, J. M. Vapor-liquid equilibria at high pressures: calculation of partial molar volumes in nonpolar liquid mixtures. **AIChE Journal**, v. 13, n. 6, p. 1099–1107, 1967.

COLEMAN, H. W.; STEELE, W. G. Engineering application of experimental uncertainty analysis. **AIAA Journal**, v. 33, n. 10, p. 1888–1896, 1995.

COMUÑAS, M. J. P.; BAZILE, J.; BAYLAUCQ, A.; BONED, C. Density of diethyl adipate using a new vibrating tube densimeter from (293.15 to 403.15) K and up to 140 MPa: calibration and measurements. **Journal of Chemical & Engineering Data**, v. 53, p. 986–994, 2008.

CONSTANTINOU, L.; GANI, R. New group contribution method for estimating properties of pure compounds. **AIChE Journal**, v. 40, n. 10, p. 1697–1710, 1994.

COSTA, M. F. L. da; DE MEDEIROS, H. A.; ARAÚJO ALVES, A. A. *et al.* Volumetric properties of three nonylphenol ethoxylated nonionic surfactant mixtures with methanol: experimental study and modeling with Tammann-Tait and PC-SAFT equation of state. **Fluid Phase Equilibria**, v. 581, p. 114076, 2024.

COSTA, M. F. L. da; MEDEIROS, H. A. D.; ALVES, A. A. A. *et al.* Phase behavior of supercritical CO_2 + nonionic ethoxylated surfactants + methanol: experimental data and modeling with PC-SAFT equation of state. **Fluid Phase Equilibria**, v. 583, p. 114130, 2024.

CUNHA, D. L.; COUTINHO, J. A. P.; DARIDON, J. L.; REIS, R. A.; PAREDES, M. L. L. An atomic contribution model for the prediction of speed of sound. **Fluid Phase Equilibria**, v. 358, p. 108–113, 2013.

DAMANIK, N.; ONG, H. C.; TONG, C. W.; MAHLIA, T. M. I.; SILITONGA, A. S. A review on the engine performance and exhaust emission characteristics of diesel engines fueled with biodiesel blends. **Environmental Science and Pollution Research**, v. 25, n. 16, p. 15307–15325, 2018.

DARIDON, J. L.; LAGRABETTE, A.; LAGOURETTE, B. Speed of sound, density, and compressibilities of heavy synthetic cuts from ultrasonic measurements under pressure. **Journal of Chemical Thermodynamics**, v. 30, n. 5, p. 607–623, 1998.

DARIDON, J.-L. Predicting and correlating speed of sound in long-chain alkanes at high pressure. **International Journal of Thermophysics**, v. 43, n. 5, p. 78, 2022a.

DARIDON, J.-L. Predicting speed of sound in fatty acid alkyl esters and biodiesels at high pressure. **Industrial & Engineering Chemistry Research**, v. 61, n. 42, p. 15620–15630, 2022b.

DARIDON, J.-L. Predicting the effect of pressure on biodiesel density at pressures of up to 200 MPa based on fatty acid alkyl ester profiles and density values at atmospheric pressure. **Fuel**, v. 281, p. 118767, 2020.

DARIDON, J.-L.; BAZILE, J.-P. Computation of liquid isothermal compressibility from density measurements: an application to toluene. **Journal of Chemical & Engineering Data**, v. 63, n. 6, p. 2162–2178, 2018.

DARIDON, J.-L.; BAZILE, J.-P.; NASRI, D. Measurement and modeling of speed of sound in binary mixtures of methyl oleate with n-hexane or n-decane under pressure. **International Journal of Thermophysics**, v. 44, n. 7, p. 99, 2023.

DARIDON, J.-L.; BAZILE, J.-P.; NASRI, D. Speed of sound, density, and related thermophysical properties of the methyl caprate + methyl oleate binary system from 0.1 MPa to 70 MPa at 303.15 K. **International Journal of Thermophysics**, v. 43, n. 2, p. 23, 2022.

DARIDON, J.-L.; COUTINHO, J. A. P.; NDIAYE, E. H. I.; PAREDES, M. L. L. Novel data and a group contribution method for the prediction of the speed of sound and isentropic compressibility of pure fatty acids methyl and ethyl esters. **Fuel**, v. 105, p. 466–470, 2013.

DAUGBJERG, C.; SWINBANK, A. Globalization and new policy concerns: the WTO and the EU's sustainability criteria for biofuels. **Journal of European Public Policy**, v. 22, n. 3, p. 429–446, 2015.

DÁVILA, M. J.; GEDANITZ, H.; SPAN, R. Speed of sound measurements of liquid C1–C4 alkanols. **Journal of Chemical Thermodynamics**, v. 93, p. 157–163, 2016.

DEMIRBAS, A.; DEMIRBAS, M. F. Importance of algae oil as a source of biodiesel. **Energy Conversion and Management**, v. 52, n. 1, p. 163–170, 2011.

DIAMANTONIS, N. I.; ECONOMOU, I. G. Evaluation of statistical associating fluid theory (SAFT) and perturbed chain-SAFT equations of state for the calculation of thermodynamic derivative properties of fluids related to carbon capture and sequestration. **Energy & Fuels**, v. 25, p. 3334–3343, 2011.

DO CARMO, F. R. et al. A new method for predicting the isobaric heat capacity of biodiesel-related esters based on the corresponding states principle. **Fluid Phase Equilibria**, v. 521, p. 112734, 2020.

DO CARMO, F. R. et al. Evaluation of optimal methods for critical properties and acentric factor of biodiesel compounds with their application on Soave–Redlich–Kwong and Peng–Robinson equations of state. **Journal of Chemical & Engineering Data**, v. 60, n. 11, p. 3358–3381, 2015.

DYMOND, J. H.; MALHOTRA, R. The Tait equation: 100 years on. **International Journal of Thermophysics**, v. 9, n. 6, p. 941–951, 1988.

DZIDA, M. Speeds of sound, densities, isobaric thermal expansion, compressibilities, and internal pressures of heptan-1-ol, octan-1-ol, nonan-1-ol, and decan-1-ol at temperatures from 293 to 318 K and pressures up to 100 MPa. **Journal of Chemical & Engineering Data**, v. 52, n. 2, p. 521–531, 2007.

DZIDA, M. Thermophysical properties of 1-butanol at high pressures. **Energies**, v. 13, n. 19, p. 5046, 2020.

DZIDA, M.; JĘŻAK, S.; SUMARA, J.; ŻARSKA, M.; GÓRALSKI, P. High pressure physicochemical properties of biodiesel components used for spray characteristics in diesel injection systems. **Fuel**, v. 111, p. 165–171, 2013.

DZIDA, M.; PRUSAKIEWICZ, P. The effect of temperature and pressure on the physicochemical properties of petroleum diesel oil and biodiesel fuel. **Fuel**, v. 87, n. 10–11, p. 1941–1948, 2008.

DZIDA, M.; ZORĘBSKI, E.; ZORĘBSKI, M. et al. Speed of sound and ultrasound absorption in ionic liquids. **Chemical Reviews**, v. 117, n. 5, p. 3883–3929, 2017.

ELLAPPAN, S.; RAJENDRAN, S. A comparative review of performance and emission characteristics of diesel engine using eucalyptus-biodiesel blend. **Fuel**, v. 284, p. 118925, 2021.

ERDIWANSYAH; MAMAT, R.; SANI, M. S. M. et al. An overview of higher alcohol and biodiesel as alternative fuels in engines. **Energy Reports**, v. 5, p. 467–479, 2019.

EVANGELISTA, N. S.; DO CARMO, F. R.; DE SANT'ANA, H. B. Estimation of physical constants of biodiesel-related fatty acid alkyl esters: normal boiling point, critical temperature, critical pressure, and acentric factor. **Industrial & Engineering Chemistry Research**, v. 57, n. 25, p. 8552–8565, 2018.

EVANGELISTA, N. S.; DO CARMO, F. R.; DE SANT'ANA, H. B. Estimation of vapor pressures and enthalpies of vaporization of biodiesel-related fatty acid alkyl esters. Part 1. Evaluation of group contribution and corresponding states methods. **Industrial & Engineering Chemistry Research**, v. 56, n. 8, p. 2298–2309, 2017.

EVANGELISTA, N. S.; DO CARMO, F. R.; DE SANT'ANA, H. B. Estimation of vapor pressures and enthalpies of vaporization of biodiesel-related fatty acid alkyl esters. Part 2. New parameters for classic vapor pressure correlations. **Industrial & Engineering Chemistry Research**, v. 56, n. 29, p. 8349–8357, 2017.

FEITOSA, F.; RODRIGUES, M. L.; VELOSO, C. B. et al. Viscosities and densities of binary mixtures of coconut + colza and coconut + soybean biodiesel at various temperatures. **Journal of Chemical & Engineering Data**, v. 55, p. 3909–3914, 2010.

FERNÁNDEZ-RODRÍGUEZ, D.; LAPUERTA, M.; GERMAN, L. Progress in the use of biobutanol blends in diesel engines. **Energies**, v. 14, n. 11, p. 3215, 2021.

FERREIRA, A. G. M.; SANTOS, J. B.; BAPTISTA, J. et al. Effect of isobutanol addition on the biodiesel density. **Journal of Chemical & Engineering Data**, v. 66, n. 12, p. 4542–4562, 2021.

FIGURA, L. O.; TEIXEIRA, A. A. Mass density. *In*: FIGURA, L. O.; TEIXEIRA, A. A. **Food physics:** physical properties-measurement and applications. Cham: Springer International Publishing, 2023. p. 59-100.

FREITAS, S. V. D.; CUNHA, D. L.; REIS, R. A. et al. Application of Wada's group contribution method to the prediction of the speed of sound of biodiesel. **Energy & Fuels**, v. 27, n. 3, p. 1365–1370, 2013.

FREITAS, S. V. D.; PAREDES, M. L. L.; DARIDON, J.-L.; LIMA, Á. S.; COUTINHO, J. A. P. Measurement and prediction of the speed of sound of biodiesel fuels. **Fuel**, v. 103, p. 1018–1022, 2013.

FREITAS, S. V. D.; PRATAS, M. J.; CERIANI, R.; LIMA, Á. S.; COUTINHO, J. A. P. Evaluation of predictive models for the viscosity of biodiesel. **Energy & Fuels**, v. 25, n. 1, p. 352–358, 2011.

GALADIMA, A.; MURAZA, O. Biodiesel production from algae by using heterogeneous catalysts: A critical review. **Energy**, v. 78, p. 72–83, 2014.

GARCÍA-MORALES, R.; DOMENZAÍN-GONZÁLEZ, J.; VERÓNICO-SÁNCHEZ, F. J. et al. Density Measurements and PC-SAFT Modeling for Beef Tallow Fatty Acid Methyl Esters (FAME Mixture) + Alkane up to 70 MPa. **Journal of Chemical & Engineering Data**, v. 68, n. 5, p. 1091–1104, 2023.

GARCÍA-MORALES, R.; VERÓNICO-SÁNCHEZ, F. J.; DOMENZAÍN-GONZÁLEZ, J. et al. Liquid to solid phase transition detection by using a vibrating tube densimeter along with densities up to 137 MPa of beef tallow fatty acid alkyl esters. **The Journal of Chemical Thermodynamics**, v. 192, p. 107259, 2024.

GERPEN, J. van. Biodiesel processing and production. **Fuel Processing Technology**, v. 86, n. 10, p. 1097–1107, 2005.

GHANBARI, M.; AHMADI, M.; LASHANIZADEGAN, A. A comparison between Peng-Robinson and Soave-Redlich-Kwong cubic equations of state from modification perspective. **Cryogenics**, v. 84, p. 13–19, 2017.

GIAKOUMIS, E. G. A statistical investigation of biodiesel physical and chemical properties, and their correlation with the degree of unsaturation. **Renewable Energy**, v. 50, p. 858–878, 2013.

GRENNER, A.; KONTOGEORGIS, G. M.; VON SOLMS, N.; MICHELSEN, M. L. Modeling phase equilibria of alkanols with the simplified PC-SAFT equation of state and generalized pure compound parameters. **Fluid Phase Equilibria**, v. 258, n. 1, p. 83–94, 2007.

GROSS, J.; SADOWSKI, G. Application of the Perturbed-Chain SAFT Equation of State to Associating Systems. **Industrial & Engineering Chemistry Research**, v. 41, n. 22, p. 5510–5515, 2002b.

GROSS, J.; SADOWSKI, G. Modeling polymer systems using the perturbed-chain statistical associating fluid theory equation of state. **Industrial and Engineering Chemistry Research**, v. 41, n. 5, p. 1084–1093, 2002a.

GROSS, J.; SADOWSKI, G. Perturbed-Chain SAFT: An Equation of State Based on a Perturbation Theory for Chain Molecules. **Industrial & Engineering Chemistry Research**, v. 40, n. 4, p. 1244–1260, 2001.

GROSS, J.; VRABEC, J. An equation-of-state contribution for polar components: Dipolar molecules. **AIChE Journal**, v. 52, n. 3, p. 1194–1204, 2006.

GROSSO, V. A. del; MADER, C. W. Speed of Sound in Pure Water. **The Journal of the Acoustical Society of America**, v. 52, n. 5B, p. 1442–1446, 1972.

GÜLÜM, M.; BILGIN, A. Measurements and empirical correlations in predicting biodiesel-diesel blends' viscosity and density. **Fuel**, v. 199, p. 567–577, 2017.

HABRIOUX, M. **Caractérisation thermophysique des fluides sous pression à l'aide d'un dispositif unique de mesures acoustiques:** application aux biodiesels et à leurs constituants. 2015. Tese (Doutorado em Génie des Procédés) – Université de Pau et des Pays de l'Adour, Pau, 2015.

HABRIOUX, M.; FREITAS, S. V. D.; COUTINHO, J. A. P.; DARIDON, J. L. High Pressure Density and Speed of Sound in Two Biodiesel Fuels. **Journal of Chemical & Engineering Data**, v. 58, n. 12, p. 3392–3398, 2013.

HABRIOUX, M.; NASRI, D.; COUTINHO, J. A. P.; DARIDON, J.-L. Measurement and prediction of the volumetric and acoustic properties of two biodiesel fuels up to 200 MPa. **Fuel**, v. 349, p. 128677, 2023.

HABRIOUX, M.; NASRI, D.; DARIDON, J. L. Measurement of speed of sound, density compressibility and viscosity in liquid methyl laurate and ethyl laurate up to 200 MPa by

using acoustic wave sensors. **The Journal of Chemical Thermodynamics**, v. 120, p. 1–12, 2018.

HAZRAT, M. A.; RASUL, M. G.; MOFIJUR, M. et al. A Mini Review on the Cold Flow Properties of Biodiesel and its Blends. **Frontiers in Energy Research**, v. 8, 2020.

HELD, C.; RESCHKE, T.; MOHAMMAD, S.; LUZA, A.; SADOWSKI, G. ePC-SAFT revised. **Chemical Engineering Research and Design**, v. 92, n. 12, p. 2884–2897, 2014.

HEMPTINNE, J.-C. de; KONTOGEORGIS, G. M.; DOHRN, R. et al. A View on the Future of Applied Thermodynamics. **Industrial & Engineering Chemistry Research**, v. 61, n. 39, p. 14664–14680, 2022.

HIDEGH, G. T.; CSEMÁNY, D.; DARALI, O. et al. Comparison of thermophysical properties and combustion characteristics of various biodiesels in a non-MILD ultra-low emission swirl burner. **Fuel**, v. 334, p. 126583, 2023.

HOANG, A. T.; TABATABAEI, M.; AGHBASHLO, M. et al. Rice bran oil-based biodiesel as a promising renewable fuel alternative to petrodiesel: A review. **Renewable and Sustainable Energy Reviews**, v. 135, p. 110204, 2021.

HOSSEINIFAR, P.; SHAHVERDI, H. A predictive method for constructing the distillation curve of petroleum fluids using their physical bulk properties. **Journal of Petroleum Science and Engineering**, v. 200, p. 108403, 2021.

HUANG, S. H.; RADOSZ, M. Equation of State for Small, Large, Polydisperse, and Associating Molecules. **Industrial & Engineering Chemistry Research**, v. 29, n. 11, p. 2284–2294, 1990.

ILIĆ PAJIĆ, J.; IVANIŠ, G.; RADOVIĆ, I. *et al.* Experimental densities and derived thermodynamic properties of pure p-cymene, α-pinene, limonene and citral under high pressure conditions. **The Journal of Chemical Thermodynamics**, v. 144, p. 106065, 2020.

IMTENAN, S.; MASJUKI, H. H.; VARMAN, M.; FATTAH, I. M. R. Evaluation of n-butanol as an oxygenated additive to improve combustion-emission-performance characteristics of a diesel engine fuelled with a diesel-calophyllum inophyllum biodiesel blend. **RSC Advances**, v. 5, n. 22, p. 17160-17170, 2015.

INTERNATIONAL ORGANIZATION FOR STANDARDIZATION. *Guide to the expression of uncertainty in measurement*. 1. ed. Geneva: ISO, 2008.

ISMAIL, H. M. et al. Development of thermophysical and transport properties for the CFD simulations of in-cylinder biodiesel spray combustion. **Energy & Fuels**, v. 26, n. 8, p. 4857-4870, 2012.

IVANIŠ, G. R.; RADOVIĆ, I. R.; VELJKOVIĆ, V. B.; KIJEVČANIN, M. L. Biodiesel density and derived thermodynamic properties at high pressures and moderate temperatures. **Fuel**, v. 165, p. 244-251, 2016a.

IVANIŠ, G. R.; RADOVIĆ, I. R.; VELJKOVIĆ, V. B.; KIJEVČANIN, M. L. Thermodynamic properties of biodiesel and petro-diesel blends at high pressures and temperatures: experimental and modeling. **Fuel**, v. 184, p. 277-288, 2016b.

JCGM. **Evaluation of measurement data**: guide to the expression of uncertainty in measurement. Paris: BIPM, 2008. Disponível em: http://www.bipm.org. Acesso em: 14 jun. 2025.

JIN, C.; YAO, M.; LIU, H.; LEE, C. F.; JI, J. Progress in the production and application of n-butanol as a biofuel. **Renewable and Sustainable Energy Reviews**, v. 15, n. 8, p. 4080-4106, 2011.

JOBACK, K. G.; REID, R. C. Estimation of pure-component properties from group-contributions. **Chemical Engineering Communications**, v. 57, n. 1-6, p. 233-243, 1987.

KAMIL, M. *et al.* Effect of engine speed on common rail injection system for hydrogen engine. *In*: NATIONAL CONFERENCE IN MECHANICAL ENGINEERING RESEARCH AND POSTGRADUATE STUDENTS, 1., 2010, Kota Bharu. **Anais** [...]. Kota Bharu: Universiti Malaysia Kelantan, 2010. p. 26-27.

KHASANSHIN, T. S. *et al.* Acoustic and thermodynamic properties of the binary liquid mixture n-octane + n-dodecane. **Journal of Engineering Physics and Thermophysics**, v. 87, n. 1, p. 213-224, 2014.

KHASANSHIN, T. S.; SAMUILOV, V. S.; SHCHEMELEV, A. P. The sound velocity in liquid binary mixtures of n-alkanes. **High Temperature**, v. 47, n. 4, p. 527-532, 2009.

KHASANSHIN, T. S.; SAMUILOV, V. S.; SHCHEMELEV, A. P. Thermodynamic properties of liquid binary mixtures of n-alkanes: n-decane + n-hexadecane. **High Temperature**, v. 48, n. 5, p. 665-672, 2010.

KHELLADI, H.; PLANTIER, F.; DARIDON, J. L. A phase comparison technique for sound velocity measurement in strongly dissipative liquids under pressure. **The Journal of the Acoustical Society of America**, v. 128, n. 2, p. 672-678, 2010.

KILLOL, A. *et al.* Experimental studies of a diesel engine run on biodiesel n-butanol blends. **Renewable Energy**, v. 135, p. 687-700, 2019.

KNOTHE, G.; KRAHL, J.; GERPEN, J. V. *The biodiesel handbook*. 2. ed. Urbana: AOCS Press, 2010.

KOLESINSKA, B. *et al.* Butanol synthesis routes for biofuel production: trends and perspectives. **Materials**, v. 12, n. 3, p. 350, 2019.

KOLSKÁ, Z. *et al.* Estimation of the heat capacity of organic liquids as a function of temperature by a three-level group contribution method. **Industrial & Engineering Chemistry Research**, v. 47, n. 6, p. 2075-2085, 2008.

KONTOGEORGIS, G. M. *et al.* Industrial requirements for thermodynamic and transport properties: 2020. **Industrial & Engineering Chemistry Research**, v. 60, n. 13, p. 4987-5013, 2021.

KOOHSHEKAN, O. *et al.* Biodiesel-petrodiesel blends physicochemical characterization and economic assessment of designing a plant in Iran. **Journal of Environmental Health and Sustainable Development**, v. 8, n. 1, p. 1897-1914, 2023.

KORTBEEK, P. J. *et al.* Apparatus for sound velocity measurements in gases up to 10 kbar: experimental data for argon. **Review of Scientific Instruments**, v. 56, n. 6, p. 1269-1273, 1985.

KOSYCHOVA, L. *et al.* Experimental Determination of Distillation Curves of Alcohols/Gasoline Blends as Bio-Fuel for SI Engines. **Machines. Technologies. Materials.**, v. 9, n. 8, p. 18-21, 2015.

KURCZYŃSKI, D. *et al.* Determination of the effect of the addition of second-generation biodiesel BBuE to diesel fuel on selected parameters of “B” fuels. **Energies**, v. 16, n. 19, 2023.

KUSZEWSKI, H. *et al.* Investigation of auto-ignition properties of 1-butanol–biodiesel blends under various temperature conditions. **Fuel**, v. 346, p. 128388, 2023.

LAFITTE, T. *et al.* Simultaneous estimation of phase behavior and second-derivative properties using the statistical associating fluid theory with variable range approach. **The Journal of Chemical Physics**, v. 124, n. 2, 2006.

LAGOURETTE, B. *et al.* Densimeter calibration method versus temperature and pressure. **Measurement Science and Technology**, v. 3, n. 8, p. 699-703, 1992.

LAKKIREDDY, V. *et al.* Diesel oxidation catalyst performance with biodiesel formulations. In: **SAE TECHNICAL PAPER SERIES**, 2024. Disponível em: https://www.sae.org/content/2024-01-2711. Acesso em: 25 ago. 2025.

LEE, B. I.; KESLER, M. G. A generalized thermodynamic correlation based on three-parameter corresponding states. **AIChE Journal**, v. 21, n. 3, p. 510-527, 1975.

LEONARDO, R. S.; MURTA VALLE, M. L.; DWECK, J. Thermovolumetric and thermogravimetric analysis of diesel S10: comparison with ASTM D86 standard method. **Journal of Thermal Analysis and Calorimetry**, v. 139, n. 2, p. 1507-1514, 2020.

LIANG, X. *et al.* Approach to improve speed of sound calculation within PC-SAFT framework. **Industrial & Engineering Chemistry Research**, v. 51, n. 45, p. 14903-14914, 2012.

LIU, X. *et al.* Experimental and correlational study of isobaric molar heat capacities of fatty acid esters: ethyl nonanoate and ethyl dodecanoate. **Fluid Phase Equilibria**, v. 479, p. 47-51, 2019.

LIU, X. *et al.* Heat capacities of fatty acid methyl esters from 300 K to 380 K and up to 4.25 MPa. **Fuel**, v. 157, p. 240-244, 2015.

LIU, X. *et al.* Isobaric heat capacities of ethyl heptanoate and ethyl cinnamate at pressures up to 16.3 MPa. **The Journal of Chemical Thermodynamics**, v. 93, p. 70-74, 2016.

LIU, X. *et al.* Isobaric molar heat capacities of binary mixtures containing methyl caprate and methyl laurate at pressures up to 16.2 MPa. **Thermochimica Acta**, v. 651, p. 43-46, 2017.

LIU, Y. et al. A study of effects of volatility on butanol-biodiesel-diesel spray and combustion. Warrendale: **SAE International**, 2011. (SAE Technical Paper 2011-01-1928).

LLOVELL, F.; VEGA, L. F. Prediction of thermodynamic derivative properties of pure fluids through the soft-SAFT equation of state. **The Journal of Physical Chemistry B**, v. 110, n. 23, p. 11427-11437, 2006.

LOVESTEAD, T. M.; WINDOM, B. C.; BRUNO, T. J. Investigating the unique properties of cuphea-derived biodiesel fuel with the advanced distillation curve method. **Energy & Fuels**, v. 24, n. 6, p. 3665-3675, 2010.

MALIK, S. *et al.* Densities and excess molar volumes of mixtures containing diesel, biodiesel and alkanols at temperatures from 288.15 to 313.15 K. **Chinese Journal of Chemical Engineering**, v. 34, p. 198-207, 2021.

MANSIR, N. *et al.* Modified waste egg shell derived bifunctional catalyst for biodiesel production from high FFA waste cooking oil: a review. **Renewable and Sustainable Energy Reviews**, v. 82, p. 3645-3655, 2018.

MAO, Y. *et al.* The thermodynamic properties of non-associating and associating fluids: a systematic evaluation of SAFT-type equations of state. **International Journal of Thermophysics**, v. 44, n. 3, p. 32, 2023.

MARCZAK, W. Water as a standard in the measurements of speed of sound in liquids. **The Journal of the Acoustical Society of America**, v. 102, n. 5, p. 2776-2779, 1997.

MCCORMICK, R. L. *et al.* Properties that potentially limit high-level blends of biomass-based diesel fuel. **Energy & Fuels**, v. 38, n. 10, p. 8829-8841, 2024.

MESQUITA, F. M. R. *et al.* Experimental density data and excess molar volumes of coconut biodiesel + n-hexadecane and coconut biodiesel + diesel at different temperatures. **Brazilian Journal of Chemical Engineering**, v. 31, n. 2, p. 543-551, 2014.

MESQUITA, F. M. R. *et al.* Density, excess volumes, and partial volumes of binary mixtures of soybean biodiesel + diesel and soybean biodiesel + n-hexadecane at different temperatures and atmospheric pressure. **Journal of Chemical & Engineering Data**, v. 56, n. 1, p. 153-157, 2011.

MOHAMMADKHANI, R.; PAKNEJAD, A.; ZAREI, H. Thermodynamic properties of amines under high temperature and pressure: experimental results correlating with a new modified Tait-like equation and PC-SAFT. **Industrial & Engineering Chemistry Research**, v. 57, n. 49, p. 16978-16988, 2018.

MOKHTARI, Z.; PAKRAVESH, A.; ZAREI, H. High-pressure densities of 2-(dimethylamino) ethanol and 2-(diethylamino) ethanol: measurement and modeling with new modified Tait and PC-SAFT equations of state. **Fluid Phase Equilibria**, v. 572, 2023.

MOLLENHAUER, K.; SCHREINER, K. History and fundamental principles of the diesel engine. *In:* **Handbook of diesel engines**. Berlin: Springer, 2010. p. 3-30.

MORADI, G. R.; KARAMI, B.; MOHADESI, M. Densities and kinematic viscosities in biodiesel–diesel blends at various temperatures. **Journal of Chemical & Engineering Data**, v. 58, n. 1, p. 99-105, 2013.

MORÉ, J. J. The Levenberg-Marquardt algorithm: implementation and theory. *In:* **Numerical analysis**: proceedings of the biennial conference held at Dundee, 1977. Berlin: Springer, 2006. p. 105-116.

MUÑOZ RUJAS, N. **Investigación sobre propiedades de nuevos fluidos industriales de bajo impacto ambiental como sustitutivos de gases fluorados para reducción del cambio climático**. 2018. Tese (Doutorado em Ingeniería Electromecánica) – Universidad de Burgos, Burgos, 2018.

MURINGER, M. J. P.; TRAPPENIERS, N. J.; BISWAS, S. N. The effect of pressure on the sound velocity and density of toluene and n-heptane up to 2600 bar. **Physics and Chemistry of Liquids**, v. 14, n. 4, p. 273-296, 1985.

MURNAGHAN, F. D. The compressibility of media under extreme pressures. **Journal of the Franklin Institute**, v. 197, n. 1, p. 98, 1924.

NANCARROW, P.; LEWIS, M.; ABOUCHACRA, L. Group contribution methods for estimation of ionic liquid heat capacities: critical evaluation and extension. **Chemical Engineering and Technology**, v. 38, n. 4, p. 632-644, 2015.

NARVÁEZ, P. C. *et al.* Determination of some physical and transport properties of palm oil and of its methyl esters. **Latin American Applied Research**, v. 38, p. 1-6, 2008.

NDIAYE, E. H. I. *et al.* Speed of sound, density, and derivative properties of ethyl myristate, methyl myristate, and methyl palmitate under high pressure. **Journal of Chemical & Engineering Data**, v. 58, n. 5, p. 1371-1377, 2013.

NDIAYE, E. H. I. *et al.* Speed of sound, density, and derivative properties of methyl oleate and methyl linoleate under high pressure. **Journal of Chemical & Engineering Data**, v. 58, n. 8, p. 2345-2354, 2013.

NDIAYE, E. I. Caractérisation thermophysique des biodiesels: vitesse du son, densité, compressibilité. 2012. Tese (Doutorado em Génie des Procédés) — Université de Pau et des Pays de l'Adour, Pau, 2012.

NDIAYE, E. H. I.; NASRI, D.; DARIDON, J. L. Speed of sound, density, and derivative properties of fatty acid methyl and ethyl esters under high pressure: methyl caprate and ethyl caprate. **Journal of Chemical & Engineering Data**, v. 57, n. 10, p. 2667-2676, 2012.

NICULESCU, R.; NĂSTASE, M.; CLENCI, A. On the determination of the distillation curve of fatty acid methyl esters by gas chromatography. **Fuel**, v. 314, 2022.

NOGUEIRA, C. A. *et al.* Densities and viscosities of binary mixtures of babassu biodiesel + cotton seed or soybean biodiesel at different temperatures. **Journal of Chemical & Engineering Data**, v. 55, n. 11, p. 5305-5310, 2010.

NOGUEIRA, C. A. *et al.* Density and viscosity of binary systems containing (linseed or corn) oil, (linseed or corn) biodiesel and diesel. **Journal of Chemical & Engineering Data**, v. 60, n. 11, p. 3120-3131, 2015.

NOGUEIRA, C. A. *et al.* Viscosities and densities of ternary blends of diesel + soybean biodiesel + soybean oil. **Journal of Chemical & Engineering Data**, v. 57, n. 11, p. 3233-3241, 2012.

ONKEN, U. *et al.* Estimation of physical properties. *In:* **Ullmann's encyclopedia of industrial chemistry**. Weinheim: Wiley, 2008.

PAPADAKIS, E. P. Ultrasonic attenuation caused by scattering in polycrystalline metals. **The Journal of the Acoustical Society of America**, v. 37, n. 4, p. 711–717, 1965.

PAPADOPOULOS, C. E.; YEUNG, H. Uncertainty estimation and Monte Carlo simulation method. **Flow Measurement and Instrumentation**, v. 12, n. 4, p. 291–298, 2001.

PARENTE, R. C. *et al.* Excess volumes and deviations of viscosities of binary blends of sunflower biodiesel + diesel and fish oil biodiesel + diesel at various temperatures. **Journal of Chemical & Engineering Data**, v. 56, n. 7, p. 3061–3067, 2011.

PAULY, J.; DARIDON, J.-L.; COUTINHO, J. A. P. Heat capacity measurements of pure fatty acid methyl esters and biodiesels from 250 to 390 K. **Fuel**, v. 137, p. 21–27, 2014.

PAYRI, R. *et al.* The effect of temperature and pressure on thermodynamic properties of diesel and biodiesel fuels. **Fuel**, v. 90, n. 3, p. 1172–1180, 2011.

PENG, D.-Y.; ROBINSON, D. B. A new two-constant equation of state. **Industrial & Engineering Chemistry Fundamentals**, v. 15, n. 1, p. 59–64, 1976

PLANTIER, F.; DARIDON, J. L.; LAGOURETTE, B. Nonlinear parameter (B/A) measurements in methanol, 1-butanol and 1-octanol for different pressures and temperatures. **Journal of Physics D: Applied Physics**, v. 35, n. 10, p. 315, 2002.

PLANTIER, F. *et al.* Isentropic thermophysical properties of pure n-paraffins as a function of temperature and chain length. **High Temperatures-High Pressures**, v. 32, n. 3, p. 305–310, 2000.

PRATAS, M. J. *et al.* Biodiesel density: experimental measurements and prediction models. **Energy & Fuels**, v. 25, n. 5, p. 2333–2340, 2011.

PRAUSNITZ, J. M.; LICHTENTHALER, R. N.; AZEVEDO, E. G. Molecular thermodynamics of fluid-phase equilibria. 3. ed. Upper Saddle River: Prentice Hall, 1999.

PRIETO, N. M. C. T. *et al.* Correlation and prediction of biodiesel density for extended ranges of temperature and pressure. **Fuel**, v. 141, p. 23–38, 2015.

REID, R.; PRAUSNITZ, J. M.; POLING, B. E. *The properties of gases and liquids*. 4. ed. New York: McGraw-Hill, 1987.

REID, R. C.; SHERWOOD, T. K.; STREET, Robert E. The properties of gases and liquids. **Physics Today**, v. 12, n. 4, p. 38–40, 1959.

RIAZI, M. R.; DAUBERT, T. E. Characterization parameters for petroleum fractions. **Industrial & Engineering Chemistry Research**, v. 26, n. 4, p. 755–759, 1987.

RŮŽIČKA, V.; DOMALSKI, E. S. Estimation of the heat capacities of organic liquids as a function of temperature using group additivity. I. Hydrocarbon compounds. **Journal of Physical and Chemical Reference Data**, v. 22, n. 3, p. 597–618, 1993.

RŮŽIČKA, V.; DOMALSKI, E. S. Estimation of the heat capacities of organic liquids as a function of temperature using group additivity. II. Compounds of carbon, hydrogen, halogens, nitrogen, oxygen, and sulfur. **Journal of Physical and Chemical Reference Data**, v. 22, n. 3, p. 619–657, 1993.

RAJAGOPALAN, G.; KRISHNAN, C. Production of cellulosic butanol by clostridial fermentation: a superior alternative renewable liquid fuel. In: **Biofuels and bioenergy**. Amsterdam: Elsevier, 2022. p. 263–289.

RAJENDRAN, S. A comparative study of performance and emission characteristics of neat biodiesel operated diesel engine: a review. **Journal of Thermal Analysis and Calorimetry**, v. 146, n. 3, p. 1015–1025, 2021.

RAKOPOULOS, D. C. et al. Effects of butanol–diesel fuel blends on the performance and emissions of a high-speed DI diesel engine. **Energy Conversion and Management**, v. 51, n. 10, p. 1989–1997, 2010.

RASMUSSEN, E. G.; WILTHAN, B. Speed of sound for understanding metals in extreme environments. **Applied Physics Reviews**, v. 11, n. 4, 2024.

RAZZAQ, L. *et al.* Modeling viscosity and density of ethanol-diesel-biodiesel ternary blends for sustainable environment. **Sustainability**, v. 12, n. 12, p. 5186, 2020.

SALINA, F. H.; DE ALMEIDA, I. A.; BITTENCOURT, F. R. RenovaBio opportunities and biofuels outlook in Brazil. *In:* **Renewable energy and sustainable buildings**: selected papers from the World Renewable Energy Congress WREC 2018. Cham: Springer International Publishing, 2019. p. 391-399.

TAMILSELVAN, P.; NALLUSAMY, N.; RAJKUMAR, S. A comprehensive review on performance, combustion and emission characteristics of biodiesel fuelled diesel engines. **Renewable and Sustainable Energy Reviews**, v. 79, p. 1134–1159, 2017.

TAT, M. E.; VAN GERPEN, J. H. Speed of sound and isentropic bulk modulus of alkyl monoesters at elevated temperatures and pressures. **Journal of the American Oil Chemists' Society**, v. 80, n. 12, p. 1249–1256, 2003.

TAT, M. E.; VAN GERPEN, J. H. The specific gravity of biodiesel and its blends with diesel fuel. **Journal of the American Oil Chemists' Society**, v. 77, n. 2, p. 115–119, 2000.

TAYLOR, A. M. K. P. Science review of internal combustion engines. **Energy Policy**, v. 36, n. 12, p. 4657–4667, 2008.

THAKKAR, K. *et al.* Combustion investigation of ternary blend mixture of biodiesel/n-butanol/diesel: CI engine performance and emission control. **Renewable and Sustainable Energy Reviews**, v. 137, p. 110468, 2021.

TIBURCIO, R. S.; MACÊDO, T. R.; NETO, A. M. P. Brazilian biofuels policy (RenovaBio): overview and generation of decarbonization credits by biodiesel production facilities. **Energy for Sustainable Development**, v. 77, p. 101334, 2023.

TORÍN-OLLARVES, G. A.; MARTÍN, M. C.; SEGOVIA, J. J. Thermophysical properties of 1,2,4-trimethylbenzene in admixtures with 1-butanol or 2-butanol at high pressures. **The Journal of Chemical Thermodynamics**, v. 111, p. 41–51, 2017.

TORRES-JIMENEZ, E. *et al.* Physical and chemical properties of ethanol-diesel fuel blends. **Fuel**, v. 90, n. 2, p. 795–802, 2011.

ULUSOY, Y. *et al.* Investigation of performance and emission characteristics of waste cooking oil as biodiesel in a diesel engine. **Petroleum Science**, v. 15, n. 2, p. 396–404, 2018.

VALERO, A. M. C. *et al.* Density and volumetric behavior of ternary CO2 + n-decane + cis-decalin (or + trans-decalin) mixtures at high pressure and high temperature. **Journal of Chemical & Engineering Data**, v. 66, n. 4, p. 1684–1693, 2021.

VALERO, A. M. C.; FEITOSA, F. X.; DE SANT'ANA, H. B. Density and volumetric behavior of binary CO2 + n-decane and ternary CO2 + n-decane + naphthalene systems at high pressure and high temperature. **Journal of Chemical & Engineering Data**, v. 65, n. 7, p. 3499–3509, 2020.

VAN DER WAALS, J. D. On the continuity of the gaseous and liquid states. 1873. Tese (Doutorado) – *Universiteit Leiden*, Leiden, 1873.

VAN GERPEN, J. Biodiesel processing and production. **Fuel Processing Technology**, v. 86, n. 10, p. 1097–1107, 2005.

VAN MILTENBURG, J. C.; MICHALIK, R. A.; MEIRELLES, A. J. A. Thermal properties of ethyl undecanoate and ethyl tridecanoate by adiabatic calorimetry. **Journal of Chemical & Engineering Data**, v. 50, n. 4, p. 1348–1353, 2005.

VARGAS-IBÁÑEZ, L. T. *et al.* Physical properties of biodiesel blended with hexanol isomers at different temperatures: surface tension, density, viscosity, and refractive index. **Journal of Chemical & Engineering Data**, v. 65, n. 7, p. 3706–3727, 2020.

VARGAS-IBÁÑEZ, L. T. *et al.* Thermophysical and excess properties of diesel + biodiesel with octanol isomers at different temperatures. **Journal of Molecular Liquids**, v. 363, p. 119779, 2022.

VENY, H. *et al.* Density of jatropha curcas seed oil and its methyl esters: measurement and estimations. **International Journal of Thermophysics**, v. 30, n. 2, p. 529–541, 2009.

VERA-ROZO, J. R. *et al.* Cetane index prediction based on biodiesel distillation curve. **Fuel**, v. 321, p. 124063, 2022.

VERMA, P.; SHARMA, M. P. Comparative analysis of effect of methanol and ethanol on Karanja biodiesel production and its optimisation. **Fuel**, v. 180, p. 164–174, 2016.

VIEIRA, B.; NADALETI, W. C.; SARTO, E. The effect of the addition of castor oil to residual soybean oil to obtain biodiesel in Brazil: energy matrix diversification. **Renewable Energy**, v. 165, p. 657–667, 2021.

VILLAZÓN-LEÓN, R.; ÁLVAREZ, V. H. Calculation of liquid Cp of pure compounds using an improved thermodynamic model based on group contributions and artificial neural networks. **Fluid Phase Equilibria**, v. 576, p. 113709, 2023.

WANG, X. *et al.* Viscosity measurement and correlation research of one biodiesel component (methyl octanoate) with five 1-alcohols. **Fuel**, v. 324, p. 124441, 2022.

WANG, X. *et al.* High-pressure liquid densities of fatty acid methyl esters: measurement and prediction with PC-SAFT equation of state. **Fluid Phase Equilibria**, v. 471, p. 8–16, 2018.

WANG, X. *et al*. Development of a reduced n-butanol/biodiesel mechanism for a dual fuel engine. **Fuel**, v. 157, p. 87–96, 2015.

WEBSTER, J. G. *Mechanical variables measurement – solid, fluid, and thermal.* Boca Raton: CRC Press, 2023.

WILHELMSEN, Ø. et al. Thermodynamic modeling with equations of state: present challenges with established methods. **Industrial & Engineering Chemistry Research**, v. 56, n. 13, p. 3503–3515, 2017.

WILSON, W. D. Speed of sound in distilled water as a function of temperature and pressure. **The Journal of the Acoustical Society of America**, v. 31, n. 8, p. 1067–1072, 1959.

WILSON, W.; BRADLEY, D. Speed of sound in four primary alcohols as a function of temperature and pressure. **The Journal of the Acoustical Society of America**, v. 36, n. 2, p. 333–337, 1964.

WIRAWAN, S. S. *et al.* Biodiesel implementation in Indonesia: experiences and future perspectives. **Renewable and Sustainable Energy Reviews**, v. 189, p. 113911, 2024.

WOLBACH, Jeffrey P.; SANDLER, Stanley I. Using molecular orbital calculations to describe the phase behavior of cross-associating mixtures. **Industrial & engineering chemistry research**, v. 37, n. 8, p. 2917-2928, 1998.

WOLBACH, J. P.; SANDLER, S. I. Using molecular orbital calculations to describe the phase behavior of hydrogen-bonding fluids. **Industrial & Engineering Chemistry Research**, v. 36, p. 4041–4051, 1997.

YAMANE, K.; UETA, A.; SHIMAMOTO, Y. Influence of physical and chemical properties of biodiesel fuels on injection, combustion and exhaust emission characteristics in a direct injection compression ignition engine. **International Journal of Engine Research**, v. 2, n. 4, p. 249–261, 2001.

ZÁBRANSKÝ, M. et al. Heat capacity of liquids: critical review and recommended values. Supplement II. **Journal of Physical and Chemical Reference Data**, v. 39, n. 1, p. 3–404, 2010.

ZÁBRANSKÝ, Milan; RŮŽIČKA JR, Vlastimil. Estimation of the heat capacities of organic liquids as a function of temperature using group additivity: an amendment. **Journal of physical and chemical reference data**, v. 33, n. 4, p. 1071-1081, 2004.

ZÁBRANSKÝ, M.; RŮŽIČKA, V. Estimation of the heat capacities of organic liquids as a function of temperature using group additivity: an amendment. **Journal of Physical and Chemical Reference Data**, v. 33, n. 4, p. 1071–1081, 2004.

ZAHARIN, M. S. M. et al. Effects of physicochemical properties of biodiesel fuel blends with alcohol on diesel engine performance and exhaust emissions: a review. **Renewable and Sustainable Energy Reviews**, v. 79, p. 475–493, 2017.

ZAMBRANO, J. *et al.* Viscosities of binary mixtures containing 1-butanol + 2,2,4-trimethylpentane or + 1,2,4-trimethylbenzene at high pressures for the thermophysical characterization of biofuels. **The Journal of Chemical Thermodynamics**, v. 102, p. 140–146, 2016.

ZARIPOV, Z. I.; NAKIPOV, R. R.; MAZANOV, S. V.; GALIULLIN, A. A. Modeling heat capacity of saturated hydrocarbon in liquid phase over a wide range of temperature and pressure. **Journal of Molecular Liquids**, v. 319, p. 114068, 2020.

ŻARSKA, M.; BARTOSZEK, K.; DZIDA, M. High pressure physicochemical properties of biodiesel components derived from coconut oil or babassu oil. **Fuel**, v. 125, p. 144–151, 2014.

ŻARSKA, M.; ZORĘBSKI, M.; DZIDA, M. High pressure thermophysical characteristics of butyl caprate and butyl laurate as fully biorenewable components of biodiesel fuel. **Fuel**, v. 323, p. 124274, 2022.

ZHENG, Z.; WANG, X.; LIU, H.; CHENG, C.; YAO, M. Experimental study on the combustion and emissions fueling biodiesel/n-butanol, biodiesel/ethanol and biodiesel/2,5-dimethylfuran on a diesel engine. **Energy**, v. 115, p. 539–549, 2016.

ZVIRIN, Y.; GUTMAN, M.; TARTAKOVSKY, L. *Fuel effects on emissions*. *In: Internal combustion engines*. [S. l.]: Woodhead Publishing Limited, 1998.

APPENDIX A1 – ESTIMATING EXPERIMENTAL UNCERTAINTY IN DENSITY AND SOUND VELOCITY MEASUREMENTS AT HIGH PRESSURES

Evaluating and quantifying the uncertainties associated with experimental measurements are essential steps in ensuring the reliability and traceability of the data obtained. In this work, the density and speed of sound of fuel mixtures were experimentally determined over a wide temperature range and at pressures of up to 100 MPa for density and up to 200 MPa for speed of sound. In accordance with the guidelines established by the *Guide to the Expression of Uncertainty in Measurement* (GUM, JCGM 100:2008), all significant sources of uncertainty, both systematic and random, were considered. Based on the relationship presented in Equation (A1), the combined standard uncertainty, $u_c(y)$, was estimated by propagating the individual uncertainties associated with the input variables.

$$u_c^2(y) = \sum_{i=1}^{N} \left(\frac{\partial f}{\partial x_i}\right)^2 u^2(i) \quad \text{(A1-1)}$$

here, $f(x_1, x_2, \ldots, x_N)$ represents the function that relates the variable of interest (such as density or speed of sound) to the directly measured variables x_i. The term $u(i)$ denotes the standard uncertainty associated with the variable x_i, and $\frac{\partial f}{\partial x_i}$ is the sensitivity coefficient of the function with respect to that variable.

The expanded uncertainty U_y was obtained by multiplying the combined standard uncertainty by the coverage factor $k = 2$, corresponding to a confidence level of approximately 95%.

$$U_y = k \cdot u_c(y) \quad \text{(A1-2)}$$

-Uncertainties Associated with the Equipment Used

The experimental uncertainties were assessed based on the technical and operational characteristics of the two main instruments used in this study: the vibrating-tube densimeter, employed for density measurements, and the transit-time-based system, used to measure the speed of sound. Detailed specifications of this equipment are provided in Chapter 2 of this thesis. The individual contributions of each variable associated with the instruments were quantified and propagated according to the methodology presented here. Tables A.1 and A.2 below present the corresponding uncertainty budgets for both properties under a representative experimental condition.

-Uncertainty Budget Tables

Tables A.1 and A.2 present the representative uncertainty budgets for density and speed of sound measurements, respectively, under typical experimental conditions. For each source of uncertainty, the estimated standard deviation, relative sensitivity, and individual contribution to the combined uncertainty are indicated.

Table A.1 Uncertainty budget for density measurement (typical condition: T = 293.15 – 473.15 K, P =0.1 – 100 MPa)

Source of uncertainty $u(i)$	Values	Units

Temperature $u(T)$	0.02	K
Pressure $u(P)$	0.03	MPa
Repeatability u_ρ	0.01	$\mathrm{kg \cdot m^{-3}}$
Composition $u(x)$	0.02	%

Table A.2 Uncertainty budget for measuring the speed of sound (typical condition: T = 293.15 – 473.15 K, P =0.1 – 200 MPa)

Source of uncertainty $u(i)$	Values	Units
Temperature $u(T)$	0.1	K
Pressure $u(P)$ range P [0.1 – 100MPa]	0.02	%
Pressure $u(P)$ range P [100 – 200MPa]	0.05	%
$U_{r,calcul}\ (c) = \ [u_r(\Delta t)]^2 + [u_r(\Delta L)]^2$	0.03	%
Composition $u(x)$	0.02	%

The uncertainty values obtained for each set of experimental data, considering all evaluated pressure and temperature conditions, are presented in the specific chapters of this thesis that address the density and speed of sound measurements. This approach enables a contextualized analysis of uncertainty at each experimental stage and reinforces the traceability of the results discussed throughout the work.

- Validation of the High-Pressure Densimeter

Results of the calibration validation using pure toluene are detailed in Table A.3. Experimental density measurements (ρ) were compared with reference values from the NIST database (ρNIST), and the respective average deviations (AD%) were calculated to assess the accuracy of the apparatus under different temperature and pressure conditions.

Table A.3 Density measurements for pure toluene (ρ) compared with reference data from NIST (ρNIST) and respective absolute deviations (AD%). Measurements were performed at temperatures ranging from 303.15 K to 468.15 K and pressures up to 130 MPa.

P (MPa)	T (K)	ρ (kg/m³)	ρNIST (kg/m³)	AD (%)	P (MPa)	T (K)	ρ (kg/m³)	ρNIST (kg/m³)	AD (%)
1.1	303.15	858.32	858.39	0.008	2.5	348.15	817.49	817.34	0.020
2.1	303.15	859.13	859.19	0.007	5.1	348.15	820.1	820.05	0.007
3.1	303.15	859.90	859.99	0.011	7.6	348.15	822.68	822.59	0.011
4.1	303.15	860.69	860.79	0.012	10.1	348.15	825.11	825.05	0.008
5.1	303.15	861.47	861.57	0.012	20.0	348.15	834.26	834.17	0.011
7.1	303.15	863.03	863.12	0.010	25.0	348.15	838.45	838.45	0.001
8.1	303.15	863.75	863.89	0.016	30.0	348.15	842.46	842.55	0.010
9.1	303.15	864.52	864.65	0.015	40.0	348.15	850.2	850.24	0.005
20	303.15	872.36	872.55	0.022	49.3	348.15	856.79	856.9	0.012

33	303.15	880.98	881.18	0.023	60.0	348.15	863.96	864.06	0.011
47	303.15	889.45	889.71	0.029	75.0	348.15	873.22	873.32	0.011
55	303.15	893.99	894.28	0.032	78.8	348.15	875.47	875.55	0.008
78	303.15	906.08	906.42	0.038	100.0	348.15	887.09	887.2	0.012
90	303.15	911.88	912.25	0.041	122.5	348.15	893.39	893.54	0.017
130	303.15	929.23	929.75	0.056	125.0	348.15	899.39	899.55	0.017
P (MPa)	T (K)	ρ (kg/m³)	ρNIST (kg/m³)	AD (%)	P (MPa)	T (K)	ρ (kg/m³)	ρNIST (kg/m³)	AD (%)
3.0	373.15	793.02	793.67	0.082	3.0	428.15	735.86	736.72	0.117
11.5	373.15	803.05	803.68	0.078	11.5	428.15	750.68	751.59	0.121
30.0	373.15	821.49	822.15	0.080	30.0	428.15	775.88	776.85	0.125
47.5	373.15	836.09	836.79	0.084	47.5	428.15	794.59	795.59	0.126
55.5	373.15	842.11	842.82	0.084	55.5	428.15	802.16	803.09	0.116
68.0	373.15	850.79	851.58	0.093	68.0	428.15	812.91	813.79	0.108
72.0	373.15	853.47	854.24	0.090	72.0	428.15	816.1	817	0.110
89.5	373.15	864.45	864.15	0.035	89.5	428.15	829.2	829.99	0.095
100.0	373.15	870.48	871.21	0.084	100.0	428.15	836.3	837.11	0.097
P (MPa)	T (K)	ρ (kg/m³)	ρNIST (kg/m³)	AD (%)	P (MPa)	T (K)	ρ (kg/m³)	ρNIST (kg/m³)	AD (%)
3.0	443.15	719.14	719.87	0.101	3.0	468.15	689.14	689.89	0.109
11.5	443.15	735.97	736.67	0.095	11.5	468.15	710.1	710.91	0.114
30.0	443.15	763.61	764.33	0.094	30.0	468.15	742.56	743.28	0.097
47.5	443.15	783.53	784.4	0.111	47.5	468.15	765.13	765.77	0.084
55.5	443.15	791.54	792.35	0.102	55.5	468.15	773.91	774.53	0.080
68.0	443.15	802.59	803.64	0.131	68.0	468.15	786.08	786.86	0.099
72.0	443.15	806.31	807.01	0.087	72.0	468.15	789.82	790.51	0.087
89.5	443.15	820.04	820.62	0.071	89.5	468.15	804.68	805.19	0.063
100.0	443.15	827.52	828.04	0.063	100.0	468.15	812.75	813.14	0.048

APPENDIX A2 – ASSOCIATIVE TERM OF THE COMPRESSIBILITY FACTOR OF THE PC-SAFT EQUATION OF STATE

The associative contribution for the compressibility factor is expressed inPC-SAFT as follows:

$$\boldsymbol{Z^{assoc}} = \sum_i \boldsymbol{X_i} \frac{\boldsymbol{\mu_i^{assoc}}}{\boldsymbol{RT}} - \frac{\boldsymbol{a^{assoc}}}{\boldsymbol{RT}} \tag{A2.1}$$

Corresponding to the associative part of the Helmholtz energy:

$$\frac{\boldsymbol{a^{assoc}}}{\boldsymbol{RT}} = \mathbf{ln}(\boldsymbol{X^A}) - \frac{\boldsymbol{X^A}}{\mathbf{2}} + \mathbf{ln}(\boldsymbol{X^B}) - \frac{\boldsymbol{X^B}}{\mathbf{2}} + \mathbf{1} \tag{A2-2}$$

In this work, the above expressions are used considering two association sites (A and B), but only for the butanol molecules, which are known to form hydrogen bonds. The biodiesel components were treated as non-associative and thus do not contribute to the associative term. Here, $\boldsymbol{X^A}$ is the fraction of molecules not bonded at the association site A. It can be calculated by:

$$\boldsymbol{X^A = \left[1 + N_{AV} \sum_{B_j} \rho X^B \Delta^{AB}\right]^{-1}} \quad \text{(A2-3)}$$

where $\boldsymbol{\Delta^{AB}}$ is the strength of association between sites A and B corresponding to:

$$\boldsymbol{\Delta^{AB} = \sigma_{ij}^3 g_{ij}^{HS}(d_{ij}) \kappa^{A_i B_j} \left[exp\left(\frac{\varepsilon^{A_i B_j}}{kT} - 1\right)\right]} \quad \text{(A2-4)}$$

The summation $\sum_{B_j}$ indicates that the summation is carried out over the association sites of molecule $\boldsymbol{j}$. The chemical potential associated with the association contribution $\boldsymbol{\mu_i^{assoc}}$ is expressed in the following form, as developed by Chapman et al Chapman et al. (1990b):

$$\frac{\mu_i^{assoc}}{RT} = \sum_{A_i}\left[\ln(X^{A_i}) - \frac{X^{A_i}}{2}\right] + \frac{1}{2}M_i + \sum_j \rho_j \sum_{A_j}\left[\left(\frac{\partial X^{A_j}}{\partial \rho_i}\right)_{T,\rho_{j\neq i}}\left[\frac{1}{X^{A_j}} - \frac{1}{2}\right]\right] \quad \text{(A2-5)}$$

where X_i is the mole fraction of component i, X^{A_i} is the mole fraction of component i not bound in site A, M_i is the number of association sites in component i and ρ_j is the molar density of component j ($\rho_j = X_j\rho$). In this expression, the derivative $((\partial X^{A_j})/(\partial \rho_i))_{T,\rho_{j\neq i}}$ is further expanded as:

$$\left(\frac{\partial X^{A_j}}{\partial \rho_i}\right)_{T,\rho_{j\neq i}} = -\left(X^{A_j}\right)^2\left[N_{AV}\sum_{B_i} X^{B_i}\Delta^{A_jB_i} + \sum_k \sum_{B_k} N_{AV}\rho_k\left[\Delta^{A_jB_k}\left(\frac{\partial X^{B_k}}{\partial \rho_i}\right)_{T,\rho_{j\neq i}} + X^{B_k}\left(\frac{\partial \Delta^{A_jB_k}}{\partial \rho_i}\right)_{T,\rho_{j\neq i}}\right]\right] \quad \text{(A2-7)}$$

where$\Delta^{A_jB_k}$ is the interaction force between the A site of molecule j and the B site of molecule k. The subscripts i, j and k are only used to differentiate molecules. Since the association scheme was approximated using the 2B model (two associating sites per molecule), it is

assumed that $X^{Ai} = X^{Bi}$ for each molecule i, i.e., the fraction of non-bonded sites is the same for both association sites within the same molecule.

The derivative of the interaction force is calculated as:

$$\left(\frac{\partial \Delta^{A_j B_k}}{\partial \rho_i}\right)_{T,\rho_{j\neq i}} = \sigma_{jk}^3 \left[\left(\frac{\partial g_{jk}^{HS}(d_{jk})}{\partial \rho_i}\right)_{T,\rho_{j\neq i}}\right] \kappa^{A_j B_k} \left[exp\left(\frac{\varepsilon^{A_j B_k}}{kT} - 1\right)\right] \quad \text{(A2-8)}$$

finally,

$$\left(\frac{\partial g_{jk}^{HS}(d_{jk})}{\partial \rho_i}\right)_{T,\rho_{j\neq i}} = \frac{\pi N_{AV}}{6} m_i \left[\frac{d_i^3}{(1-\zeta_3)^2} + 3\frac{d_j d_k}{d_j + d_k}\left[\frac{d_i^2}{(1-\zeta_3)^2} + 2\frac{d_i^3 \zeta_2}{(1-\zeta_3)^3}\right] + 2\left(\frac{d_j d_k}{d_j + d_k}\right)^2 \left[\frac{2d_i^2 \zeta_2}{(1-\zeta_3)^3} + 3\frac{d_i^3 (\zeta_2)^2}{(1-\zeta_3)^4}\right]\right] \quad \text{(A2-9)}$$

Where, m_i is the chain length parameter and d is the temperature-dependent segment diameter. All the parameters are discussed in more detail throughout the text. This part of the work was based on the work of Baird et al (BAIRD et al., 2019).

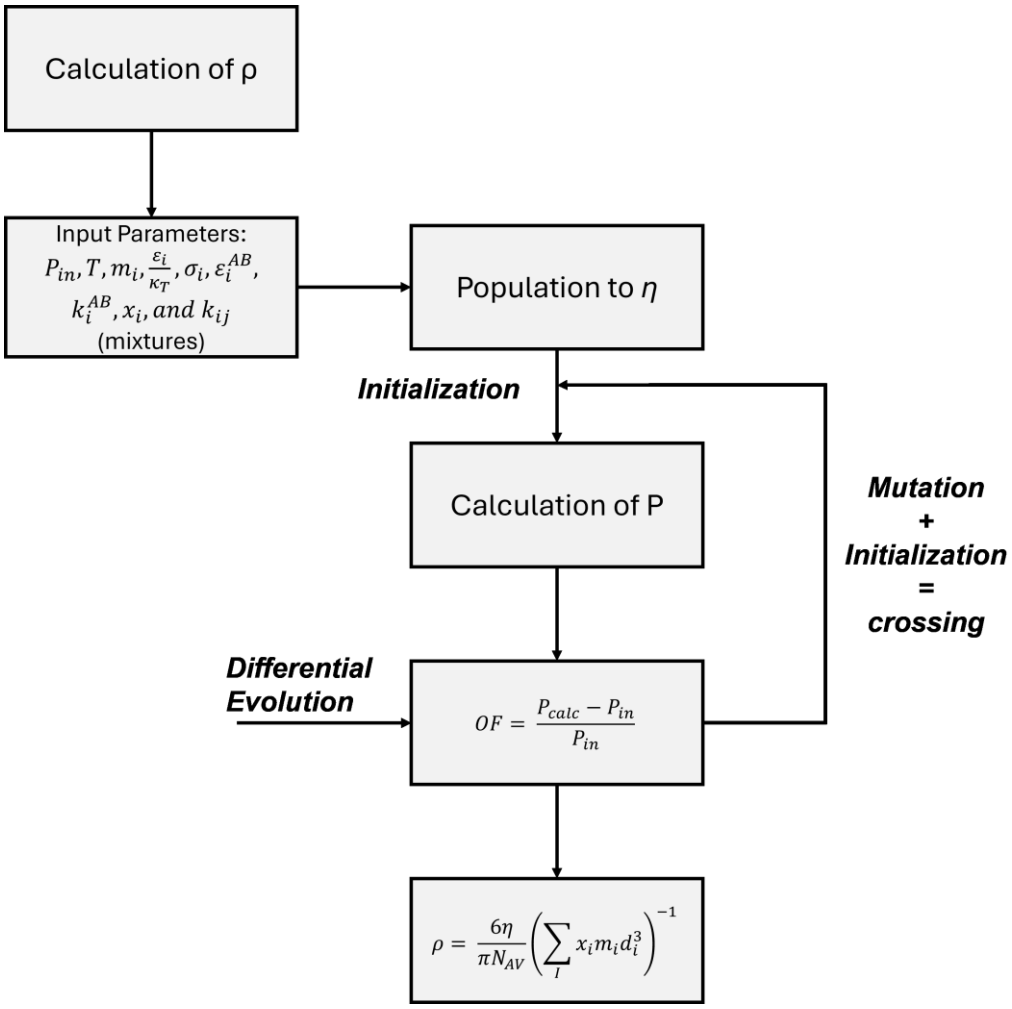

Figure A2.1 Flowchart of the iterative procedure for calculating molar density using the PC-SAFT equation of state, applied to pure compounds and mixtures, with the Differential Evolution solver.

APPENDIX B – COMPLEMENTARY MATERIAL TO CHAPTER 3

This document provides complementary information to chapter 3 of this thesis, with a detailed description of its contents described below:

Table B1 – B2. Calculated Isentropic compressibility (κ_s) data and calculated Acoustic impedance (Z) data for coconut, sucupira and canola biodiesels as a function of pressure (0.1-200 MPa) and temperature (293.15-373.15 K).

Figure B1 – B3. Graphs of the properties studied (ρ, c, κ_s and Z) for coconut, sucupira, and canola biodiesel. The (●) indicate data at 313 K, while the (▲) represent 353 K.

Table B3. PC-SAFT parameters obtained in this work.

Table B1. Calculated Isentropic compressibility (κ_s) data (GPa^{-1}) for coconut, sucupira and canola biodiesels as a function of pressure (0.1-200 MPa) and temperature (293.15-373.15 K)

P/MPa	T/K	$\kappa s/Gpa^{-1}$	T/K	$\kappa s/Gpa^{-1}$	T/K	$\kappa s/Gpa^{-1}$	T/K	$\kappa s/Gpa^{-1}$	T/K	$\kappa s/Gpa^{-1}$
coconut biodiesel										
0.1	293.15	0.62	313.15	0.71	333.15	0.81	353.15	0.93	373.15	-
10	293.15	0.58	313.15	0.65	333.15	0.74	353.15	0.84	373.15	0.95
20	293.15	0.54	313.15	0.61	333.15	0.68	353.15	0.76	373.15	0.85
30	293.15	0.51	313.15	0.56	333.15	0.63	353.15	0.70	373.15	0.77
40	293.15	0.48	313.15	0.53	333.15	0.58	353.15	0.64	373.15	0.71
50	293.15	0.45	313.15	0.50	333.15	0.55	353.15	0.60	373.15	0.66
60	293.15	0.43	313.15	0.47	333.15	0.52	353.15	0.56	373.15	0.61
70	293.15	0.41	313.15	0.45	333.15	0.49	353.15	0.53	373.15	0.58
80	293.15	0.39	313.15	0.43	333.15	0.46	353.15	0.50	373.15	0.54
90	293.15	0.38	313.15	0.41	333.15	0.44	353.15	0.48	373.15	0.51
100	293.15	0.36	313.15	0.39	333.15	0.42	353.15	0.45	373.15	0.49
120	293.15	0.34	313.15	0.36	333.15	0.39	353.15	0.42	373.15	0.44
140	293.15	0.32	313.15	0.34	333.15	0.36	353.15	0.38	373.15	0.41
160	293.15	0.30	313.15	0.32	333.15	0.34	353.15	0.36	373.15	0.38
180	293.15	-	313.15	0.30	333.15	0.32	353.15	0.33	373.15	0.35
200	293.15	-	313.15	0.28	333.15	0.30	353.15	0.31	373.15	0.33
sucupira biodiesel										
0.1	293.15	0.55	313.15	0.62	333.15	0.70	353.15	0.79	373.15	-
10	293.15	0.52	313.15	0.58	333.15	0.65	353.15	0.73	373.15	0.82
20	293.15	0.49	313.15	0.54	333.15	0.60	353.15	0.67	373.15	0.74
30	293.15	0.46	313.15	0.51	333.15	0.56	353.15	0.62	373.15	0.68
40	293.15	0.43	313.15	0.48	333.15	0.53	353.15	0.58	373.15	0.63

50	293.15	0.41	313.15	0.45	333.15	0.50	353.15	0.54	373.15	0.59
60	293.15	0.40	313.15	0.43	333.15	0.47	353.15	0.51	373.15	0.55
70	293.15	0.38	313.15	0.41	333.15	0.45	353.15	0.48	373.15	0.52
80	293.15	0.36	313.15	0.39	333.15	0.43	353.15	0.46	373.15	0.49
90	293.15	0.35	313.15	0.38	333.15	0.41	353.15	0.44	373.15	0.47
100	293.15	0.34	313.15	0.36	333.15	0.39	353.15	0.42	373.15	0.45
120	293.15	0.31	313.15	0.34	333.15	0.36	353.15	0.38	373.15	0.41
140	293.15	0.29	313.15	0.31	333.15	0.34	353.15	0.36	373.15	0.38
160	293.15	0.28	313.15	0.30	333.15	0.31	353.15	0.33	373.15	0.35
180	293.15	-	313.15	0.28	333.15	0.30	353.15	0.31	373.15	0.33
200	293.15	-	313.15	0.27	333.15	0.28	353.15	0.30	373.15	0.31
canola biodiesel										
0.1	293.15	0.57	313.15	0.64	333.15	0.73	353.15	0.82	373.15	0.94
10	293.15	0.53	313.15	0.60	333.15	0.67	353.15	0.75	373.15	0.84
20	293.15	0.50	313.15	0.55	333.15	0.62	353.15	0.69	373.15	0.76
30	293.15	0.47	313.15	0.52	333.15	0.58	353.15	0.63	373.15	0.70
40	293.15	0.45	313.15	0.49	333.15	0.54	353.15	0.59	373.15	0.65
50	293.15	0.42	313.15	0.46	333.15	0.51	353.15	0.55	373.15	0.60
60	293.15	0.40	313.15	0.44	333.15	0.48	353.15	0.52	373.15	0.57
70	293.15	0.39	313.15	0.42	333.15	0.46	353.15	0.49	373.15	0.53
80	293.15	0.37	313.15	0.40	333.15	0.43	353.15	0.47	373.15	0.51
90	293.15	0.36	313.15	0.38	333.15	0.42	353.15	0.45	373.15	0.48
100	293.15	0.34	313.15	0.37	333.15	0.40	353.15	0.43	373.15	0.46
120	293.15	0.32	313.15	0.34	333.15	0.37	353.15	0.39	373.15	0.42
140	293.15	0.30	313.15	0.32	333.15	0.34	353.15	0.36	373.15	0.39
160	293.15	0.28	313.15	0.30	333.15	0.32	353.15	0.34	373.15	0.36
180	293.15	0.27	313.15	0.29	333.15	0.30	353.15	0.32	373.15	0.34
200	293.15	0.25	313.15	0.27	333.15	0.28	353.15	0.30	373.15	0.32

a The maximum combined expanded uncertainties U (level of confidence = 0.95) are $U(\kappa_s) = 0.007\ \kappa_s$.

Table B2. Calculated Acoustic impedance (Z) data ($MPa \cdot m \cdot s^{-1}$) for coconut, sucupira and canola biodiesels as a function of pressure (0.1-200 MPa) and temperature (293.15-373.15 K)

P /MPa	T /K	Z /$MPa \cdot m \cdot s^{-1}$	T /K	Z /$MPa \cdot m \cdot s^{-1}$	T /K	Z /$MPa \cdot m \cdot s^{-1}$	T /K	Z /$MPa \cdot m \cdot s^{-1}$	T /K	Z /$MPa \cdot m \cdot s^{-1}$
coconut biodiesel										
0.1	293.15	1.18	313.15	1.10	333.15	1.02	353.15	0.94	373.15	-
10	293.15	1.23	313.15	1.15	333.15	1.07	353.15	1.00	373.15	0.93
20	293.15	1.28	313.15	1.20	333.15	1.12	353.15	1.05	373.15	0.99
30	293.15	1.32	313.15	1.24	333.15	1.17	353.15	1.10	373.15	1.04
40	293.15	1.37	313.15	1.29	333.15	1.22	353.15	1.15	373.15	1.09
50	293.15	1.41	313.15	1.33	333.15	1.26	353.15	1.20	373.15	1.13
60	293.15	1.45	313.15	1.37	333.15	1.30	353.15	1.24	373.15	1.18

70	293.15	1.49	313.15	1.41	333.15	1.34	353.15	1.28	373.15	1.22
80	293.15	1.52	313.15	1.45	333.15	1.38	353.15	1.32	373.15	1.26
90	293.15	1.56	313.15	1.49	333.15	1.42	353.15	1.36	373.15	1.30
100	293.15	1.59	313.15	1.52	333.15	1.46	353.15	1.40	373.15	1.34
120	293.15	1.66	313.15	1.59	333.15	1.53	353.15	1.47	373.15	1.41
140	293.15	1.72	313.15	1.65	333.15	1.59	353.15	1.53	373.15	1.48
160	293.15	1.78	313.15	1.72	333.15	1.66	353.15	1.60	373.15	1.54
180	293.15	-	313.15	1.77	333.15	1.71	353.15	1.66	373.15	1.61
200	293.15	-	313.15	1.83	333.15	1.77	353.15	1.71	373.15	1.66
sucupira biodiesel										
0.1	293.15	1.28	313.15	1.19	333.15	1.11	353.15	1.04	373.15	-
10	293.15	1.32	313.15	1.24	333.15	1.16	353.15	1.09	373.15	1.02
20	293.15	1.37	313.15	1.29	333.15	1.21	353.15	1.14	373.15	1.07
30	293.15	1.41	313.15	1.33	333.15	1.26	353.15	1.19	373.15	1.12
40	293.15	1.45	313.15	1.38	333.15	1.30	353.15	1.23	373.15	1.17
50	293.15	1.49	313.15	1.42	333.15	1.35	353.15	1.28	373.15	1.22
60	293.15	1.53	313.15	1.46	333.15	1.39	353.15	1.32	373.15	1.26
70	293.15	1.57	313.15	1.50	333.15	1.43	353.15	1.36	373.15	1.30
80	293.15	1.60	313.15	1.53	333.15	1.46	353.15	1.40	373.15	1.34
90	293.15	1.64	313.15	1.57	333.15	1.50	353.15	1.44	373.15	1.38
100	293.15	1.67	313.15	1.60	333.15	1.54	353.15	1.48	373.15	1.42
120	293.15	1.74	313.15	1.67	333.15	1.61	353.15	1.55	373.15	1.49
140	293.15	1.80	313.15	1.73	333.15	1.67	353.15	1.61	373.15	1.56
160	293.15	1.86	313.15	1.79	333.15	1.73	353.15	1.67	373.15	1.62
180	293.15	-	313.15	1.85	333.15	1.79	353.15	1.73	373.15	1.68
200	293.15	-	313.15	1.91	333.15	1.85	353.15	1.79	373.15	1.74
canola biodiesel										
0.1	293.15	1.24	313.15	1.16	333.15	1.08	353.15	1.01	373.15	0.93
10	293.15	1.29	313.15	1.21	333.15	1.13	353.15	1.06	373.15	0.99
20	293.15	1.34	313.15	1.26	333.15	1.18	353.15	1.11	373.15	1.05
30	293.15	1.38	313.15	1.30	333.15	1.23	353.15	1.16	373.15	1.10
40	293.15	1.42	313.15	1.35	333.15	1.27	353.15	1.21	373.15	1.15
50	293.15	1.46	313.15	1.39	333.15	1.32	353.15	1.25	373.15	1.19
60	293.15	1.50	313.15	1.43	333.15	1.36	353.15	1.29	373.15	1.23
70	293.15	1.54	313.15	1.46	333.15	1.40	353.15	1.33	373.15	1.27
80	293.15	1.57	313.15	1.50	333.15	1.43	353.15	1.37	373.15	1.31
90	293.15	1.61	313.15	1.54	333.15	1.47	353.15	1.41	373.15	1.35
100	293.15	1.64	313.15	1.57	333.15	1.51	353.15	1.45	373.15	1.39
120	293.15	1.70	313.15	1.64	333.15	1.57	353.15	1.52	373.15	1.46
140	293.15	1.77	313.15	1.70	333.15	1.64	353.15	1.58	373.15	1.53
160	293.15	1.82	313.15	1.76	333.15	1.70	353.15	1.64	373.15	1.59
180	293.15	1.88	313.15	1.82	333.15	1.76	353.15	1.70	373.15	1.65

200	293.15	1.94	313.15	1.87	333.15	1.81	353.15	1.76	373.15	1.71

a The maximum combined expanded uncertainties U (level of confidence = 0.95) are $U(Z) = 0.004\,Z$.

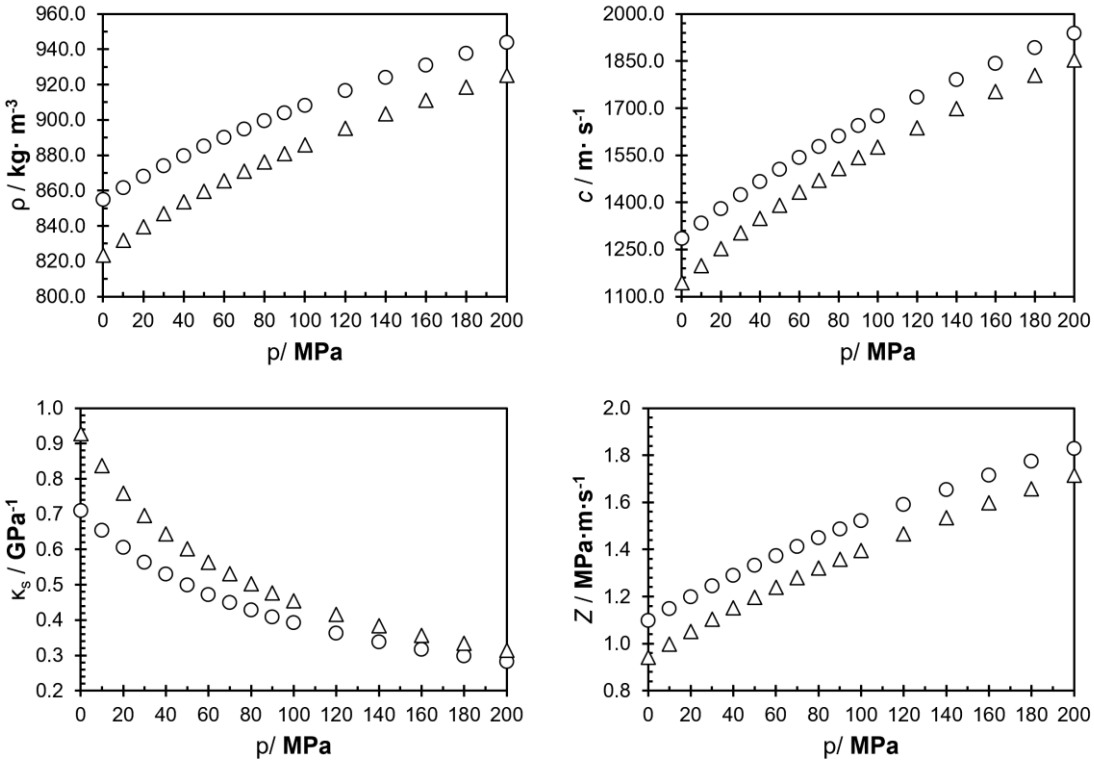

Figure B1. Graphs of the properties studied (ρ, c, κ_s and Z) for coconut biodiesel. The (●) indicate data at 313 K, while the (▲) represent 353 K.

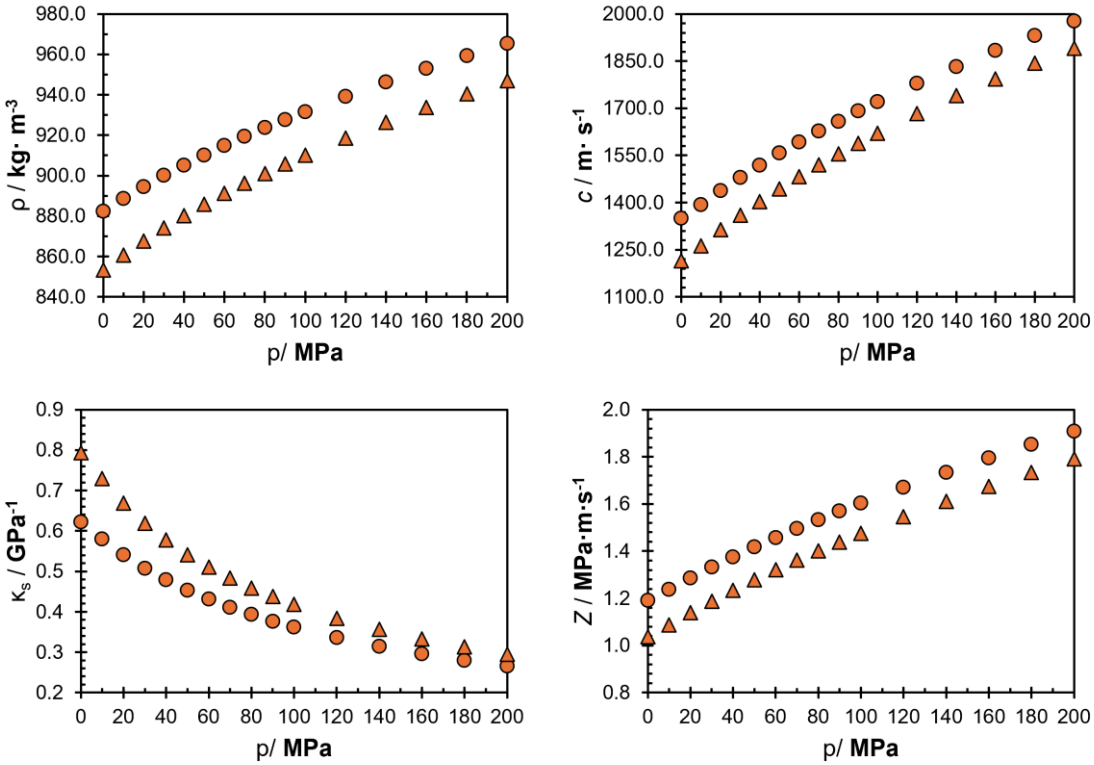

Figure B2. Graphs of the properties studied (ρ, c, κ_s and Z) for sucupira biodiesel. The (●) indicate data at 313 K, while the (▲) represent 353 K.

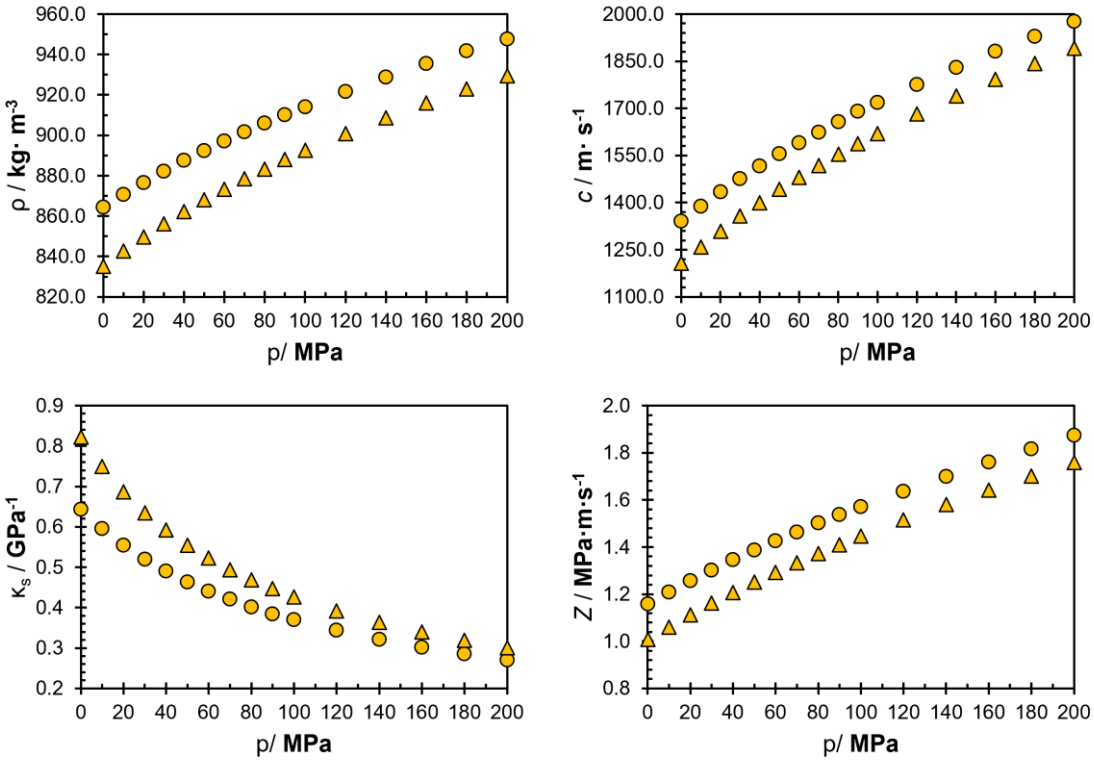

Figure B3. Graphs of the properties studied (ρ, c, κ_s and Z) for Canola biodiesel. The (●) indicate data at 313 K, while the (▲) represent 353 K.

Table B3. PC-SAFT parameters obtained in this work.

PC-SAFT Parameters	$M/g.mol-1$	m_i	σ_i (Å)	ε_i/k (K)
Coconut	222.95	18.982421	2.587297	174.236752
Sucupira	292.12	23.800270	2.607757	175.651154
Canola	295.11	24.052038	2.627133	176.679660

APPENDIX C – COMPLEMENTARY MATERIAL TO CHAPTER 4

This document provides complementary information to Chapter 4 of this thesis, with a detailed description of its contents presented below:

Table C1. Experimental conditions of heat capacity data atmospheric pressure of biodiesels collected from open literature.

Table C2. Properties of pure esters used as a basis for determining critical properties. Includes name of ester, molecular formula, acronym, molar mass (MW), critical temperature (T_c), critical volume (V_c), and acentric factor (ω).

Table C3 – C4. Matrix of heat capacities (C_P) obtained by the model studied for each pure methyl ester (Me) and ethyl ester (Ee) present in biodiesel at various temperatures (T).

Table C5. Biodiesel profiles collected from open literature with FAME and FAEE-type compositions, indicating the molar percentage of methyl (Me) and ethyl (Ee) esters of fatty acids.

Table C1. Experimental conditions of heat capacity data atmospheric pressure of biodiesels collected from open literature.

ref.	year	soucer biodiesel	acronym[a]	T range /K	data type	Uncertainty
FAME						
Narváez et al. (2008)	2008	palm	TG	303 - 343	correlation[1]	Not Specified
Habrioux et al. (2013a)	2013	soybean	S	293 - 393	correlation[2]	Not Specified
Habrioux et al. (2013a)	2013	rapeseed	R	293 - 393	correlation[3]	Not Specified
Pauly et al. (2014)	2014	rapeseed	BR	300 - 390	data	0.5%
Pauly et al. (2014)	2014	soybean	BS	300 - 390	data	0.5%
Pauly et al. (2014)	2014	PL + RS + SB[b]	B1	290 - 390	data	0.5%
Pauly et al. (2014)	2014	PL + RS + SB[b]	B2	300 - 390	data	0.5%
Habrioux et al. (2023)	2023	sunflower	MB-SF	293 - 393	correlation[4]	Not Specified
Habrioux et al. (2023)	2023	PL + RS + SB[b]	MB-PRS	293 - 393	correlation[5]	Not Specified
FAEE						
De Lima et al. (2011)	2011	palm	PL3	325 - 425	correlation[6]	Not Specified
De Lima et al. (2011)	2011	coconut	CCN	325 - 425	correlation[7]	Not Specified
De Lima et al. (2011)	2011	castor	CAN	325 - 425	correlation[8]	Not Specified

[a] Acronym assigned by reference; [b] PL + RS + BB: Mixture between palm biodiesel, rapeseed, and soybean.
[1] $C_P(TG) = 0.0059 \cdot (T) + 1.617$; [2] $C_P(S) = 1.184 \cdot 10^3 + 2.865 \cdot (T) + 1.617$; [3] $C_P(R) = 1.218 \cdot 10^3 + 2.760T \cdot (T)$; [4] $C_P(MB - SF) = 1.438 \cdot 10^3 + 8.289 \cdot 10^{-1} \cdot (T) + 3.260 \cdot 10^{-3} \cdot (T^2)$; [5] $C_P(MB - PRS) = 1.509 \cdot 10^3 + 6.439 \cdot 10^{-1} \cdot (T) + 3.467 \cdot 10^{-3} \cdot (T^2)$; [6] $C_P(PLN) = 1.267LN(T) - 5.567$; [7] $C_P(CCN) = 1.795LN(T) - 8.438$; [8] $C_P(CAN) = 5.637LN(T) - 30.53$; (All correlation equations are in $J\ kg^{-1}K^{-1}$).

Table C2. Properties of Pure Esters used as a basis for Determining Critical Properties. Name of ester, molecular formula, acronym, molar mass (MW), critical temperature (T_c), critical volume (V_c) and acentric factor (ω).

alternative name	molecular formula	acronym	MW_i $[g \cdot mol^{-1}]$	$T_{c,i}$ $[K]$	$V_{c,i}{}^b$ $[cm^3.mol^{-1}]$	$\omega_i{}^a$
FAME						
methyl caprylate	$C_9H_{18}O_2$	MeC8:0	158.24	646.0	567.8	0.564
methyl caprate	$C_{11}H_{22}O_2$	MeC10:0	186.29	675.0	682.0	0.649
methyl laurate	$C_{13}H_{26}O_2$	MeC12:0	214.34	709.0	796.2	0.733
methyl myristate	$C_{15}H_{30}O_2$	MeC14:0	242.40	730.0	910.5	0.815
methyl palmitate	$C_{17}H_{34}O_2$	MeC16:0	270.45	760.0	1024.7	0.895
methyl palmitoleate	$C_{17}H_{32}O_2$	MeC16:1	268.43	764.0[a]	1010.3	0.880
methyl stearate	$C_{19}H_{38}O_2$	MeC18:0	298.50	785.0	1138.9	0.973
methyl oleate	$C_{19}H_{36}O_2$	MeC18:1	296.49	777.0	1124.5	0.959
methyl ricinoleate	$C_{19}H_{36}O_3$	MeC18:1, OH	312.49	813.3[a]	1143.5	1.103
methyl linoleate	$C_{19}H_{34}O_2$	MeC18:2	294.47	778.0	1110.1	0.945
methyl linolenate	$C_{19}H_{32}O_2$	MeC18:3	292.46	779.0	1095.8	0.931
methyl arachidate	$C_{21}H_{42}O_2$	MeC20:0	326.56	802.3[a]	1253.1	1.050
methyl gadoleate	$C_{21}H_{40}O_2$	MeC20:1	324.54	805.4[a]	1238.7	1.036
methyl behenate	$C_{23}H_{46}O_2$	MeC22:0	354.61	820.7[a]	1367.3	1.125
methyl erucate	$C_{23}H_{44}O_2$	MeC22:1	352.59	817.0	1353.0	1.111
methyl lignocerate	$C_{25}H_{50}O_2$	MeC24:0	382.66	837.8[a]	1481.6	1.198
FAEE						
ethyl caprylate	$C_{10}H_{20}O_2$	EeC8:0	172.26	655.0	624.9	0.606
ethyl caprate	$C_{12}H_{24}O_2$	EeC10:0	200.32	687.0	739.1	0.691
ethyl laurate	$C_{14}H_{28}O_2$	EeC12:0	228.37	718.0	853.3	0.774
ethyl myristate	$C_{16}H_{32}O_2$	EeC14:0	256.42	740.0	967.6	0.855
ethyl palmitate	$C_{18}H_{36}O_2$	EeC16:0	284.48	767.0	1081.8	0.934
ethyl palmitoleate	$C_{18}H_{34}O_2$	EeC16:1	282.46	768.2[a]	1067.4	0.920
ethyl stearate	$C_{20}H_{40}O_2$	EeC18:0	312.53	786.6[a]	1196.0	1.012
ethyl oleate	$C_{20}H_{38}O_2$	EeC18:1	310.51	789.7[a]	1181.6	0.998
ethyl ricinoleate	$C_{20}H_{38}O_3$	EeC18:1, OH	326.51	836.4[a]	1200.6	1.140
ethyl linoleate	$C_{20}H_{36}O_2$	EeC18:2	308.50	792.9[a]	1167.2	0.984
ethyl linolenate	$C_{20}H_{34}O_2$	EeC18:3	306.48	796.2[a]	1152.9	0.970
ethyl arachidate	$C_{22}H_{44}O_2$	EeC20:0	340.58	806.7[a]	1310.2	1.088
ethyl gadoleate	$C_{22}H_{42}O_2$	EeC20:1	338.57	809.6[a]	1295.8	1.074
ethyl behenate	$C_{24}H_{48}O_2$	EeC22:0	368.64	825.3[a]	1424.4	1.162
ethyl erucate	$C_{24}H_{46}O_2$	EeC22:1	366.62	828.0[a]	1410.1	1.148
ethyl lignocerate	$C_{26}H_{52}O_2$	EeC24:0	396.69	842.7[a]	1538.7	1.234

[a]Obtained from Evangelista et al. Do Carmo; Evangelista; Fernandes, Fabiano A. N.; et al. (2015b).
[b]Estimated by Group Contribution methods Constantinou; Gani (1994).

Table C3. Matrix of Heat Capacities (C_P) Obtained by the Model Studied for Each Pure Ester Methylic (Me) Present in Biodiesel at Various Temperatures (T).

Acronym ester	C_P values obtained for the esters from the model studied																				
	293.15	298.15	303.15	308.15	313.15	318.15	323.15	328.15	333.15	338.15	343.15	348.15	353.15	358.15	363.15	368.15	373.15	378.15	383.15	388.15	393.15
MeC8:0	313.09	315.18	317.28	319.39	321.52	323.67	325.82	327.99	330.17	332.36	334.56	336.76	338.98	341.20	343.43	345.66	347.90	350.15	352.40	354.66	356.92
MeC10:0	371.25	373.79	376.34	378.91	381.49	384.09	386.70	389.32	391.96	394.60	397.25	399.91	402.57	405.25	407.92	410.60	413.29	415.97	418.67	421.36	424.05
MeC12:0	430.60	433.57	436.55	439.55	442.58	445.61	448.66	451.73	454.80	457.89	460.98	464.08	467.18	470.29	473.41	476.52	479.64	482.76	485.89	489.01	492.13
MeC14:0	489.05	492.47	495.91	499.37	502.85	506.34	509.85	513.38	516.91	520.45	524.01	527.56	531.13	534.70	538.27	541.84	545.42	549.00	552.57	556.15	559.72
MeC16:0	549.05	552.89	556.76	560.65	564.56	568.49	572.44	576.40	580.37	584.36	588.35	592.35	596.35	600.36	604.37	608.38	612.40	616.41	620.42	624.43	628.44
MeC16:1	533.27	537.04	540.84	544.66	548.50	552.35	556.22	560.10	563.99	567.89	571.79	575.70	579.61	583.52	587.44	591.35	595.27	599.18	603.08	606.99	610.88
MeC18:0	608.82	613.10	617.40	621.73	626.08	630.45	634.83	639.24	643.65	648.08	652.52	656.96	661.41	665.87	670.32	674.78	679.24	683.70	688.15	692.60	697.05
MeC18:1	591.30	595.54	599.80	604.09	608.39	612.71	617.05	621.40	625.76	630.12	634.50	638.88	643.26	647.64	652.02	656.40	660.78	665.16	669.53	673.89	678.25
Me-C18:1, OH	630.53	634.47	638.45	642.46	646.50	650.56	654.65	658.77	662.90	667.04	671.20	675.37	679.56	683.75	687.94	692.14	696.35	700.55	704.76	708.96	713.16
MeC18:2	575.11	579.29	583.49	587.71	591.95	596.20	600.47	604.74	609.02	613.31	617.60	621.89	626.19	630.48	634.77	639.06	643.34	647.62	651.89	656.16	660.41
MeC18:3	558.92	563.04	567.19	571.34	575.51	579.70	583.89	588.09	592.29	596.50	600.71	604.92	609.12	613.33	617.53	621.72	625.91	630.09	634.27	638.43	642.58
MeC20:0	667.72	672.44	677.19	681.97	686.78	691.60	696.45	701.31	706.18	711.07	715.96	720.87	725.78	730.69	735.60	740.52	745.43	750.35	755.25	760.16	765.06
MeC20:1	651.89	656.54	661.23	665.94	670.67	675.42	680.18	684.96	689.76	694.56	699.37	704.18	709.00	713.82	718.63	723.45	728.27	733.08	737.88	742.68	747.48
MeC22:0	726.98	732.14	737.33	742.56	747.81	753.09	758.38	763.69	769.02	774.36	779.71	785.07	790.43	795.80	801.17	806.53	811.90	817.27	822.63	827.98	833.33
MeC22:1	710.00	715.11	720.26	725.43	730.63	735.85	741.08	746.33	751.59	756.86	762.14	767.42	772.71	778.00	783.28	788.57	793.85	799.13	804.40	809.66	814.91
MeC24:0	786.17	791.77	797.41	803.08	808.78	814.51	820.26	826.02	831.80	837.60	843.40	849.22	855.03	860.86	866.68	872.50	878.33	884.14	889.96	895.76	901.56

Table C4. Matrix of Heat Capacities (C_P) Obtained by the Model Studied for Each Pure Ester Ethylic (Ee) Present in Biodiesel at Various Temperatures (T).

Acronym ester	C_P values obtained for the esters from the model studied																				
	293.15	298.15	303.15	308.15	313.15	318.15	323.15	328.15	333.15	338.15	343.15	348.15	353.15	358.15	363.15	368.15	373.15	378.15	383.15	388.15	393.15
EeC8:0	341.56	343.88	346.21	348.57	350.93	353.32	355.71	358.12	360.54	362.96	365.40	367.84	370.29	372.75	375.21	377.68	380.15	382.63	385.11	387.59	390.08
EeC10:0	400.33	403.09	405.87	408.67	411.48	414.31	417.15	420.00	422.87	425.74	428.62	431.51	434.40	437.30	440.21	443.11	446.03	448.94	451.85	454.77	457.69
EeC12:0	459.64	462.83	466.05	469.29	472.54	475.81	479.09	482.39	485.70	489.01	492.34	495.67	499.01	502.35	505.70	509.04	512.39	515.75	519.10	522.45	525.80
EeC14:0	518.34	521.98	525.64	529.33	533.04	536.76	540.50	544.26	548.02	551.79	555.58	559.36	563.16	566.96	570.76	574.56	578.36	582.17	585.97	589.77	593.57
EeC16:0	420.11	421.87	423.68	425.52	427.41	429.32	431.27	433.25	435.25	437.28	439.34	441.41	443.51	445.62	447.75	449.90	452.06	454.24	456.42	458.62	460.83
EeC16:1	561.96	565.97	570.01	574.06	578.14	582.23	586.34	590.46	594.59	598.73	602.87	607.02	611.17	615.32	619.47	623.63	627.78	631.92	636.07	640.21	644.34
EeC18:0	637.17	641.69	646.23	650.81	655.40	660.02	664.65	669.30	673.96	678.63	683.31	688.00	692.69	697.39	702.09	706.79	711.49	716.19	720.88	725.57	730.26
EeC18:1	621.33	625.78	630.26	634.76	639.29	643.83	648.38	652.95	657.53	662.12	666.71	671.31	675.91	680.52	685.12	689.72	694.32	698.92	703.51	708.10	712.68
Ee-C18:1, OH	662.67	666.79	670.94	675.14	679.36	683.61	687.89	692.19	696.52	700.85	705.21	709.57	713.95	718.34	722.73	727.13	731.53	735.93	740.34	744.74	749.14
EeC18:2	605.49	609.88	614.29	618.72	623.17	627.64	632.12	636.61	641.10	645.60	650.11	654.62	659.13	663.64	668.15	672.66	677.16	681.65	686.14	690.62	695.09
EeC18:3	589.65	593.98	598.32	602.68	607.06	611.45	615.85	620.26	624.67	629.09	633.51	637.93	642.35	646.77	651.18	655.59	659.99	664.39	668.77	673.15	677.51
EeC20:0	696.57	701.53	706.51	711.53	716.57	721.63	726.71	731.81	736.92	742.05	747.18	752.32	757.46	762.61	767.77	772.92	778.07	783.21	788.36	793.50	798.63
EeC20:1	680.68	685.57	690.49	695.44	700.40	705.39	710.40	715.42	720.45	725.49	730.53	735.58	740.64	745.70	750.75	755.81	760.86	765.91	770.95	775.98	781.01
EeC22:0	755.89	761.29	766.72	772.18	777.66	783.18	788.71	794.26	799.82	805.40	810.98	816.58	822.18	827.78	833.38	838.99	844.59	850.19	855.79	861.37	866.96
EeC22:1	740.02	745.35	750.71	756.10	761.52	766.95	772.41	777.88	783.36	788.85	794.35	799.86	805.37	810.88	816.39	821.90	827.40	832.90	838.39	843.87	849.35
EeC24:0	815.14	820.97	826.85	832.75	838.69	844.65	850.63	856.63	862.65	868.68	874.72	880.77	886.83	892.89	898.94	905.00	911.06	917.11	923.16	929.20	935.23

Table C5. Biodiesel profiles collected in the open literature with FAME and FAEE type profiles, depending on the methyl (Me) and ethyl (Ee) esters of fatty acids in mol%.

biodiesels collected in the open literature (acronyms)[a]													
FAME	BR	BS	B1	B2	MB-SF	MB-PRS	S	R	TG	**FAEE**	CCN	PLN	CAN
MeC8:0	0.00	0.00	0.00	0.00	0.00	0.00	0.00	0.00	0.00	EeC8:0	6.00	0.00	0.00
MeC10:0	0.00	0.00	0.00	0.00	0.00	0.02	0.00	0.02	0.00	EeC10:0	4.97	0.00	0.00
MeC12:0	0.14	0.14	0.14	0.14	0.03	0.19	0.00	0.06	0.00	EeC12:0	45.12	0.40	0.00
MeC14:0	0.12	0.12	0.24	0.12	0.08	0.46	0.08	0.09	2.22	EeC14:0	20.90	1.78	0.00
MeC16:0	5.39	11.47	10.49	7.12	6.95	20.40	11.65	5.70	46.27	EeC16:0	10.52	42.50	1.83
MeC16:1	0.33	0.22	0.22	0.22	0.10	0.15	0.08	0.22	0.00	EeC16:1	0.00	0.00	0.00
MeC18:0	1.50	4.45	2.18	1.98	4.15	3.20	3.86	1.60	4.27	EeC18:0	2.09	4.81	0.94
MeC18:1	60.51	23.42	56.12	57.43	23.68	41.71	22.67	61.81	37.82	EeC18:1	7.96	38.77	3.15
MeC18:1, OH	0.00	0.00	0.00	0.00	0.00	0.00	0.00	0.00	0.00	EeC18:1,OH	0.00	0.00	89.35
MeC18:2	19.40	51.47	20.17	22.73	64.02	27.59	53.22	21.11	9.42	EeC18:2	2.44	10.73	3.91
MeC18:3	10.38	7.58	8.49	8.30	0.12	4.63	7.03	7.01	0.00	EeC18:3	0.00	0.29	0.00
MeC20:0	0.46	0.36	0.45	0.45	0.03	0.40	0.34	0.54	0.00	EeC20:0	0.00	0.70	0.29
MeC20:1	1.19	0.27	1.00	1.00	0.14	0.47	0.21	1.23	0.00	EeC20:1	0.00	0.00	0.00
MeC22:0	0.25	0.33	0.25	0.25	0.63	0.27	0.66	0.29	0.00	EeC22:0	0.00	0.00	0.53
MeC22:1	0.25	0.00	0.17	0.17	0.07	0.11	0.20	0.16	0.00	EeC22:1	0.00	0.00	0.00
MeC24:0	0.08	0.15	0.08	0.08	0.00	0.40	0.00	0.17	0.00	EeC24:0	0.00	0.00	0.00
M $/gmol^{-1}$	294.86	292.52	293.47	294.37	293.82	290.85	292.77	295.07	283.14	-	245.64	297.16	324.66

APPENDIX D – COMPLEMENTARY MATERIAL TO CHAPTER 5

This document provides complementary information to Chapter 5 of this thesis, with a detailed description of its contents presented below:

Table D1: Density data (ρ) collected in the literature for comparison purposes (1-butanol) at temperatures (T) and pressure (P)

Table D2: Densities measured at atmospheric pressure for 1-butanol + biodiesel systems in Anton Paar SVM 3000 equipment.

Table D3. Calculated Isothermal compressibility (κ_T) for Blending 1-Butanol with Linseed Biodiesel, 0, 5, 13, 22, 34, 61, and 100 ϕ_{But}, at temperatures (T) and pressure (P)[a].

Table D4. Calculated Isothermal compressibility (κ_T) for Blending 1-Butanol with Soybean Biodiesel, 0, 5, 13, 22, 34, 61, and 100 ϕ_{But}, at temperatures (T) and pressure (P)[a].

Table D5. Calculated Isobaric thermal expansivities (α_P) for Blending 1-Butanol with Linseed Biodiesel, 0, 5, 13, 22, 34, and 61 ϕ_{But}, at temperatures (T) and pressure (P)[a].

Table D6. Calculated Isobaric thermal expansivities (α_P) for Blending 1-Butanol with Soybean Biodiesel, 0, 5, 13, 22, 34, and 61 ϕ_{But}, at temperatures (T) and pressure (P)[a].

Figure D1: Isothermal compressibility (κ_T) as a function of pressure for 1-butanol and soybean biodiesel blends.

Figure D2. Isothermal compressibility as a function of the volume fraction of 1-butanol (ϕ_{But}) at temperature $T = 293.15\ K$ and pressure, for 1-butanol and soybean biodiesel blends.

Table D1: Density data (ρ) collected in the literature for comparison purposes (1-butanol) at temperatures (T) and pressure (P)

P/MPa	T/K				
	293.15	313.15	333.15	353.15	373.15
			Sarafov et al. 2015		
0.1	809.6	794.4	778.3	760.9	742.4
5	813.1	798.5	782.8	765.8	748.2
10	816.7	802.1	786.7	770.1	753.0
20	823.0	808.7	794.0	778.9	762.6
30	829.0	815.5	801.4	786.8	771.5
40	834.7	821.3	807.7	793.4	778.9
50	840.0	827.3	814.2	800.7	786.7
60	845.0	832.4	819.8	806.6	793.0
70	849.7	837.8	825.5	812.9	799.8
80	854.3	842.6	830.7	818.1	805.5
90	858.6	847.3	835.8	823.9	811.6
100	862.5	851.4	840.2	828.5	816.5
			Ait belale et al. 2021		
0.1	-	794.1	778.3	760.9	-
10	-	801.6	786.8	770.6	753.4
20	-	809.1	794.6	779.2	763.3
30	-	815.4	801.7	787.1	772.2
40	-	821.4	808.4	794.3	780
50	-	827.2	814.6	800.9	787.2
60	-	832.6	820.3	807.7	793.8
70	-	837.8	825.6	813.2	800.2
80	-	842.6	830.8	818.9	805.8
90	-	847.3	836.0	823.9	811.5
100	-	851.6	840.5	828.8	817.0
			Tórin-Ollarves et al. 2012		
0.1	809.6	794.1	778	-	-
5	813.1	798	782.4	-	-
10	816.5	801.8	786.5	-	-
20	822.9	808.9	794.4	-	-
30	829.0	815.5	801.6	-	-
40	834.7	821.6	808.2	-	-
50	840.0	827.4	814.4	-	-
60	845.0	832.7	820.1	-	-
70	849.8	837.8	825.6	-	-
80	854.4	842.7	830.7	-	-
90	858.7	847.3	835.6	-	-
100	862.9	851.7	840.3	-	-

Table D2: Densities measured at atmospheric pressure for 1-butanol + biodiesel systems in Anton Paar SVM 3000 equipment [a]

ϕ_1	w_1	x_1	Temperature / K				
vol	*mass*	*mol*	293.15	313.15	333.15	353.15	373.15
1-Butanol + Linseed Biodiesel							
1.00	1.00	1.00	809.9	794.4	778.3	761.2	743.1
0.96	0.96	0.99	813.3	797.8	781.7	764.6	746.5
0.89	0.88	0.97	819.0	803.5	787.5	770.5	752.5
0.81	0.80	0.94	825.1	809.6	793.6	776.7	758.9
0.70	0.68	0.89	833.7	818.2	802.3	785.5	768.0
0.61	0.59	0.85	840.6	825.2	809.4	792.7	775.4
0.43	0.41	0.74	853.9	838.6	822.9	806.7	790.0
0.34	0.32	0.65	861.1	845.9	830.4	814.5	798.2
0.22	0.20	0.50	870.5	855.6	840.3	824.8	809.1
0.13	0.12	0.35	877.3	862.5	847.5	832.3	817.1
0.05	0.04	0.15	883.9	869.3	854.5	839.8	825.2
0.00	0.00	0.00	886.6	872.2	857.6	843.1	828.8
1-Butanol + Soybean Biodiesel							
0.96	0.96	0.99	813.0	797.5	781.5	764.4	746.2
0.89	0.88	0.97	819.1	803.8	787.8	770.8	752.6
0.82	0.80	0.94	826.1	810.8	794.8	778.0	760.0
0.70	0.68	0.89	836.8	821.6	805.6	788.9	771.5
0.61	0.59	0.85	845.5	830.2	814.4	797.8	780.7
0.44	0.41	0.73	861.0	845.8	830.1	813.8	797.2
0.34	0.32	0.65	868.8	853.7	838.2	822.2	805.6
0.22	0.20	0.50	878.4	863.4	848.1	832.6	816.2
0.13	0.12	0.35	885.0	870.2	855.2	840.0	823.8
0.05	0.04	0.15	891.8	877.2	862.3	847.6	832.1
0.00	0.00	0.00	895.7	881.3	866.5	852.1	837.0
0.96	0.96	0.99	813.0	797.5	781.5	764.4	746.2

[a] The standard uncertainties are $u(T) = 0.01\ K$, $u(P) = 0.01\ MPa$, and $u(x_i) = 4 \cdot 10^{-5}$. Expanded uncertainty $U(\rho) = 0.50\ kg \cdot m^{-3}$, (0.95 confidence level).

Table D3. Calculated Isothermal compressibility (κ_T) for Blending 1-Butanol with Linseed Biodiesel, 0, 5, 13, and 22 ϕ_{But}, at temperatures (T) and pressure (P)[a].

P /MPa	T/K	$U(\kappa_T)$	T/K	$U(\kappa_T)$	T/K	$U(\kappa_T)$	T/K	$U(\kappa_T)$	T/K	$U(\kappa_T)$
	293.15	$U(\kappa_T)$	313.15	$U(\kappa_T)$	333.15	$U(\kappa_T)$	353.15	$U(\kappa_T)$	373.15	$U(\kappa_T)$
	But 0									
0.1	0.682	0.017	0.763	0.017	0.856	0.018	0.961	0.018	1.077	0.020
5.0	0.658	0.014	0.733	0.014	0.818	0.014	0.914	0.014	1.018	0.016
10.0	0.635	0.010	0.705	0.010	0.783	0.010	0.870	0.010	0.965	0.011
20.0	0.594	0.006	0.655	0.006	0.722	0.006	0.795	0.006	0.874	0.006
30.0	0.558	0.004	0.612	0.004	0.670	0.004	0.733	0.004	0.799	0.004
40.0	0.527	0.004	0.574	0.004	0.626	0.003	0.680	0.004	0.737	0.004
50.0	0.499	0.005	0.541	0.004	0.587	0.004	0.634	0.005	0.684	0.005
60.0	0.474	0.006	0.512	0.006	0.553	0.005	0.595	0.006	0.638	0.006
70.0	0.451	0.007	0.486	0.007	0.522	0.006	0.560	0.007	0.599	0.007
80.0	0.431	0.008	0.462	0.007	0.495	0.007	0.530	0.008	0.564	0.008
90.0	0.412	0.009	0.441	0.008	0.471	0.008	0.502	0.008	0.533	0.008
100.0	0.395	0.010	0.422	0.009	0.450	0.009	0.478	0.010	0.506	0.009
P	**But 5**									
0.1	0.686	0.018	0.768	0.018	0.863	0.016	0.972	0.023	1.095	0.019
5.0	0.662	0.014	0.738	0.015	0.826	0.013	0.924	0.018	1.035	0.015
10.0	0.639	0.010	0.710	0.011	0.790	0.009	0.881	0.013	0.981	0.010
20.0	0.598	0.006	0.660	0.007	0.729	0.006	0.805	0.007	0.888	0.006
30.0	0.562	0.004	0.617	0.004	0.676	0.004	0.742	0.004	0.812	0.004
40.0	0.530	0.004	0.579	0.003	0.631	0.004	0.688	0.004	0.748	0.004
50.0	0.502	0.005	0.546	0.004	0.592	0.004	0.642	0.005	0.694	0.005
60.0	0.477	0.007	0.516	0.005	0.558	0.005	0.602	0.007	0.648	0.006
70.0	0.455	0.008	0.490	0.006	0.527	0.006	0.567	0.008	0.607	0.007
80.0	0.434	0.009	0.466	0.007	0.500	0.007	0.536	0.009	0.572	0.008
90.0	0.415	0.010	0.445	0.008	0.476	0.007	0.508	0.010	0.541	0.008
100.0	0.398	0.011	0.426	0.009	0.454	0.008	0.483	0.011	0.513	0.009
P	**But 13**									
0.1	0.698	0.019	0.782	0.019	0.881	0.018	0.998	0.022	1.134	0.020
5.0	0.673	0.016	0.752	0.015	0.843	0.015	0.948	0.017	1.071	0.016
10.0	0.650	0.011	0.723	0.011	0.806	0.010	0.903	0.012	1.013	0.011
20.0	0.608	0.007	0.672	0.006	0.743	0.006	0.824	0.007	0.915	0.006
30.0	0.572	0.004	0.627	0.004	0.690	0.004	0.759	0.004	0.836	0.004
40.0	0.539	0.003	0.589	0.004	0.643	0.004	0.704	0.004	0.769	0.004
50.0	0.511	0.004	0.555	0.005	0.603	0.005	0.656	0.005	0.713	0.005
60.0	0.485	0.006	0.525	0.006	0.568	0.007	0.615	0.006	0.665	0.006
70.0	0.462	0.007	0.498	0.007	0.537	0.008	0.579	0.007	0.623	0.007
80.0	0.441	0.008	0.474	0.008	0.509	0.008	0.547	0.008	0.587	0.008
90.0	0.422	0.009	0.452	0.009	0.485	0.009	0.519	0.009	0.554	0.009
100.0	0.405	0.010	0.433	0.010	0.462	0.010	0.493	0.010	0.526	0.010
P	**But 22**									
0.1	0.711	0.018	0.800	0.018	0.903	0.022	1.026	0.020	1.171	0.022
5.0	0.686	0.015	0.768	0.015	0.863	0.018	0.974	0.016	1.104	0.017
10.0	0.662	0.011	0.738	0.011	0.826	0.012	0.927	0.011	1.044	0.011
20.0	0.619	0.007	0.685	0.007	0.760	0.007	0.845	0.006	0.942	0.006
30.0	0.582	0.004	0.640	0.004	0.705	0.004	0.778	0.004	0.859	0.004
40.0	0.549	0.004	0.600	0.003	0.657	0.003	0.720	0.004	0.790	0.004
50.0	0.520	0.005	0.566	0.004	0.616	0.005	0.671	0.005	0.731	0.005
60.0	0.493	0.006	0.535	0.005	0.580	0.006	0.629	0.006	0.681	0.007
70.0	0.470	0.007	0.507	0.006	0.548	0.008	0.591	0.007	0.638	0.007
80.0	0.449	0.008	0.483	0.007	0.519	0.009	0.559	0.008	0.600	0.008
90.0	0.429	0.009	0.461	0.008	0.494	0.010	0.529	0.009	0.567	0.009
100.0	0.412	0.010	0.440	0.009	0.471	0.011	0.503	0.010	0.537	0.010

[a] The standard uncertainties are $u(T) = 0.02\,K$, $u(P) = 0.03\,MPa$, $u(x_i) = 4 \cdot 10^{-5}$

Table D3. Calculated Isothermal compressibility (κ_T) for Blending 1-Butanol with Linseed Biodiesel, 34, 61 and 100 ϕ_{But}, at temperatures (T) and pressure (P)[a].

P /MPa	T/K	$U(\kappa_T)$								
	293.15	$U(\kappa_T)$	313.15	$U(\kappa_T)$	333.15	$U(\kappa_T)$	353.15	$U(\kappa_T)$	373.15	$U(\kappa_T)$
	But 34									
0.1	0.739	0.017	0.828	0.017	0.936	0.021	1.069	0.019	1.235	0.022
5.0	0.712	0.014	0.795	0.013	0.894	0.017	1.014	0.015	1.162	0.017
10.0	0.687	0.010	0.763	0.009	0.854	0.012	0.963	0.010	1.096	0.012
20.0	0.641	0.006	0.707	0.006	0.785	0.007	0.876	0.006	0.985	0.007
30.0	0.601	0.004	0.659	0.003	0.726	0.004	0.804	0.004	0.895	0.005
40.0	0.567	0.003	0.618	0.003	0.676	0.004	0.743	0.004	0.821	0.005
50.0	0.536	0.004	0.581	0.004	0.633	0.005	0.692	0.005	0.759	0.005
60.0	0.508	0.005	0.549	0.006	0.595	0.006	0.647	0.006	0.706	0.006
70.0	0.484	0.006	0.521	0.007	0.562	0.007	0.608	0.007	0.660	0.007
80.0	0.461	0.007	0.495	0.007	0.533	0.008	0.574	0.008	0.620	0.008
90.0	0.441	0.008	0.472	0.008	0.506	0.009	0.544	0.008	0.585	0.008
100.0	0.423	0.009	0.451	0.009	0.482	0.010	0.516	0.009	0.554	0.009
P	**But 100**									
0.1	0.885	0.020	1.000	0.021	1.147	0.020	1.338	0.026	-	-
5.0	0.847	0.016	0.952	0.017	1.084	0.016	1.254	0.019	1.480	0.021
10.0	0.812	0.012	0.908	0.012	1.027	0.011	1.178	0.013	1.376	0.014
20.0	0.750	0.007	0.832	0.007	0.931	0.006	1.053	0.007	1.209	0.007
30.0	0.697	0.005	0.768	0.004	0.851	0.004	0.953	0.004	1.079	0.005
40.0	0.652	0.004	0.713	0.004	0.785	0.004	0.871	0.004	0.976	0.005
50.0	0.612	0.005	0.666	0.005	0.729	0.005	0.803	0.006	0.892	0.006
60.0	0.577	0.006	0.625	0.006	0.680	0.006	0.745	0.007	0.821	0.006
70.0	0.547	0.007	0.589	0.007	0.638	0.007	0.695	0.008	0.762	0.007
80.0	0.519	0.007	0.558	0.008	0.602	0.008	0.652	0.008	0.711	0.008
90.0	0.494	0.008	0.529	0.009	0.569	0.008	0.614	0.009	0.666	0.008
100.0	0.472	0.009	0.504	0.010	0.540	0.009	0.581	0.010	0.628	0.008

P /MPa	T/K	$U(\kappa_T)$								
	293.15	$U(\kappa_T)$	313.15	$U(\kappa_T)$	333.15	$U(\kappa_T)$	353.15	$U(\kappa_T)$	373.15	$U(\kappa_T)$
	But 61									
0.1	0.806	0.020	0.909	0.018	1.036	0.022	1.196	0.019	-	-
5.0	0.773	0.016	0.868	0.014	0.983	0.017	1.126	0.015	1.307	0.023
10.0	0.742	0.012	0.829	0.010	0.934	0.011	1.062	0.010	1.222	0.015
20.0	0.689	0.007	0.763	0.006	0.851	0.006	0.956	0.006	1.084	0.008
30.0	0.642	0.004	0.706	0.004	0.781	0.004	0.869	0.004	0.974	0.004
40.0	0.602	0.004	0.658	0.004	0.723	0.004	0.798	0.004	0.886	0.004
50.0	0.567	0.005	0.616	0.005	0.673	0.006	0.738	0.005	0.813	0.006
60.0	0.536	0.007	0.580	0.006	0.630	0.007	0.687	0.006	0.752	0.007
70.0	0.508	0.008	0.548	0.007	0.592	0.008	0.642	0.007	0.699	0.008
80.0	0.483	0.009	0.519	0.007	0.559	0.009	0.604	0.007	0.654	0.009
90.0	0.460	0.010	0.493	0.008	0.529	0.009	0.570	0.008	0.615	0.010
100.0	0.440	0.011	0.470	0.009	0.503	0.010	0.539	0.009	0.580	0.011

[a] The standard uncertainties are $u(T) = 0.02\,K, u(P) = 0.03\,MPa, u(x_i) = 4 \cdot 10^{-5}$

Table D4. Calculated Isothermal compressibility (κ_T) for Blending 1-Butanol with Soybean Biodiesel, 0, 5, 13, and 22 ϕ_{But}, at temperatures (T) and pressure (P)[a].

P /MPa	T/K	$U(\kappa_T)$	T/K	$U(\kappa_T)$	T/K	$U(\kappa_T)$	T/K	$U(\kappa_T)$	T/K	$U(\kappa_T)$
	293.15	$U(\kappa_T)$	313.15	$U(\kappa_T)$	333.15	$U(\kappa_T)$	353.15	$U(\kappa_T)$	373.15	$U(\kappa_T)$
	But 0									
0.1	0.659	0.018	0.728	0.017	0.809	0.018	0.907	0.021	1.025	0.022
5.0	0.637	0.014	0.702	0.014	0.777	0.015	0.867	0.017	0.974	0.018
10.0	0.617	0.010	0.677	0.010	0.747	0.011	0.829	0.012	0.927	0.013
20.0	0.580	0.006	0.632	0.006	0.693	0.007	0.764	0.007	0.846	0.008
30.0	0.547	0.004	0.594	0.004	0.647	0.004	0.708	0.004	0.779	0.005
40.0	0.518	0.004	0.560	0.004	0.607	0.003	0.661	0.003	0.722	0.005
50.0	0.492	0.005	0.530	0.005	0.572	0.004	0.619	0.005	0.673	0.005
60.0	0.468	0.006	0.503	0.006	0.541	0.005	0.583	0.006	0.630	0.006
70.0	0.447	0.007	0.478	0.008	0.513	0.006	0.551	0.007	0.593	0.007
80.0	0.428	0.008	0.457	0.008	0.488	0.007	0.522	0.008	0.560	0.008
90.0	0.411	0.009	0.437	0.009	0.465	0.007	0.497	0.009	0.531	0.008
100.0	0.394	0.010	0.419	0.010	0.445	0.008	0.474	0.010	0.505	0.010
	But 5									
0.1	0.666	0.018	0.738	0.018	0.824	0.016	0.929	0.023	1.057	0.019
5.0	0.644	0.014	0.711	0.015	0.791	0.013	0.886	0.018	1.002	0.015
10.0	0.623	0.010	0.686	0.011	0.760	0.009	0.847	0.013	0.953	0.010
20.0	0.585	0.006	0.640	0.007	0.704	0.006	0.779	0.007	0.867	0.006
30.0	0.552	0.004	0.601	0.004	0.657	0.004	0.721	0.004	0.796	0.004
40.0	0.522	0.004	0.566	0.003	0.615	0.004	0.672	0.004	0.737	0.004
50.0	0.496	0.005	0.535	0.004	0.579	0.004	0.629	0.005	0.686	0.005
60.0	0.472	0.007	0.508	0.005	0.547	0.005	0.592	0.007	0.642	0.006
70.0	0.451	0.008	0.483	0.006	0.519	0.006	0.559	0.008	0.604	0.007
80.0	0.431	0.009	0.461	0.007	0.493	0.007	0.529	0.009	0.570	0.008
90.0	0.413	0.010	0.440	0.008	0.470	0.007	0.503	0.010	0.540	0.008
100.0	0.397	0.011	0.422	0.009	0.449	0.008	0.479	0.011	0.513	0.009
P	**But 13**									
0.1	0.680	0.019	0.763	0.019	0.860	0.018	0.973	0.022	1.106	0.020
5.0	0.657	0.016	0.734	0.015	0.823	0.015	0.927	0.017	1.046	0.016
10.0	0.635	0.011	0.707	0.011	0.789	0.010	0.884	0.012	0.992	0.011
20.0	0.596	0.007	0.658	0.006	0.729	0.006	0.809	0.007	0.899	0.006
30.0	0.561	0.004	0.616	0.004	0.678	0.004	0.747	0.004	0.823	0.004
40.0	0.530	0.003	0.579	0.004	0.634	0.004	0.694	0.004	0.760	0.004
50.0	0.503	0.004	0.547	0.005	0.595	0.005	0.648	0.005	0.705	0.005
60.0	0.478	0.006	0.518	0.006	0.562	0.007	0.609	0.006	0.659	0.006
70.0	0.456	0.007	0.492	0.007	0.532	0.008	0.574	0.007	0.618	0.007
80.0	0.436	0.008	0.469	0.008	0.505	0.008	0.543	0.008	0.583	0.008
90.0	0.418	0.009	0.448	0.009	0.481	0.009	0.515	0.009	0.551	0.009
100.0	0.401	0.010	0.429	0.010	0.459	0.010	0.490	0.010	0.523	0.010
P	**But 22**									
0.1	0.700	0.018	0.787	0.018	0.889	0.022	1.010	0.020	1.152	0.022
5.0	0.676	0.015	0.756	0.015	0.850	0.018	0.959	0.016	1.087	0.017
10.0	0.653	0.011	0.728	0.011	0.814	0.012	0.913	0.011	1.028	0.011
20.0	0.611	0.007	0.676	0.007	0.750	0.007	0.834	0.006	0.929	0.006
30.0	0.574	0.004	0.632	0.004	0.696	0.004	0.768	0.004	0.848	0.004
40.0	0.542	0.004	0.593	0.003	0.650	0.003	0.712	0.004	0.780	0.004
50.0	0.514	0.005	0.559	0.004	0.609	0.005	0.664	0.005	0.723	0.005
60.0	0.488	0.006	0.529	0.005	0.574	0.006	0.622	0.006	0.674	0.007
70.0	0.465	0.007	0.502	0.006	0.542	0.008	0.586	0.007	0.632	0.007
80.0	0.444	0.008	0.478	0.007	0.514	0.009	0.553	0.008	0.595	0.008
90.0	0.425	0.009	0.456	0.008	0.489	0.010	0.525	0.009	0.562	0.009
100.0	0.408	0.010	0.436	0.009	0.467	0.011	0.499	0.010	0.533	0.010

[a] The standard uncertainties are $u(T) = 0.02\,K$, $u(P) = 0.03\,MPa$, $u(x_i) = 4 \cdot 10^{-5}$

Table D4. Calculated Isothermal compressibility (κ_T) for Blending 1-Butanol with Soybean Biodiesel, 34, 61 and 100 ϕ_{But}, at temperatures (T) and pressure (P)[a].

	T/K	$U(\kappa_T)$										T/K									
P/MPa	293.15	$U(\kappa_T)$	313.15	$U(\kappa_T)$	333.15	$U(\kappa_T)$	353.15	$U(\kappa_T)$	373.15	$U(\kappa_T)$	P/MPa	293.15	$U(\kappa_T)$	313.15	$U(\kappa_T)$	333.15	$U(\kappa_T)$	353.15	$U(\kappa_T)$	373.15	$U(\kappa_T)$
	But 34											**But 61**									
0.1	0.712	0.019	0.800	0.020	0.906	0.019	1.032	0.021	1.185	0.024	0.1	0.791	0.019	0.892	0.019	1.016	0.021	1.168	0.019	1.361	0.021
5.0	0.687	0.015	0.769	0.016	0.866	0.015	0.980	0.016	1.118	0.018	5.0	0.760	0.015	0.853	0.015	0.965	0.016	1.102	0.015	1.272	0.017
10.0	0.663	0.011	0.740	0.012	0.829	0.011	0.933	0.011	1.057	0.012	10.0	0.731	0.011	0.817	0.011	0.919	0.011	1.042	0.010	1.193	0.011
20.0	0.621	0.007	0.687	0.007	0.764	0.006	0.852	0.006	0.954	0.007	20.0	0.679	0.007	0.753	0.007	0.839	0.006	0.941	0.006	1.062	0.006
30.0	0.584	0.004	0.642	0.004	0.709	0.004	0.784	0.004	0.870	0.004	30.0	0.635	0.005	0.699	0.005	0.773	0.004	0.858	0.004	0.959	0.004
40.0	0.551	0.004	0.603	0.004	0.661	0.004	0.727	0.004	0.800	0.004	40.0	0.596	0.004	0.652	0.005	0.716	0.004	0.790	0.004	0.874	0.004
50.0	0.522	0.005	0.569	0.005	0.620	0.005	0.677	0.005	0.741	0.006	50.0	0.562	0.005	0.612	0.006	0.668	0.005	0.732	0.005	0.804	0.005
60.0	0.496	0.007	0.538	0.006	0.584	0.006	0.635	0.006	0.691	0.007	60.0	0.532	0.007	0.576	0.007	0.626	0.007	0.682	0.006	0.745	0.005
70.0	0.473	0.008	0.511	0.007	0.552	0.007	0.597	0.007	0.647	0.008	70.0	0.505	0.008	0.545	0.008	0.589	0.008	0.639	0.007	0.694	0.006
80.0	0.452	0.009	0.486	0.008	0.524	0.008	0.564	0.008	0.609	0.009	80.0	0.481	0.009	0.517	0.008	0.557	0.008	0.601	0.007	0.650	0.006
90.0	0.432	0.010	0.464	0.009	0.498	0.009	0.535	0.009	0.575	0.009	90.0	0.459	0.009	0.492	0.009	0.528	0.009	0.568	0.008	0.612	0.007
100.0	0.415	0.010	0.444	0.010	0.475	0.010	0.509	0.010	0.545	0.010	100.0	0.439	0.011	0.469	0.010	0.502	0.010	0.538	0.009	0.578	0.008
P	**But 100**																				
0.1	0.885	0.020	1.000	0.021	1.147	0.020	1.338	0.026	-	-											
5.0	0.847	0.016	0.952	0.017	1.084	0.016	1.254	0.019	1.480	0.021											
10.0	0.812	0.012	0.908	0.012	1.027	0.011	1.178	0.013	1.376	0.014											
20.0	0.750	0.007	0.832	0.007	0.931	0.006	1.053	0.007	1.209	0.007											
30.0	0.697	0.005	0.768	0.004	0.851	0.004	0.953	0.004	1.079	0.005											
40.0	0.652	0.004	0.713	0.004	0.785	0.004	0.871	0.004	0.976	0.005											
50.0	0.612	0.005	0.666	0.005	0.729	0.005	0.803	0.006	0.892	0.006											
60.0	0.577	0.006	0.625	0.006	0.680	0.006	0.745	0.007	0.821	0.006											
70.0	0.547	0.007	0.589	0.007	0.638	0.007	0.695	0.008	0.762	0.007											
80.0	0.519	0.007	0.558	0.008	0.602	0.008	0.652	0.008	0.711	0.008											
90.0	0.494	0.008	0.529	0.009	0.569	0.008	0.614	0.009	0.666	0.008											
100.0	0.472	0.009	0.504	0.010	0.540	0.009	0.581	0.010	0.628	0.008											

[a] The standard uncertainties are $u(T) = 0.02\,K, u(P) = 0.03\,MPa, u(x_i) = 4 \cdot 10^{-5}$

Table D5. Calculated Isobaric thermal expansivities (α_P) for Blending 1-Butanol with linseed Biodiesel, 0, 5, 13, 22, 34, and 61 ϕ_{But} , at temperatures (T) and pressure (P)[a].

P	T /K					P	T /K					P/MPa	T /K				
$/MPa$	293.15	313.15	333.15	353.15	373.15	$/MPa$	293.15	313.15	333.15	353.15	373.15		293.15	313.15	333.15	353.15	373.15
			But 0						**But 5**						**But 13**		
0.1	0.826	0.839	0.853	0.867	0.881	0.1	0.823	0.845	0.869	0.893	0.918	0.1	0.828	0.861	0.896	0.933	0.971
5.0	0.808	0.819	0.830	0.841	0.853	5.0	0.805	0.824	0.845	0.866	0.888	5.0	0.809	0.840	0.871	0.903	0.937
10.0	0.791	0.799	0.808	0.817	0.827	10.0	0.787	0.805	0.823	0.841	0.861	10.0	0.792	0.820	0.848	0.876	0.906
20.0	0.760	0.765	0.770	0.775	0.782	20.0	0.756	0.770	0.783	0.798	0.813	20.0	0.760	0.783	0.806	0.829	0.852
30.0	0.733	0.735	0.737	0.740	0.745	30.0	0.728	0.739	0.750	0.761	0.774	30.0	0.732	0.752	0.771	0.790	0.808
40.0	0.709	0.709	0.709	0.710	0.714	40.0	0.704	0.712	0.720	0.729	0.740	40.0	0.707	0.724	0.740	0.756	0.771
50.0	0.687	0.685	0.684	0.684	0.687	50.0	0.682	0.688	0.695	0.702	0.712	50.0	0.685	0.700	0.713	0.726	0.739
60.0	0.668	0.665	0.662	0.661	0.664	60.0	0.662	0.667	0.672	0.678	0.687	60.0	0.665	0.678	0.690	0.701	0.711
70.0	0.650	0.646	0.642	0.641	0.643	70.0	0.644	0.648	0.652	0.657	0.665	70.0	0.647	0.658	0.668	0.678	0.687
80.0	0.634	0.629	0.625	0.623	0.625	80.0	0.628	0.631	0.633	0.638	0.646	80.0	0.630	0.640	0.649	0.657	0.665
90.0	0.619	0.613	0.609	0.606	0.609	90.0	0.613	0.615	0.617	0.621	0.628	90.0	0.615	0.624	0.632	0.639	0.646
100.0	0.606	0.599	0.594	0.592	0.594	100.0	0.599	0.600	0.602	0.605	0.613	100.0	0.601	0.609	0.616	0.622	0.629
P			**But 22**			P			**But 34**			P			**But 61**		
0.1	0.842	0.880	0.919	0.961	1.004	0.1	0.849	0.898	0.949	1.003	1.060	0.1	0.877	0.946	1.019	1.096	1.178

5.0	0.823	0.857	0.893	0.930	0.968	5.0	0.830	0.875	0.921	0.969	1.017	5.0	0.855	0.920	0.986	1.055	1.124
10.0	0.804	0.836	0.868	0.901	0.935	10.0	0.811	0.853	0.895	0.937	0.978	10.0	0.834	0.895	0.956	1.017	1.076
20.0	0.771	0.798	0.825	0.852	0.878	20.0	0.778	0.815	0.850	0.883	0.912	20.0	0.798	0.851	0.903	0.953	0.996
30.0	0.742	0.765	0.788	0.810	0.831	30.0	0.750	0.781	0.811	0.837	0.857	30.0	0.766	0.814	0.859	0.900	0.933
40.0	0.716	0.737	0.756	0.774	0.792	40.0	0.724	0.752	0.777	0.798	0.812	40.0	0.738	0.781	0.822	0.856	0.880
50.0	0.693	0.711	0.728	0.743	0.758	50.0	0.701	0.726	0.748	0.765	0.773	50.0	0.713	0.753	0.789	0.819	0.836
60.0	0.673	0.688	0.703	0.716	0.729	60.0	0.681	0.703	0.722	0.735	0.740	60.0	0.691	0.728	0.761	0.786	0.799
70.0	0.654	0.668	0.681	0.692	0.704	70.0	0.662	0.683	0.699	0.709	0.711	70.0	0.671	0.706	0.736	0.758	0.766
80.0	0.637	0.649	0.661	0.671	0.681	80.0	0.645	0.664	0.678	0.686	0.685	80.0	0.653	0.686	0.714	0.733	0.738
90.0	0.621	0.632	0.642	0.652	0.661	90.0	0.630	0.647	0.660	0.666	0.662	90.0	0.637	0.668	0.693	0.710	0.713
100.0	0.607	0.617	0.626	0.634	0.642	100.0	0.616	0.632	0.643	0.647	0.641	100.0	0.622	0.652	0.675	0.690	0.690

[a] The standard uncertainties are $u(T) = 0.1\,K$, $u(P) = 0.02\,MPa$, $u(x_i) = 4 \cdot 10^{-5}$ and $u(\alpha_P) = 0.017$.

Table D6. Calculated Isobaric thermal expansivities (α_P) for Blending 1-Butanol with Soybean Biodiesel, 0, 5, 13, 22, 34, and 61 ϕ_{But} , at temperatures (T) and pressure (P)[a].

P	T /K					P	T /K					P/MPa	T /K				
$/MPa$	293.15	313.15	333.15	353.15	373.15	$/MPa$	293.15	313.15	333.15	353.15	373.15		293.15	313.15	333.15	353.15	373.15
			But 0						**But 5**						**But 13**		
0.1	0.797	0.818	0.841	0.864	0.888	0.1	0.796	0.829	0.863	0.899	0.937	0.1	0.827	0.862	0.898	0.935	0.975
5.0	0.781	0.800	0.820	0.839	0.858	5.0	0.780	0.810	0.841	0.872	0.903	5.0	0.809	0.841	0.873	0.907	0.941
10.0	0.767	0.784	0.800	0.816	0.830	10.0	0.765	0.793	0.820	0.847	0.873	10.0	0.792	0.821	0.850	0.880	0.911

20.0	0.741	0.753	0.765	0.774	0.781	20.0	0.738	0.761	0.783	0.803	0.820	20.0	0.760	0.785	0.810	0.834	0.858
30.0	0.717	0.727	0.734	0.739	0.740	30.0	0.714	0.733	0.751	0.766	0.776	30.0	0.733	0.754	0.775	0.795	0.814
40.0	0.696	0.703	0.708	0.709	0.705	40.0	0.692	0.709	0.723	0.733	0.738	40.0	0.708	0.727	0.744	0.761	0.777
50.0	0.678	0.682	0.684	0.682	0.675	50.0	0.672	0.687	0.698	0.705	0.705	50.0	0.686	0.702	0.717	0.731	0.745
60.0	0.661	0.663	0.663	0.658	0.648	60.0	0.655	0.667	0.676	0.680	0.677	60.0	0.666	0.680	0.693	0.706	0.717
70.0	0.645	0.646	0.644	0.637	0.624	70.0	0.639	0.649	0.656	0.657	0.652	70.0	0.648	0.660	0.672	0.683	0.693
80.0	0.631	0.630	0.626	0.618	0.603	80.0	0.624	0.633	0.638	0.637	0.629	80.0	0.631	0.642	0.653	0.662	0.671
90.0	0.618	0.616	0.611	0.601	0.584	90.0	0.611	0.618	0.621	0.619	0.609	90.0	0.616	0.626	0.635	0.643	0.652
100.0	0.606	0.603	0.596	0.585	0.567	100.0	0.598	0.604	0.606	0.603	0.591	100.0	0.602	0.611	0.619	0.627	0.634
P			**But 22**			*P*			**But 34**			*P*			**But 61**		
0.1	0.840	0.876	0.915	0.955	0.996	0.1	0.846	0.890	0.936	0.984	1.034	0.1	0.881	0.946	1.014	1.086	1.163
5.0	0.822	0.855	0.889	0.925	0.961	5.0	0.827	0.867	0.909	0.951	0.995	5.0	0.859	0.919	0.982	1.047	1.113
10.0	0.804	0.834	0.865	0.897	0.929	10.0	0.809	0.846	0.883	0.922	0.960	10.0	0.838	0.895	0.953	1.011	1.068
20.0	0.772	0.798	0.823	0.849	0.873	20.0	0.776	0.808	0.839	0.870	0.899	20.0	0.802	0.852	0.902	0.949	0.994
30.0	0.744	0.766	0.787	0.808	0.827	30.0	0.747	0.774	0.801	0.826	0.849	30.0	0.770	0.815	0.859	0.899	0.934
40.0	0.719	0.738	0.756	0.773	0.788	40.0	0.721	0.745	0.768	0.789	0.807	40.0	0.742	0.783	0.822	0.856	0.884
50.0	0.696	0.713	0.728	0.742	0.755	50.0	0.698	0.719	0.739	0.757	0.771	50.0	0.717	0.755	0.790	0.820	0.842
60.0	0.676	0.690	0.704	0.715	0.726	60.0	0.677	0.696	0.714	0.728	0.740	60.0	0.695	0.730	0.762	0.788	0.806
70.0	0.657	0.670	0.682	0.691	0.700	70.0	0.658	0.675	0.691	0.703	0.713	70.0	0.675	0.708	0.737	0.760	0.775

80.0	0.640	0.652	0.662	0.670	0.677	80.0	0.640	0.656	0.670	0.681	0.688	80.0	0.657	0.688	0.715	0.736	0.748
90.0	0.625	0.635	0.644	0.651	0.657	90.0	0.625	0.639	0.651	0.661	0.667	90.0	0.640	0.670	0.695	0.714	0.723
100.0	0.611	0.620	0.627	0.634	0.639	100.0	0.610	0.623	0.634	0.642	0.647	100.0	0.625	0.653	0.677	0.694	0.702

[a] The standard uncertainties are $u(T) = 0.1\ K$, $u(P) = 0.02\ MPa$, $u(x_i) = 4 \cdot 10^{-5}$ and $u(\alpha_P) = 0.017$

Table D6 Calculated Isobaric thermal expansivities (α_P) for 1-Butanol at temperatures (T) and pressure (P)[a].

P/MPa	T/K				
	293.15	313.15	333.15	353.15	373.15
	But 100				
0.1	0.891	0.987	1.089	1.198	1.315
5.0	0.866	0.957	1.051	1.147	1.245
10.0	0.844	0.929	1.016	1.102	1.184
20.0	0.803	0.880	0.955	1.025	1.084
30.0	0.769	0.839	0.905	0.963	1.005
40.0	0.739	0.803	0.863	0.912	0.941
50.0	0.712	0.772	0.826	0.868	0.887
60.0	0.688	0.745	0.794	0.830	0.842
70.0	0.667	0.721	0.766	0.798	0.803
80.0	0.648	0.699	0.742	0.769	0.769
90.0	0.631	0.680	0.719	0.743	0.739
100.0	0.615	0.662	0.699	0.720	0.713

[a] The standard uncertainties are $u(T) = 0.1\ K$, $u(P) = 0.02\ MPa$, $u(x_i) = 4 \cdot 10^{-5}$ and $u(\alpha_P) = 0.017$.

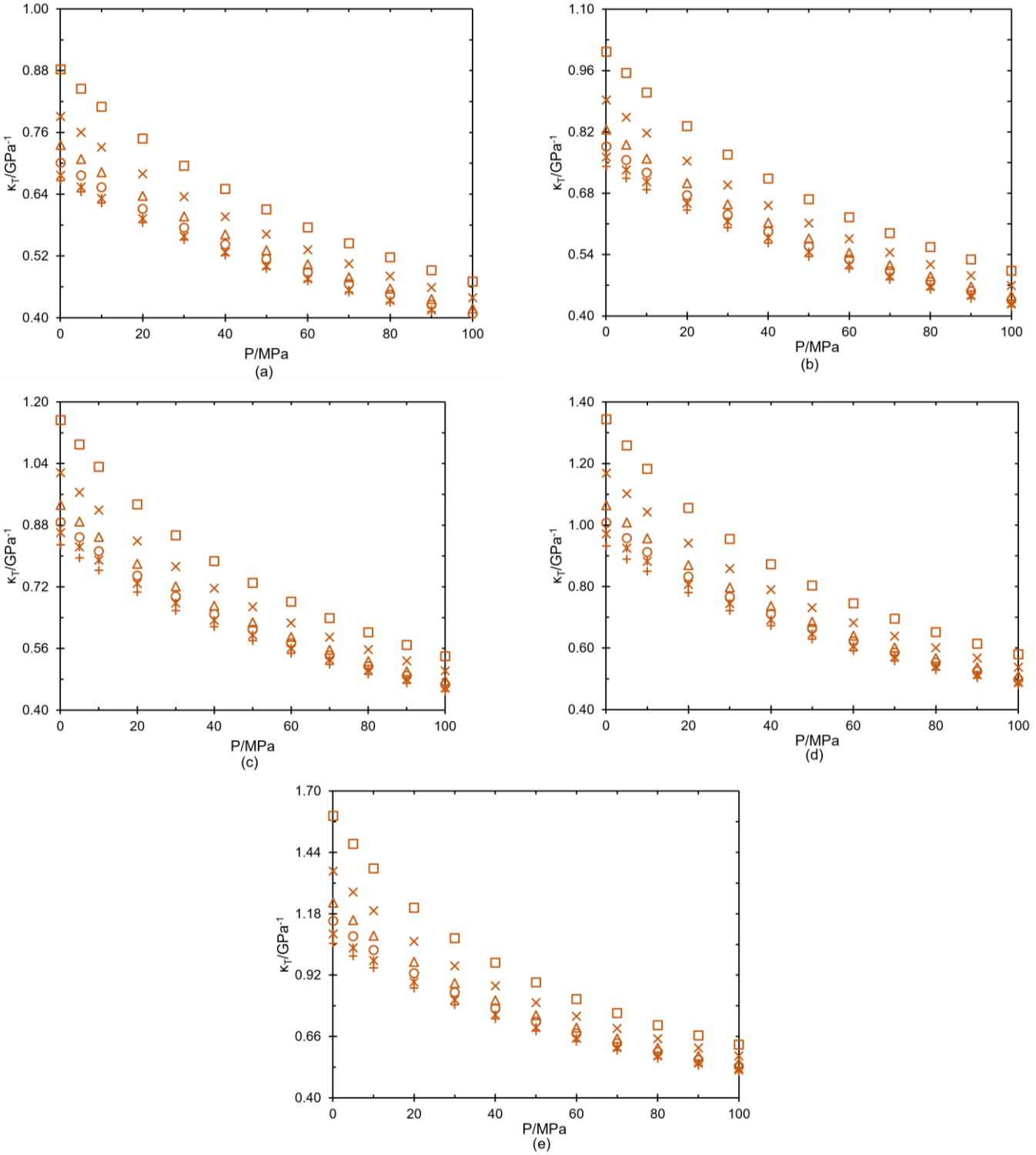

Figure D1. Isothermal compressibility (κ_T) as a function of pressure for 1-butanol and soybean biodiesel blends. Each symbol refers to a mixture, where: (□, brown open square) But 100 – Bio 0, (×, brown cross) But 61 – Bio 39, (△, brown open triangle) But 34 – Bio 66, (○, open brown circle) But 22 – Bio 78, (∗, brown asterisk) But 13 – Bio 87, and (+, brown plus signal) But 5 – Bio 95. The isothermal graphs presented are respectively: (a) 293.15 K, (b) 313.15 K, (c) 333.15 K, (d) 353.15 K, (e) 373.15 K.

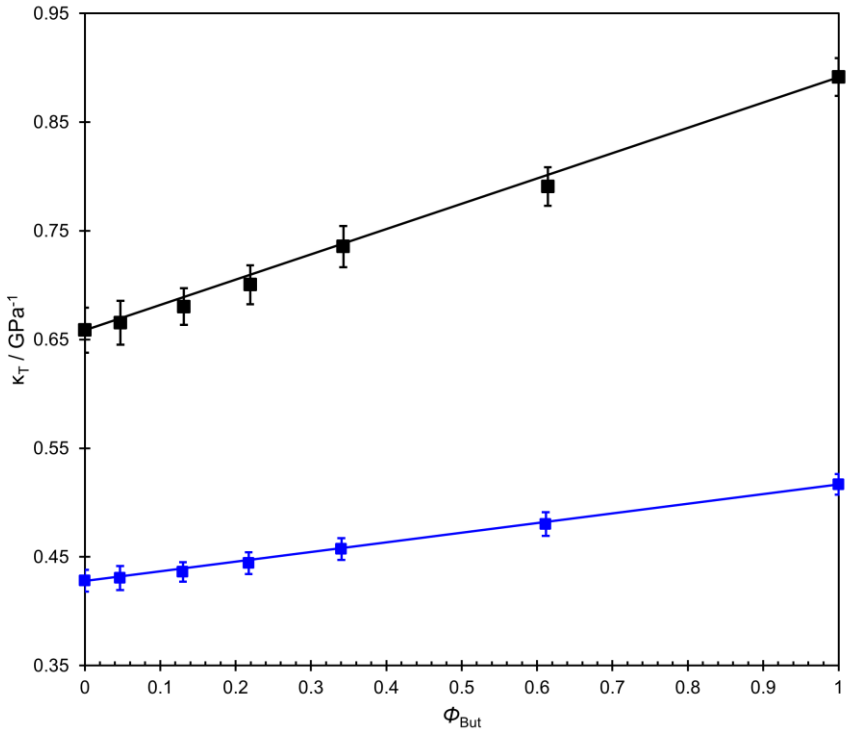

Figure D2. Isothermal compressibility as a function of the volume fraction of 1-butanol (ϕ_{But}) at temperature $T = 293.15\ K$ and pressure, for 1-butanol and soybean biodiesel blends. P: (■, black square), $0.1\ MPa$; (■, blue square), $90\ MPa$. Straight lines, ideal behavior. Error bars indicate the expanded uncertainty corresponding to a 95% confidence level.

APPENDIX E –COMPLEMENTARY MATERIAL TO CHAPTER 6

This document provides complementary information to Chapter 6 of this thesis, with a detailed description of its contents presented below:

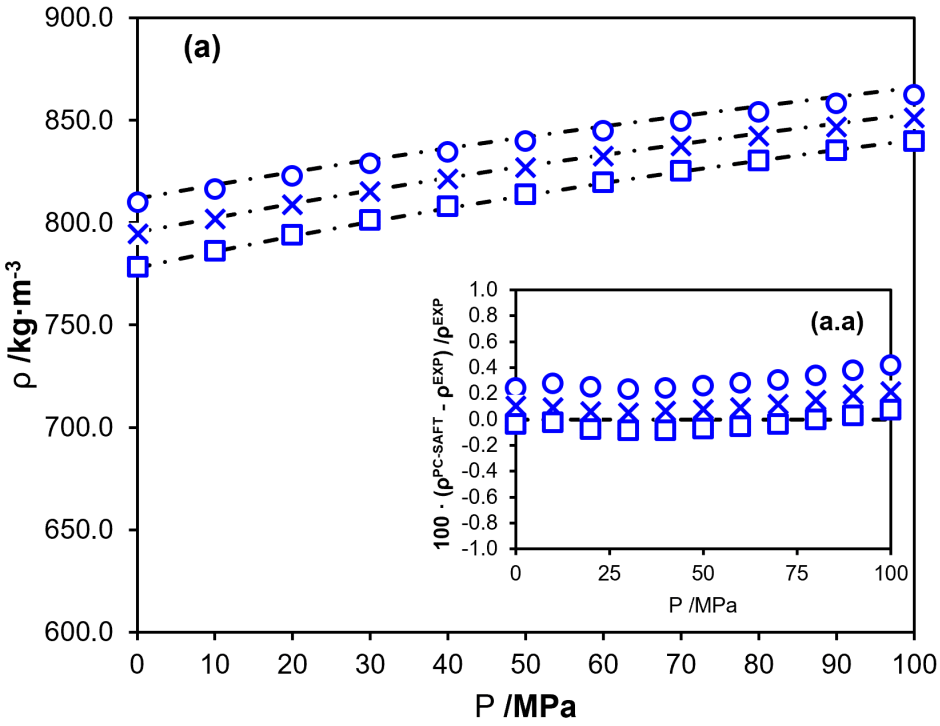

Figure E1 Density as a function of pressure for three isotherms: (○) 293,15 K, (×) 313,15 K e (□) 333,15 K. Graph (a) shows the comparison between the experimental data (symbols) and the values estimated by the PC-SAFT equation of state (dotted lines). Graph (a.a) shows the corresponding relative deviations as a function of pressure, for the same conditions.

APPENDIX F – COMPLEMENTARY MATERIAL TO CHAPTER 7

This document provides complementary information to Chapter 7 of this thesis, with a detailed description of its contents presented below:

Table F1: Technical description of the experimental apparatus studied in this work: Diana 700, SVM 3000, DSA 5000, Abbemat 300, and PMA 500.

Table F2: Specifications Imposed by ASTM for Biodiesel (B100) and Diesel (Diesel S10).

Table F3: Name, Molecular Formula, Acronym, CAS Registry Number, and Boiling Temperatures of Hydrocarbons and Esters Found in Diesel Profiles and the Three Investigated Biodiesels.

Table F4 – F6: Experimental distillation curve values for diesel, grape seed biodiesel, corn biodiesel, linseed biodiesel, and blends (20, 40, 60, and 80%). Data obtained by the Anton Paar Diana 700 atmospheric distillation analyzer used to measure the distillation curves using the ASTM D86 standard.

Table F7: Reference, source, acronym, viscosity at 40°C, density at 15°C, and temperature at 10, 50, and 90 percentual of volume recovered.

Table F8: Parameters adjusted for a correlation set for application in equations 2 – 4, which used to obtain distillation temperatures at 10, 50, and 90% distillation (T_{10}, T_{50}, and T_{90}).

Table F9: Parameters adjusted for correlation set for application in equations 5 – 8 a used to obtain the distillation curve for blends diesel + biodiesel.

Equation F1 – F15: Equations used to calculate the cetane number, **ASTM D 4737**, **D 976**, and **modified ASTM D4737** for biodiesel**.**

Figure F1. Values for the difference between temperatures (●) T_{90}-T_{10} and (■) T_{50}-T_{10} for diesel, biodiesel, and blends diesel + biodiesel. Symbols green (grape seed biodiesel), yellow (corn biodiesel), and brown (linseed biodiesel).

Table F1. Technical description of the experimental apparatus studied in this work: Diana 700, SVM 3000, DSA 5000, Abbemat 300, and PMA 500.

Apparatus/ Property studied	Technical information on the experimental apparatus[a]	Apparatus illustration[d]
Diana 700 (Boiling temperature)	Condenser system and sample chamber: Cooling technology: Peltier, without the use of liquids. Temperature range: 0 °C to 80 °C, with a resolution of 0.1 °C. Steam Temperature Sensor: Pt100, class A, with a range of 0 °C to 450 °C and a resolution of 0.1 °C. Pressure correction: Automatic, based on barometric pressure. Sample volume: Detection system: Static optical with contact image sensor. Analysis: Measurement of the initial volume before the test and automatic calculation of residue losses in the chamber. Volume range: 0 mL to 103.5 mL, with a resolution of 0.01 mL and accuracy of ± 0.1 mL Uncertainty[b]: 2 °C	
SVM 3000 (kinematic viscosity)	Measuring range: 0.2 to 20,000 mPa·s Temperature range: 15°C to 105°C Uncertainty: 0.02 mPa·s Digital resolution: 0.0001 mPa-s Minimum sample volume: 2.5 to 5 mL	
DSA 5000 (Density)	Measuring range: 0 to 3 g/cm3 Temperature range: 0°C to 100°C Uncertainty[c]: 0.0005 g/cm3 Digital resolution: 0.000001 g/cm3 Minimum sample volume: 2.5 to 5 mL	
Abbemat 300 (refractive index)	Range nD: 1.26 to 1.72 Temperature range 4 to 85 °C Uncertainty[c]: 0.001 Digital resolution nD: ± 0.00001 Minimum sample volume: 0.2mL	
PMA 500 (flash point)	Temperature range: Above ambient temperature up to 410 °C. Ignition type: Electric (encapsulated hot wire). Barometric pressure correction: The flash point is automatically corrected for barometric pressure. Flash detection: Automatic detection by thermoelement. Uncertainty[b]: 2°C	

a: Information taken from the company's website; *b*: Maximum experimental uncertainty obtained by repeatability; *c*: Maximum combined experimental uncertainty; *d*: Information taken from the company's website.

Table F2. Specifications Imposed by ASTM for Biodiesel (B100) and Diesel (Diesel S10)

studied Properties	units	test method ASTM[a]	diesel S10 test limit ASTM D975	biodiesel (B100) test limit ASTM D6751
density at 15 °C	$g \cdot cm^{-3}$	D1298	0.82 – 0.86	0.86 – 0.90
kinematic viscosity at 40 °C	$mm^2 \cdot s^{-1}$	D445	1.3 – 4.1	1.9 – 6.0
refractive index 20°C	nD	D1218	[b]N.S.	maximum 1.47
flash point	$°C$	D93	minimum 52	minimum 130
acid number	$mgKOH \cdot g^{-1}$	D664	maximum 0.5	maximum 0.5
cetane number	$°C$	D4737	minimum 40	minimum 47
distillation curve	$°C$	D1078	T_{10} min. 205; max. 300	-
			T_{50} min. 240; max. 338	-
			T_{90} min. 270; max. 371	T_{90} max. 365

[a]American Society for Testing and Materials; [b]Not Specified.

Cetane Index calculation

Equations are used to calculate the cetane number, which is explained in section 6.2.3 of the manuscript. **ASTM D 4737** (equation F1 – F6) and **D 976** (equation F7 – F9) are used for diesel and modified ASTM D4737 is used for biodiesel (equation F10 – F15).

ASTM D 4737:

$$DN = density\ at\ 15°C\ (kg/liter) - 0.85 \quad \text{(F1)}$$

$$B = [\exp(-3.5 \cdot DN)] - 1 \quad \text{(F2)}$$

$$T_{10N} = T_{10} - 215 \quad \text{(F3)}$$

$$\mathrm{T_{90N}} = T_{50} - 260 \quad \text{(F4)}$$

$$\mathrm{T_{90N}} = T_{90} - 310 \quad \text{(F5)}$$

$$\begin{aligned}\mathrm{CCI} = {} & 45.2 + 0.0892 \cdot (\mathrm{T_{10N}}) + 0.131 \cdot (\mathrm{T_{50N}}) + 0.0523 \cdot (\mathrm{T_{90N}}) \\ & + 0.901 \cdot \mathrm{B} \cdot (\mathrm{T_{50N}}) - 0.420 \cdot \mathrm{B} \cdot (\mathrm{T_{90N}}) + 4.9\mathrm{x}10^{-4} \\ & \cdot (\mathrm{T_{10N}})^2 - 4.9\mathrm{x}10^{-4} \cdot (\mathrm{T_{90N}})^2 + 107 \cdot \mathrm{B} + 60 \cdot \mathrm{B}^2\end{aligned} \quad \text{(F6)}$$

ASTM D 976:

$$D = fuel\ density\ at\ 15°C\ (g/ml) \quad \text{(F7)}$$

$T_{50} =$ 50% point on the distillation curve in (°C) (F8)

$$\mathrm{CCI} = 454.74 - 1641.416 \cdot \mathrm{D} + 774.74 \cdot \mathrm{D}^2 - 0.554 \cdot \mathrm{T_{50}} + 97.803 \cdot [\log_{10}(\mathrm{T_{50}})]^2 \quad \text{(F9)}$$

ASTM D 4737 modified for biodiesel:

$DN = density\ at\ 15°C\ (kg/liter) - 0.8743$ (F10)

$B = [\exp(-3.5 \cdot DN)] - 1$ (F11)

$T_{10N} = T_{10} - 321.1$ (F12)

$\mathrm{T_{90N}} = T_{50} - 327.5$ (F13)

$\mathrm{T_{90N}} = T_{90} - 339.9$ (F14)

$$\mathrm{CCI} = 56.46 + 0.4412 \cdot (\mathrm{T_{10N}}) + (14.62 \cdot \mathrm{B} - 0.6264) \cdot (\mathrm{T_{50N}}) + (0.002716 - 25.8 \cdot \mathrm{B}) \cdot (\mathrm{T_{90N}}) + 0.002199 \cdot [(\mathrm{T_{10N}})^2 - (\mathrm{T_{90N}})^2] + 77.02 \cdot \mathrm{B} - 2\,143 \cdot \mathrm{B}^2 \quad \text{(F15)}$$

Where: T_{10}, T_{50}, and T_{90} are temperatures at 10%, 50%, and 90% volume distilled in degrees °C.

Table F3. Name, Molecular Formula, Acronym, CAS Registry Number, and Boiling Temperatures of Hydrocarbons and Esters Found in Diesel Profiles and the Three Investigated Biodiesels.

name	molecular formula	[a]acronym	CAS Reg. No.	[b]boiling temperature / °C
hydrocarbons present in the diesel profile				
heptane	C_7H_{16}	C7	142-82-5	98.35
octane	C_8H_{18}	C8	111-65-9	125.55
nonane	C_9H_{20}	C9	111-84-2	150.65
decane	$C_{10}H_{22}$	C10	124-18-5	174.05
undecane	$C_{11}H_{24}$	C11	1120-21-4	194.85
dodecane	$C_{12}H_{26}$	C12	112-40-3	215.85
tridecane	$C_{13}H_{28}$	C13	629-50-5	233.85
tetradecane	$C_{14}H_{30}$	C14	629-59-4	249.85
pentadecane	$C_{15}H_{32}$	C15	629-62-9	266.85
hexadecane	$C_{16}H_{34}$	C16	544-76-3	280.85
heptadecane	$C_{17}H_{36}$	C17	629-78-7	301.85
octadecane	$C_{18}H_{38}$	C18	593-45-3	316.15
nonadecane	$C_{19}H_{40}$	C19	629-92-5	329.75
eicosane	$C_{20}H_{42}$	C20	112-95-8	343.05
henicosane	$C_{21}H_{44}$	C21	629-94-7	356.55

docosane	$C_{22}H_{46}$	C22	629-97-0	368.65
tricosane	$C_{23}H_{48}$	C23	638-67-5	380.05
tetracosane	$C_{24}H_{50}$	C24	646-31-1	391.35
esters present in biodiesel profiles				
methyl palmitate	$C_{17}H_{34}O_2$	ME-C16:0	112-39-0	163.55
methyl stearate	$C_{19}H_{38}O_2$	ME-C18:0	112-61-8	215.05
methyl oleate	$C_{19}H_{36}O_2$	ME-C18:1	112-62-9	218.55
methyl linoleate	$C_{19}H_{34}O_2$	ME-C18:2	112-63-0	192.05
methyl linolenate	$C_{19}H_{32}O_2$	ME-C18:3	301-00-8	182.05

[a]nomenclature used for compounds: diesel hydrocarbons, "CX", where: C refers to the compound carbon, X number of carbons present in the hydrocarbon chain. For compounds of biodiesel, "ME-CX: Y", where ME refers to the type of (methyl) ester, C refers to the carbon compound, X refers to the number of carbons in the main chain of the ester, and Y refers to the amount of unsaturation. [b]data from NIST Chemistry WebBook.

Table F4. Experimental distillation curve values for diesel, grape seed biodiesel, and blends (20, 40, 60 and 80%). Data obtained by the Anton Paar Diana 700 atmospheric distillation analyzer was used to measure the distillation curves using the ASTM D86 standard.

Distilled Volume (%)	Boiling Temperature (°C)					
	0%	20%	40%	60%	80%	100%
	Grape Seed Biodiesel					
IBP	157.5	152.5	155.0	145.4	130.2	325.6
5	192.7	200.4	217.4	238.9	270.3	344.0
10	208.0	213.8	231.5	257.1	295.5	345.3
20	226.4	237.2	255.6	284.4	317.9	346.3
30	241.0	254.9	277.7	306.8	327.4	347.4
40	253.5	271.5	297.5	321.0	331.9	348.1
50	266.2	288.3	314.0	329.3	335.3	348.9
60	280.0	305.4	325.9	334.3	337.4	349.5
70	296.0	320.8	333.5	337.8	339.4	351.4
80	315.3	333.3	339.4	341.4	341.4	350.3
90	345.2	348.3	349.4	349.7	345.6	350.6
95	373.4	366.5	361.1	357.7	-	-
Recovered Volume (%)	97.9	97.6	98.3	98.3	94.9	93.1
Loss (mL)	0.6	0.4	0.3	0.5	1.2	3.2
Residue (mL)	1.5	2.0	1.4	1.2	3.9	3.7

Mean repeatability for IBP is ± 4.7 °C, and for T_{10}, T_{50}, and T_{90} is ± 1.6 °C.

Table F5. Experimental distillation curve values for diesel, corn biodiesel, and blends (20, 40, 60, and 80%). Data obtained by the Anton Paar Diana 700 atmospheric distillation analyzer used to measure the distillation curves using the ASTM D86 standard.

Distilled Volume (%)	Boiling Temperature (°C)					
	0%	20%	40%	60%	80%	100%
	Corn Biodiesel					
IBP	157.5	154.7	151.6	143.1	110.1	331.1
5	192.7	200.8	213.5	228.6	272.3	340.5

10	208.0	214.7	229.3	256.4	296.5	343.3
20	226.4	237.2	254.1	283.1	317.2	344.7
30	241.0	254.9	276.3	305.6	326.4	345.7
40	253.5	271.5	295.6	319.6	331.5	346.6
50	266.2	288.3	312.0	327.6	334.2	347.3
60	280.0	305.1	323.9	333.1	336.5	348.6
70	296.0	320.1	332.0	336.9	337.9	350.1
80	315.3	332.8	338.6	340.5	340.9	350.2
90	345.2	348.4	350.0	349.0	346.0	351.7
95	373.4	367.7	361.7	354.4	-	-
Recovered Volume (%)	97.9	98.2	98.8	98.3	94.5	93.4
Loss (mL)	0.6	0.4	0.4	0.5	1.4	3.1
Residue (mL)	1.5	1.4	0.8	1.2	4.0	3.5

Mean repeatability for IBP is ± 4.7 °C, and for T_{10}, T_{50}, and T_{90} is ± 1.6 °C.

Table F6. Experimental distillation curve values for diesel, linseed biodiesel, and blends (20, 40, 60 and 80%). Data obtained by the Anton Paar Diana 700 atmospheric distillation analyzer used to measure the distillation curves using the ASTM D86 standard.

Distilled Volume (%)	Boiling Temperature (°C)					
	0%	20%	40%	60%	80%	100%
	Linseed Biodiesel					
IBP	157.5	159.0	153.0	140.8	94.8	320.5
5	192.7	198.4	214.7	240.0	242.2	341.8
10	208.0	215.3	230.6	257.1	297.3	343.5
20	226.4	238.1	256.8	284.3	316.3	345.1
30	241.0	254.7	277.3	305.8	326.4	345.8
40	253.5	271.0	297.0	319.8	330.9	346.7
50	266.2	287.3	313.4	328.1	333.9	347.9
60	280.0	304.3	324.6	333.1	336.3	348.9
70	296.0	319.5	338.4	336.7	338.1	350.6
80	315.3	332.9	338.7	340.1	340.5	348.6
90	345.2	348.2	348.6	347.8	342.5	349.6
95	373.4	367.1	360.7	355.3	-	-
Recovered Volume (%)	97.9	97.2	98.3	98.3	98.0	93.3
Loss (mL)	0.6	0.4	1.7	0.5	2.0	3.1
Residue (mL)	1.5	2.4	0.0	1.2	0.0	3.6

Mean repeatability for IBP is ± 4.7 °C, and for T_{10}, T_{50}, and T_{90} is ± 1.6 °C.

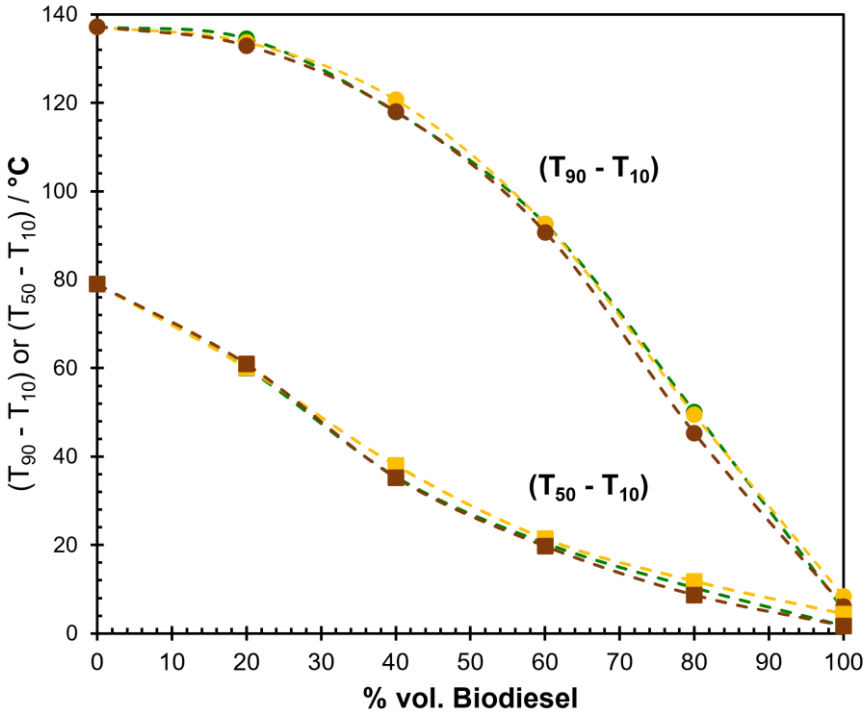

Figure F1. Values for the difference between temperatures (●) T_{90}-T_{10} and (■) T_{50}-T_{10} for diesel, biodiesel, and blends diesel + biodiesel. Symbols green (grape seed biodiesel), yellow (corn biodiesel), and brown (linseed biodiesel).

Table F8. Reference, source, acronym, viscosity at 40°C, density at 15°C, and temperature at 10, 50, and 90 percentual of volume recovered.

Ref, Year	**source**	**acronym**	Viscosity (40°C)	Density (15°C)	T_{10}	T_{50}	T_{90}
			$mm^2 \cdot s^{-1}$	$kg \cdot m^{-3}$	°C	°C	°C
This work, 2024	linseed	LS1	4.44	889.3	343.45	347.85	349.55
This work, 2024	corn	CR	4.86	887.8	343.30	347.30	351.70
This work, 2024	grape seed	GS	4.48	886.8	345.30	348.90	350.60
Hidegh et al. (2023)	Palm	PME	4.22	874.1	343.20	346.60	366.67
Hidegh et al. (2023)	Waste cooking	WCO	4.27	881.5	352.66	357.57	370.55
Hidegh et al. (2023)	Coconut	CME	2.72	874.3	276.74	300.22	364.13
Aburudyna et al. (2015)	Sunflower	SF1	4.39	885.3	325.00	336.00	341.00
Benjumea et al. (2008)	Palm	PL1	4.71	871.6	310.16	326.43	335.55
Bachler et al. (2010)	S. Rapessed	SRME	4.51	883.0	352.62	358.32	360.77
Berman et al. (2011)	Castor	CST1	15.17	924.4	368.94	377.25	393.88

Giakoumis (2013)	Beef tallow	BT	4.83	874.3	329.20	344.20
Giakoumis (2013)	Canola	CN	4.40	881.6	325.00	354.30
Giakoumis (2013)	Castor	CST2	14.52	917.6	327.00	381.60
Giakoumis (2013)	Croton	CRT	4.48	883.2	352.00	358.00
Giakoumis (2013)	Fish	FS	4.30	887.3	339.00	358.00
Giakoumis (2013)	Jatropha	JT	4.72	878.7	333.30	341.20
Giakoumis (2013)	Karanja	KR	5.04	882.9	334.00	345.40
Giakoumis (2013)	Lard	LD	4.89	873.0	329.00	337.00
Giakoumis (2013)	Linseed	LS2	4.06	891.5	338.00	361.00
Giakoumis (2013)	Palm	PL2	4.61	874.7	327.70	339.30
Giakoumis (2013)	Rapeseed	RP	4.63	882.2	340.70	344.30
Giakoumis (2013)	Rice bran	RB	4.70	880.9	336.00	346.00
Giakoumis (2013)	Soybean	SB1	4.29	882.8	336.30	345.00
Giakoumis (2013)	Sunflower	SF2	4.53	882.9	355.70	356.50
Giakoumis (2013)	Waste cooking	WC	4.75	880.6	340.40	350.30
Candeia et al. (2009)	soybean	SB2	5.75	882.8	334.00	352.00

Table F8. Parameters adjusted for a correlation set for application in equations 7.2 – 7.4, which used to obtain distillation temperatures at 10, 50 and 90% distillation (T_{10}, T_{50}, and T_{90})

Distillation temperatures (°C)	Adjusted parameters		
	$a/10^{-2}$	$b/10^{-6}$	$c/10^{-5}$
T_{10}	69949.5950	-41401.8780	68940.0595
T_{50}	66814.2747	-21174.5869	50424.7248
T_{90}	60410.7914	37345.2893	30981.2792

Table F9. Parameters adjusted for correlation set for application in equations 7.6–7.9 used to obtain the distillation curve for blends diesel + biodiesel.

Adjusted parameters	$D(x_D)$ **Eq. 7.6**	Adjusted parameters	$E(x_D)$ **Eq. 7.7**	Adjusted parameters	$F(x_D)$ **Eq. 7.8**
$d_2\ /10^{-4}$	-8430.9424	$e_2\ /10^{-4}$	1734.7110	$f_2\ /10^{-5}$	7114.6969
$d_1\ /10^{-4}$	2268.8265	$e_1\ /10^{-4}$	-2035.9666	$f_1\ /10^{-6}$	-1679.1348
$d_0/10^{-4}$	2273.6701	$e_0/10^{-3}$	1096.5223	$f_0/10^{-4}$	-5091.9071